Open Research Online

The Open University's repository of research publications
and other research outputs

The Photochemistry of *N*-Arylsulfonyl Amino Acids and Peptides

Thesis

How to cite:

Moore, Sharon Ann (2001). The Photochemistry of N-Arylsulfonyl Amino Acids and Peptides. PhD thesis. The Open University.

For guidance on citations see FAQs.

© 2001 Sharon Ann Moore

Version: Version of Record

Copyright and Moral Rights for the articles on this site are retained by the individual authors and/or other copyright owners. For more information on Open Research Online's data policy on reuse of materials please consult the policies page.

oro.open.ac.uk

UNRESTRICTED.

The Photochemistry of *N*-Arylsulfonyl Amino Acids and Peptides

A thesis submitted for the degree of

Doctor of Philosophy in Chemistry

to

The Open University

by

Sharon Ann Moore, BSc (Hons), AMRSC

October 2001

Department of Chemistry

The Open University

Walton Hall

Milton Keynes MK7 6AA

United Kingdom

SUBMISSION DATE: 7 NOVEMBER 2001
AWARD DATE: 20 DECEMBER 2001

ProQuest Number: C808762

All rights reserved

INFORMATION TO ALL USERS
The quality of this reproduction is dependent upon the quality of the copy submitted.

In the unlikely event that the author did not send a complete manuscript and there are missing pages, these will be noted. Also, if material had to be removed, a note will indicate the deletion.

ProQuest C808762

Published by ProQuest LLC (2019). Copyright of the Dissertation is held by the Author.

All rights reserved.
This work is protected against unauthorized copying under Title 17, United States Code
Microform Edition © ProQuest LLC.

ProQuest LLC.
789 East Eisenhower Parkway
P.O. Box 1346
Ann Arbor, MI 48106 – 1346

ABSTRACT

The photochemistry of arylsulfonamides has received continuing interest for the last four decades for three main reasons: 1) arylsulfonamides offer convenient acceptor properties for studying photo-induced electron transfer (PIET) processes in chromophorically modified peptide models, 2) arylsulfonamides have potential as photoremovable protecting groups in organic synthesis, but this has so far remained largely unrealized, 3) arylsulfonamide pharmaceuticals are generally photolabile and photostability is an important consideration in the development of new drugs.

We have studied a series of *p*-toluenesulfonyl amino acid derivatives and undertaken comprehensive product analysis to elucidate the photoproducts and identify common pathways of photodegradation. We found that the tosyl α-amino acids formed toluenesulfinic acid as a major photoproduct in conjunction with ammonia, carbon dioxide and a carbonyl compound. Upon changing the carboxylate to an ester or an amide, a C_α-H abstraction became the dominant process to give a carbonyl compound, toluenesulfinic acid and ammonia. These were also the major photoproducts with a tosyl β-amino acid. A mechanism is proposed that involves an initial electron transfer (ET) from the carboxyl function to the sulfonyl moiety to give a biradical intermediate that could react to produce most of the observed products.

Some differences in product distribution were found with different amino acid side-chains, although bulky aliphatic or sulfur containing side-chains produced little variation. A tyrosine derivative underwent side-chain cleavage, implying electron transfer from the side-chain rather than the carboxyl function. Peptide bond cleavages occurred in the majority of amide derivatives, which can also be explained by an electron transfer mechanism. The results showed that S-N cleavage to form the free amino acid moiety occurs in very poor yield due to a complex array of competing photoreactions.

A photoyellowing was seen in many of the amide compounds which may be due to photochromism, a process that is consistent with our photo-induced electron transfer hypothesis.

STATEMENT

I declare that the work included in this thesis was carried out by the author at the Open University Chemistry Department between 1st October 1998 and 30th September 2001 under the supervision of Dr Roger Hill and Dr David Roberts. The material embodied in this thesis has not been submitted nor is currently being submitted for any other degree.

The work is the result of my own investigations apart from the following which are fully acknowledged:

Departmental NMR service run by Mr Gordon Howell

Accurate mass data acquired by Pfizer Global R & D

Elemental analysis carried out by Medac Ltd

Parts of the work have been presented or published as listed below:

R. R. Hill, G. E. Jeffs, D. R. Roberts and S. A. Wood*, *Chem. Commun.*, **1999**, 1735-1736, Photodegradation of aryl sulfonamides: *N*-tosylglycine (*published in my previous name of Wood)

RSC Organic Reaction Mechanisms Group, Student Conference, Roche Discovery, Welwyn, UK, September 1999 (poster)

The European Photochemistry Association, Graduate Student Symposium in Photochemistry, University of Fribourg, Switzerland, February 2000 (poster)

Pfizer Organic Chemistry Poster Symposium, Café Royal, London, December 2000 (poster)

Sharon Ann Moore, October 2001

ACKNOWLEDGEMENTS

I would like to express my sincere gratitude to my supervisors, Dr Roger Hill and Dr David Roberts, for their patient support, guidance and continued enthusiasm and encouragement throughout the course of my project.

I would also like to thank the staff and students in the Open University Chemistry Department for their assistance during the last three years. In particular, Graham Jeffs, who has been of immense help in all technical aspects of the project, most notably HPLC and GC, and I must thank him for suffering the "electrickery" that I have performed upon his instruments.

I must also thank Dr Stephen Robinson and his colleagues at Pfizer Global R & D for their advice and assistance in acquiring LC-MS data and allowing me the use of LC-MS equipment on many occasions. I also thank Pfizer Global R & D for funding a large proportion of this project and allowing me to attend a number of courses and conferences. The Open University has also funded part of my studies, for which I am very grateful.

Finally, I must thank family and friends who have given me support and encouragement, not only during my PhD but also throughout my first degree. I would especially like to thank my children, Rebecca and Sean, for their (sometimes wavering) understanding of the need for peace and quiet at times of stress. And, last but not least, Paschalis for the greatly appreciated synthetic advice on numerous occasions.

SYMBOLS AND ABBREVIATIONS

ΔG	molar free-energy change
ε	molar absorption coefficient
λ_{max}	wavelength of maximum absorption
Boc	*t*-butyloxycarbonyl, $(CH_3)_3COCO$-
CT	charge transfer
DCM	dichloromethane
DMSO	dimethyl sulfoxide
DNA	deoxyribonucleic acid
DNMBS	4-(4′,8′-dimethoxynaphthylmethyl)benzenesulfonyl
DNP	2,4-dinitrophenylhydrazone
ET	electron transfer
FTIR	Fourier transform infrared spectroscopy
GC	gas chromatography
HPLC	high performance liquid chromatography
IC	internal conversion
ICH	International Conference on Harmonisation
ISC	inter system crossing
LC-MS	liquid chromatography-mass spectrometry
LRET	long range electron transfer
M	molar
MV	methyl viologen
PDA	photodiode array detector
PIET	photo-induced electron transfer
Ts or tosyl	*p*-toluenesulfonyl
UV-vis	Ultra violet-visible spectroscopy
VR	vibrational relaxation

The standard one or three letter abbreviations are used for amino acids and their derivatives. The *N*-*p*-toluenesulfonyl compounds are all abbreviated as Ts followed by the single letter abbreviation for the amino acid, e.g. G for glycine, and end with the carboxyl function i.e. OH, OMe (methyl ester) or NMA (N′-methyl amide). Tosylglycine is therefore abbreviated to TsGOH.

CONTENTS

Chapter 1: Introduction

1.1 Outline

Photochemistry is of literally vital importance for life on Earth, both in its origins and in many naturally occurring processes today. Photobiological processes such as photosynthesis are complex and generally involve pigments within a protein matrix. Photo-induced electron transfer (PIET) is known to play an important role within these matrices for the conversion of light energy to energy that is available to the plant for carbohydrate synthesis. A substantial proportion of current research is aimed at elucidating the mechanisms involved, and hence the understanding of the photochemistry of small organic molecules such as peptides, amino acids and related compounds is expected to give insights into these processes. A considerable amount of research is based upon model compounds of these proteins and typically involves small peptides attached to a light absorbing component. However, there are many issues that remain unresolved. The project described in this thesis involved the investigation of the photochemistry of *p*-toluenesulfonyl (tosyl) derivatives of amino acids and peptides (**1**). This is an area that has received a limited but continuing amount of study over the past thirty years.

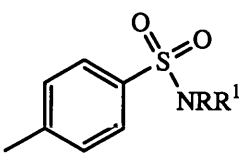

NRR^1 = amino acid or peptide

1

Four main reasons have been identified for an in-depth study of arylsulfonamide photochemistry:

- Arylsulfonyl groups offer convenient acceptor properties for studying the PIET processes in amino acid derivatives,[1]
- The potential of arylsulfonyls as photoremovable protecting groups in organic synthesis,[2,3]
- Arylsulfonamide pharmaceuticals are generally photolabile,[4,5]
- The ambiguity that remains over the mechanisms of the reactions in the aforementioned areas.

In the remainder of this chapter recent research in PIET of compounds related to amino acids and peptides, the photochemistry of a number of different arylsulfonamide protecting groups and the importance of drug photostability are reviewed. Evidence for different types of mechanisms in each area is examined. In the final section the objectives for the project are discussed and the relevance of our studies to the aforementioned areas considered. First, though it is necessary to review some of the fundamentals of photochemistry.

1.2 Fundamentals of photochemistry

1.2.1 Light absorption

Light-driven processes, such as photosynthesis, are initiated by the absorption of a photon, which excites an electron in a molecule to a higher energy level. The excited state of a molecule has different physical and chemical properties from the ground state, resulting in chemistry that is always kinetically controlled due to its short lifetime. The reactions that can be brought about photochemically are often not possible thermally or only occur over a long timescale.

The absorption of light energy is a prerequisite for photochemistry to occur – the Grotthuss-Draper law.[6] One of the advantages of photochemistry is the selective excitation of particular molecules or parts of molecules in the presence of less absorbing ones. The principal molecular feature responsible for absorption of a particular wavelength of light is the chromophore, which usually has double bonds and/or heteroatoms. Hence, the absorptions usually excite the electrons in the π orbitals of unsaturated molecules ($\pi \rightarrow \pi^*$) and the non-bonding electrons of molecules with heteroatoms ($n \rightarrow \pi^*$). An increase in conjugation or the presence of heteroatoms both serve to increase the wavelength at which light is most likely to be absorbed (λ_{max}) and the molar absorption coefficient (ε) of a molecule. In a simplified model the energy difference between the highest occupied orbital and lowest unoccupied orbital determines the lowest energy absorption.

1.2.2 Dissipation of excess energy

The absorption of light energy is very fast, ~10^{-18} s. When no interactions with other molecules occur, the excited molecule can return to the ground state by intramolecular photophysical processes, dissipating all the energy as heat or undergo a unimolecular photochemical reaction. Figure 1.1 shows the excitation of a molecule and the possible routes for return to the ground state. Most molecules are in a singlet ground state (S_0), and after excitation, a singlet excited state is expected if the excited electron maintains its original spin state. A change in spin state is not a formally allowed transition but this can occur to give a triplet excited state (T_1). The triplet excited state is longer-lived than the singlet excited state as the return to the singlet ground state would entail the forbidden change in spin state. Photochemical processes occur from the lowest vibrational energy of the lowest excited state i.e. S_1 or T_1. Higher electronically excited states have very short lifetimes (10^{-13} s) due to rapid decay via photophysical processes such as internal conversion (IC) and vibrational relaxation (VR). IC occurs from one energy level to a lower one when their vibrational energy levels overlap. VR occurs in any energy state

if the electron is not in the lowest vibrational level of that state, it is observed as an increase in thermal motion.

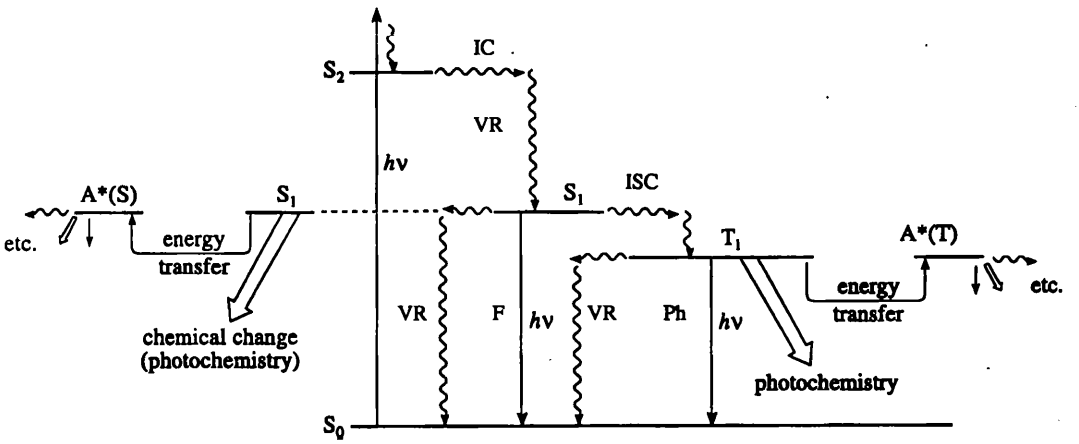

Figure 1.1 A Jablonski diagram[7] extended to show photochemical processes. Wavy arrows indicate non-radiative processes (VR, IC, ISC). Straight arrows are radiative processes (F = fluorescence, Ph = phosphorescence). Wide arrows show photochemical routes.

The lifetime of the lowest singlet excited state (S_1) is ~10^{-7}-10^{-9} s. The electron can return to S_0 from S_1 by IC or by fluorescence. To the eye, fluorescence ceases as soon as illumination stops. This reflects the short lifetime of the S_1 excited state. Intersystem crossing (ISC) from S_1 to T_1 can also occur although this is not a formally allowed transition as a change of spin state is involved. The lifetime of the lowest triplet excited state (T_1) is longer as it must return to the singlet ground state (S_0) via ISC or phosphorescence, a transition that is not formally allowed due to the change in spin state. The longer lifetime in T_1 is observed by phosphorescence continuing for up to 10^2 s after illumination stops.

A molecule may also return to the ground state by transferring its energy to another molecule (A). Singlet-singlet energy transfer requires the overlap of the emission spectra of the donor with the absorption spectra of the acceptor, whereas the Forster mechanism involves the coupling of the transition dipoles of two molecules. Energy transfer can occur from the excited molecule to a vibrational level of a slightly lower energy electronic state of A. Each transfer of energy results in some loss of energy due to

VR of the acceptor. If there is enough energy, A^* may undergo photochemical change. This is the case in photosynthesis.

Photochemical events are comparatively rare as they are in competition with the more spontaneous photophysical ones. They are more likely to occur from T_1 due to the longer lifetime of the excited state but can also occur from S_1 if the reaction is faster than 10^{-7} s. Photochemistry is a quantum process, only one photon of light per absorbing molecule is required to induce chemical change – the Stark-Einstein law.[6] The resulting excited state is so short-lived that it is unlikely that another photon will be absorbed before a chemical change has occurred.

1.2.3 The chemistry of the excited state.

According to the Franck-Condon principle,[6] the initial conformation of the excited state is the same as that of the ground state. However, this immediately relaxes to a more stable conformation, an equilibrium excited state that has different bond lengths, bond angles and charge distribution from the ground state. These changes are the cause of the differences between ground state chemistry and that of the excited state.

Often there are a number of possible products in a photochemical reaction. The one that is produced will be the product with the fastest formed intermediate as the reaction is kinetically controlled. When a number of intermediates can be formed quickly then the most stable intermediate will predominate. Reactions from S_1 are often stereospecific whereas those from T_1 are not. This is due to difference in lifetimes of the two states, which allows more opportunity for changes in conformation prior to reaction from T_1.

1.2.4 Electron acceptor/donor properties of the excited state

So, the absorption of a photon of sufficient energy by a molecule, M, causes excitation of the molecule in which an electron is promoted to a higher energy level generating an electronically excited state, M^*. The excited state is modelled as one electron being promoted from the highest occupied molecular orbital to a low energy unoccupied

orbital, with the remaining electrons staying in their original orbitals (Figure 1.2). M^* is both a better electron acceptor and a better electron donor than M, as less energy is required to remove an electron from M^* than from M ($I^* < I$), and more energy is released when an electron is accepted by M^* than by M ($A^* > A$). Thus, both electron donation and electron acceptance are favoured more from the excited state than the ground state. Electron transfer may be intermolecular or intramolecular depending upon the compounds involved. Intramolecular electron transfer occurs from one part of a molecule to another part resulting in a charge separation within the excited molecule.

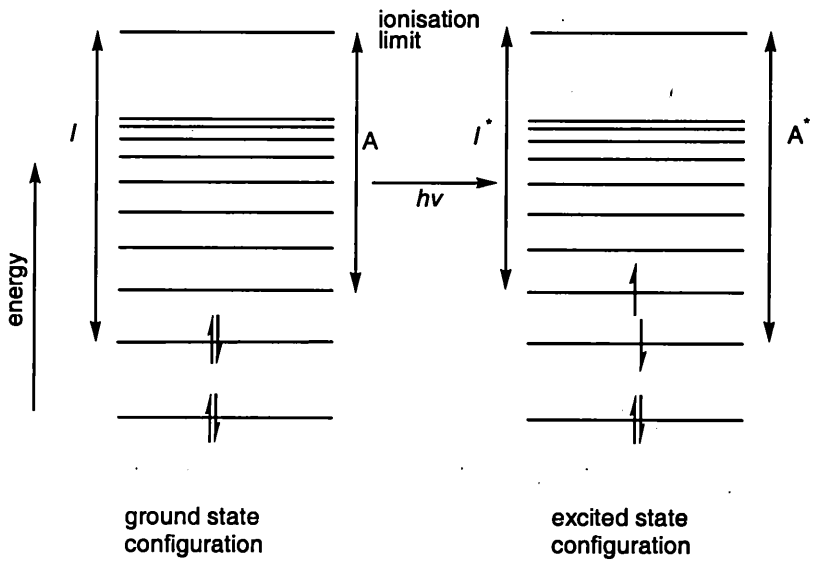

Figure 1.2 Schematic representation of the better electron donor and electron acceptor properties of an excited state compared with the ground state.

PIET is particularly relevant to the photobiological context of this project, although it is by no means the only outcome of a photochemical process. Bond homolysis leading to radical intermediates is also common.

1.3 PIET in amino acids and peptides

In photosynthesis the absorption of solar radiation by the two light-harvesting antennae excites a pigment (chlorophyll) in the reaction centres, which are called P680 and P700 in green plants, and initiates the transfer of an electron over long distances through a protein matrix that contains the other key molecules such as pheophytin and plastoquinone.[7] Hence, photo-induced electron transfer (PIET) plays a pivotal role in photosynthesis, and results in a primary charge separation that is maintained by the electron being rapidly transferred away from the original donor molecule as shown in Scheme 1.1. The arrangement of the membrane proteins ensures that PIET from the reaction centres is a very efficient process that is virtually irreversible.

P680 (Chlorophyll *a*) Pheophytin *a* Plastoquinone

$\downarrow h\nu$

P680 (Chlorophyll *a*)* Pheophytin *a* Plastoquinone

$\downarrow$

P680 (Chlorophyll *a*)$^+$ Pheophytin *a*$^-$ Plastoquinone

$\downarrow$

P680 (Chlorophyll *a*)$^+$ Pheophytin *a* Plastoquinone$^-$

Scheme 1.1 The sequence of events resulting in the primary charge separation within the P680 photosynthetic reaction centre of green plants. Pheophytin and plastoquinone are pigments participating in ET.

The role of the protein matrix also remains unclear but the capacity of a peptide chain to mediate ET is clearly of interest. Much work has been done to investigate the ET properties of photosynthetic reaction centres by using peptide-based model compounds. The remainder of this section looks at a number of studies where amino acid residues were chosen for their ability to influence the secondary structure of the peptide producing α-

helices, β-strands, β-sheets and helical bundles as required, and for conformational flexibility or restraint and ET capacity. The mechanisms of ET have been investigated both experimentally and theoretically, and much evidence in support of both through-bond and through-space mechanisms has been acquired.

Studies in these laboratories of the photochemistry of small peptides have demonstrated the capacity of a peptide chain to mediate ET. Indeed, free peptides undergo PIET reactions.[8,9] A number of dipeptides were studied that were chosen to investigate the influence of the amino acid side-chains upon the outcome of the photochemical reaction (Figure 1.3).

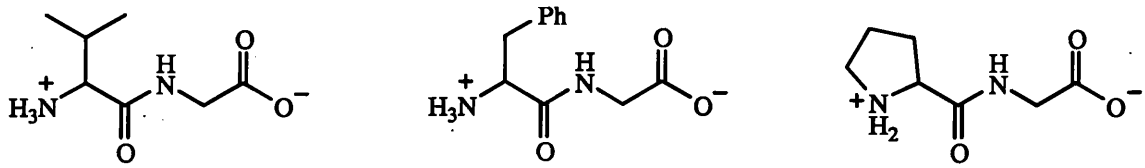

Val-Gly Phe-Gly Pro-Gly

Figure 1.3 Representative structures of the dipeptides previously studied in these laboratories.

The observed products could be explained by n → π* excitation of the molecule causing PIET from the terminal carboxylate to the peptide bond, which is also supported by a theoretical study of the electronic spectra of the electronically excited dipeptides. PIET results in a charge separation that initiates the photodegradation of the peptide, with the major products at pH 6 resulting from decarboxylation and deamination (Scheme 1.2). High or low pH values were shown to influence the product distribution, as were different side-chains. Bulky aliphatic side-chains as in valylglycine reduced the efficiency of deamination, whilst phenyl side-chains reduced the yield of the expected products presumably due to undetected products resulting from competing pathways involving the aromatic ring. Prolyl dipeptides gave analogous products to the other aliphatic ones but with a ring opening rather than deamination. These studies have shown

the importance of peptide structure upon the photochemistry of the peptides. It was concluded that aliphatic peptides generally photodegrade by similar routes, but the presence of bulky or aromatic side chains, for example, may alter the degradation pathways. *Ab initio* calculations revealed an absorption band corresponding to a charge transfer (CT) transition between peptide units in addition to the known $n \rightarrow \pi^*$ and $\pi \rightarrow \pi^*$ transitions.[10]

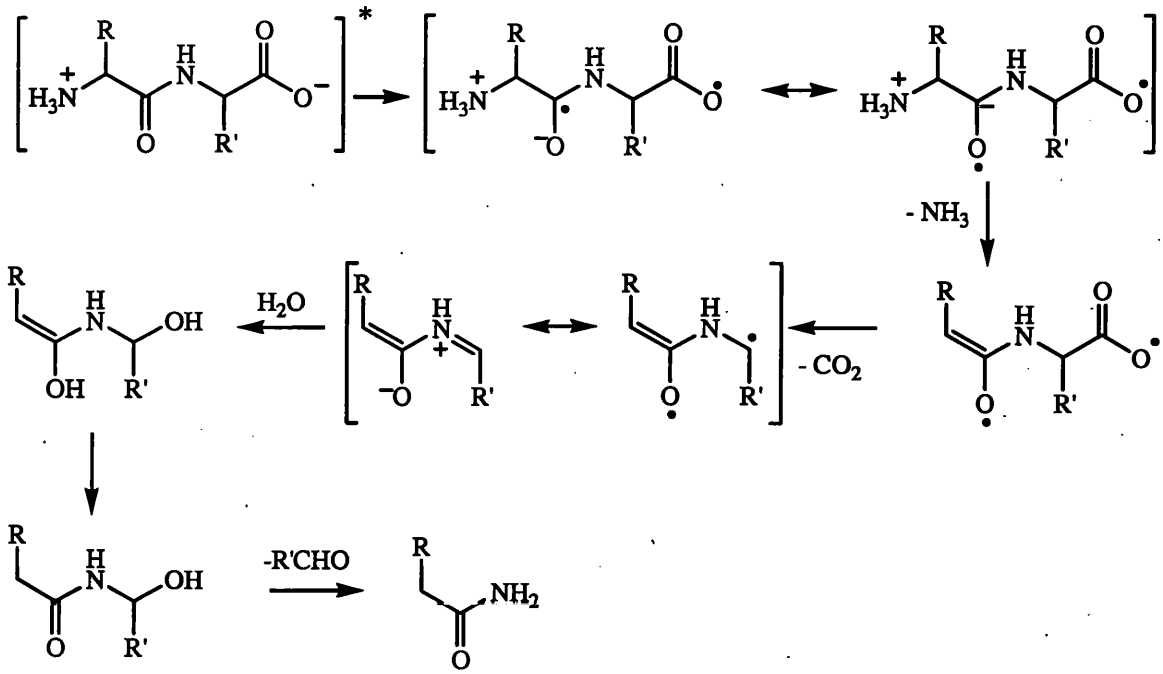

Scheme 1.2 Major degradation route for dipeptides.

The elucidation of the structure of bacterial reaction centres[11,12] has enabled much progress in the understanding of green plant photosynthesis. Many models that can undergo PIET have been designed that are based upon these reaction centres and these have proved to be valuable models for the green plant reaction centres. The focus of much research has been upon the mechanisms of electron transfer both within the proteins and between the subunits, the latter being non-covalently bound to one another. Typical work involves the linking of a porphyrin donor molecule to a quinone acceptor in order to mimic ET from chlorophyll to plastoquinone.

For example, one study showed the importance of hydrogen bonding from the porphyrin donor to the quinone acceptor via a β-turning depsipeptide bridge (Figure 1.4).[13] Through backbone ET involves 10 bonds whilst that via the H-bond involves only 6 bonds. In dichloromethane (DCM) an electron transfer rate of $k_{et} = 1.1 \times 10^9$ s^{-1} was observed but in dimethylsulfoxide (DMSO) this was almost an order of magnitude lower, $k_{et} = 3.5 \times 10^8$ s^{-1}. The difference in rates shows the importance of the hydrogen bond in contributing to a faster rate of ET, as it would be disrupted in the more polar solvents such as DMSO. This was also supported by the observation of fluorescence in DMSO but not in DCM.

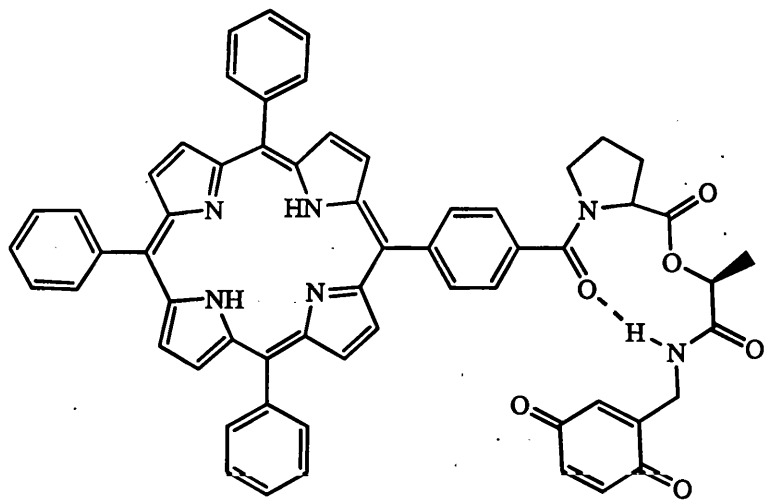

Figure 1.4 The porphyrin-quinone donor-acceptor complex with a β–turn-forming depsipeptide bridge.

Electron transfer within proteins is frequently modelled using bischromophoric peptides i.e. a short peptide chain with a donor and acceptor at either end or within the chain. The unnatural amino acid 2-amino-*iso*-butyric acid (Aib, **2**) is often used in the peptide chain to induce a helical conformation similar to that found in native proteins.

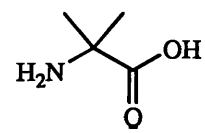

2

An example of this is a study that compared two helical oligopeptides consisting of Ala and Aib residues with a dimethylaniline donor and a pyrene acceptor, and differing only in the positional reversal of the donor and acceptor moieties (Figure 1.5).[14] The α-helix dipole is thought to generate an electrostatic field along the helix axis producing a positive charge at the amino end and a negative charge at the carboxyl end of the α-helix. PIET from the donor to the acceptor generates a charge-separated pair that is aligned against the helix dipole in **3** but with the dipole in **4**. The potential energy of the two systems is expected to differ leading to a greater driving force and hence faster rate for PIET in **3** due to a more negative ΔG for PIET in **3** than in **4**. Measurements of ET rates supported this hypothesis in many solvents and at different temperatures, with a faster ET rate in **3** by a factor of 5-27 times dependent upon conditions. Absorption and fluorescence spectra of the two systems were identical although the fluorescence quantum yield of **4** was twice that of **3**, indicating that **3** is a more efficient quencher. The effects of the helix dipole were further investigated by measuring ET rates in polar protic solvents, which cause helix unfolding due to disruption of the hydrogen bond system. Both compounds exhibited a lower ET rate than in the helical conformation and upon complete unfolding had identical ET rates providing further support for the role of the α-helix.[15]

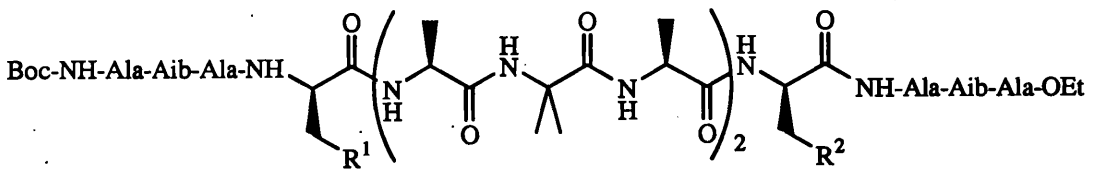

3 $R^1 = A, R^2 = D$

4 $R^1 = D, R^2 = A$

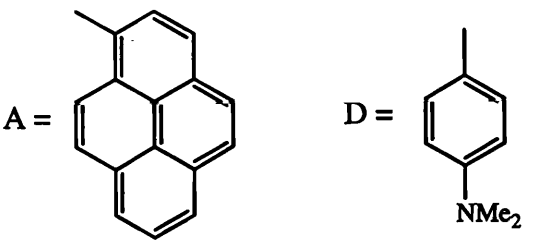

Figure 1.5 Structures of the pyrene-*N,N*-dimethyl-*p*-aniline bichromophoric peptides differing only in the positions of the donor and acceptor.

Helix unfolding was also investigated in a similar system that had Pro residues instead of Aib, which induce helix breaks. This enabled comparison of a non-helical system with the α-helix conformation of **3** and **4** under identical conditions. A slower rate by about one order of magnitude was found in the Pro systems than in the Aib systems. A higher fluorescence quantum yield was observed in **5** than **6** and the ET rate was highest in **6**, which is the opposite of the differences observed between **3** and **4**. This supports the role of the α-helix dipole in influencing ET rates and of the importance of the hydrogen bond network although it does not exclude the effects of conformation as the systems are not rigid and may vary according to the solvent used.

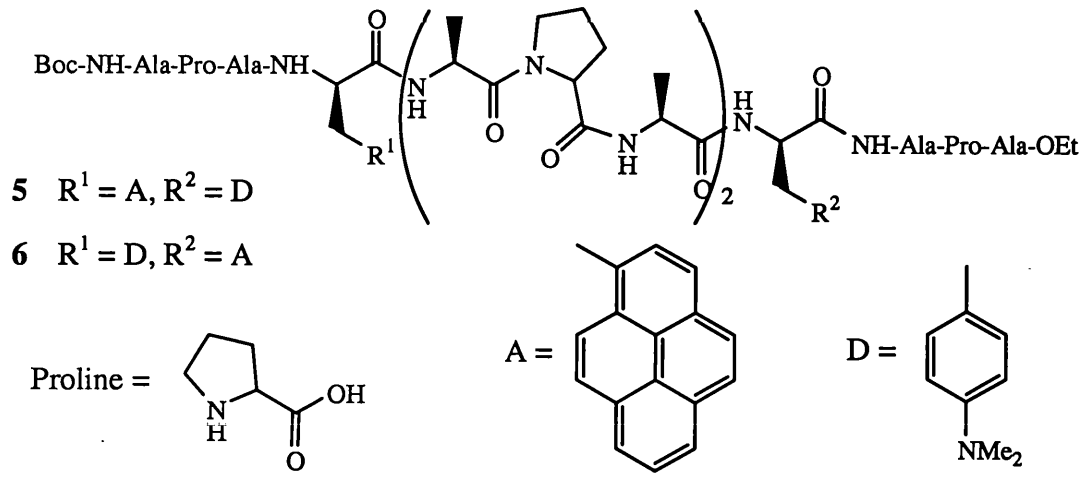

Figure 1.6 The pyrene-*N,N*-dimethyl-*p*-aniline bichromophoric peptides with Aib replaced by Pro.

A similar result was found in a dyad with metal-to-ligand PIET via a peptide linker being affected by the solvent.[16] The peptide linker consisted of Aib, Ala and functionalised Glu residues (Figure 1.7). Chlorinated hydrocarbons were found to favour a helical structure which brings the chromophores close enough for a through-space ET of 1100-1200 pm. Evidence for an ET came from the loss of luminescence. Full luminescence

was observed in protic solvents which again cause helix unfolding by disrupting hydrogen bonding.

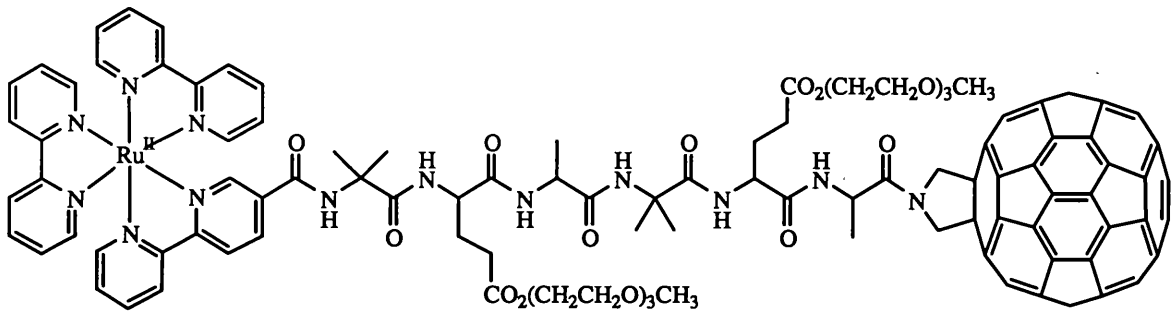

Figure 1.7 A [ruthenium-(2,2'-bipyridine)$_3^{2+}$]-hexapeptide-C_{60} dyad.

An experimental study that supported the through-bond mechanism compared two rigid bischromophoric molecules with the same through bond distance but differing in conformation.[17] Both of the molecules had a 1,4-dimethoxybenzene donor and a 7,7-dicyanobenzoquinone acceptor joined by alkyl linkers, but one was a stacked system whilst the other was unstacked giving through space distances of 360 and 470 pm respectively. The stacked system had a larger value for the absorption coefficient of the CT band at 450 nm indicating greater electronic coupling between the donor and acceptor of the stacked system. However, the two systems gave the same back-electron transfer dynamics despite the differences in electronic coupling and the increase in through space distance of 25% for the unstacked system. Theory predicts that there should be an order of magnitude difference in the rate of electron transfer if a through space mechanism is occurring. All of the evidence in this study supports a through bond mechanism for a rigid system. The same conclusions were reported for two oligoprolines with center-to center distances of 1150 and 1850 pm.[18]

In a third example of this type of work ET from a Trp residue to a distant pyrene of the same subunit was found in protein aggregates with higher-order structures consisting of eight helix bundles. The pyrene chromophores are able to form dimers

(Figure 1.8) reminiscent of the bacteriochlorophyll special pair in photosynthetic bacteria, although there is an equilibrium of monomer-dimer-octamer. The use of methyl viologen (MV) as a photooxidiser gave evidence of fluorescence quenching of the aggregate. Phototransients assigned to $MV^{+\bullet}$, $pyr^{+\bullet}$ and $Trp^{+\bullet}$ were observed in this species. A transient analogous to the latter was not observed in a peptide aggregate where the Trp was replaced by Phe. It was thought that the electron transfer rate of 5.5×10^5 s^{-1} is indicative of a through space mechanism involving hydrogen bonds for the long-range electron transfer (LRET).[19]

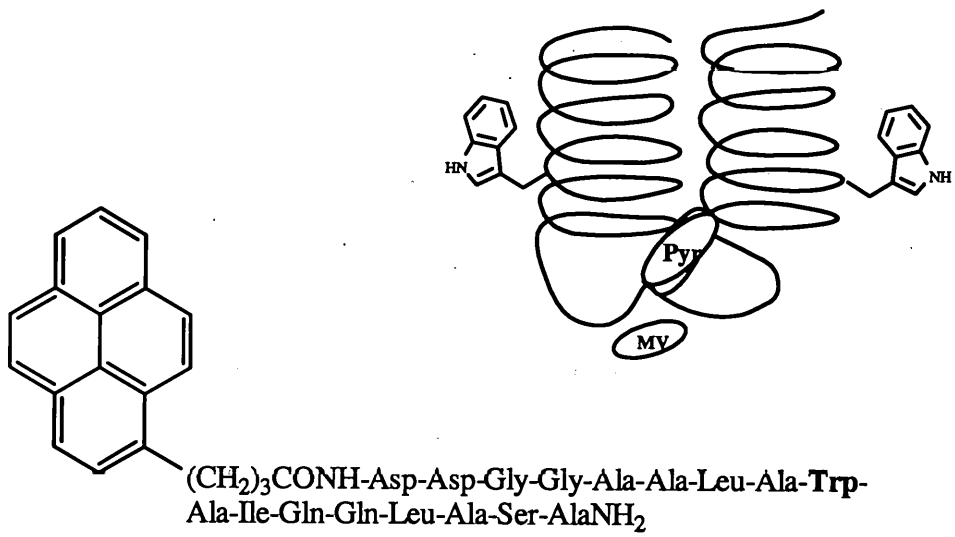

Figure 1.8 Primary structure of the pyrene peptide and a schematic representation of a two helix dimer (pyr = pyrene, MV = methyl viologen).

All of the aforementioned studies have illustrated the importance of hydrogen bonding for efficient ET within a protein thus supporting a through-space mechanism for PIET in flexible molecules, although through-bond ET seems to predominates in rigid molecules with short bridges.

Photoinduced LRET is also relevant to the damage and repair processes occurring in DNA, as electrons are known to travel ~ 20 nm along DNA strands. Studies involving donor-bridge-acceptor systems with DNA as the bridge have provided evidence

for the transfer of an electron from a tryptophan residue of a peptide to DNA with subsequent damage at distant guanines.[20]

Many of the examples discussed have been studies of the mechanism of ET between proteins that were modelled using a donor-bridge-acceptor system where the bridge was a covalently bound peptide linker. However, electron transfer *in vivo* occurs, at least in part, across the non-covalently bound interface between proteins. Consequently, biomimetic systems have been developed where the donor and acceptor molecules are noncovalently linked through electrostatic or hydrogen bonds. An example of this type of work is a study that investigated the importance of electrostatic interactions between a cationic metalloporphyrin and a pentapeptide chain consisting of four Glu residues and a terminal Trp or Tyr residue (Figure 1.9). The side-chain carboxylates of the Glu residues were expected to form an ion-pair complex with a tetracationic Pd(II) porphyrin unit. Complexation of either pentapeptide resulted in fluorescence quenching of the porphyrin T_1 state indicating that the electrostatic bonds had facilitated ET from the peptide donor to the porphyrin acceptor.[21]

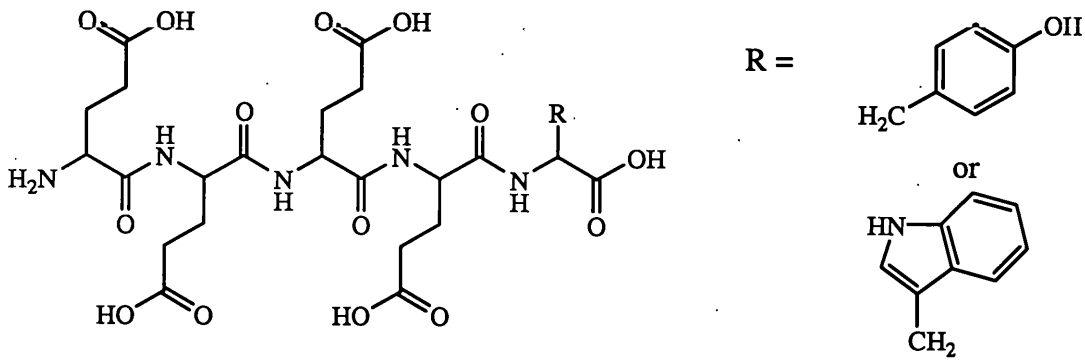

Figure 1.9 The pentapeptides Glu-Glu-Glu-Glu-Tyr and Glu-Glu-Glu-Glu-Trp used for ET studies to a non-covalently bound metallporphyrin.

This section has given a brief overview of the importance of PIET in biological systems. PIET is a very wide field and many more examples could have been cited. The ones discussed were chosen to highlight the significance of amino acids and peptides in ET

studies and to show that there is still much work to be done in elucidating the mechanisms. One purpose of this project was to see if the photochemistry of a series of amino acids derivatives attached to a tosyl chromophore could contribute to this area. We shall now look at the known photochemistry of arylsulfonamides.

1.4 The photochemistry of arylsulfonamides

The excited arylsulfonyl group is a more readily generated electron acceptor than the excited peptide bond. This is due primarily to the structure of each moiety, which causes differences in the wavelengths absorbed and the molar absorption coefficients of each group as observed in the differences between the UV-vis spectra of the two groups. The sulfonyl group also reduces the nucleophilicity of the adjacent nitrogen making it part of an electron acceptor and therefore offering an opportunity for more convenient study of PIET in peptides.

N-arylsulfonyl derivatives of peptides have been studied photochemically over the past 30 years, primarily to establish their usefulness as photochemically removable protecting groups. Current methods of removal are by electrolysis[22,23] or chemical cleavage.[3,24] However, many other functional groups are also unstable under these conditions, so there was a need for a mild selective method of deprotection.

D'Souza[25,26] reported a photochemical cleavage of various aryl sulfonyl derivatives of peptides and amino acids (Figure 1.10). However, the fate of the arylsulfonyl group was not reported and the yield for regeneration of the peptide or amino acid was found to vary greatly depending upon conditions and the structure of the molecule. Tosylated amino acids gave yields of 21-57% whilst dansyl derivatives varied from 5-97%. Irradiation at 180 nm was found to cause more destruction of the amino acids relative to the sulfonamide bond cleavage than irradiation at 254 nm. This is consistent with the peptide bond absorbing weakly near 190 nm but not at longer wavelengths, whereas the arylsulfonyl absorbs significantly at 254 nm. A low pH was found to give improved yields

(up to 95%) for glycine from dansylglycine suggesting an acid-catalysed hydrolysis of the dansyl derivatives in the excited state. A number of unwanted side reactions including deamination, decarboxylation and cleavage of peptide bonds were noted. However, this strategy for the deprotection of amino acids and peptides has continued to be pursued as we shall see from more recent examples.

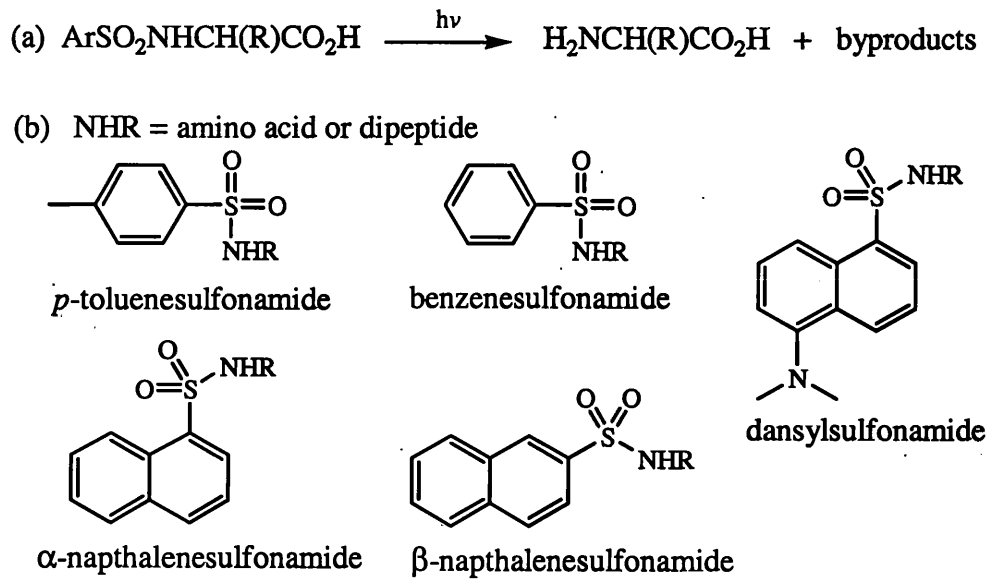

Figure 1.10 (a) General scheme for the required photocleavage; (b) the arylsulfonamide derivatives studied by D'Souza.

Pete studied the photolysis of both tosylamides and benzenesulfonamides in acid, neutral or basic solutions and a variety of solvents.[27,28] Comparable yields for the amine were found under all conditions and the structure of the aryl or amine function did not greatly affect yields, which were all about 50%. The amine was generally recovered as a salt with the sulfonic acid although some free amine was isolated. Hydrolysis of the excited state was excluded since the pH did not affect the observed yields of the amine. A number of other products were observed which suggested that both S-N and C-S cleavage were occurring. A radical mechanism was proposed with two competing pathways (Scheme 1.3).[29] Although proton abstraction from the solvent is not important for the homolytic cleavage of amide derivatives, it is necessary to explain the minor products. It

was proposed that ArH could only be produced from a C-S cleavage, as its production from the salt or radical was thought to be unlikely.

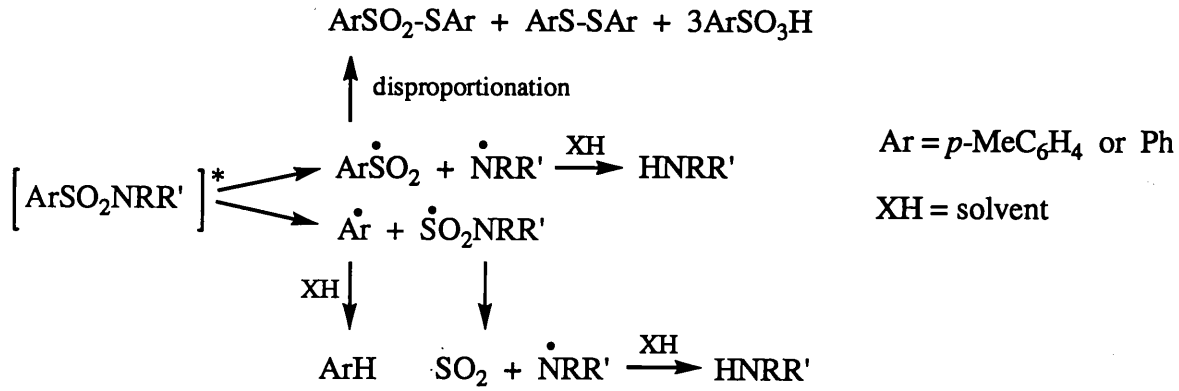

Scheme 1.3 Mechanism for photodegradation of arenesulfonamides according to Pete.

Other workers[30] excluded the C-S cleavage in *N*-arylbenzenesulfonamides as all of the products retained the $PhSO_2$ moiety with the exception of the dimer PhS-SPh. The latter was explained by disproportionation of two phenylsulfonyl radicals to benzenesulfonate and a phenyl sulfide radical which leads to the dimer as in Scheme 1.3. Increasing the viscosity of the solvent did not change the observed products but merely slowed down the rate of degradation presumably due to recombination of the initially formed radicals. The authors had also examined the thermolysis products of the same compounds and found that completely different products were formed, thus confirming the importance of the electronically excited state in determining the final products. Good yields of the amine were found, ~80% as both the free amine and as a salt formed with the benzenesulfonate. The formation of salts has been noted by a number of other workers. Another study identified similar products including the dimer, although the yields of the amines were much lower, ~20%. The dimer was explained by loss of SO_2 from the arylsulfonyl radical followed by dimerisation instead of disproportionation.[31] The formation of the proposed radicals was supported by electron spin resonance (ESR) spectroscopy.

A different study of benzenesulfonamide derivatives of primary and secondary amines in alcoholic media did find that the yields of the amines increased as the hydrogen donating ability of the solvent increased.[32] Best results were obtained in basic media, which prevented the precipitation of amine salts as reported by Pete. A mechanism involving homolytic cleavage of the S-N bond was suggested similar to the one shown in Scheme 1.3, although no products other than the amine and benzenesulfonic acid were reported. Preliminary experiments with amino acids suggested increased degradation of amino acids due to the wavelength required for excitation of the benzene chromophore, so this may be avoided if the chromophore can be modified to allow the use of a longer wavelength for excitation. Aromatic amines were found to change the nature of the chromophore such that S-N cleavage is inhibited; compounds of this type are therefore not suitable for deprotection by photolysis.

The photocleavage of tosyl groups, in the presence of the reducing agent $NaBH_4$, had been reported with over 80% yields in 6,7-dimethoxytetrahydroisoquinoline *N*-tosylates (Figure 1.11).[33] However, phenethylamine *N*-tosylates were found to give less than 40% yields.[34] Yonemitsu later proposed that two different mechanisms must be involved: the phenethylamine *N*-tosylates undergoing the radical mechanism as proposed previously and the 6,7-dimethoxytetrahydroisoquinoline *N*-tosylates undergoing an initial intramolecular ET from the 1,2-dimethoxybenzene to the tosyl prior to cleavage. This was supported by the virtual lack of fluorescence observed in these compounds unlike 1,2-dimethoxybenzene.[35]

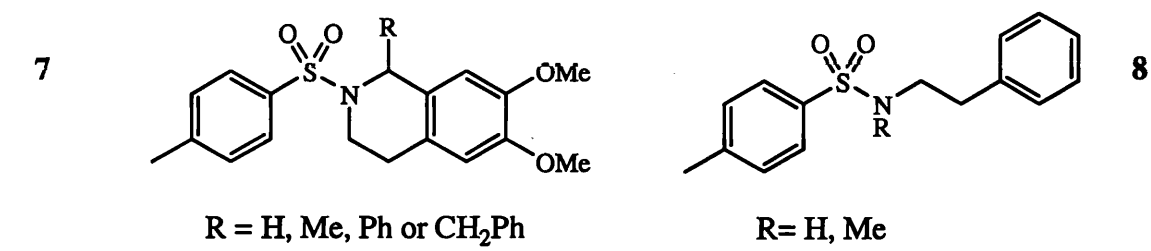

Figure 1.11 Structure of 6,7-dimethoxytetrahydroisoquinoline *N*-tosylates, **7** and phenethylamine *N*-tosylates, **8**, studied by Umezawa.

Yonemitsu extended the previous work on photodeprotection to an intermolecular ET reaction of tosylamides and naphthalenesulfonamides, which were studied in the presence of both electron donating aromatics and reducing agents.[1,2] Yields of up to 91% of the amine were achieved for the cleavage of *p*-tosylmethylphenethylamide in the presence of the aromatic donor 1,2-dimethoxybenzene and the reducing agent $NaBH_4$ (Scheme 1.4).

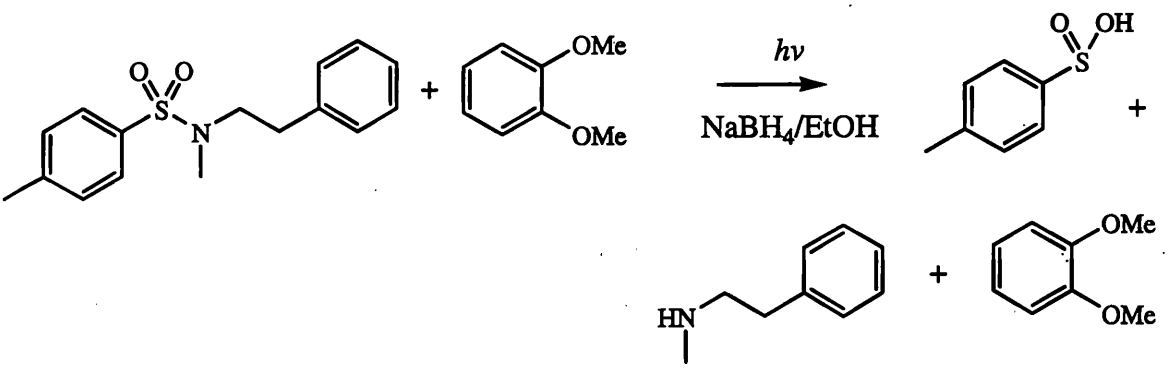

Scheme 1.4 Photocleavage of *p*-tosylmethyphenethylamide.

Higher yields were achieved when some water was present, suggesting that a radical ion pair was formed by ET and then hydrolysed. ET is supported by calculations of free enthalpy change for the donors, where ΔG is negative for reactions involving donors that resulted in a cleavage, and by measurements of fluorescence quenching of the donors by *N*-tosylmethylamine. A possible mechanism is shown in eq 1-4 where the radical anion is identical to the known species generated in the initial step of $Na\text{-}NH_3$, Na-naphthalene and electrochemical reduction.[36] A similar scheme was proposed for cleavage in the presence of $NaBH_4$ with the sulfinic acid being formed instead of the sulfonic acid (eq 1-2, then 5-6).

1 $ArSO_2NRR' + {}^1D^* \longrightarrow ArSO_2NRR'^{\bullet-} \cdots D^{\bullet+}$

2 $ArSO_2NRR'^{\bullet-} \xrightarrow{H_2O} ArSO_2^{\bullet} + RR'NH + {}^-OH$

3 $ArSO_2^{\bullet} + {}^-OH \longrightarrow ArSO_3H^{\bullet-}$

4 $ArSO_3H^{\bullet-} + D^{\bullet+} \longrightarrow ArSO_3H + D$

5 $ArSO_2^{\bullet} \xrightarrow{NaBH_4} ArSO_2H^{\bullet-}$

6 $ArSO_2H^{\bullet-} + D^{\bullet+} \longrightarrow ArSO_2H + D$

Further evidence for the proposed mechanisms came from isolation of either toluenesulfonic acid or toluenesulfinic acid depending upon conditions, and the recovery of the aromatic donor. The use of naphthalenesulfonyl instead of tosyl allowed irradiation at longer wavelengths but showed very little difference in yields of the free amine under otherwise identical conditions. A number of lysine peptides were protected at the side-chain amine with a tosyl group (Figure 1.12) and yields of 68-96% were reported in the presence of an electron donor and $NaBH_4$ with no damage to the peptide or the Boc group that was also present in these compounds.

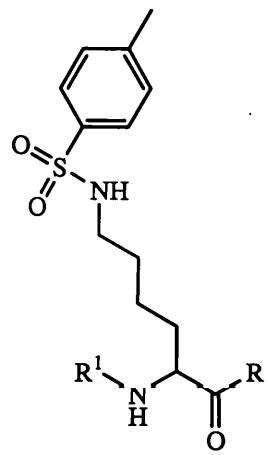

R = OH, OMe,

R^1 = Boc, Boc-Gly-, Boc-Gly-Pro

Figure 1.12 The side-chain protected lysine derivatives studied by Yonemitsu.

Yonemitsu also studied a number of other groups for use as intramolecular electron donors including 4,8-dimethoxynaphthyl and 3-methoxybenzyl groups (Figure

1.13).[2] The former has the advantage of absorbing at > 300 nm, thus minimizing the risk of destroying the amines liberated, as noted by other workers, unlike the latter which required a shorter wavelength excitation (< 300 nm). The highest disappearance quantum yields were observed with a 4-(4′,8′-dimethoxynaphthylmethyl)benzenesulfonyl (DNMBS, $n = 1$) which also gave the highest degree of fluorescence quenching relative to the free aromatic donor, suggesting that intramolecular electron transfer is occurring to the benzenesulfonyl moiety upon photolysis. The efficiency of quenching and degradation (in the presence of a reducing agent) decreased with an increase in the methylene chain length for both types of derivatives. The mechanism proposed was the same as for the tosyl and naphthalenesulfonyl amides (*cf* eq 1-6). Fluorescence quenching measurements and disappearance quantum yields were higher in the naphthyl systems than the benzyl derivatives for similar values of n, suggesting that the naphthyl is the better electron donor. The photocleavage of DNMBS protected amines was investigated and yields for the free amine of 77-91% were reported with ammonia borane as the reducing agent. The amines contained a number of potentially labile groups, including an indole, benzyl, tosyl, Boc, Cbz and a mesyl, all of which remained intact upon photolysis.

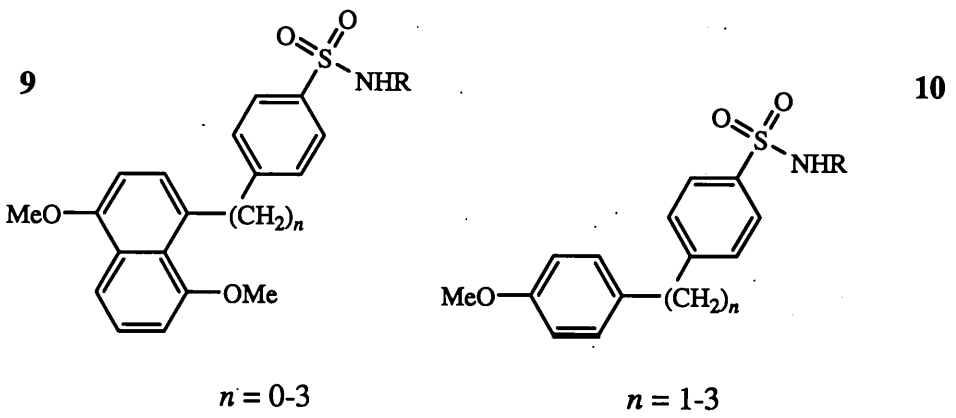

Figure 1.13 The 4,8-dimethoxynaphthyl (**9**) and 3-methoxybenzyl (**10**) systems studied by Yonemitsu.

Corrie studied the photocleavage of a modified DNMBS protected glycine and reported yields of only 6% in aqueous buffered solution.[37] A competitive decarboxylative reaction was proposed, as compounds without a carboxylate group such as glycine esters gave improved yields of 44%. Increasing the methylene chain between the sulfonamide and carboxylate groups of the amino acid, as in β-alanine, gave improved yields of up to 24%. This is consistent with the high yields reported by Yonemitsu for tosyl protected lysine side-chains, where the carboxylate is separated from the sulfonamide moiety by five carbon atoms. The mechanism that was proposed (Scheme 1.5) for decarboxylation was oxidation of the glycine carboxylate group after S-N cleavage by the biradical to give a carboxylate radical. Glycine could then be decarboxylated and other products formed which were not identified. Evidence for the formation of CO_2 came from flash photolysis studies coupled with FTIR spectroscopy.

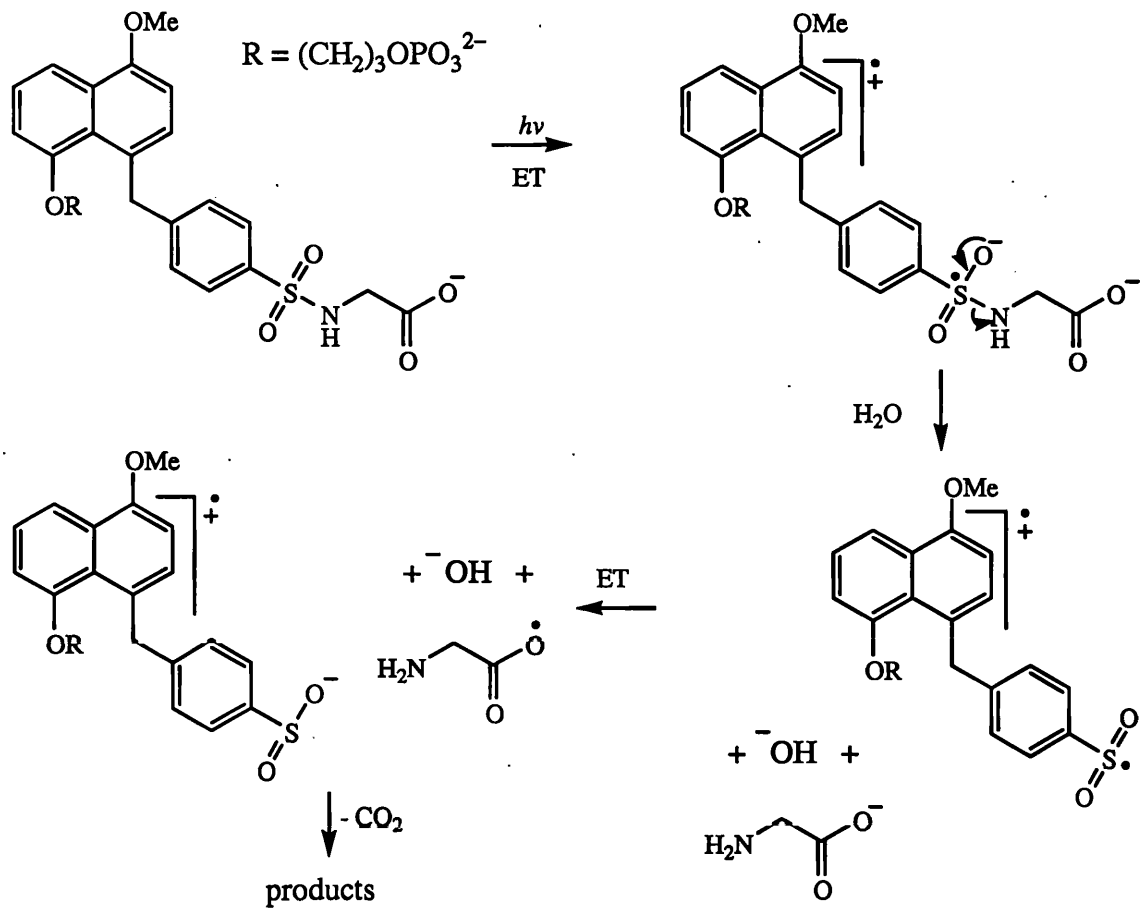

Scheme 1.5 Proposed mechanism for S-N cleavage followed by glycine decarboxylation.

An attempt was made to prevent the decarboxylation by the introduction of a sacrificial carboxylate at the ortho position of a benzylsulfonyl moiety (Figure 1.14, **12**).[38] An intermolecular reaction was investigated that gave improved yields for glycine from **12a** (31%) relative to that from tosylglycine (4%), in the presence of an electron donor (**11**). An acetic acid (**12b**) or oxyacetic acid group (**12c**) were found to give faster degradation relative to **12a** as well as improved yields relative to tosylglyine, so a protecting group incorporating one oxyacetic acid group plus a second sacrificial carboxylate was investigated (**13a-b**).

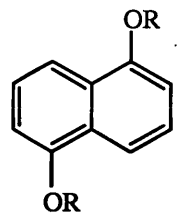

11 $R = (CH_2)_3OPO_3^{2-}$

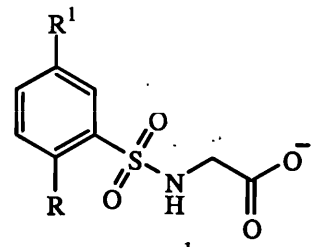

12 a $R = CO_2H$, $R^1 = H$
b $R = CH_2CO_2H$, $R^1 = H$
c $R = OCH_2CO_2H$, $R^1 = Me$

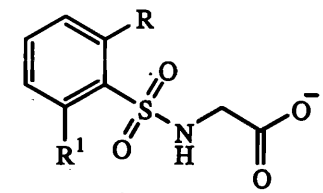

13 a $R = CO_2H$, $R^1 = OCH_2CO_2H$
b R, R1 = OCH_2CO_2H

Figure 1.14 The aromatic donor (**11**) and the glycine molecules with protecting groups incorporating a sacrificial carboxylate (**12, 13**) investigated for an intermolecular deprotection reaction.

However, two sacrificial carboxylates gave no further improvements leading to the suggestion that the biradical generated in the intramolecular DNMBS reaction (Scheme 1.5) by initial ET can cleave by an additional route to give a sulfinate anion and an aminyl radical (Scheme 1.6). This type of cleavage has been suggested previously for electrochemical methods[36] and the aminyl radical is known to readily decarboxylate.[39] Thus the method of S-N cleavage may be homolytic or heterolytic, with the former possibly explaining the low yields of the free glycine.

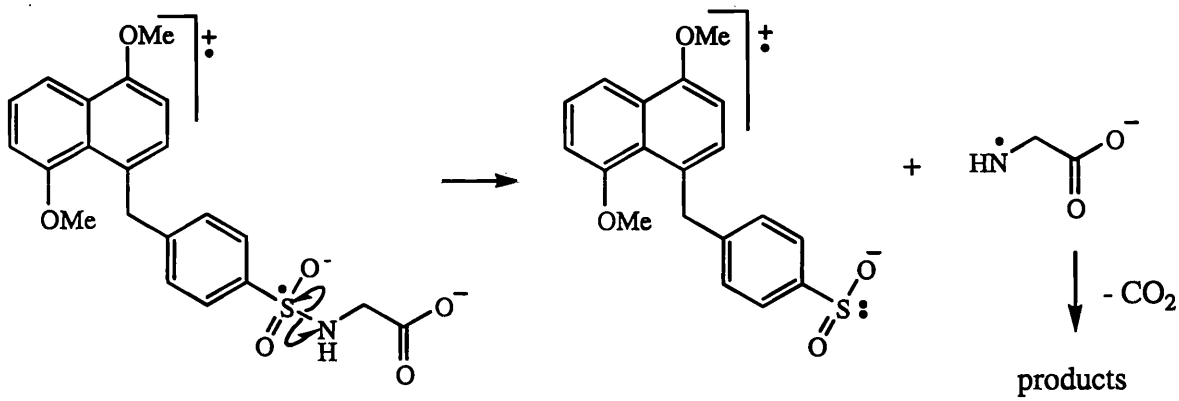

Scheme 1.6 Biradical cleavage to give an aminyl radical.

The photocleavage of tosyl and 2-carboxybenzenesulfonyl protected derivatives γ-aminobutyric acid was investigated and yields of 17% and 34% respectively were reported thus providing further support for the sacrificial role of the additional carboxylate on the protecting group.

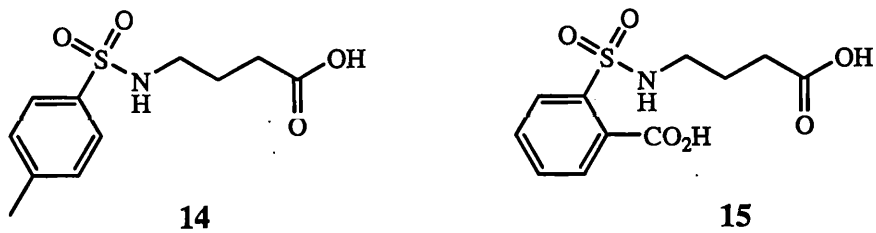

14 **15**

Figure 1.15 Tosyl (**14**) and 2-carboxybenzenesulfonyl (**15**) protected γ-aminobutyric acid.

Intramolecular electron transfer in arylsulfonamides is further supported by studies of fluorescence quenching. This has been observed in the pyrenesulfonamide group,[40,41] where electron transfer from Trp or a C-terminal donor to the chromophore was thought to be responsible for the fluorescence quenching. In Pyr or NPyr donor-acceptor systems the fluorescence was diminished by the attachment of Trp or dimethyl-1,4-benzenediamine (DMPD) directly to the acceptor (Figure 1.16). The efficiency of fluorescence quenching decreased with an increase in chain length when intervening Ala

residues were introduced. This supports other PIET studies as described in Section 1.3. Flash photolysis provided evidence for a radical anion of the pyrenesulfonyl chromophore and a Trp radical cation, consistent with the mechanisms suggested for PIET in DMBS systems.

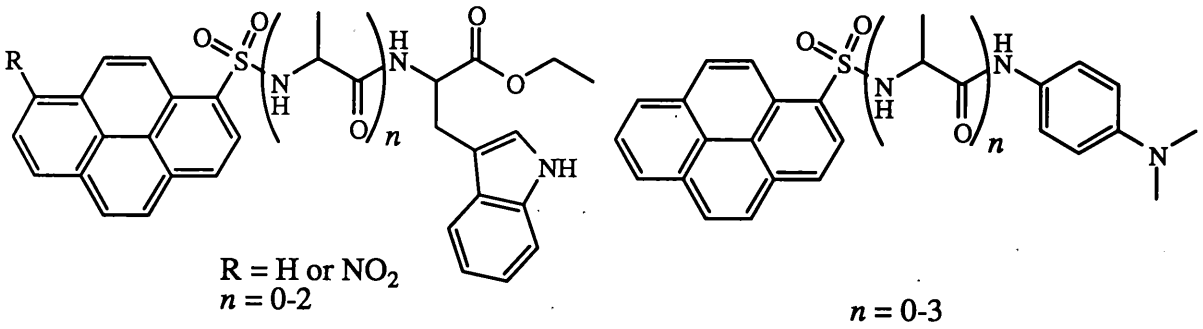

Figure 1.16 The 1-pyrenesulfonyl (pyr or NPyr) peptides studied for fluorescence quenching.

This section has shown that the photodeprotection strategy of arylsulfonamides has been largely unsuccessful for reasons that remain unclear, and that the mechanisms of photodegradation are also not known. Better yields have been achieved in the presence of electron donors and this has led to two main routes being proposed; a radical pathway or an initial ET. We hope that by examining the effects of small structural changes we may be able to gain insight into the mechanisms of photodegradation.

1.5 The photostability of drugs

Arylsulfonamides are prominent among drugs identified as photolabile. Drug development is an expensive process and anticipation or detection of potential photoinstability is desirable at an early stage. However, few specific studies have been carried out and most of the general literature on sulfonamide photochemistry has focused on the yield of products from simple S-N cleavage. Only a few of the studies have attempted to identify any competing reactions and their mechanisms. Hence, the

understanding of the mechanisms of arylsulfonamide photochemistry may lead to a prediction of the likelihood of a particular arylsulfonamide drug candidate being photolabile.

The photostability of drugs is an important issue for several reasons (Figure 1.17).[42] Firstly there is the problem of shelf-life, which when identified can be addressed by use of appropriate packaging materials such as opaque containers. However, this could be considered a minor problem if it can be resolved unlike more serious consequences such as loss of drug potency potentially leading to a therapeutically inactive compound. Photodegradation products of any of the components in the drug formulation may lead to phototoxic effects,[43] which is a term that encompasses any adverse effects of the drug *in vivo* including photosensitivity[44] which is known to be an unwanted side-effect of sulfonamide drugs. In Finland in 1966, 187 out of 464 reported adverse drug reactions were due to sulfonamides, 9 of which were photosensitivity reactions.[45] Photosensitisation is where the drug or a photodegradation product absorbs light *in vivo* and then reacts with cellular components to give irreparable damage. Phototoxic effects can include severe burning of the skin, painful sensation and development of skin cancer.[46]

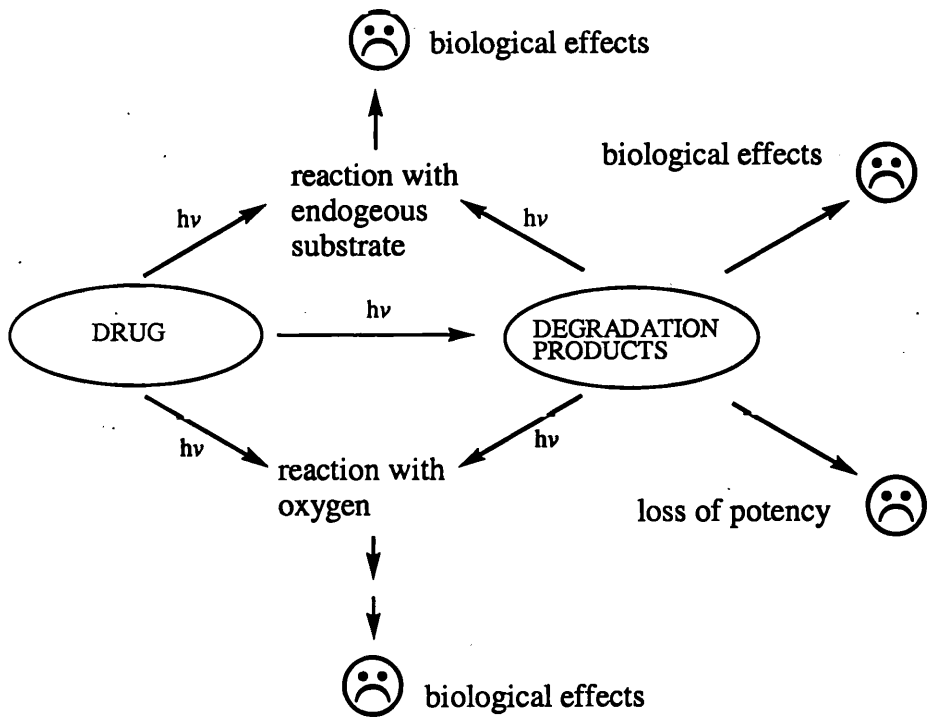

Figure 1.17 The possible consequences of drug photoinstability.

There is a large group of sulfonamide compounds related to the anti-bacterial drug sulfanilamide (Figure 1.18), many of which have known phototoxic effects. Sulfanilamide type drugs are known to be photolabile, with S-N and C-S cleavage involved in the main photodegradation route.[5,4]

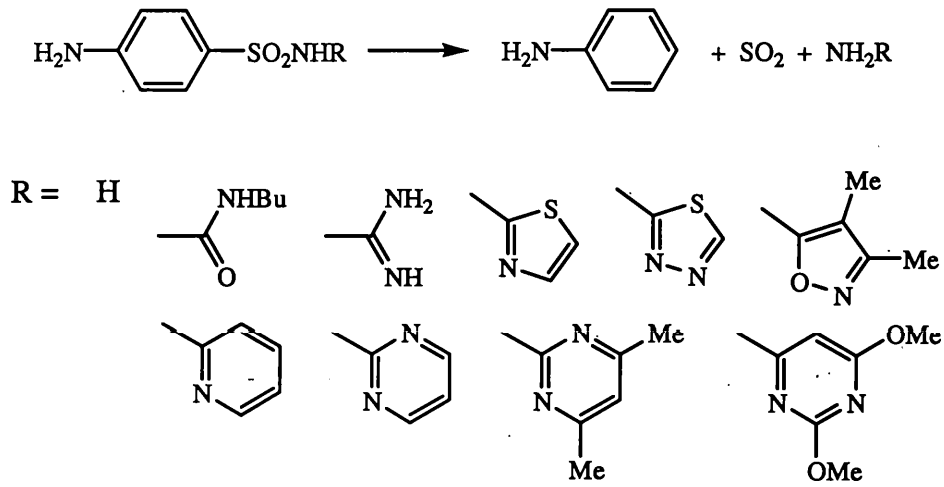

Figure 1.18 Structures of some sulfonamide drugs and their main photoreaction.

A report regarding the phototoxicity of sulfadoxine (Scheme 1.7),[44] which is a component of an antimalarial drug, reported severe light-induced adverse cutaneous effects in patients that are known to be allergic to sulfonamide drugs. Sulfadoxine was shown to rapidly decompose in light to give a complex mixture of products. Degradation pathways corresponding to α, α′ and β-cleavages were proposed that lead to radicals that may dimerize or polymerize. These products or the radical precursors may react with cellular components *in vivo*. However, the only products positively identified were those arising from the α-cleavage of the S-N bond, possibly by a homolytic cleavage followed by the addition of water. The amine was found in 29% yield but only traces of sulfanilic acid were found suggesting that is degraded after cleavage. Hence, much of the photodegraded compound has not been accounted for and important products are likely to have been missed, which may have phototoxic effects.

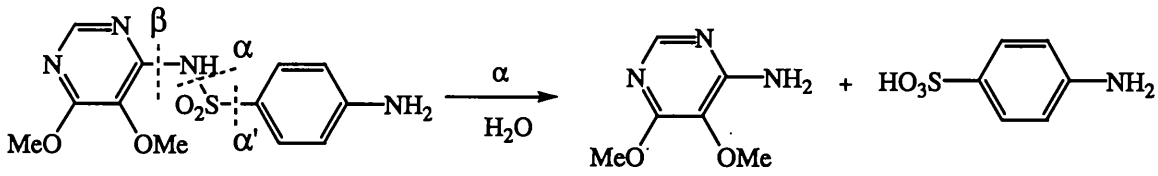

Scheme 1.7 Three possible cleavages in sulfadoxine.

The methods used for photostability testing in the past have varied widely and hence comparison of the data is difficult. Many researchers have been aware for some time of the need for a standardised photostability testing protocol.[5] It is only recently that the International Conference on Harmonisation (ICH) guidelines for the photostability testing of pharmaceutical compounds have been introduced,[47] and these were implemented in 1998. The guidelines identify the circumstances in which more than a basic degradation study should be carried out, and the conditions that should be used in order to identify possible photodegradation products and suitable methods for analysis. These types of studies should enable identification of possible phototoxic products or photosensitizers. The ICH guidelines on photostability testing should encourage companies to perform in-depth studies and potentially lead to a greater understanding of photodegradative pathways in all drugs. The project described in this thesis may help identify the possible outcomes of light absorption by arylsulfonamide drugs, both *in vitro* and *in vivo*.

1.6 Objectives of the project

The review of the literature has shown that whilst the photochemistry of arylsulfonamides is an area of current interest there is very little comprehensive product analysis. So, we have chosen to perform an extensive study of the photochemistry of a range of tosylated amino acids, dipeptides and their derivatives in order to:

(a) Investigate PIET processes in chromophorically modified peptide models and the reactions that occur following ET.

(b) Clarify the scope of photodeprotection in arylsulfonyl protected amine compounds and identify competitive pathways responsible for the low yields of the required products.

(c) Identify common pathways relevant to sulfonamide drug photodegradation in order to identify the most likely outcomes of a photochemical reaction.

(d) Propose general mechanisms that may be applied in the aforementioned areas.

These objectives were pursued by:

1. Performing the photolyses in mainly aqueous solution in order to facilitate ET and to be relevant to processes occurring in biological systems and in the photodegradation of pharmaceutical compounds in storage.

2. Carrying out a comprehensive product analysis for twenty-seven compounds; eight tosylated amino acids and their ester and amide derivatives, four tosyl dipeptides and five tosylated alkyl amines to enable quantification of products at an early point in the degradation in order to identify the primary processes occurring.

The initial stages of the project involved examination of a number of tosyl amino acids, which were chosen for a specific reason such as conformational or steric restraints and side-chain reactivity. These results then prompted further studies with alkyl amines, dipeptides, and ester and amide derivatives. The comprehensive product data obtained has enabled mechanisms to be proposed.

The literature suggests that we should observe S-N cleavage as the primary process in the photolysis of simple tosylated amino acids and peptides. The presence of a COOH group may cause some unwanted side reactions such as decarboxylation and deamination. Much of the work reviewed has involved electron donation either inter or intramolecularly from an excited donor molecule or group, the use of reducing agents to give the sulfinic acid and an amine. Our work has been performed in aqueous solution with no electron donors or reducing agents present, hence the side reactions suggested by other workers may prove to be important, especially as the toluenesulfonamide group is a good electron acceptor. The use of wavelengths of < 300 nm may lead to degradation of the released amino acids, as may prolonged irradiation. We have analysed the product yields near the beginning of the degradation process in order to determine the primary processes that are occurring.

The next chapter of this thesis describes the experimental procedures used in the photodegradation experiments and product analyses along with synthetic details for compounds and standards. The subsequent chapters contain the results and discussion for each compound, which are grouped according to structure. Finally the results are summarised and the conclusions regarding the effects of structure upon the photodegradation pathways of *N*-arylsulfonyl amino acids and peptides are discussed.

Chapter 2: Experimental

2.1 Instrumentation

2.1.1 Physical measurements

Melting points (m.p.) were determined in capillary tubes on an Electrothermal apparatus and are uncorrected. Infrared spectra (IR) were recorded as potassium bromide discs or as thin films between sodium chloride plates using either a Perkin-Elmer 1710 or Nicolet 205 infrared spectrometer. Nuclear magnetic resonance (NMR) spectra were obtained on a JEOL LAMBDA300 or JEOL EX400. Chemical shifts are reported as parts per million (ppm) downfield of tetramethylsilane which was used as an internal standard. The coupling constants (*J*), where appropriate, are expressed in Hz with multiplicities; s-singlet, d-doublet, t-triplet, q-quartet and m-multiplet. The prefix br-broad is used where applicable. Microanalytical data were obtained from Medac Ltd, Analytical and Consultancy Services. Accurate mass data were obtained by Pfizer Global R & D, Sandwich, Kent. UV spectra were recorded in 1 cm quartz cuvettes on a Kontron Model 860 spectrophotometer, or were extracted from HPLC data. Accurate weighing of samples (< 20 mg) was performed on a Perkin-Elmer AD2Z Autobalance.

2.1.2 HPLC equipment

HPLC operations were performed using the following systems:

HPLC System 1: Waters 616 pump, 600S controller, 717 plus autosampler, 996 photodiode array detector (200-700nm), Waters Millenium Software version 2.15 or 3.05. The software allowed peak areas and UV-Vis spectra to be obtained for individual peaks. The diagnostic software enables extraction and integration at wavelengths other than that of primary detection and identification of peaks by comparison with libraries of known compounds.

HPLC System 2: Waters 474 scanning fluorescent detector, 712 WISP autosampler and a 600 Multisolvent Delivery System and Millenium Software version 3.05 as described for System 1.

HPLC System 3: Waters Deltaprep 3000 pump, 600E System Controller, 484 Tunable Absorbance Detector and a 745B Data Module.

Stationary phases for analytical HPLC:

I Phenomenex Luna C18 250 mm × 4.60 mm with a C18 guard column or security guard cartridge.

II Phenomenex Luna phenyl hexyl 150 mm × 4.60 mm

III Novapak 4 μm C18 150 × 3.9 mm with a C18 guard column

Stationary phase for preparative HPLC:

IV Jones Apex ODS 8 μm, 250 × 21 mm column

2.1.3 LC-MS equipment

LC-MS operations were performed on a Waters Alliance System with a Waters 996 PDA detector, MS in positive ion-mode detection.

2.1.4 GC equipment

GC operations were performed on a Unicam ATI 610GC with a Unicam methaniser fitted into the injection port. The column was a 10′ × 1/8′′ SS Porapak Q column, with a mesh size of 80-100. Peak areas were determined using a Spectra-Physics Chromjet integrator.

2.2 Materials

2.2.1 Reagents

O-Methyl-L-tyrosine was supplied by Acros. Ammonium chloride, benzyl alcohol, *tert*-butylamine, *trans*-cinnamic acid, *o*-cresol, 1,4-diaminobutane, *N,N*-dimethylformamide, ethylenediamine, ethyl glycolate, formaldehyde solution, glycollic acid, glycine methyl ester hydrochloride, glycylglycine, glyoxylic acid monohydrate, guaiacol, methionine methyl ester hydrochloride, methylamine (40% aq. wt. soln), methylamine (2M solution in methanol), oxalyl chloride, phenylacetaldehyde, L-phenylalanine, phenylalanine methyl ester hydrochloride, phenyllactic acid, toluenesulfinic acid (Li salt), *p*-toluenesulfonamide, toluenesulfonic acid monohydrate 98% and tosyl chloride were supplied by Aldrich Chemical Company. Ammonium acetate, 37% hydrochloric acid, magnesium sulphate (anhydrous), potassium bromide (Spectrosol) and sodium hydroxide were supplied by BDH Chemical Company. Ninhydrin was supplied by East Anglia Chemicals. Acetone, acetonitrile (far UV), dichloromethane, diethyl ether, ethyl acetate, hexane, methanol, tetrahydrofuran and trifluoroacetic acid were supplied by Fisher Chemical Company. Sodium hydrogen carbonate, tetrabutylammonium bromide, *N*-cetyl trimethylammonium bromide and tri-sodium citrate were supplied by Fisons Scientific Equipment. Ethanol was supplied by Hayman Ltd. 2,4-Dinitrophenylhydrazine was supplied by Hopkins and Williams. 2-Amino-*iso*-butyric acid, 2-butylamine, *iso*-butylamine, *iso*-butyraldehyde, methyl 3,3-dimethoxypropionate, methyl methacrylate, phenethylamine, 2-phenyl-5-oxazalone, phenylpyruvic acid Na salt, L-proline and triethylamine were supplied by Lancaster Chemicals. β-Alanine, glycyl-DL-alanine, glycylproline, glycyl-DL-valine, hydrochloric acid (ACS), pyruvic acid ethyl ester and tosylglycine were supplied by Sigma Chemical Company. NMR solvents were supplied by Cambridge Isotope Laboratories except for D_2O supplied by Goss Scientific Instruments.

All solvents were reagent grade unless stated otherwise. Bottled, compressed gases were supplied by Air Products and nitrogen was high purity. Silica gel for chromatography was Kieselgel 60 (220-240 mesh). Water used in solutions and as eluants for HPLC was purified by reverse osmosis and ion exchange to produce Grade 2 purified water (according to ISO3696/BS3978) and finally by PureOne polishing.

2.2.2 General points for syntheses

Solvents were dried and distilled, where appropriate: tetrahydrofuran (THF) from potassium, methanol from magnesium turnings, dichloroethane from CaH_2. Column chromatography was performed under medium pressure using silica gel (Kieselgel 60; 220-240 mesh). Organic extracts were dried over anhydrous magnesium sulphate ($MgSO_4$). Solvents were removed under reduced pressure.

2.2.3 Syntheses of tosylated compounds

2.2.3.1 General procedure for tosylation of amines

An established method was used for these compounds.[48] The amine component was dissolved in H_2O/THF (2:1) and stirred with three equivalents of Et_3N. One equivalent of tosyl chloride was added in small aliquots over 30 min at 0 °C. The solution was stirred at 20 °C for at least 3 h and the THF removed. The aqueous layer was extracted with ether ($2 \times 20\ cm^3$), acidified with conc. HCl to pH 2 and extracted with ethyl acetate ($3 \times 20\ cm^3$). The combined organic extracts were washed with H_2O ($20\ cm^3$), dried ($MgSO_4$), filtered and the solvent removed. The purity was checked by HPLC prior to recrystallisation.

2.2.3.2 *N-p*-Tosyl-2-amino-*iso*-butyric acid

Tosyl chloride (2.0 g, 10.5 mmol) was added to a solution of 2-amino-*iso*-butyric acid (1.0 g, 9.70 mmol), H_2O ($30\ cm^3$), THF ($15\ cm^3$) and Et_3N ($4\ cm^3$, 29 mmol) and stirred at 20 °C for 3 h. 1.8 g of a gummy substance was obtained (72% yield). 0.75 g

was purified by prep HPLC (System 3, Column IV, detection at 228 nm, eluant 60% H_2O, 30% acetonitrile and 10% 0.1 M TFA) gave two peaks at RT 6.2 and 9.1 min. The fractions from the 9.1 min peak were combined and the solvent reduced *in vacuo*. The residual solid was dissolved in ethyl acetate, dried and the solvent removed to give 0.48 g of a white solid that was recrystallised from ethyl acetate / methanol. m.p. 146-147 °C (lit:[49] 149-150 °C); δ_H (300 MHz; CD_3CN) 1.33 (6H, s, 2 × CH_3), 2.38 (3H, s, $ArCH_3$), 6.01 (1H, br s, NH), 7.33 (2H, d, *J* 8.3, Ar), 7.71 (2H, d, *J* 8.3, Ar).

2.2.3.3 *N-p*-Tosyl-β-alanine

Tosyl chloride (3.09 g, 16 mmol) was added to a solution of β-alanine (1.42 g, 16 mmol) in H_2O (30 cm^3), THF (15 cm^3) and Et_3N (6.5 cm^3, 47 mmol) at 20 °C and stirred for 3 h. 2.28 g of the crude product was obtained (59% yield) and recrystallised from ethyl acetate / hexane. m.p. 118-120 °C (lit:[50] 119.5–121 °C); δ_H (300 MHz; CD_3CN) 2.41 (3H, s, CH_3), 2.43 (2H, t, *J* 6.1, $COCH_2$), 3.05 (2H, q, *J* 6.1, NCH_2) 5.68 (1H, br s, NH), 7.38 (2H, d, *J* 8.2, Ar), 7.71 (2H, d, *J* 8.2, Ar).

2.2.3.4 *N-p*-Tosyl-*sec*-butylamine

Tosyl chloride (2.82 g, 15 mmol) was added to a solution of *sec*-butylamine (1.5 cm^3, 15 mmol), H_2O (30 cm^3), THF (15 cm^3) and Et_3N (6 cm^3, 43 mmol) and stirred for 3 h at 20 °C. 2.8 g of a white solid was obtained (83% yield) by recrystallisation from diethyl ether. m.p. 54-56 °C (lit:[51] 54-55 °C). δ_H (300 MHz; $CDCl_3$) 0.79 (3H, t, *J* 7.4, CH_2CH_3), 0.94 (3H, d, *J* 5.7, $CHCH_3$), 1.38-1.47 (2H, m, CH_2), 2.42 (3H, s, $ArCH_3$), 3.15-3.29 (1H, m, CH), 5.04 (1H, br s, NH), 7.29 (2H, d, *J* 8.4, Ar), 7.80 (2H, d, *J* 8.4, Ar).

2.2.3.5 *N-p*-Tosyl-*tert*-butylamine

Tosyl chloride (2.72 g, 14 mmol) was added to a solution of *tert*-butylamine (1.5 cm^3, 14 mmol), H_2O (30 cm^3), THF (15 cm^3) and Et_3N (6 cm^3, 43 mmol) and stirred for 3 h at 20°C. 2 g of a white solid was obtained (62% yield) by recrystallisation from

ethyl acetate. m.p. 112-115 °C (lit:[52] 113-114 °C). δ_H (300 MHz; $CDCl_3$) 1.21 (9H, s, 3 × CH_3) 2.41 (3H, s, $ArCH_3$), 5.26 (1H, br s, NH), 7.28 (2H, d, *J* 8.1, Ar), 7.81 (2H, d, *J* 8.1, Ar).

2.2.3.6 *N-p*-Di-tosyl-1,4-diaminobutane

Tosyl chloride (4.00 g, 20 mmol) was added to a solution of 1,4-diaminobutane (1.00 g, 11 mmol), H_2O (30 cm^3), THF (15 cm^3) and Et_3N (4.5 cm^3, 32 mmol) and stirred for 3 h at 20 °C. 3.39 g (75% yield) of a white solid was obtained by recrystallisation from methanol m.p. 122-124 °C (lit:[53] 124-125 °C). δ_H (300 MHz; $CDCl_3$) 1.44-1.50 (4H, m, 2 × CH_2), 2.42 (6H, s, 2 × CH_3), 2.87 (4H, td, *J* 5.4 and 6.2, 2 × NCH_2), 4.98 (2H, t, *J* 6.2, 2 × NH), 7.30 (4H, d, *J* 8.4, Ar), 7.73 (4H, d, *J* 8.4, Ar).

2.2.3.7 *N-p*-Tosylethylamine

Tosyl chloride (2.00 g, 11 mmol) was added to a solution of ethylamine (1 cm^3 70% aq. sol, 12 mmol), H_2O (30 cm^3), THF (15 cm^3) and Et_3N (4 cm^3, 29 mmol) and stirred for 3 h at 20 °C. 1.5 g (72% yield) of a white solid was obtained by recrystallisation from (ethyl acetate/hexane). m.p. 49-59 °C (lit:[54]58 °C). δ_H (300 MHz; $CDCl_3$) 1.09 (3H, t, *J* 7.2, CH_3), 2.42 (3H, s, $ArCH_3$), 2.97 (2H, m, *J* 7.2, CH_2), 5.12 (1H, br s, NH), 7.33 (2H, d, *J* 8.7, Ar), 7.78 (2H, d, *J* 8.7, Ar).

2.2.3.8 *N-p*-Di-tosylethylenediamine

Synthesized by a standard procedure.[55] Ethylenediamine (0.65 cm^3, 10 mmol) gave a white solid, which was recrystallised to give 0.06 g (5% yield) of white crystals was obtained by recrystallisation from ethanol m.p. 161 °C (lit:[55] 160 °C). δ_H (300 MHz; $CDCl_3$) 2.43 (6H, s, $ArCH_3$), 3.06 (4H, s, CH_2), 5.02 (2H, br s, NH), 7.31 (4H, d, *J* 8.2, Ar), 7.71 (4H, d, *J* 8.2, Ar).

2.2.3.9 *N-p*-Tosylglycylalanine

Tosyl chloride (2.3 g, 12.1 mmol) was added to a solution of glycylalanine (1.41 g, 10 mmol), H_2O (20 cm^3), THF (10 cm^3) and Et_3N (4.2 cm^3, 30 mmol) and stirred at 20 °C for 3 h. 1.70 g (59% yield). of the crude product was obtained which was recrystallised from ethyl acetate) m.p. 168–171 °C (lit:[56] 167 °C) δ_H (300 MHz; CD_3CN) 1.28 (3H, d, *J* 7.2, $CHCH_3$), 2.41 (3H, s, $ArCH_3$), 3.52 (2H, d, *J* 6.0, CH_2), 4.26 (1H, m, NCH) 5.99 (1H, br t, *J* 6.0, SNH), 6.98 (1H, br d, *J* 5.7, CONH), 7.36 (2H, d, *J* 8.4, Ar), 7.72 (2H, d, *J* 8.4, Ar).

2.2.3.10 *N-p*-Tosylglycylglycine

Tosyl chloride (24.4 g, 128 mmol) was added to a solution of glycylglycine (15 g, 114 mmol), H_2O (180 cm^3), THF (90 cm^3) and Et_3N (36.6 cm^3, 263 mmol) and stirred at 20 °C for 3 h. 15.28 g (47% yield) of the crude product was obtained and recrystallised from ethyl acetate. m.p. 173–179 °C (lit:[48] 178-179 °C) δ_H (400 MHz; CD_3OD) 2.42 (3H, s, $ArCH_3$), 3.53 (2H, s, $SNCH_2$), 3.87 (2H, s, CH_2COO), 7.37 (2H, d, *J* 8.4, Ar), 7.74 (2H, d, *J* 8.4, Ar).

2.2.3.11 *N-p*-Tosylglycylproline

Tosyl chloride (1.22 g, 6.4 mmol) was added to a solution of glycylproline (1 g, 5.81 mmol), H_2O (20 cm^3), THF (10 cm^3) and Et_3N (2.5 cm^3, 18 mmol), and stirred at 20 °C for 3 h. 1.15 g (61% yield) of the crude product was obtained and recrystallised from ethyl acetate to give white crystals. m.p. 182-184 °C (lit:[57]183-184 °C); δ_H (300 MHz; CD_3CN) 1.85-2.17 (4H, m, $CHCH_2CH_2$), 2.40 (3H, s, CH_3), 3.28-3.46 (2H, m, NCH_2), 3.72 (2H, t, *J* 4.9, $NHCH_2$), 4.22 (1H, dd, *J* 3.8 and 4.5, CH), 5.85 (1H, br s, NH), 7.36 (2H, d, *J* 8.4, Ar), 7.72 (2H, d, *J* 8.4, Ar).

2.2.3.12 *N-p*-Tosylglycyl-DL-valine

Tosyl chloride (1.1 g, 5.74 mmol) was added to a solution of glycyl-DL-valine (1 g, 5.74 mmol), H_2O (20 cm^3), THF (10 cm^3) and Et_3N (2.5 cm^3, 18 mmol) at 20 °C for 3 h. 1.30 g (69% yield) of the crude product was obtained as a white solid and recrystallised from ethyl acetate / hexane. m.p. 132–137 °C (lit:[58] 131 °C); δ_H (300 MHz; CD_3CN) 0.80 (3H, d, *J* 7.0, $CHCH_3$), 0.83 (3H, d, *J* 7.0, $CHCH_3$), 1.83-1.91 (1H, m, $CH(CH_3)_2$), 2.37 (3H, s, $ArCH_3$), 3.52 (2H, s, CH_2), 4.16 (1H, dd, *J* 5.3 and 8.4, NCH), 5.99 (1H, br s, SNH), 6.84 (1H, br d, *J* 8.4, CONH), 7.33 (2H, d, *J* 8.4, Ar), 7.67 (2H, d, *J* 8.4, Ar).

2.2.3.13 *N-p*-Tosyl-DL-methionine

Tosyl chloride (3.19 g, 18 mmol) was added to a solution of DL-methionine (2.5 g, 17 mmol), H_2O (40 cm^3), THF (20 cm^3) and Et_3N (7 cm^3, 50 mmol) and stirred for 16 h at 20°C. 4.82 g (95% yield) of a white solid was obtained and recrystallised from ethyl acetate / hexane. m.p. 117-118 °C (lit:[59] 104-105 °C); δ_H (300 MHz; CD_3CN) 1.76-1.89 (1H, m, $CHCH_2$), 1.91-2.05 (1H, m, $CHCH_2$), 2.00 (3H, s, SCH_3), 2.33-2.53 (2H, m, SCH_2), 2.42 (3H, s, $ArCH_3$), 3.95-4.05 (1H, m, NCH), 5.05 (1H, br s, OH), 6.08 (1H, d, *J* 9.0, NH), 7.38 (2H, d, *J* 8.5, Ar), 7.73 (2H, d, *J* 8.5, Ar).

2.2.3.14 *N-p*-Tosylmethylamine

Synthesized by a standard procedure:[55] Tosyl chloride (5.72 g, 30 mmol) was added in small aliquots to a solution of methylamine (2 M sol. in methanol, 15 cm^3, 15 mmol) in 10% aq. NaOH (40 cm^3) with stirring at 0 °C. The solution was stirred at 20 °C for 1 h, heated to 55 °C, cooled and acidified to pH 2 with 2 M HCl. The precipitate was filtered, washed with H_2O and recrystallised from ethanol to give 1.12 g (36% yield) of white crystals. m.p. 71.5 °C (lit:[55] 75 °C); δ_H (300 MHz; $CDCl_3$) 2.43 (3H, s, $ArCH_3$), 2.64 (3H, s, NCH_3), 4.55 (1H, br s, NH), 7.32 (2H, d, *J* 8.3, Ar), 7.75 (2H, d, *J* 8.3, Ar).

2.2.3.15 *N-p*-Tosyl-*O*-methyl-L-tyrosine

Tosyl chloride (1 g, 5.2 mmol) was added to a solution of *O*-methyl-L-tyrosine (0.96 g, 4.9 mmol), H_2O (20 cm^3), THF (10 cm^3) and Et_3N (2 cm^3, 14 mmol) and stirred for 18 h at 20 °C. 1.60 g (93% yield) of white crystals were obtained by recrystallisation from ethyl acetate / hexane. m.p. 139-141 °C (lit:[60] 138-140 °C). δ_H (300 MHz; $CDCl_3$) 2.39 (3H, s, $ArCH_3$), 2.92 (1H, dd, *J* 6.6 and 14.0, CH_2), 3.03 (1H, d, *J* 6.6 and 14.0, CH_2), 3.77 (3H, s, OCH_3), 4.12-4.19 (1H, m, CH), 5.19 (1H, d, *J* 8.8, NH), 6.74 (2H, d, *J* 8.6, OAr), 6.98 (2H, d, *J* 8.6, OAr), 7.20 (2H, d, *J* 8.3, SAr), 7.58 (2H, d, *J* 8.3, SAr).

2.2.3.16 *N-p*-Tosylphenethylamine

Tosyl chloride (2.44 g, 13 mmol) was added to a solution of phenethylamine (1.55 cm^3, 13 mmol), H_2O (18 cm^3), THF (9 cm^3) and Et_3N (5.5 cm^3, 39 mmol) and stirred for 3 h at 20 °C. 3 g of a white solid was obtained by recrystallisation from hexane / ether. m.p. 62-64 °C (lit:[61] 65-66 °C); δ_H (300 MHz; $CDCl_3$) 2.42 (3H, s, CH_3), 2.76 (2H, t, *J* 6.6, $PhCH_2$), 3.21 (2H, q, *J* 6.6, NCH_2), 4.45 (1H, t, *J* 6.6, NH), 7.06 (2H, d, *J* 8.2, S-Ar), 7.19-7.29 (5H, m, C-Ar), 7.69 (2H, d, *J* 8.2, Ar).

2.2.3.17 *N-p*-Tosylphenylalanine

Tosyl chloride (5.00 g, 26 mmol) was added to a solution of phenylalanine (4.33 g, 26 mmol), H_2O (36 cm^3), THF (18 cm^3) and Et_3N (11 cm^3, 79 mmol) and stirred for 3 h at 20 °C. A white solid was obtained by recrystallisation from ethanol. m.p. 145-155 °C (lit:[62] 165.5-167); δ_H (300 MHz; $CDCl_3$) 2.40 (3H, s, CH_3), 3.00 (1H, dd, *J* 6.3 and 13.9, CH_2), 3.10 (1H, dd, *J* 6.3 and 13.9, CH_2), 4.21 (1H, m, CH), 5.04 (1H, d, *J* 9.0, NH), 7.08 (2H, d, *J* 8.4, S-Ar), 7.20-7.26 (5H, m, C-Ar), 7.59 (2H, d, *J* 8.4, S-Ar).

2.2.3.18 *N-p*-Tosylproline

Tosyl chloride (4.97 g, 26 mmol) was added to a solution of proline (3 g, 26 mmol), H_2O (20 cm^3), THF (10 cm^3) and Et_3N (10 cm^3, 72 mmol) and stirred for 18 h at 20

°C. 4.94 g (71% crude yield) of a pale yellow gum was obtained. Purification of 1.90 g by column chromatography on silica gel (1:1 v/v ethyl acetate: hexane) gave 1.7 g of a clear gum. δ_H (300 MHz; CD_3CN) 1.54-1.65 (1H, m, $CH_2CH_2CH_2$), 1.76-1.85 (1H, m, $CH_2CH_2CH_2$), 1.86-1.97 (2H, m, $CHCH_2$), 2.42 (3H, s, $ArCH_3$), 3.12-3.23 (1H, m, NCH_2), 3.35-3.46 (1H, m, NCH_2), 4.14 (1H, t, *J* 6.4, NCH), 7.40 (2H, d, *J* 8.1, Ar), 7.73 (2H, d, *J* 8.1, Ar); δ_C (75 MHz; CD_3CN) 21.02 ($ArCH_3$), 24.86 ($CH_2CH_2CH_2$), 31.07 ($CHCH_2$), 49.24 (NCH_2), 60.91 (NCH), 127.91 (Ar-CH), 130.31 (Ar-CH), 135.03 (Ar-C), 144.65 (Ar-C), 173.22 (CO).

2.2.3.19 *N-p*-Tosyl-*iso*propylamine

Tosyl chloride (2.23 g, 12 mmol) was added to a solution of *iso*-propylamine (1 cm^3, 12 mmol), H_2O (30 cm^3), THF (15 cm^3) and Et_3N (4 cm^3, 29 mmol) and stirred for 3 h at 20 °C. 2 g (80% yield) of a white solid was obtained by recrystallisation from diethyl ether. m.p. 47-49 °C (lit:[63] 48-50 °C). δ_H (300 MHz; $CDCl_3$) 1.07 (6H, d, *J* 6.4, 2 × CH_3) 2.42 (3H, s, $ArCH_3$), 4.91 (1H, d, *J* 7.5, NH), 3.37-3.52 (1H, m, CH), 7.30 (2H, d, *J* 8.1, Ar), 7.79 (2H, d, *J* 8.1, Ar).

2.2.3.20 *N-p*-Tosyl L-valine

Tosyl chloride (4.88 g, 26 mmol) was added to a solution of L-valine (3 g, 26 mmol), H_2O (30 cm^3), THF (15 cm^3) and Et_3N (10 cm^3, 72 mmol) and stirred for 16 h at 20 °C. 5.81 g (84% yield). of a white solid was obtained by recrystallisation from ethyl acetate / hexane. m.p. 148-149 °C (lit:[64] 149.5-150.5 °C). δ_H (300 MHz; CD_3CN) 0.74 (3H, d, *J* 6.8, CH_3), 0.81 (3H, d, *J* 6.8, CH_3), 1.85-2.02 (1H, m, $CH(CH_3)_2$), 2.31 (3H, s, $ArCH_3$), 3.62 (1H, dd, *J* 5.3 and 9.4, NCH), 5.21 (1H, br s, OH), 5.88 (1H, d, *J* 9.4, NH), 7.23 (2H, d, *J* 8.6, Ar), 7.62 (2H, d, *J* 8.6, Ar).

2.2.4 Syntheses of the ester and amide derivatives of tosyl amino acids

2.2.4.1 *N-p*-Tosylglycine methyl ester

Tosyl chloride (6.00 g, 30 mmol) was added to a solution of glycine methyl ester hydrochloride (3.95 g, 31 mmol), H_2O (50 cm^3), THF (25 cm^3) and Et_3N (12 cm^3, 86 mmol) and stirred for 15 h at 20 °C. The organic extract was washed with saturated Na_2CO_3 (20 cm^3) and H_2O (20 cm^3), then dried to give 3.8 g (50% yield) of a white solid was obtained by recrystallisation from diethyl ether. m.p. 90-93 °C (lit:[65] 92-93 °C). δ_H (300 MHz; $CDCl_3$) 2.42 (3H, s, $ArCH_3$), 3.63 (3H, s, OCH_3), 3.78 (2H, d, *J* 5.6, CH_2), 5.38 (1H, br t, *J* 5.6, NH), 7.30 (2H, d, *J* 8.3, Ar), 7.75 (2H, d, *J* 8.3, Ar).

2.2.4.2 *N-p*-Tosylphenylalanine methyl ester

TsFOH (32.86 g, 103 mmol) was refluxed in methanol (300 cm^3) and conc. H_2SO_4 (4 cm^3) for 5 h, cooled to room temperature and neutralized with aq. ammonia. The precipitated ammonium sulphate was removed by filtration and the filtrate reduced in volume *in vacuo*. The resulting precipitate was collected by filtration and recrystallised from methanol to give 35 g (100% yield) of white crystals. m.p. 86-88 °C (lit:[66] 95°C); δ_H (300 MHz; $CDCl_3$) 2.40 (3H, s, $ArCH_3$), 3.02 (2H, d, *J* 6.1, CH_2), 3.48 (3H, s, OCH_3), 4.20 (1H, dt, *J* 6.1 and 9.1, CH), 5.18 (1H, d, *J* 9.1, NH), 7.07 (2H, d, *J* 8.4, SAr), 7.18-7.27 (5H, m, OAr), 7.63 (2H, d, *J* 8.4, SAr).

2.2.4.3 *N-p*-Tosylglycine *N'*-methyl amide

Methylamine (10 cm^3, 40% aq. wt. soln) was added to a solution of TsGOMe (2 g, 8.2 mmol) in THF (20 cm^3) and stirred for 6 days at 20 °C. Extracted with ethyl acetate (3 × 20 cm^3) and 2 M aq. HCl (2 × 20 cm^3). White crystals were obtained by recrystallisation from diethyl ether. m.p. 131-133 °C (lit:[67] 130 °C). δ_H (300 MHz; $CDCl_3$) 2.39 (3H, s, $ArCH_3$), 2.61 (3H, d, *J* 5.0, NCH_3), 3.42 (2H, d, *J* 6.0, CH_2), 6.10 (1H, br s, SNH), 6.72 (1H, br s, CONH), 7.36 (2H, d, *J* 8.2, Ar), 7.70 (2H, d, *J* 8.2, Ar).

2.2.4.4 *N-p*-Tosylphenylalanine *N'*-methyl amide

Methylamine (122 cm^3, IMS sol) was added to a solution of TsFOMe (30 g) in ethanol (20 cm^3) and stirred for 10 days at 20 °C. The solvent was removed and a white solid was obtained. 5.5 g was dissolved in ethyl acetate (50 cm^3) and extracted with 2 M aq. HCl (3 × 20 cm^3) and H_2O (20 cm^3), the organic extracts were dried to give a white solid that was recrystallised from ethyl acetate / hexane. m.p. 160 °C; ν_{max} (KBr) / cm^{-1} 3322 (NH), 3263 (NH), 1660, 1334, 1163, 1156, 1091, 1078, 669, 540; δ_H (300 MHz; $CDCl_3$) 2.43 (3H, s, $ArCH_3$), 2.74 (3H, d, *J* 4.6, NCH_3), 2.86 (1H, dd, *J* 6.2 and 13.9, CH_2), 2.96 (1H, dd, *J* 7.0 and 13.9, CH_2), 3.83 (1H, q, *J* 6.8, CH), 4.82 (1H, s, *J* 6.8, SNH), 6.27 (1H, br d, *J* 4.6, CONH), 6.91 (2H, d, *J* 8.4, Ph), 7.14-7.26 (5H, m, Ar), 7.53 (2H, d, *J* 8.4, SAr); δ_C (100 MHz, $CDCl_3$) 21.58 ($ArCH_3$), 26.34 (NCH_3), 38.19 (CH_2), 57.88 (CH), 127.16 (Ar-CH), 127.27 (Ar-CH), 128.93 (Ar-CH), 129.01 (Ar-CH), 129.83 (Ar-CH), 135.24 (SAr-C), 135.55 (Ar-C), 143.96 (SAr-C), 170.63 (CO); Found: C, 61.25%; H, 6.09%; N, 8.37% ($C_{18}H_{22}N_2O_4S$ requires: C, 61.43%; H, 6.06%; N, 8.42%).

2.2.4.5 *N-p*-Tosyl-β-alanine *N'*-methyl amide

Ts-β-AOH (5.42 g, 21 mmol) was dissolved in methanol (50 cm^3) and conc HCl (5 cm^3), and refluxed for 2 h. The solution was cooled and added slowly to H_2O (25 cm^3) at 0 °C. The methanol was removed and the aqueous solution extracted with ethyl acetate (3 × 40 cm^3), washed with sat. Na_2CO_3 (20 cm^3) and H_2O (20 cm^3). The solvent was removed to give 5.28 g of a white solid which was dissolved in methanol (10 cm^3). Methylamine (40 cm^3, 40% aq. wt. soln) was added and the solution stirred at 20 °C for 4 days. The solvent was reduced in volume, extracted with ethyl acetate (3 × 50 cm^3), 10% Na_2CO_3 (25 cm^3), 2 M aq. HCl (2 × 20 cm^3) and H_2O (25 cm^3). The organic extracts were dried and the solvent removed to give 1.28 g (23% yield) of a white solid that was recrystallised from ethyl acetate. m.p. 127-129 °C (lit:[68] 127-130 °C); δ_H (300 MHz; CD_3CN) 2.23 (3H, t, *J* 6.7, NCH_2) 2.40 (3H, s, $ArCH_3$), 2.60 (3H, d, *J* 4.7, NCH_3) 3.06

(2H, t, *J* 6.7, $COCH_2$), 5.83 (1H, br s, NH), 6.29 (1H, br s, CONH), 7.37 (2H, d, *J* 8.4, Ar), 7.70 (2H, d, *J* 8.4, Ar).

2.2.4.6 *N-p*-tosylmethionine *N'*-methyl amide

Tosyl methionine methyl ester was synthesized according to the general procedure: Tosyl chloride (2.87 g, 15 mmol) was added to a solution of methionine methyl ester hydrochloride (3 g, 15 mmol), H_2O (40 cm^3), THF (20 cm^3) and Et_3N (6 cm^3, 43 mmol) and stirred for 16 h at 20 °C. The organic extract was washed with saturated Na_2CO_3 (20 cm^3) and H_2O (20 cm^3), then dried to give 3.59 g of a white solid (75% yield), which was converted to the amide according to the procedure for TsVNMA: TsMOMe (3.59 g) in methanol (10 cm^3) and methylamine (40 cm^3 40% aq. wt. sol) stirred for 4 days at 20 °C to give 1.94 g (41% yield) of white crystals recrystallised from ethyl acetate. m.p. 160-162 °C; ν_{max} (KBr) / cm^{-1} 3359 (NH), 3325 (NH), 1653, 1647, 1347, 1326, 1162, 673, 573, 553; δ_H (300 MHz; CD_3CN) 1.60-1.73 (1H, m, $CHCH_2$), 1.75-1.85 (1H, m, $CHCH_2$), 1.93 (3H, s, SCH_3), 2.20-2.36 (2H, m, SCH_2), 2.38 (3H, s, $ArCH_3$), 2.46 (3H, d, *J* 4.8, NCH_3), 3.72 (1H, br s, CH), 5.97 (1H, br s, SNH), 6.52 (1H, br s, $NHCH_3$), 7.33 (2H, d, *J* 8.2, Ar), 7.67 (2H, d, *J* 8.2, Ar); δ_C (75 MHz; CD_3CN) 14.66 ($CHCH_2$), 21.00 ($ArCH_3$), 25.67 (NCH_3), 29.89 (SCH_3), 32.93 (SCH_2), 56.28 (NCH), 127.57 (Ar-CH), 130.08 (Ar-CH), 137.63 (Ar-C), 144.44 (Ar-C), 171.21 (CO); Found: C, 49.47%; H, 6.47%; N, 8.84% ($C_{13}H_{20}N_2O_3S_2$ requires: C, 49.34%; H, 6.37%; N, 8.85%).

2.2.4.7 *N-p*-Tosyl-*O*-methyl-L-tyrosine *N'*-methyl amide

Synthesized according the procedure for Ts-β-ANMA: TsY(OMe)OH (1.35 g) was converted to the ester (20 cm^3 methanol and 2 cm^3 conc. HCl) and then to the amide (10 cm^3 methanol and 40 cm^3 40% aq. methylamine) after 4 days at 20°C (53% yield). White crystals were obtained by recrystallisation from ethyl acetate / hexane. m.p. 166 °C; ν_{max} (KBr) / cm^{-1} 3321 (NH), 3362 (NH), 1654, 1561, 1513, 1334, 1234, 1157, 1088; δ_H (300 MHz; $CDCl_3$) 2.43 (3H, s, $ArCH_3$), 2.74 (3H, d, *J* 4.8, NCH_3), 2.84 (1H, d, *J* 6.5,

CH_2), 2.86 (1H, d, *J* 6.5, CH_2), 3.77 (3H, s, OCH_3), 3.81 (1H, m, CH), 4.97 (1H, d, *J* 6.8, SNH), 6.38 (1H, br d, *J* 4.8, NHMe), 6.68 (2H, d, *J* 8.7, OAr-CH), 6.82 (2H, d, *J* 8.7, OAr-CH), 7.22 (2H, d, *J* 8.2, SAr-CH), 7.53 (2H, d, *J* 8.2, SAr-CH); δ_C (75 MHz; CCl_3) 21.58 ($ArCH_3$), 26.34 (NCH_3), 37.32 (CH_2), 55.21 (OCH_3), 58.06 (CH), 114.26 (OAr-CH), 127.12 (OAr-C), 127.17 (SAr-CH), 129.77 (SAr-CH), 130.12 (OAr-CH), 135.68 (SAr-C), 143.93 (SAr-C), 158.81 (OAr-C), 170.79 (CO); Found: C, 59.77%; H, 6.15%; N, 7.69% ($C_{18}H_{22}N_2O_4S$ requires: C, 59.65%; H, 6.12%; N, 7.73%).

2.2.4.8 *N-p*-Tosyl-*N'*-methyl-2-amino-*iso*-butyramide

AibNMA was tosylated by the general procedure: Tosyl chloride (1.91 g, 10 mmol) was added to a solution of AibNMA (1.53 g, 13 mmol), H_2O (10 cm^3), THF (5 cm^3) and Et_3N (4 cm^3, 29 mmol) and stirred for 15 h at 20 °C. 0.90 g (25% yield) of white crystals were obtained by recrystallisation from diethyl ether / methanol. m.p. 174-176 °C; ν_{max} (KBr) / cm^{-1} 3146 (NH), 1653, 1646, 1645, 1540, 1523, 1330, 1158, 1096, 993, 809, 678, 538; δ_H (300 MHz; CD_3CN) 1.26 (6H, s, 2 × CH_3), 2.40 (3H, s, $ArCH_3$), 2.59 (3H, d, *J* 4.8, NCH_3), 6.01 (1H, br s, SNH), 6.66 (1H, br s, CONH), 7.34 (2H, d, *J* 7.9, Ar), 7.71 (2H, d, *J* 7.9, Ar); δ_C (75 MHz; CD_3CN) 20.98 ($ArCH_3$) 25.79 (2×CH_3), 26.13 (NCH_3), 59.78 (SNC), 127.20 (Ar-CH), 130.03 (Ar-CH), 140.67 (Ar-C), 143.85 (Ar-C), 174.81 (C=O); Found: C, 53.17%; H, 6.72%; N, 10.30% ($C_{12}H_{18}N_2O_3S$ requires: C, 53.31%; H, 6.71%; N, 10.36%).

2.2.4.9 *N-p*-Tosylproline *N'*-methyl amide

Synthesized according the procedure for Ts-β-ANMA: TsPOH (3.04 g, mmol) converted to the ester (50 cm^3 methanol and 5 cm^3 conc. HCl) and then to the amide (10 cm^3 methanol and 40 cm^3 40% aq. methylamine) after 5 days at 20 °C (72% yield). Recrystallisation from ethyl acetate / hexane. m.p. 122-124 °C; ν_{max} (KBr) / cm^{-1} 3433 (NH), 3374 (NH), 1669, 1658, 1518, 1347, 1341, 1157, 815, 667, 595, 551; δ_H (300 MHz; CD_3CN) 1.44-1.63 (2H, m, $CH_2CH_2CH_2$), 1.65-1.76 (1H, m, $CHCH_2$), 1.85-1.96 (1H, m,

$CHCH_2$), 2.41 (3H, s, $ArCH_3$), 2.69 (3H, d, *J* 4.7, NCH_3), 3.12-3.20 (1H, m, NCH_2), 3.42-3.49 (1H, m, NCH_2), 3.97 (1H, dd, *J* 4.3 and 8.3, CH), 6.99 (1H, br s, NH), 7.40 (2H, d, *J* 8.3, Ar), 7.72 (2H, d, *J* 8.3, Ar); δ_C (75 MHz; CD_3CN) 21.05 ($ArCH_3$), 24.55 ($CH_2CH_2CH_2$), 25.80 (NCH_3), 30.86 ($CHCH_2$), 49.96 (NCH_2), 63.09 (CH), 128.23 (Ar-CH), 130.40 (Ar-CH), 134.02 (Ar-C), 144.90 (Ar-C), 172.62 (CO); Found: C, 55.30%; H, 6.44%; N, 9.85% ($C_{13}H_{18}N_2O_3S$ requires: C, 55.30%; H, 6.43%; N, 9.92%).

2.2.4.10 *N-p*-Tosylvaline *N'*-methyl amide

Synthesized according the procedure for Ts-β-ANMA: TsVOH (3.55 g, 13.1 mmol) converted to the ester (50 cm^3 methanol and 5 cm^3 conc. HCl) and then to the amide (10 cm^3 methanol and 40 cm^3 40% aq. methylamine) after 4 days at 20 °C. 1.24 g (33% yield) of white crystals was obtained by recrystallisation from ethyl acetate. m.p. 204-206 °C; ν_{max} (KBr) / cm^{-1} 3347 (NH), 3259 (NH),1654, 1320, 1168, 1085, 1068, 664, 576; δ_H (300 MHz; CD_3CN) 0.78 (3H, d, *J* 6.7, $CHCH_3$), 0.81 (3H, d, *J* 6.7, $CHCH_3$), 1.83 (1H, m, *J* 6.7, $CHCH_3$), 2.38 (3H, s, $ArCH_3$), 2.39 (3H, d, *J* 4.8, NCH_3), 3.38 (1H, dd, *J* 6.2 and 8.8, NCH), 5.80 (1H, br d, *J* 8.8, SNH), 6.35 (1H, br s, $NHCH_3$), 7.32 (2H, d, *J* 8.4, Ar), 7.65 (2H, d, *J* 8.4, Ar); δ_C (75 MHz; CD_3CN) 17.60 ($CHCH_3$), 18.85 ($CHCH_3$), 20.98 ($ArCH_3$), 25.44 (NCH_3), 31.88 ($CH(CH_3)_2$), 62.68 (NCH), 127.61 (Ar-CH), 129.89 (Ar-CH), 137.84 (Ar-C), 144.08 (Ar-C), 171.08 (CO); Found: C, 54.86%; H, 7.12%; N, 9.73% ($C_{13}H_{20}N_2O_3S$ requires: C, 54.91%; H, 7.09%; N, 9.85%).

2.2.5 Syntheses of 2,4-dinitrophenylhydrazone derivatives

2.2.5.1 Acetone DNP

DNPH (2 g, 10 mmol) was added to acetone (20 cm^3) and conc. HCl (2 cm^3) and heated to boiling. A yellow solid precipitated upon cooling. Filtered and dried ($MgSO_4$) then recrystallised from methanol to give 1.78 g (74% yield) of yellow crystals. m.p. 121-125 °C (lit:[69] 123-125 °C); δ_H (300 MHz; DMSO) 2.05 (3H, s, CH_3), 2.08 (3H, s, CH_3), 7.80 (1H, d, *J* 9.7, Ar), 8.33 (1H, dd, *J* 2.6 and 9.7, Ar), 8.82 (1H, d, *J* 2.6, Ar).

2.2.5.2 Benzaldehyde DNP

Synthesized by a known method:[55] benzaldehyde (500 µl, 49 mmol) in 250 cm^3 Brady's reagent gave 0.61 g of orange crystals after recrystallisation from ethyl acetate. m.p. 235-241 °C (lit:[70] 233-234 °C). δ_H (300 MHz; $CDCl_3$) 7.46-7.49 (3H, m, CAr), 7.77-7.80 (2H, m, CAr), 8.11 (1H, d, *J* 9.5, NAr), 8.14 (1H, s, N=CH), 8.37 (1H, dd, *J* 2.6 and 9.5, NAr), 9.16 (1H, d, *J* 2.6, NAr), 11.33 (1H, br s, NH).

2.2.5.3 Formaldehyde DNP

Synthesized by a known method:[55] formaldehyde solution (10 cm^3) gave 0.05 g of yellow crystals after recrystallisation from ethanol. m.p. 164 °C (lit:[71] 166 °C); δ_H (300 MHz; $CDCl_3$) 6.74 (1H, d, *J* 10.8, N=CH), 7.16 (1H, dd, *J* 0.9 and 10.8, N=CH) 7.97 (1H, d, *J* 9.5, Ar), 8.34 (1H, dd, *J* 0.9, 2.6 and 9.5, Ar) 9.13 (1H, d, *J* 2.6, Ar), 11.13 (1H, br s, NH).

2.2.5.4 Glyoxylic acid DNP

DNPH (2 g, 10 mmol) was dissolved in acetonitrile (20 cm^3) and conc. HCl (2 cm^3) by heating to boiling point. Glyoxylic acid monohydrate (1 g, 11 mmol) was dissolved in H_2O (1 cm^3) and added to the warm solution of DNPH. The precipitate formed upon cooling was filtered, dissolved in acetonitrile, dried ($MgSO_4$) and recrystallised from ethyl acetate to give 2 g (78% yield) of a yellow crystals. HPLC analysis gave two peaks. m.p. 188-190 °C (lit:[72] 195 °C); δ_H (300 MHz; CD_3CN) 5.17 (1H, br s, OH), 7.10 (1H, s, N=CH), 7.98 (1H, d, *J* 9.4, Ar), 8.39 (1H, dd, *J* 2.6 and 9.4, Ar), 8.75 (1H, d, *J* 2.6, Ar), 11.79 (1H, br s, NH).

2.2.5.5 Methyl glyoxylate DNP

Methyl glyoxylate was synthesized by a known procedure[73] and 0.30 g (3.4 mmol) was converted to the DNP derivative[55] giving orange crystals after recrystallisation from methanol (0.23 g, 34% yield). HPLC gave two peaks at 12.8 min (minor) and 15.5

min (major); these became equal in size after two days in 50% aq. acetonitrile in daylight. m.p. 198-200 °C (lit:[74] 200.5-201 °C); δ_H (300 MHz; CD_3CN) 3.83 (3H, s, CH_3), 7.70 (1H, s, N=CH), 8.00 (1H, d, *J* 9.5, Ar), 8.40 (1H, dd, *J* 2.6 and 9.5, Ar), 8.97 (1H, d, *J* 2.6, Ar), 11.33 (1H, br s, NH).

2.2.5.6 *N*-Methylglyoxamide DNP

Synthesized by known procedures:[75,55] Dimethoxymethyl acetate (1.02 g, 7.60 mmol) was converted to the amide and then the DNP derivative to give 0.1 g of an orange solid. HPLC analysis showed two products. Recrystallisation from ethanol gave a solid with a single peak by HPLC, which was found to convert to the second peak upon standing in solution (50% aq. acetonitrile) in daylight for 2 days. m.p. 258-261 °C (lit:[75] 244-245 °C); δ_H (300 MHz; DMSO) 2.75 (3H, d, *J* 4.6, CH_3), 7.15 (1H, s, N=CH), 8.03 (1H, d, *J* 9.5, Ar), 8.43 (1H, dd, *J* 2.6 and 9.5, Ar), 8.88 (1H, d, *J* 2.6, Ar), 9.02 (1H, br d, *J* 4.6, NH).

2.2.5.7 *N*-Methylphenylpyruvamide DNP

Phenylpyruvic acid sodium salt (0.50 g, 2.45 mmol) was dissolved in 50 cm^3 0.5 M HCl and extracted with diethyl ether (2 × 25 cm^3), dried, and the solvent removed to give phenylpyruvic acid (0.5 g) which was dissolved in dry THF (10 cm^3) and *N,N*-dimethylformamide (20 µl) under N_2 at 0 °C. Oxalyl chloride (0.4 cm^3, 4.6 mmol) was added slowly and stirred for 30 min. until effervescence ceased. After warming to 20 °C, the solvent and excess $(COCl)_2$ were removed to give 0.5 g of an oil which was dissolved in THF (2 cm^3) and added dropwise to methylamine (5 cm^3, 40% aq. wt. sol.) at 0 °C and stirred for 1 hr, then warmed to 20 °C and the THF removed. The aqueous layer was extracted with diethyl ether (2 × 20 cm^3) and the organic extracts were washed with 2 M HCl (20 cm^3) and H_2O (20 cm^3), dried and the solvent removed to give 0.2 g of an oil, which was dissolved in 1 cm^3 acetonitrile and converted to the DNP derivative by a known method:[55] 0.11 g of yellow crystals were obtained by recrystallisation from ethanol. m.p.

168 °C; ν_{max} (KBr) / cm^{-1} 3354 (NH), 1654, 1623, 1522, 1341, 1314, 1259, 1133, 1113; δ_H (300 MHz; CD_3CN) 2.89 (3H, d, *J* = 4.95, CH_3), 4.12 (2H, s, CH_2), 7.20-7.33 (5H, m, CAr), 7.59 (1H, broad s, N*H*-CH_3), 8.12 (1H, d, *J* 9.51, NAr), 8.37 (1H, dd, *J* 2.55 and 9.51, NAr) 8.92 (1H, d, *J* 2.55, NAr), 11.06 (1H, broad s, NH-Ar); δ_C (75 MHz; CD_3CN) 26.07 (CH_3), 30.75 (CH_2), 117.67 (Ar-CH), 123.24 (Ar-CH), 127.59 (Ar-CH), 129.00 (Ar-CH), 129.50 (Ar-CH), 130.48 (Ar-CH), 131.65 (Ar-C), 134.88 (Ar-C), 140.01 (Ar-C), 144.68 (Ar-C), 148.96 (C=N), 164.35 (C=O); Found: C, 52.8%; H, 4.4%; N, 19.3%; ($C_{16}H_{15}N_5O_5$.0.25 H_2O requires: C, 53.1%; H, 4.3%; N, 19.4%).

2.2.5.8 Methyl phenylpyruvate DNP

Synthesized by known procedures:[76,55] phenylpyruvic acid sodium salt monohydrate (1.02 g, 5.00 mmol) was dissolved in 0.5 M HCl (50 cm^3) and extracted with diethyl ether (2 × 25 cm^3) to give phenylpyruvic acid (0.68 g, 4.14 mmol), which was converted to the ester and then the DNP to give 0.2 g of orange crystals after recrystallisation from ethyl acetate. HPLC gave a single peak at 29.9 min, another peak at 23.8 min was found after standing in 50% aq. acetonitrile in daylight for two days. m.p. 169-170 °C (lit:[77] 169–169.5 °C); δ_H (300 MHz; CD_3CN) .384 (3H, s, CH_3), 3.95 (2H, s, CH_2), 7.22-7.36 (5H, m, Ph), 8.02 (1H, d, *J* 9.5, NAr), 8.35 (1H, dd, *J* 2.6 and 9.5, NAr), 8.97 (1H, d, *J* 2.6, NAr), 14.03 (1H, br s, NH).

2.2.5.9 *N*-Methylpyruvamide DNP

N-Methylpyruvamide was synthesized by a known method:[78] 10 cm^3 ethyl lactate gave 0.8 g of a pale yellow oil which was converted to the DNP derivative and obtained as yellow crystals (0.15 g, 0.6% yield) by recrystallisation from ethanol, m.p. 185 °C (lit:[78] 186.5-187.5 °C); δ_H (300 MHz; CD_3CN) 2.05 (3H, s, N=CCH_3), 2.12 (3H, s, $NHCH_3$), 7.89 (1H, d, *J* 9.7, Ar), 8.28 (1H, dd, *J* 2.6 and 9.7, Ar), 8.96 (1H, d, *J* 2.6, Ar), 11.33 (1H, br s, NH).

2.2.5.10 *N*-Oxo-acetylglycine DNP

N-oxo-acetylglycine was synthesized by a known method:[79] 2-phenyl-5-oxazolone (1.0146 g, 6.30 mmol) was converted to *N*-oxo-acetylglycine which was converted to its DNP derivative[55] and 140 mg of a yellow solid was obtained. HPLC analysis showed two products which were separated by prep HPLC (45% H_2O : 45% acetonitrile : 10% 0.1 mol dm^{-3} TFA / 5% aq. methanol) and recrystallised from ethanol. Product 1: m.p. 223 °C; found MH^+ 312.0585 ($C_{10}H_{10}N_5O_4$ requires 312.0580); δ_H (300 MHz; CD_3OD) 4.07 (2H, s, CH_2), 7.77 (1H, s, N=CH), 8.31 (1H, d, *J* 9.5, Ar), 8.42 (1H, dd, *J* 2.6 and 9.5, Ar), 9.05 (1H, d, *J* 2.6, Ar). Product 2: m.p. 236 °C; found MH^+ 312.0591 ($C_{10}H_{10}N_5O_4$ requires 312.0580) δ_H (300 MHz; CD_3OD) 4.05 (2H, s, CH_2), 7.15 (1H, s, N=CH), 8.16 (1H, d, *J* 9.5, Ar), 8.41 (1H, dd, *J* 2.6 and 9.5, Ar), 9.06 (1H, d, *J* 2.6, Ar). All data are consistent with *N*-oxoacetylglycine DNP *syn* and *anti* stereoisomers. The literature m.p. (ethanol:[79] 214-215° C) was lower than either of the two products formed.

2.2.5.11 3-Oxo-propionic acid DNP

Synthesized according to known procedures:[80,55] 3,3-dimethoxypropionate (2 g, 14 mmol) was converted to the acid, of which 1 g was converted to the DNP derivative. 1.3 g (34% yield) of orange crystals were obtained after recrystallisation from ethyl acetate. m.p. 146-148 °C (lit:[71] 150 °C); δ_H (300 MHz; CD_3CN) 2.04 (2H, d, *J* 5.3, CH_2), 7.70 (1H, 2t, *J* 5.3, N=CH), 7.87 (1H, d, *J* 9.7, Ar), 8.26 (1H, dd, *J* 2.6 and 9.7, Ar), 8.93 (1H, d, *J* 2.6, Ar), 10.92 (1H, br s, NH).

2.2.5.12 Phenylpyruvic acid DNP

Synthesized by a known method:[55] phenylpyruvic acid sodium salt (0.50g, 25 mmol) gave 0.77 g of an orange solid (91% yield). HPLC analysis of a sample (1 mg / cm^3) showed two products which were separated by prep HPLC on System 3 (Column IV, detection at 228 nm, eluant 30% H_2O: 60% acetonitrile: 10% 0.1 M TFA in 5% methanol) gave two peaks with RT 8.1 and 12.8 min.. The solvents were removed and the residual

solids were dissolved in DCM, washed with H_2O, dried and recrystallised from ethyl acetate to give yellow crystals; 0.53 g from peak 1 and 0.17 g from peak 2. Product 1: m.p. 160-162 °C (lit:[81] 192-194 °C); δ_H (300 MHz; CD_3CN) 4.11 (2H, s, CH_2), 7.25-7.36 (5H, m, CAr), 8.18 (1H, d, *J* 9.5, NAr), 8.33 (1H, dd, *J* 2.6 and 9.5, NAr), 8.92 (1H, d, *J* 2.6, NAr), 11.14 (1H, br s, NH); Found: C, 52.30%; H, 3.57%; N, 16.07%; ($C_{15}H_{12}N_4O_6$ requires: C, 52.33%; H, 3.51%; N, 16.27%). Product 2: m.p. 192-194 °C (lit:[81] 192-194 °C); δ_H (300 MHz; CD_3CN) 3.94 (2H, s, CH_2), 7.24-7.35 (5H, m, CAr), 8.02 (1H, d, *J* 9.5, NAr), 8.34 (1H, dd, *J* 2.5 and 9.5, NAr), 8.97 (1H, d, *J* 2.5, NAr), 14.12 (1H, br s, NH); Found: C, 52.10%; H, 3.59%; N, 15.72%; ($C_{15}H_{12}N_4O_6$ requires: C, 52.33%; H, 3.51%; N, 16.27%). Samples of the two phenylpyruvic acid DNP stereoisomers (1 mg / cm^3 50% aq. acetonitrile) were left standing in solution in daylight. HPLC analysis showed that the stereoisomers interconvert to give equal amounts of both stereoisomers in either case.

2.2.6 Miscellaneous syntheses

2.2.6.1 Glycine *N*-methylamide

Methylamine (10 cm^3, 40% wt. aq. sol) was added to a solution of glycine methyl ester hydrochloride (1 g) in H_2O (10 cm^3) and stirred at 20 °C for 6 days. Methylamine was removed on a rotary evaporator and the aqueous solution was acidified to pH 7 and extracted with ethyl acetate (4 × 20 cm^3). 650 mg of an oil was obtained (93% yield). δ_H (300 MHz; D_2O) 3.73 (3H, s, CH_3), 3.84 (2H, s, CH_2), 4.65 (1H, s, NH).

2.2.6.2 *N*-Methyl-2-amino-*iso*-butyramide

2-Amino-*iso*-butyric acid (4.12 g) was converted to AibOMe.HCl by a known procedure:[82] 5.85 g of an off-white solid was obtained (96% yield) m.p. 185 °C (lit:[82] 182-183 °C); δ_H (300 MHz; D_2O) 1.47 (6H, s, $2CH_3$), 3.72 (3H, s, OCH_3). 4 g of AibOMe.HCl was converted to the title compound by the method described for GNMA; 1.68 g of an oil was obtained (55% yield); δ_H (300 MHz; D_2O) 1.26 (6H, s, $2CH_3$), 2.61 (3H, s, NCH_3).

2.2.6.3 *N*-Methylmethacrylamide

The amide was synthesized by the same procedure as for GNMA: Methylamine (50 cm^3, 40% wt. sol) added to a solution of methyl methacrylate (5 cm^3, 5.04 mmol) in methanol (20 cm^3) at 0 °C, then stirred at 20 °C for 6 days. 1.48 g of an oil was obtained which was purified by column chromatography on silica gel (1:1 v/v ethyl acetate: hexane) to give 1.40 g of a clear oil. δ_H (300 MHz; CD_3Cl_3) 1.96 (3H, dd, *J* 0.9 and 1.5, CCH_3), 2.82 (3H, d, *J* 4.1, NCH_3), 5.31 (1H, m, C=CH), 5.69 (1H, m, C=CH).

2.2.6.4 Phenylalanine *N*-methylamide

Phenyalanine methyl ester hydrochloride (0.51g, 2.36 mmol) was dissolved in 20 cm^3 dry THF under N_2 and 10 cm^3 methylamine (2 M in methanol, 10 mmol) was added to the solution and stirred for 7 days. 5 cm^3 H_2O was added to the solution and the volatile components removed *in vacuo*. The aqueous layer was extracted with DCM (2 × 20 cm^3), dried and solvent removed to give 0.2 g of an oil (48% yield). δ_H (300 MHz; $CDCl_3$) 1.26 (2H, br s, NH_2), 2.60 (1H, dd, *J* 9.5 and 13.7, CH_2), 2.75 (3H, d, *J* 4.9, CH_3), 3.22 (1H, dd, *J* 4.0 and 13.7, CH_2), 3.53 (1H, dd, *J* 4.0 and 9.5, CH), 7.14-7.31 (5H, m, Ar). The ^1H nmr spectrum was consistent with the literature:[83] δ_H ($CDCl_3$) 1.38 (2H, br s), 2.68 (1H, dd, *J* 9.5 and 13.7), 2.82 (3H, d, *J* 5.0), 3.29 (1H, dd, *J* 4.0 and 13.7), 3.61 (1H, dd, *J* 4.0 and 9.5), 7.1-7.6 (5H, m).

2.3 Photolysis procedures

2.3.1 Irradiation protocols

2.3.1.1 Standard irradiation protocol

A 10^{-2} M solution of the compound in water, either unadjusted or pH 9 (by addition of 1M NaOH), or in 40% aq. acetonitrile was purged with nitrogen for ~1 hr whilst being stirred. Quartz carousel tubes were filled with ~14 cm^3 of the solution, and purged for a further 2 minutes prior to subasealing. The tubes were irradiated in an Applied

Photophysics carousel in the inner or outer rings with a 400 W medium pressure Hg lamp for periods of 1-240 min, with an inversion every 30 minutes to ensure homogeneous mixing and hence irradiation of the solution. The reactions were quenched by cooling in ice for at least 30 min, which also ensures that all of the CO_2 and NH_3 are in solution. Two tubes were required at each irradiation time for CO_2 and NH_3 analysis by the gas electrode techniques or one at each irradiation time for NH_3 analysis by AccQTag™ derivatisation. The analyses were performed on the day of irradiation unless time was limiting, when the samples were stored in a refrigerator.

2.3.1.2 Irradiation protocol for CO_2 measurements by GC

10 cm^3 of a solution of the compound under study (10^{-2} mol dm^{-3} in 40% acetonitrile in H_2O) was transferred to a quartz irradiation tube and the tube was subasealed. The tube and the solution were purged with N_2 for 5 min via tubing inserted through the subaseal. The sample was irradiated in the carousel as described previously and cooled in ice for a minimum of 30 min with frequent inverting. The sample was analysed for CO_2 as described in Section 2.3.2.6, and the sample degradation was calculated by analysis of the treated sample by HPLC as described in Table 2.5.

2.3.2 Analytical methods

2.3.2.1 General

All of the irradiated samples were analysed by HPLC to calculate the degradation of the substrate and to identify and quantify products as detailed in Table 2.5. Analyses of the raw photolysates by HPLC required sample dilutions of 1: 9 with either H_2O or 20% acetonitrile in H_2O to give analyte concentrations in the linear range of the PDA detector. Typical injection volumes were 10 µl for the raw photolysate analyses and 10-40 µl for the analyses of the DNP derivatives. The parameters and the linearity of response were determined for each compound using solutions of known concentration,

which were made volumetrically from commercial or synthesized samples either dissolved in H_2O or 40% acetonitrile in H_2O. The UV-vis spectra were extracted from the HPLC raw data files and kept as library references. The identity of a photolysate peak was assumed when its retention time and UV-Vis spectrum matched those of an authentic sample under identical analytical conditions, and a spiking experiment gave a positive result. Quantitation of products was by external standard calibration. Standard solutions were typically injected four times to check the repeatability. AccQTag™ derivatised samples typically required injections of 5 µl and dilutions were made volumetrically in H_2O with a dilution factor of ten, to give analyte concentrations in the linear range of the fluorescence detector. The pH or apparent pH of substrates was measured before photolysis and after 60 min irradiation.

2.3.2.2 Sample preparation for DNP analysis

1 cm^3 photolysate solution was added to 1 cm^3 Brady's reagent (0.26 g 2,4-dinitrophenylhydrazine in 100 cm^3 6M HCl) and left for 15 min before adding 2 cm^3 acetonitrile. Product quantitation was relative to formaldehyde DNP if an authentic sample was not available.

2.3.2.3 Sample preparation for AccQtag™ analysis

70 µl AccQFluorBorate Buffer was added to 10 µl photolysate sample and vortexed prior to the addition of 20 µl AccQFluor reagent, and vortexed again. The derivatised sample was left at 20°C for 1 min, then heated @ 55 °C for 10 min. Product quantitation was relative to an authentic sample.

2.3.2.4 HPLC gradients

The gradients for the HPLC analyses are shown in Tables 2.1–2.4, and the methods used for each substrate and the analyte retention times in Table 2.5. For all methods the time intervals denote either isocratic periods or linear gradients, and the flow

rate = 1 cm^3 min^{-1} unless stated otherwise.

Table 2.1 HPLC methods for the raw photolysate analyses: System 1, Column 1, column temperature = 37 °C.

Method	Time / min	H_2O / %	acetonitrile / %	0.1 M H_3PO_4 / %
A1	0	80	10	10
	20	10	80	10
A2	As A1 plus an additional 5 min at 10% A, 80% B, 10% C			
A3	0-20	as A1		
	20-25	0	90	10
A4	0	80	10	10
	15	45	45	10
	25	10	80	10
	30	0	90	10
A5	As A1 plus an additional 10 min at 10% A, 80% B, 10% C			
A6	0	80	10	10
	20	30	60	10
	30	10	80	10
A7	0	80	10	10
	15	80	10	10
	20	55	35	10
	35	10	80	10

Table 2.2 HPLC methods for the DNP analyses: System 1, Column 1, temperature = 37 °C.

Method	Time / min	H_2O / %	acetonitrile / %	0.1 M H_3PO_4 / %
B1	0	80	10	10
	30	0	90	10
	30-35	0	90	10
B2	0	80	10	10
	5	35	55	10
	20	25	65	10
	25	0	90	10
B3	As B2 plus an additional 10 min at 90% B, 10% C			
B4	0	80	10	10
	10	30	60	10
	30	0	90	10
B5	0	80	10	10
	5	35	55	10
	40	0	90	10

The conditions for LC-MS analyses were determined on System 1, Column 2 prior to analysis at Pfizer by the methods detailed in Table 2.3. Peak identity was checked by comparison with data acquired by the methods in Table 2.1 and Table 2.2, and from the MS data.

Table 2.3 LC-MS methods: System 2, Column 2, temperature = 25 °C, A= 10 mmol ammonium trifluoroacetate (pH 3.0)

Method	Time / min	Eluant A / %	acetonitrile / %
D1	0	90	10
	5	80	20
	15	25	75
	25	25	75
D2	0-5	80	20
	15	25	75
	25	25	75

Table 2.4 HPLC parameters for analysis of AccQTag derivatives: System 3, Column 3, column temp = 35 °C, eluant B = 140 mM sodium acetate and 17 mM triethylamine (pH 5.04, H_3PO_4).

Method	Time / min	60% H_2O : 40% acetonitrile / %	Eluant B / %
C1	0	0	100
	0.5	2	98
	15	10	90
	25	33	67
	30	100	0
	40	100	0
C2	0	0	100
	0.5	2	98
	10	33	67
	15	100	0
	25	100	0
C3	0	0	100
	0.5	2	98
	5	10	90
	15	33	67
	20	100	0
	25	100	0
C4	0	0	100
	0.5	2	98
	15	7	93
	19	10	90
	32	33	67
	33	33	67
	34	100	0
	40	100	0
C5	As C4 but column temp = 32 °C		
C6	0-25 min as C3 plus an additional 15 min at 100% A		

Table 2.5 Substrate HPLC analysis method and analyte retention times.

Substrate	HPLC method	Analyte retention time / min
TsGOH	A1	TsOH (10.5), TsH (11.7), $TsNH_2$ (13.1), TsGOH (13.4), TsNHMe (16.0), $(TsNH_2CH_2)_2$ (20.1)
	B1	HCHO (23.5) glyoxylic acid (22.8 + 25.5)
	C1	Gly (13.4), NH_3 (18.6),
TsVOH	A2	TsOH (9.8), TsH (11.4), TsVOH (16.4)
	B2	acetone (15.9), *iso*-butyraldehyde (20.6, 24.4)
	C2	NH_3 (11.4), valine (13.9), *iso*-butylamine (18.0)
TsPOH	A2	TsOH (9.7), TsH (11.5), $TsNH_2$ (12.3), unknown (13.7), TsPOH (15.4), unknown (16.7)
	B2	unknown (7.4)
	C2	NH_3 (11.4), proline (11.9)
TsMOH	A2	TsOH (9.8), TsH (11.4), $TsNH_2$ (12.3), TsMOH (16.2)
	B2	7.2, 13.7, 15.9, 18.3, 19.0, 20.2
	C2	NH_3 (11.4), methionine (14.2)
TsFOH	A3	TsOH (10.1), unknown (11.7), TsH (11.9), $TsNH_2$ (12.9), TsFOH (18.7), TsPhenethylamine (20.1)
	B3	phenylpyruvic acid (24.9 +28.5), benzaldehyde DNP (29.8), phenylacetaldehyde DNP (30.0)
	C3	NH_3 (13.7), Phe (20.6), phenethylamine (23.9)
TsY(OMe)OH	A4	TsOH (10.5), TsH (12.8), 13.1, 13.6, $TsNH_2$ (13.8), TsY(OMe)OH (22.0) 24.7
	B3	glyoxylic acid DNP (10.1, 13.0), 15.9, 19.3, 21.3, 25.3
	C2	NH_3 (11.5), Y(OMe) (16.3)
TsAibOH	A1	TsOH (10.0), TsH (12.0), $TsNH_2$ (13.0), TsAibOH (15.6)
	B2	acetone DNP (20.2)
	C2	NH_3 (11.1), Aib (12.2), *iso*-propylamine (16.9)
Ts-β-AOH	A1	TsOH (9.6), TsH (11.2), $TsNH_2$ (11.7), Ts-β-AOH (13.4)
	B1	3-oxo-propionic acid DNP (24.5)
	C4	NH_3 (21.8), β-Ala (24.5),
TsGOMe	A1	TsOH (9.4), TsH (11.3), $TsNH_2$ (12.2), TsGOH (12.8), TsGOMe (15.6)
	B2	glyoxylic acid DNP (10.1 and 13.2), methyl glyoxylate DNP (13.0 and 17.2)
	C4	Gly (18.6), NH_3 (22.4), GOMe (25.3)

Table 2.5 cont. Substrate HPLC analysis method and analyte retention times.

Substrate	HPLC method	Analyte retention time / min
TsFOMe	A5	TsOH (9.9), TsH (11.5), 11.8 (240 nm), $TsNH_2$ (12.2), TsFOH (18.5), 291 nm (19.3), TsFOMe (21.0)
	B5	methyl glyoxylate DNP (13.0 and 17.2), phenylpyruvic acid (16.1 and 22.8), methyl phenylpyruvate DNP (23.8 and 29.9), benzaldehyde DNP (25.7)
	C2	NH_3 (11.2), Phe (16.0), phenethylamine (18.8)
TsGGOH	A6	TsOH (10.6), TsH (13.2), TsGGOH (13.9), $TsNH_2$ (14.5), TsGOH (15.9), TsGNMA (14.3)
	B1	*N*-oxoacetylglycine DNP (16.8 + 19.5) HCHO DNP (23.1 glyoxylic acid (22.5))
	C5	NH_3 (25.6), Gly (22.3), GlyGly (23.6)
	C4	NH_3 (23.2), Gly (19.8), GlyGly (21.0)
TsGAOH	A1	TsOH (9.4), TsH (11.3), TsGAOH (12.4), TsGOH (13.0)
	B4	*N*-oxoacetylalanine DNP (12.6 and 14.2), unknown (17.5)
	C4	glyAla (20.8), NH_3 (20.3), Gly (17.3), Ala (22.3)
	D1	TsGAOH (9.6), TsGOH (10.0), *N*-oxoacetylalanine DNP (12.6 and 13.9), unknown (16.0)
TsGVOH	A1	TsOH (9.4), TsH (11.3), TsGVOH (14.6), TsGOH (13.0)
	B4	*N*-oxoacetylvaline DNP (14.0 and 16.1), (19.5, 22.7))
	C6	NH_3 (13.5), Gly (12.5), GlyVal (16.1), Val (17.7)
	D1	TsGVOH (11.6), *N*-oxoacetylvaline DNP (13.4 and 15.1), unknown (16.6 and 17.7)
TsGPOH	A1	TsOH (9.4), TsH (11.3), TsGOH (13.0), TsGPOH (13.4), $TsNH_2$ (12.2),
	B4	*N*-oxoacetylproline DNP (12.5 and 14.2), unknown (17.5)
	C6	NH_3 (14.0), Gly (12.5), Pro (14.5), GlyPro (15.2)
	D1	TsGAOH (10.8), TsGOH (10.0), *N*-oxoacetylproline DNP (12.5 and 14.4)
TsGNMA	A7	TsOH (17.3), TsH (24.2), $TsNH_2$ (24.7), TsGNMA (25.2), TsGOH (26.3)
	B2	methyl glyoxamide DNP (9.9 and 12.2)
	C2	Gly (10.0), NH_3 (11.2), GNMA (11.8), methylamine (12.6)
TsVNMA	A2	TsOH (10.0), TsH (11.5), (12.8), TsVNMA (14.5)
	B2	13.6, 15.1, 18.1, *iso*-butyraldehyde (21.0, 24.4)
	C2	NH_3 (11.4), methylamine (12.9), valine (13.9), *iso*-butylamine (18.0)

Table 2.5 cont. Substrate HPLC analysis method and analyte retention times.

Substrate	HPLC method	Analyte retention time / min
TsPNMA	A1	TsOH (9.4), TsH (10.9), TsPNMA (14.1), 16.3
	B2	7.1, 7.3, 7.8, 13.5
	C2	NH_3 (11.5), proline (11.9), methylamine (13.1), unknown (12.5, 13.5, 14.0, 14.3)
TsMNMA	A2	TsOH (10.0), TsH (11.6), $TsNH_2$ (12.3), TsMNMA (14.8)
	B2	14.9 and 17.3 (unknown)
	C2	NH_3 (11.4), (12.3), methylamine (12.9), methionine (14.2)
TsFNMA	A3	TsOH (10.3), unknown (11.4 and 11.7), TsH (12.0), $TsNH_2$ (12.9), TsFNMA (17.6), TsFOH (18.7)
	A4	TsOH (9.9), TsH (12.6), unknown (12.9 and 13.6), $TsNH_2$ (14.0), TsFNMA (21.2), TsFOH
	B4	*N*-methyl glyoxamide DNP (12.8 and 14.9), *N*-methyl phenylpyruvamide (18.9), benzaldehyde DNP (29.5)
	C2	NH_3 (11.6), methylamine (15.8), Phe (16.6), PheNMA (17.6), phenethylamine (23.7)
	D2	TsOH (2.1), unknown (8.5 and 9.6), TsH (3.5), TsFNMA (14.5), unknown (16.7)
	D1	TsOH (3.3), unknown (8.5 and 9.6), TsH (3.8), TsFNMA (13.2), TsFOH (13.9), *N*-methyl glyoxamide DNP (12.7), phenylpyruvic acid (24.9 and 28.5), benzaldehyde DNP (29.8), phenylacetaldehyde DNP (30.0)
TsY(OMe)NMA	A4	TsOH (10.4), TsH (12.7), unknown (13.1), TsY(OMe)NMA (20.5), unknown (24.7)
	B3	*N*-methyl glyoxamide DNP (9.9, 12.1), 17.4
	C2	NH_3 (11.5), methylamine (13.1), Y(OMe)NMA (16.7)
TsAibNMA	A1	TsOH (9.1), TsH (11.1), $TsNH_2$ (12.1), TsAibNMA (13.2), TsAibOH (14.5)
	B2	*N*-methylpyruvamide DNP (11.9), acetone DNP (18.9)
	C2	NH_3 (11.3), methylamine (12.8), AibNMA (13.6), *iso*-propylamine (16.9)
Ts-β-ANMA	A1	TsOH (9.5), TsH (11.3), Ts-β-ANMA (12.1)
	B2	DNPs (9.8 + 15.8)
	C4	NH_3 (24.0), methylamine (29.7), β-AlaNMA (32.5)
TsNHMe	A1	TsOH (9.7), TsH (11.4), $TsNH_2$ (12.3), TsNHEt (16.9)
	B2	formaldehyde DNP (13.7)
	C2	NH_3 (11.4), methylamine (13.0)
TsNHEt	A1	TsOH (9.6), TsH (11.3), $TsNH_2$ (12.2), TsNHEt (16.9)
	B2	acetaldehyde DNP (15.9)
	C2	NH_3 (11.4), ethylamine (15.1)

Table 2.5 cont. Substrate HPLC analysis method and analyte retention times.

Substrate	HPLC method	Analyte retention time / min
TsNH-*i*-Pr	A1	TsOH (9.8), TsH (11.5), $TsNH_2$ (12.3), TsNH-*i*-Pr (18.5)
	B2	acetaldehyde DNP (15.9), acetone DNP (18.7)
	C2	NH_3 (11.4), *iso*-propylamine (16.9)
TsNH-2-Bu	A2	TsOH (9.8), TsH (11.5), $TsNH_2$ (12.3), TsNH-2-Bu (20.0)
	B2	acetaldehyde DNP (15.9), DNP (23.8)
	C2	NH_3 (11.5), 2-butylamine (17.9)
TsNH-*t*-Bu	A2	TsOH (9.6), TsH (11.5), $TsNH_2$ (12.4), 13.8, 16.8, TsNH-*t*-Bu (20.2)
	B2	13.8, acetone DNP (18.9)
	C2	NH_3 (11.3), *tert*-butylamine (18.3)

2.3.2.5 CO_2 and NH_3 analysis by gas electrodes

The substrates that were irradiated in aqueous solution were analysed for carbon dioxide and ammonia by the gas electrode methods. The samples were treated as detailed below and analysed immediately by insertion of the electrode into the stirred solution. The measurements were performed in a water bath at 25 °C with a stirrer in the solution at 300 rpm. The electrode responses (mV) were measured with a PTI-6 meter and recorded on a chart recorder. Standard solutions were used to obtain a calibration plot and at least two measurements are required for each sample to ensure reliability. Trial irradiations showed that the results were unaffected by leaving either CO_2 or NH_3 analysis for 24 h if tubes remained subasealed and stored at < 5 °C until required.

NH_3 analysis

Measurements were made with a Unicam IS-NH_3 electrode. 10^{-2} M NH_3 standard (NH_4Cl, 0.382 g in 100 cm^3 H_2O) was diluted by factors of 5, 10, 20, 100 and 1000 with serial dilutions. A calibration plot showed that a linear response was given across the entire range of standards, $R^2 > 0.99$.

Standard and sample measurement:

250 µl 1M NaOH (40 g / 100 cm^3 H_2O) was added to 2.5 cm^3 sample. This ensured that samples have pH 11-13 so that all ammonium ions were converted to NH_3.

The effect of amines in the photolysate solution upon the measurement of NH_3 was checked by the addition of glycine and glycylglycine to an aq. TsGGOH solution to give concentrations of 10^{-4} M. The original solution gave a reading of 121 mV, and the treated solution gave a reading of 124 mV. This is within the limits of analytical error. Thus amines in the concentration likely to be observed in the photolysates have no effect upon NH_3 measurements.

CO_2 analysis:

Measurements were made with an Orion 95-02 CO_2 electrode. 10^{-2} M CO_2 standard ($NaHCO_3$, 0.4768 g in 250 cm^3 H_2O) was diluted as for the NH_3 standards, and a linear response was given across the entire range, $R^2 > 0.99$.

Standard and sample measurement:

250 µl buffer (74 g tri-sodium citrate in 250 cm^3 H_2O adjusted to pH 4.5 with conc HCl) was added to 2.5 cm^3 sample. This ensures that samples have a pH of 4.8-5.2, which converts all carbonate and bicarbonate to CO_2.

2.3.2.6 CO_2 analysis by gas chromatography

Analysis protocol for CO_2 by the GC methaniser

The sample, in a sealed carousel tube, was placed in a beaker of H_2O at 40 °C, 1 cm^3 1M HCl was added to the tube and the sample purged for 2 min with N_2 into a 500 cm^3 gas bag that had been previously evacuated. A sample of the gas was withdrawn into a 5 cm^3 SGE syringe fitted with an integral on/off valve, and 1 cm^3 of the gas sample was injected through a 25 µl loop (to ensure complete flushing of the loop) and 25 µl injected

into the GC via the methaniser column. CO_2 is converted to CH_4 in the methaniser column and detected at a RT of ~2.3 mins. A minimum of three repeat injections were carried out for each sample. Standards were injected between samples throughout a run. Acetonitrile is also present in the gas samples but has an RT of ~ 75 min. Analysis for CO_2 can be carried out on 4 min. run times for a continuous period of 75 min., after which the column temperature must be increased to 200 °C for 30 min. to remove all acetonitrile from the column. A blank of 40% acetonitrile in H_2O, a substrate t_0 sample and the CO_2 standards ($NaHCO_3$ in 40% aq. acetonitrile) are treated in the same manner for analysis as the irradiated samples.

GC operating conditions for CO_2 analyses

Hydrogen flow:	10 psi
Helium flow:	20 psi
Air flow:	26 psi
Injector temp:	370 °C
Column temp:	90 °C
Detector temp:	300 °C

Method development for the CO_2 methaniser

Variation on a daily basis was tested by filling a 500 cm^3 gas bag with air from the compressed air cylinder and injecting samples over a 3 day period. The peak areas were repeatable each day with 0.4% variation for 5 injections. CO_2 standard calibration plots were found to be linear in H_2O and 40% aq. acetonitrile up to 10^{-2} M CO_2 ($NaHCO_3$ as standard). The methaniser method was compared to the gas electrode by irradiating TsGOH (in aq. sol) for 30 min. (20% degradation) and comparing with the data obtained via the gas electrode method. Result: CO_2 mole fraction of a 20% degraded sample by gas electrode – 0.32; by methaniser – 0.31. Irradiation of TsGOH in 40% aq. acetonitrile for 30 min gave 33% degradation with a mole fraction of 0.46. Degradation was higher in 40%

aq. acetonitrile than for the same irradiation time in H_2O but the mole fraction is comparable to a similarly degraded sample in water. The measurements were performed on samples that were treated with acid only (as described in the analysis protocol) and samples that had 1 cm^3 1M NaOH added prior to cooling (to convert all CO_2 to HCO_3^- to prevent losses). There was no difference between the two methods.

2.4 Data handling

2.4.1 Calculation procedures for product quantitation

The peak area in a chromatogram is directly proportional to the amount of the compound in the solution being analysed. Therefore, accurate preparation of the substrate solution enables the amount of degradation of the substrate to be calculated. Photolysis products can also be quantified by comparison with accurately prepared standard solutions. The responses of the PDA and fluorescence detectors were shown to be linear by injecting varying amounts of a standard solution to give a calibration plot with $R^2 > 0.99$. The standard solutions had concentrations similar to those in the photolysates. All calculations were carried out in a Microsoft Excel spreadsheet. Typical calculation procedures are shown below. Peak area values were adjusted to allow for dilution factors.

$$\text{Substrate \% degradation at } t_x = \left(\frac{\text{peak area } t_x}{\text{peak area } t_0} \right) \times 100$$

Moles of substrate/dm^3 degraded at t_x= substrate conc at t_0 × % degradation at t_x.x.0.01

$$\text{Molar conc. of product at } t_x = \left(\frac{\text{peak area } t_x}{\text{standard peak area}} \right) \times \text{standard conc}$$

$$\text{Product mole fraction at } t_x = \left(\frac{\text{moles product formed at } t_x}{\text{moles substrate degraded at } t_x} \right)$$

These calculations were performed for all samples on every product identified in the analyses. The data were used to plot graphs in Microsoft Excel such as substrate degradation rates and product yield monitoring, where the product mole fractions were plotted against substrate percentage degradation. A product is likely to be a primary one if its yield plot has a zero or negative gradient, and a secondary product if the yield plot has a positive gradient. Correlation plots were also obtained for one product against another at degradation points on the linear part of the degradation plots. These plots were used to obtain R^2, slope and intercept values.

2.4.2 Error analyses

An experiment in which 16 TsGOH samples were all irradiated for 90 min each, was performed to calculate the errors in the substrate degradation and quantitation of products. All of the samples were taken from the same solution, 10^{-2} mol dm^{-3} aq. TsGOH and irradiated according to the standard protocol. All samples were analysed for substrate degradation, and for the production of TsH and TsOH. Samples 1-8 were also analysed for CO_2 and samples 9-16 for NH_3 and formaldehyde, with the latter by DNP analysis and both CO_2 and NH_3 by the gas electrode methods. Analysis for CO_2 and NH_3 was split into two further comparisons, with the first four of each sample sets analysed immediately and the second four analysed 24 h later after storing overnight in the fridge. The quantitation of products was as described previously.

Where there was only one source of error in a measurement the standard error on the mean was calculated using the following set of formulas, and expressed as the percentage error:

arithmetic mean, AVERAGE[1] = $\frac{(x_1 + x_2 ..... + x_n)}{n}$

standard deviation of the population, STDEVP[1] = $\sqrt{\frac{n\sum x^2 - (\sum x)^2}{n^2}}$

standard error on the means, $s_m = \frac{\text{STDEVP}}{(n-1)^{1/2}}$

% error = $\left(\frac{s_m}{\text{AVERAGE}}\right) \times 100\%$

Where there was more than one measurement involved in obtaining a value the resultant error, ΔZ was calculated. A and B are the measurements involved in calculating Z, and ΔA and ΔB are the errors in those measurements. A photolysis product quantitation is calculated from the product or ratios of two measurements (Section 2.4.1), so ΔZ is calculated from the expression:

$$\frac{\Delta Z}{Z} = \sqrt{\left(\frac{\Delta A}{A}\right)^2 + \left(\frac{\Delta B}{B}\right)^2}$$

% error in Z = $\frac{\Delta Z}{Z} \times 100\%$

Table 2.6 Percentage errors in product quantitation.

Calculated quantity	measurements used in error calculation	% error
TsGOH t_0 peak area	t_0 p.a.	0.58
TsGOH degradation	t_0 p.a., t_x p.a.	1.20
TsH mole fraction	TsH std p.a., t_x TsH p.a., TsGOH t_0 p.a., TsGOH t_x p.a.	1.95
HCHO DNP mole fraction	HCHO std p.a., t_x HCHO p.a., TsGOH t_0 p.a., TsGOH t_x p.a.	1.99
CO_2 mole fraction	t_x CO_2, TsGOH t_0 p.a., TsGOH t_x p.a.	1.58
NH_3 mole fraction	NH_3 std., t_x NH_3, TsGOH t_0 p.a., TsGOH t_x p.a.	1.32

[1] A Microsoft Excel statistical function

2.5 Specific studies

2.5.1 Thermal stability of TsGOH and TsGGOH

The Hg lamp emits considerable heat and subsequently, the photolysates become warm during irradiation. The effects of temperature were investigated by preparing TsGOH and TsGGOH samples, both unadjusted and pH 9 in aq. solution, as for a standard irradiation. The tubes were placed in a water bath at 50 °C for 2 h under normal lab lighting, and cooled upon removal. The solutions were analysed by HPLC before and after treatment and the peak areas for the substrate compared and the chromatograms checked for any products of a thermal reaction. No changes in the solution were detected.

2.5.2 Identification of some minor products of TsGOH photolyses

2.5.2.1 Ninhydrin test for glycine

The ninhydrin test was used to investigate the possibility of glycine in a TsGOH photolysate that was 50% degraded. 100 µl sample, 100 µl sodium acetate and a few drops of ninydrin reagent heated @ 80 °C until a purple colour was seen. A glycine sample (10^{-2} M) was treated similarly. Further studies were carried out by the AccQTag™ analyses as detailed in Section 2.3.2.

2.5.2.2 Toluenesulfonamide, tosylmethylamide and 1,2-*bis*-(toluene-4-sulfonylamino)-ethane by TLC

10 µl of saturated solutions of standards in DCM were applied to a silica gel plate. 20 µl of 50% degraded TsGOH solution was applied to a plate and the water evaporated prior to visualisation by UV lamp.

Table 2.7 TLC conditions for TsGOH product identification.

Compound	Eluant	R_f
Toluenesulfonamide	100% methanol	0.8
Tosylmethylamide	1% methanol in DCM + 0.1% Et_3N	0.8
1,2-*bis*-(toluene-4-sulfonylamino)-ethane	1% methanol in DCM + 0.1% ET_3N	0.7
TsGOH photolysate	100% methanol	0.8
	1% methanol in DCM + 0.1% ET_3N	0.7, 0.8

2.5.2.3 Isolation and identification of the insoluble material of TsGOH photolysis

Two methods were utilized to isolate the insoluble material from a TsGOH photolysate. In each case 500 cm^3 of an aq. TsGOH solution (10^{-2} mol dm^{-3}) was purged with nitrogen and irradiated in a quartz immersion well with a Hg lamp. A sample was taken for HPLC analysis to calculate the degradation of TsGOH. Other experimental details are as follows:

1. The solution was irradiated for 2.5 h and then centrifuged at 2000 rpm to give a solution that was almost clear. The supernatant was discarded and the solid was washed several times with water and then with ethanol. Drying under vacuum afforded 8 mg of solid, m.p. 145-160 °C. IR spectrum was obtained from a KBr disc and TLC analysis was performed as described in the previous section.

2. The solution was irradiated for 4 h and then adjusted to pH 9 with 1M NaOH. The aqueous solution was extracted with DCM (5 × 100 cm^3), and the DCM extracts were combined, washed with water, dried ($MgSO_4$) and the solvent was removed. A small amount of solid was obtained, which was rinsed several times with ethanol, the extracts combined and the ethanol removed. 10 mg of a solid was obtained.

2.5.3 Product confirmation in TsGGOH

2.5.3.1 TsGOH by TLC analysis

10 μl of saturated solutions of standards in DCM were applied to a silica gel plate. 20 μl of 50% degraded aq. TsGGOH solution was applied with rapid evaporation using a hot air gun (on cool setting). The plates were eluted with 1% methanol in DCM + 0.1% triethylamine and the spots were visualised by a UV lamp. TsGOH had an R_f 0.5. The photolysate had a similar R_f spot.

2.5.3.2 Isolation and identification of the insoluble compound of TsGGOH photolysis

Samples remaining from the irradiation of the unadjusted TsGGOH solution were combined to give approximately 50 cm^3 of photolysate. This was centrifuged at 2000 rpm and the supernatant discarded. The solid was washed 3 times with H_2O, then dried in a vacuum oven overnight. The dried solid (m.p. ~150 °C) was dissolved in 50% acetonitrile and analysed by HPLC. This solution was also used to spike an irradiated sample for comparison of peak overlap. A small amount of solid in DCM was analysed by TLC by the conditions stated for the analysis of TsGOH in TsGGOH photolysates. An FTIR spectrum was obtained from a KBr disc.

2.5.3.3 TLC analysis of *N*-oxo-acetylglycine DNPs

TsGGOH (10^{-2} mol dm^{-3} in H_2O) was irradiated for 120 min according to the standard irradiation protocol. 10 cm^3 of the photolysate solution was added to 10 cm^3 Brady's reagent.[55] The resulting precipitate was collected by centrifugation and washed with H_2O. A small amount of a yellow solid was obtained, to which a few drops of DCM were added and the solution was analysed by TLC.

Table 2.8 TLC analysis of *N*-oxoacetylglycine DNP in TsGGOH photolysates.

Sample	R_f in 1:1 hexane : DCM	R_f in DCM
DNP	-	0.6
Synthesized standard	0.3	0
TsGGOH photolysate	0.3	0.6

2.5.3.4 Interconversion of DNP stereoisomers

The formation of two stereoisomers of DNP derivatives of compounds where the carbonyl is α to an acid, ester or amide was investigated by isolating a single stereoisomer and looking for conversion to the other stereoisomer in daylight. The procedure is described for *N*-oxo-acetylglycine DNP: *ca* 0.1 mg of each sample was dissolved in 50% aqueous acetonitrile and analysed by RPHPLC . Half of each sample was left in daylight for 72 h and the other half of each sample was kept in the dark for 72 h. The RPHPLC analysis was then repeated on all samples for comparison of the ratio of the two peak areas.

The thermal interconversion of the two stereoisomers was also investigated: *ca* 0.1 mg of the product from peak 1 was dissolved in 50% aqueous acetonitrile and analysed by RPHPLC. The sample was then heated at 70 °C for 60 mins and reanalysed.

Table 2.9 *N*-oxoacetyglycine DNP stereoisomer interconversion experiments

Sample	Treatment	Initial ratio of peak areas 1:2	Final ratio of peak areas 1:2
Product 1	Heat	11	2
	Dark	64	39
	Light	64	1
Product 2	Dark	38	34
	Light	38	1

Other DNP derivatives that were found to exist as pairs of stereoisomers when formed in Brady's reagent[55] are those where the carbonyl is at the α-C of a carboxylate, ester or amide group i.e. glyoxylic acid, methyl glyoxylate, methyl glyoxamide, and phenylpyruvic acid.

2.5.4 Product analysis in TsGOMe

During AccQTag™ analysis of photolysate products it was noticed that GOMe is hydrolysed to glycine. This produces inaccurate values for the quantitation of glycine from a photolysate sample. Quantitation of a minimum yield of GOMe is possible by calculating the amount of glycine arising from a GOMe standard and adjusting the standard concentration accordingly. The hydrolysis was tested by heating the derivatised sample or by adding NaOH to the standard solution prior to derivatisation. Comparison with an untreated sample gave a larger peak for glycine in both cases.

2.5.5 TsFNMA: identification of benzyl alcohol as a photolysis product

Separation of benzyl alcohol and TsH was achieved by HPLC analysis using an isocratic method on a 150 cm C18 column with a guard column. The eluant system was 80% H_2O, 10% acetonitrile, 10% 0.1 M KH_2PO_4 (pH 7). Benzyl alcohol had an RT of 20.4 min, TsH 7.2 min. A 30% degraded TsFNMA photolysate was analysed by the same method, and a small peak was found at 20.4 min with a UV spectrum matching that of benzyl alcohol.

2.5.6 Molar absorption coefficients of 2,4-dinitrophenylhydrazine derivatives

The molar absorption coefficients of a range of DNP derivatives were calculated for comparison with formaldehyde DNP. The absorbance values at 354 nm were measured for 10^{-6} mol dm^{-3} solutions on a Kontron UVIKON 680 spectrophotometer. Samples were made up in 60% acetonitrile, 30% H_2O, 10% 0.1 M H_3PO_4. The same solvent mixture was used for the reference sample.

Table 2.10 Molar absorption coefficients of DNP derivatives.

DNP derivative	Concentration / 10^{-6} mol dm^{-3}	Absorbance at 354 nm	ε
formaldehyde	5.67	0.101	17813
methyl glyoxylate	7.20	0.167	23194
methyl phenylpyruvamide	7.67	0.146	19035
benzaldehyde	8.04	0.079 (0.138 @ 380 nm)	9826 (17164 @ 380 nm)
phenylpyruvic acid #1	4.39	0.063	14351
phenylpyruvic acid #2	3.86	0.062	16062

2.5.7 Acetone DNP

Low values for acetone DNP were confirmed to be due to the poor quantitation of acetone in aq. solution by DNP derivatisation. Comparison of the peak areas obtained for a solution of 1.36×10^{-3} mol dm^{-3} acetone in water derivatised by the usual procedure gave peak areas of approximately 4 times lower than that found from a synthesized sample; measured peak area: 15472208, calculated peak area: 57446536.

Chapter 3: The Photochemistry of Tosyl Amino Acids and Esters

3.1 Tosylglycine

3.1.1 Introduction

The purpose of this section is to describe in detail how one substrate was studied, before the results of all the other substrates are described, discussed and compared in later sections. The first compound chosen for study was the tosyl derivative of the simplest α-amino acid, glycine, i.e. *N*-*p*-tosylglycine (TsGOH, **16**). Glycine is the only naturally occurring α-amino acid that is not chiral, having only hydrogen atoms at the α carbon. The absence of a side-chain makes it the amino acid with the greatest amount of rotational freedom about its bonds. Being the simplest amino acid its derivatives are the most commonly studied. As described in Chapter 1, poor yields of around 5% have been obtained for both the photolysis of TsGOH and the DNMBS derivative of glycine in aqueous solution.[37,38] The addition of a sacrificial carboxylate on the arylsulfonyl moiety gave slightly improved yields of 10% which could be further improved by the use of electron donors.[26] All studies have found that the use of reducing agents gives improved yields. However, we wanted to perform our studies in aqueous solution in order to 1) facilitate PIET, 2) identify the major photoprocesses without any added complications, 3) be relevant to drug photostability.

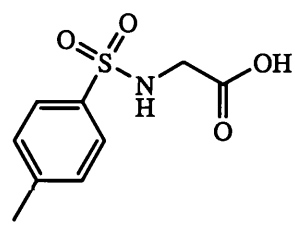

16

3.1.2 Methods

Full details are given in Chapter 2. TsGOH was irradiated in 10^{-2} mol dm^{-3} aqueous solutions that either had unadjusted pH (~3) or pH adjusted to 9. Product analysis was carried out by HPLC of the raw photolysates and derivatised samples, and by gas electrode measurements. Replicate experiments were performed to determine the reproducibility of the measurements and to calculate the errors. The results were plotted on graphs to identify a point early in the degradation where reliable data could be extracted to determine the product distribution.

The majority of compounds studied subsequently were sparingly soluble in water so for consistency it was decided to use solutions in aqueous acetonitrile for the majority of these photolyses. Acetonitrile is known to be inert under the photolysis conditions employed so was not expected to influence the product distribution. Further data were acquired for TsGOH in 40% acetonitrile/60% H_2O in order to verify that this was comparable to the data acquired in aqueous solution. These experiments revealed that the gas electrode methods could not be used for analyses of gaseous products in the photolysates performed in 40% acetonitrile/60% H_2O. New methods were developed and experiments were performed upon TsGOH to check that the results obtained by these methods were comparable to those obtained by the original methods.

3.1.3 Results

Aqueous solutions of TsGOH at pH 3 became cloudy upon irradiation and by the end of the irradiation the solutions had become opaque with a slightly creamy colouration due to a fine precipitate. The pH 9 solutions showed a similar colouration although no precipitate was observed. The extent of degradation at both pH values showed a linear increase up to ~ 30 min but slowed down after 30 min 66% in the acidic solution and 84% in the alkaline solution after 240 min. irradiation. The rate of degradation was not significantly affected by the pH of the solution (Figure 3.1), although the long irradiation times did give a higher degradation for the alkaline solution.

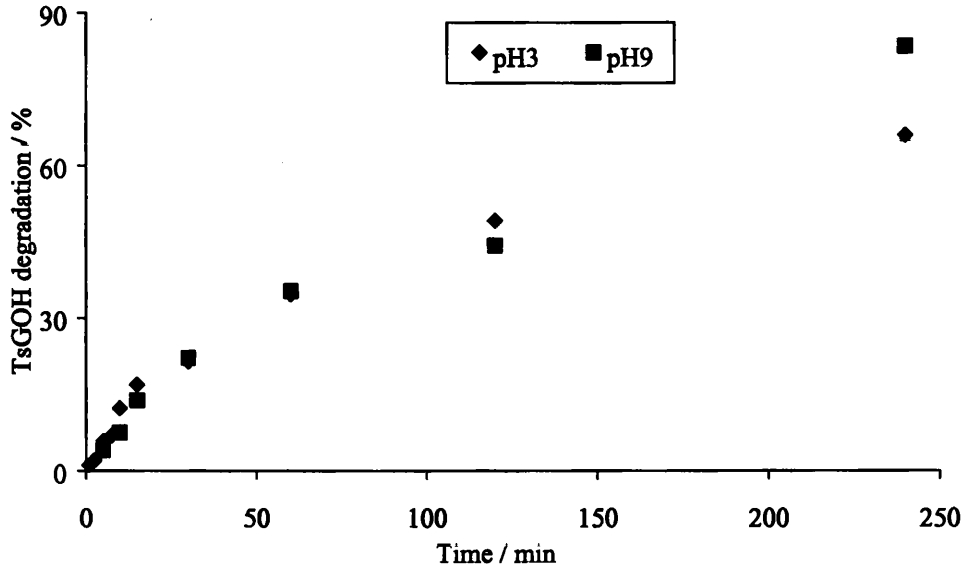

Figure 3.1 Comparison of TsGOH degradation rates at pH 3 and pH 9.

The aromatic products of the irradiations could be observed in a single chromatogram together with the starting material. A typical chromatogram with detection at 228 nm (Figure 3.2) shows that toluenesulfinic acid (TsH) was the major aromatic product of the irradiation. A number of other products were also identified: toluenesulfonic acid (TsOH), toluenesulfonamide ($TsNH_2$), tosylmethylamine ($TsNHCH_3$) and di-tosyldiethylenediamine ($(TsNHCH_2)_2$).

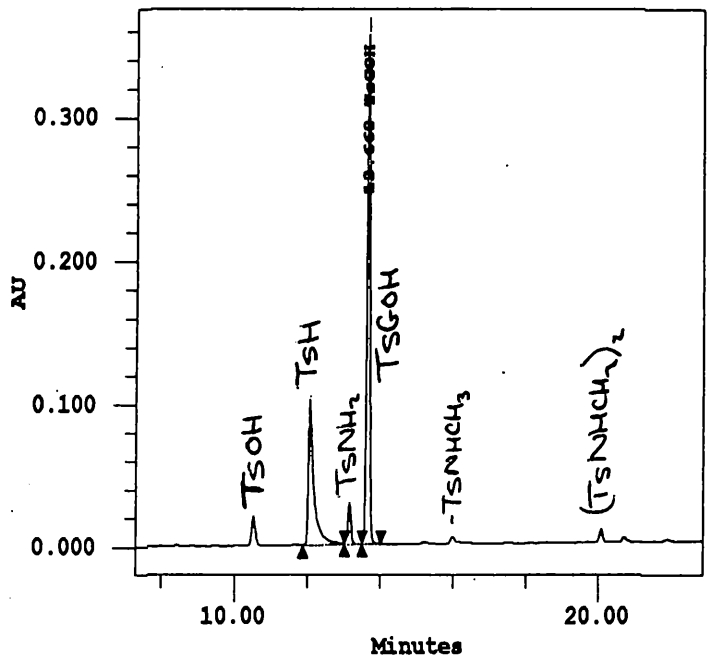

Figure 3.2 A chromatogram at 228 nm for the TsGOH irradiation.

Aldehydic compounds were identified separately as their 2,4-dinitrophenylhydrazine (DNP) derivatives. A typical chromatogram (Figure 3.3) with detection at 354 nm shows the major aldehyde to be formaldehyde (HCHO) at 23.5 min. An additional small DNP peak at 23 minutes was also observed. This peak has been identified as glyoxylic acid DNP by comparison of its retention time and UV spectrum with those of an authentic sample, and by coelution with a standard. Glycine, CO_2 and NH_3 were produced in both photolyses, although glycine was not measured at all degradation points.

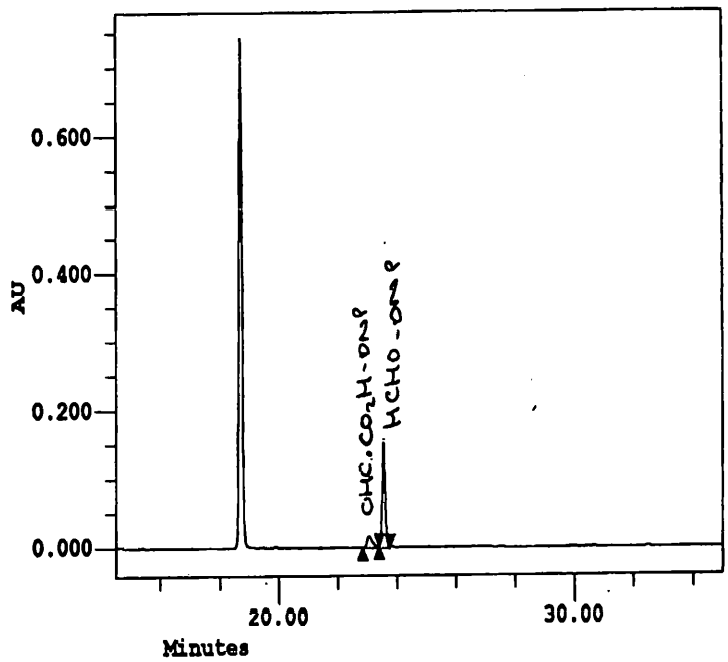

Figure 3.3 A chromatogram at 354 nm showing the DNP derivatives of TsGOH irradiation. The large peak at 19 min is unreacted DNP reagent.

A small amount of solid was isolated from the irradiated solution (pH 3) by centrifugation, giving a melting point in the range 145-160 °C. An NMR spectrum was obtained consistent with $TsNH_2$ as the major component and TLC analyses confirmed this assignment. HPLC analysis showed that a number of the other products already identified were also present. $(TsNHCH_2)_2$ is particularly insoluble in water and is therefore a likely component of the solid, although IR evidence was equivocal on this. The amount of precipitate is very small and is unlikely to affect the quantitation of products particularly in the early stages where no precipitate could be seen. It was thus decided not to pursue the identification of the insoluble material any further, as its identity was unlikely to be of much help in further clarification of the degradation pathways at early points of the degradation.

The mole fractions of each product were calculated at each degradation point and are given in Table 3.1 for the acidic solution, which does not account for any precipitate although as stated in the previous paragraph this is a minor amount and should

not greatly affect the mole fractions as calculated. Table 3.2 gives the mole fractions for the alkaline solution. Graphical plots of the product mole fractions against TsGOH degradation are shown in Figure 3.4 and Figure 3.5 for the acidic solution, and the analogous plots for the alkaline irradiation are shown in Figure 3.6 and Figure 3.7. The plots show that in general the mole fractions of products decrease with an increase in degradation. This is likely to be due to the photoinstability of some of the products. Hence, quantitation at an early stage is desirable. Comparison of the two experiments shows that the main differences are the higher mole fractions observed for CO_2 and TsH in the alkaline photolysis. The other products show a similar distribution for both experiments. Experiments with TsGOH in 40% aq. acetonitrile were compared with the results of the pH 3 aqueous solution. The degradation rate and the CO_2 mole fractions were similar, suggesting that the results from subsequent experiments with other compounds are comparable to those in aqueous solution. In these experiments CO_2 was measured by GC instead of the gas electrode, as in the aqueous measurements, thus verifying the validity of data obtained by the new GC method for CO_2.

Table 3.1 Product mole fractions for TsGOH aqueous photolysate, initially pH 3.[a]

Time/min	degradation/%	Product mole fractions									
		TsH	TsOH	$TsNH_2$	$TsNHCH_3$	$(TsNHCH_2)_2$	glycine	HCHO	glyoxylic acid	CO_2[b]	NH_3[b]
5	6	0.29	0.20	0.04	-	0.17	0.10	0.28	0.23	0.28	0.51
7.5	7	0.27	0.19	0.05	-	0.14	0.13	0.30	0.23	0.34	0.58
10	12	0.34	0.12	0.05	0.01	0.11	0.11	0.28	0.18	0.35	0.47
15	17	0.28	0.06	0.02	0.01	0.09	-	0.23	0.16	0.23	0.64
30	22	0.31	0.06	0.03	0.01	0.08	-	0.28	0.14	0.32	0.92
60	35	0.36	0.05	0.04	0.01	0.06	0.05	0.31	0.11	0.46	0.59
90[c]	53	0.38	-	-	-	-	-	0.26	-	0.49	1.00
120	49	0.34	0.06	0.05	0.01	0.05	-	0.30	0.10	0.54	0.73
240	66	0.32	0.05	0.05	0.01	0.03	-	0.21	0.07	0.31	0.81

[a] All values are the mean of two measurements unless otherwise stated. [b]Single measurement. [c]Separate experiment for error analysis involving 16 tubes

Table 3.2 Product mole fractions for TsGOH aqueous photolysate, initially pH 9.[a]

Time/min	degradation/%	Product mole fractions									
		TsH	TsOH	$TsNH_2$	$TsNHCH_3$	$(TsNHCH_2)_2$	glycine	HCHO	glyoxylic acid	CO_2[b]	NH_3[b]
5	4	0.92	0.09	0.10	0.09	0.14	n.m.	0.67	0.21	0.78	0.92
10	8	0.68	0.06	0.07	0.07	0.09	n.m.	0.51	0.13	0.80	0.68
15	14	0.49	0.04	0.05	0.05	0.05	n.m.	0.37	0.08	0.52	0.63
30	22	0.62	0.03	0.05	0.06	0.05	n.m.	0.35	0.07	0.87	0.66
60	35	0.61	0.03	0.05	0.05	0.03	n.m.	0.29	0.04	1.01	0.67
120	44	0.55	0.04	0.04	0.05	0.03	n.m.	0.33	0.03	1.08	0.56
240	84	0.44	0.02	0.04	0.02	0.01	n.m.	0.13	0.01	0.98	0.60

[a] All values are the mean of two measurements unless otherwise stated. [b]Single measurement. n.m. = not measured

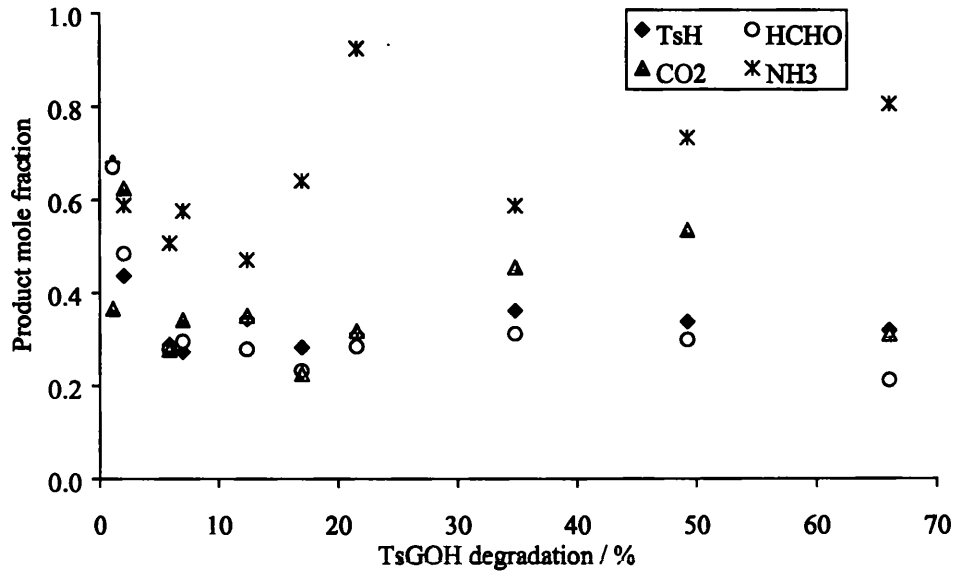

Figure 3.4 Aqueous TsGOH (pH 3) major product mole fractions.

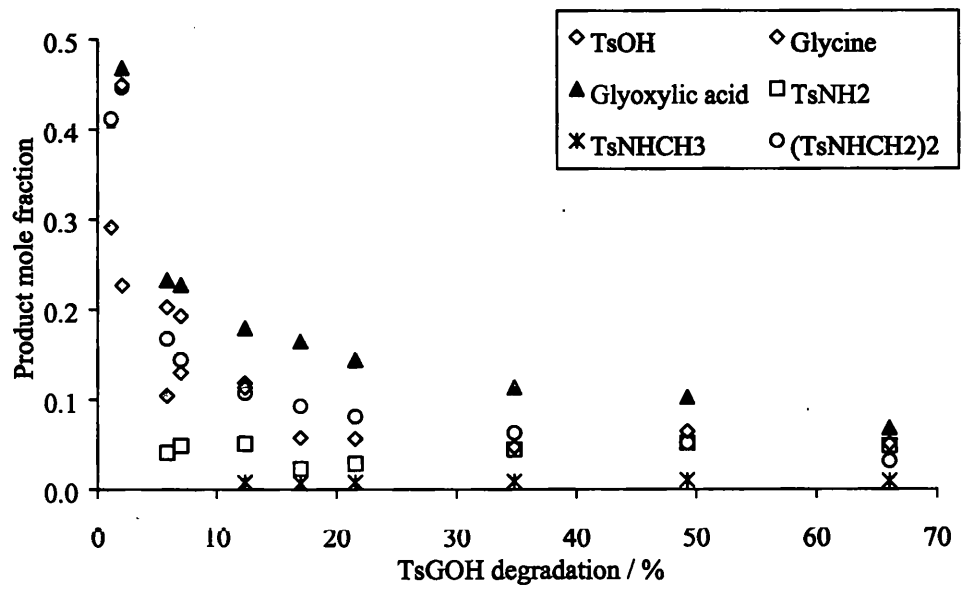

Figure 3.5 Aqueous TsGOH (pH 3) minor product mole fractions.

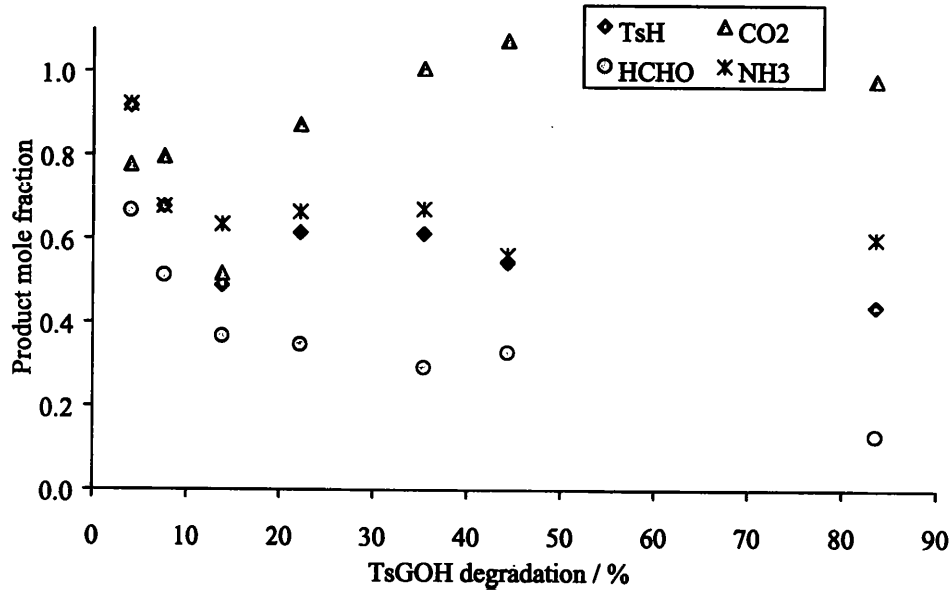

Figure 3.6 Aqueous TsGOH (pH 9) major product mole fractions.

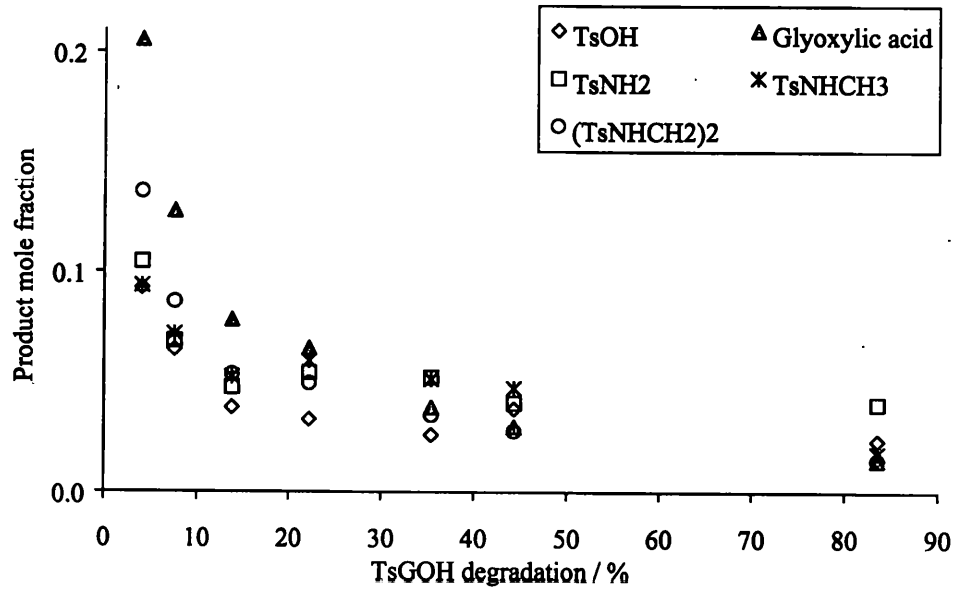

Figure 3.7 Aqueous TsGOH (pH 9) minor product mole fractions.

3.1.4 Discussion

Figure 3.1 confirms that the rate of the photochemical reaction is independent of pH and is primarily dependent upon the rate of absorption of radiation. However, the product data show that the pathways observed are partly dependent upon pH. An initial tentative working hypothesis for a degradation pathway consistent with the results for 7% degradation at pH 3 (red) and pH 9 (blue) is shown in Scheme 3.1. As will be seen shortly, the value assigned to each route corresponds to the observed yields of uniquely associated products. The accumulated values for products obtained by more than one pathway are in reasonable agreement with those obtained from the analyses e.g. in the pH 9 photolyses TsH and NH_3 had measured values of 68% and predicted values of 64% according to Scheme 3.1, whilst the corresponding values for CO_2 were 80% and 67% respectively.

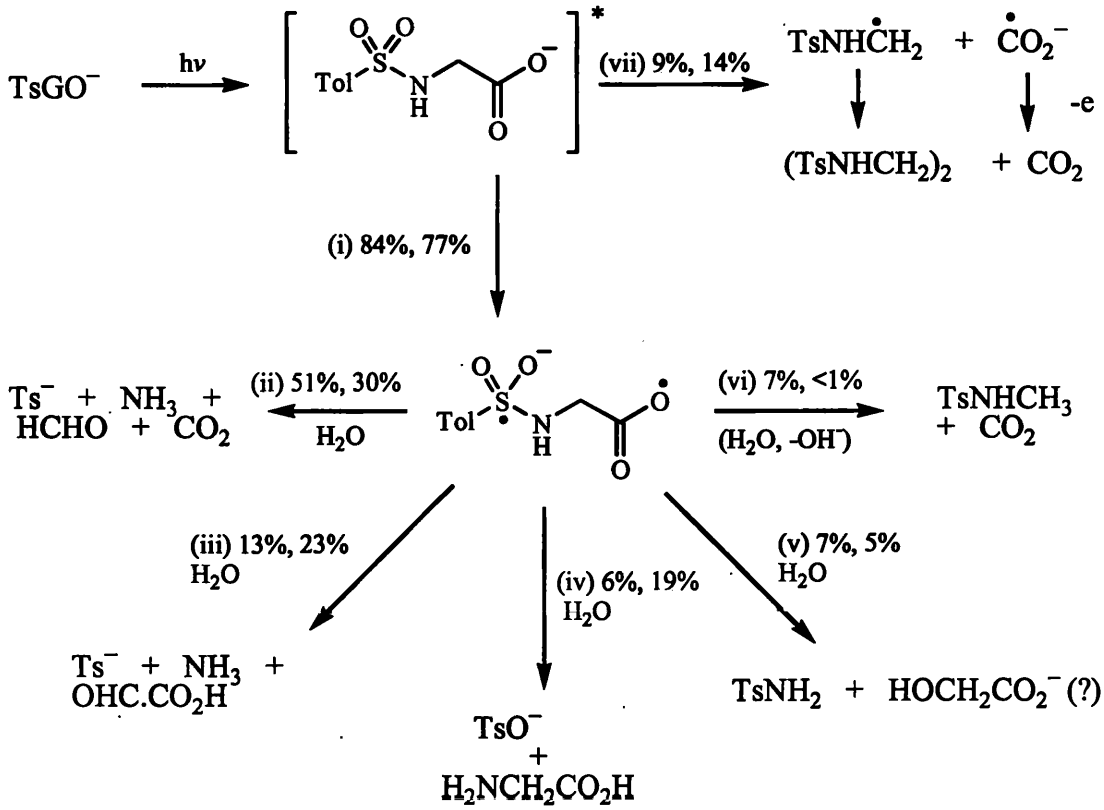

Scheme 3.1 Possible pathways of photodegradation of TsGOH (shown as the anion) at 7% degradation and accountancy for product distributions in pH 3 (red) and pH 9 (blue) aqueous photolysates.

Scheme 3.1 proposes two principal routes from the excited state. The major pathway (i) is prompted by the known behaviour of the arylsulfonyl group discussed in Chapter 1 to behave as an electron acceptor, and suggests electron or hydrogen transfer (depending upon conditions) from the carboxylate group to the sulfonyl group giving a biradical intermediate. There are a number of possibilities from this intermediate. The plots of mole fractions and the correlation coefficients support our hypothesis that the major degradation pathway from this intermediate (ii) is the production of TsH, CO_2, NH_3 and HCHO via homolytic bond cleavages that lead to some of the observed products plus an aldimine precursor of NH_3 and formaldehyde (Scheme 3.2). It is also possible that the products may be formed from a seven-membered transition state if the carboxylate group is protonated. However, as this route accounts for more of the degradation in alkaline solution than in acidic solution an electron transfer route seems more probable.

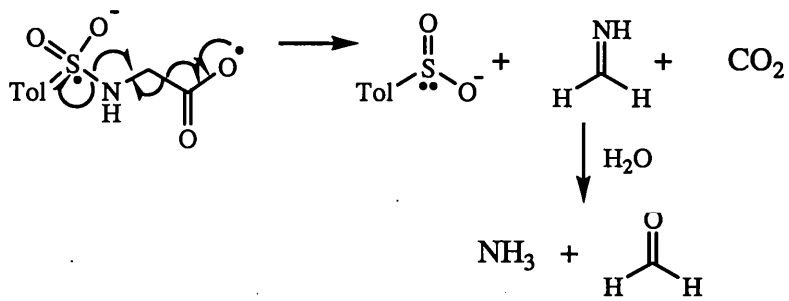

Scheme 3.2 Cleavage of bonds in the biradical intermediate for TsGOH to give the major products.

The next most important route (iii) gives glyoxylic acid, which can also be derived from the biradical intermediate via hydrogen transfer from the α-C to a sulfonyl oxygen and collapse of the biradical to give the products or precursors (Scheme 3.3).

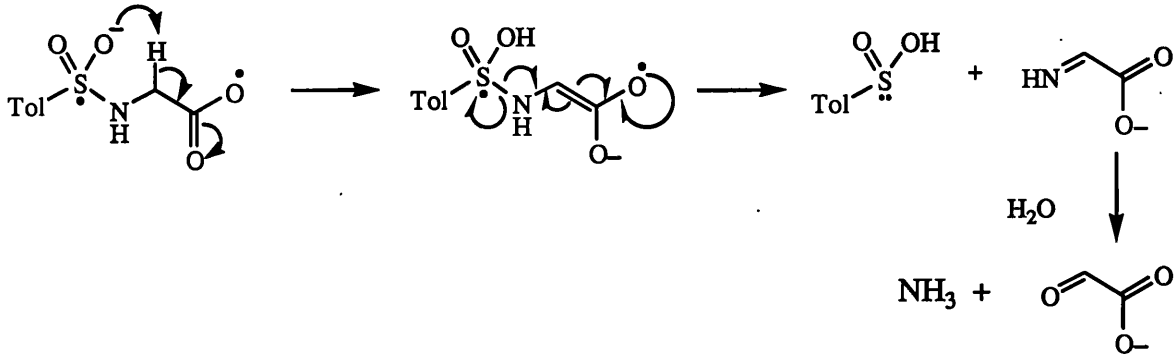

Scheme 3.3 Formation of glyoxylic acid and co-products from the biradical intermediate.

An alternative mechanism does not require ET but α-H abstraction in the excited state to give the initially formed products (Scheme 3.4). This is similar to a mechanism proposed by Jenks and co-workers for sulfone compounds in thermolysis reactions where the hydrogen atom may be in a suitable conformation to form a five-membered transition state with an oxygen atom of the sulfone.[84] This mechanism can be tested for tosylated compounds by the use of bulky side-chain groups at the α-C as described later. We generally favour the ET route for the photochemical reaction, however, as it involves a common intermediate to plausible pathways of the majority of the observed products rather than many disparate pathways.

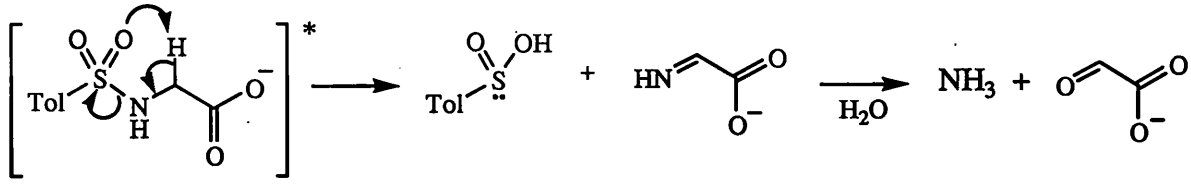

Scheme 3.4 Formation of glyoxylic acid and co-products from the excited state by C_α-H abstraction.

Glyoxylic acid was analysed as the two stereoisomers of its DNP derivative. It has been known for a long time[85] that *syn* and *anti* stereoisomers of carbonyl DNP derivatives are formed by the traditional method of preparation i.e. Brady's reagent (2,4-

dinitrophenylhydrazine in 2M HCl). The lone pair on the nitrogen can be either *syn* or *anti* to the smallest group of the carbonyl compound. A recent study[86] that investigated a wide range of carbonyl DNP derivatives by LC-MS with photodiode array detection, reported stereoisomers that were separable for α,β-unsaturated carbonyls and carbonyls with other oxygen-bearing substituents. Symmetrical ketones will give a single peak but it is possible that *syn* and *anti* stereoisomers are produced with unsymmetrical carbonyl compounds even if they do not have sufficiently different properties to elute at different RT. For all carbonyls, two peaks were observed if there was a polar substituent. As we shall see in subsequent sections, many examples have been found of separable stereoisomers by HPLC analysis during the course of this project.

The other routes suggested for TsGOH may explain how some minor products can also be derived from the biradical intermediate formed after ET in the excited state. A net S-N hydrolysis giving TsOH and glycine (iv) could occur via a cyclic intermediate (Scheme 3.5), which as we shall see is analogous to a mechanism suggested for peptide bond cleavage (Section 4.3.3). The yields for the production of the free amino acid, which shall be referred to as a S-N cleavage from hereon, are low, only 19% in acidic solution or 6% in alkaline solution as calculated from the yields of TsOH. Glycine is slightly lower for the acidic solution and was not measured in alkaline solution so assumed to be the same as for TsOH. The poor yields contrast with those found in the photodeprotection studies (Chapter 1) where reducing agents compensated for the oxidising component of the ET process to give higher yields.

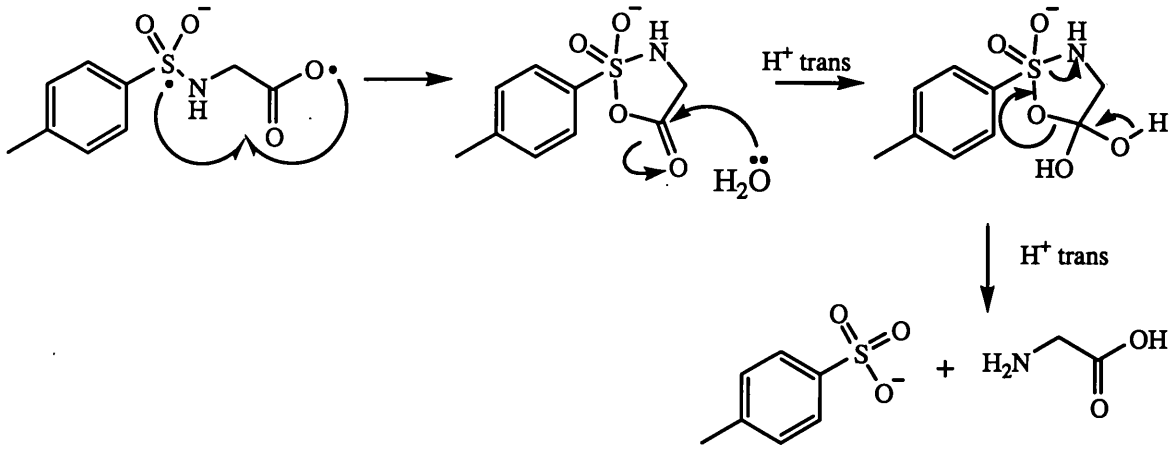

Scheme 3.5 Mechanism for S-N cleavage to give glycine and TsOH.

$TsNH_2$ could be the outcome of a net hydrolysis of the C-N bond (v), although its anticipated co-product glycollic acid was not detected (the concentration would be below our levels of detection). A speculative mechanism is shown in Scheme 3.6.

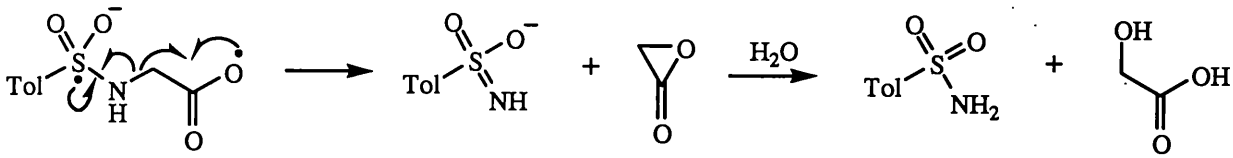

Scheme 3.6 A possible mechanism for $TsNH_2$ formation.

Loss of CO_2 alone would give $TsNHCH_3$ (vi), while the related dehydrodimer may result from reaction (vii) and involve C-C homolysis to give two radicals, with the dimerization of the relatively stable α-amido radical and facile oxidation of the formate radical to CO_2 by an unknown constituent.

One way of testing whether two products are produced by the same route is to plot the concentration of one against the other for each point in the degradation. The equation obtained for a linear trendline ($y = mx + c$) will show how good the correlation between the two products is (R^2), whilst a value for the gradient (m) of close to 1 indicates that the two products may be produced together and a value for the intercept (c) of close to zero indicates that were initially produced at the same time. These values have been

obtained for the graphical analysis of the results from the TsGOH photolyses early in the degradation (up to 30%). A typical plot is shown in Figure 3.8. The correlations are summarised in Table 3.3 for the pH 3 irradiation, and Table 3.4 for the pH 9 irradiation.

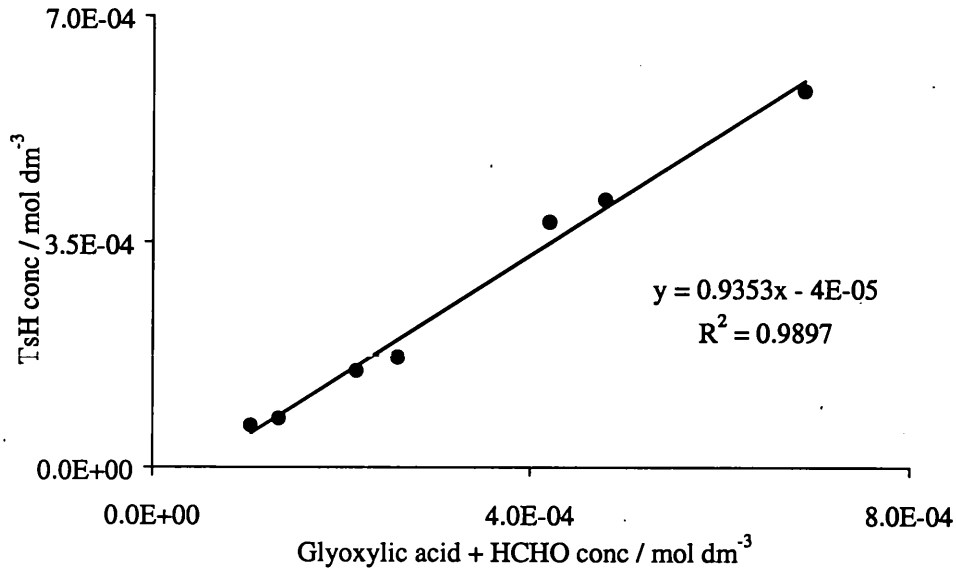

Figure 3.8 Correlation plot for TsH vs glyoxylic acid and HCHO at < 30% degradation.

Table 3.3 Correlations for the pH 3 aqueous TsGOH irradiation.

Products			R^2	Gradient	Intercept
TsH	vs	NH_3	0.92	0.32	0.00007
TsH	vs	Glyoxylic acid + HCHO	0.98	0.94	-0.00005
HCHO	vs	CO_2	0.98	0.82	0.000009
NH_3	vs	Glyoxylic acid + HCHO	0.93	2.63	-0.0003
TsOH	vs	Glycine	0.82	0.57	0.00006

[a]The first product is taken to be the *y*-axis and the second product(s) to be the *x*-axis

Table 3.4 Correlations for the pH 9 aqueous TsGOH irradiation.

Products			R^2	Gradient[a]	Intercept
TsH	vs	NH_3	0.98	0.83	0.0001
TsH	vs	Glyoxylic acid + HCHO	0.93	1.78	-0.0003
HCHO	vs	CO_2	0.97	0.30	0.0002
NH_3	vs	Glyoxylic acid + HCHO	0.99	1.65	-0.0002

[a]The first product is taken to be the *y*-axis and the second product(s) to be the *x*-axis

The best correlation in alkaline solution is that between TsH and NH_3 supporting their release by the same pathways (i, ii). The poor correlation coefficient observed for TsOH and glycine may betray some adventitious oxidation of TsH. The worst is that observed for CO_2 with HCHO at pH 9 supporting the evidence for additional decarboxylation by the two other routes (vi, vii). NH_3 and CO_2 would not be degraded under the photochemical conditions whereas the organic products may be, leading to poor correlation coefficients for associated products.

The intercepts are all very close to zero supporting the proposed co-products. However, the lowest concentration of products detected is usually in the region of 10^{-5} M so the value of interpreting the intercept values may be limited. But a point worthy of mention is the intercept values obtained for correlations involving NH_3. This is a product of a secondary process involving hydrolysis of an imine precursor, and as such its mole fraction may be expected to be less than those of the co-products which are formed in the initial step, such as TsH, or can be detected from the imine precusor as the DNP derivative, as is the case for HCHO and glyoxylic acid. In all such cases the intercept values predict the formation of NH_3 starting at a later point than the associated product(s).

A gradient of close to one is found in the acidic photolysis for the correlation between TsH and the two aldehyde products supporting TsH as being the co-product of the other two. However, a poor correlation for the same products was found in the alkaline solution which may suggest that TsH was degraded under these conditions. The correlations between NH_3 and the two aldehyde products support the later production of NH_3 by a hydrolysis reaction as discussed above. Similar comparisons can be made for all the values in the two tables, which in general support the proposed degradation scheme.

The mass balance at a given point of the degradation may be determined by considering the individual product mole fractions at that point. The mole fraction for each product at 7% and 20% degradation are shown in Table 3.5. The mass balance is calculated by using values for products that are unique to a particular pathway as suggested in Scheme 3.1. While a high mass balance is found early in the degradation process,

quantitation at higher percentage conversion is more accurate but then there is more scope for the complication by secondary processes leading to a lower mass balance.

Table 3.5 Mole fractions of TsGOH at ~7 % and ~20 % degradation.

Product	~7 % degradation[a]		~20 % degradation[b]	
	pH 3	pH 9	pH 3	pH 9
TsH	0.27	0.68	0.31	0.62
HCHO	0.30	0.51	0.29	0.35
CO_2	0.34	0.80	0.32	0.87
NH_3	0.58	0.68	0.50	0.66
glyoxylic acid	0.23	0.13	0.14	0.07
TsOH	0.19	0.06	0.06	0.03
$(TsNHCH_2)_2$	0.14	0.09	0.08	0.05
$TsNH_2$	0.05	0.07	0.03	0.05
$TsNHCH_3$	0	0.07	0.01	0.06
glycine	0.13	Not measured	0.08	Not measured
Mass balance[c]	0.91	0.93	0.60	0.61

[a]Error < ± 0.04. [b]Error < ± 0.02. [c]According to Scheme 3.1 error < ± 0.11 and ± 0.6 at 7 and 20% degradation respectively.

The higher mole fractions for TsH and HCHO in alkaline solution are evidence for hydrogen transfer being less competitive than electron transfer to the sulfonyl group when the molecule is deprotonated. The higher value for $TsNHCH_3$ and CO_2 shows that alkaline solution also enhances decarboxylation, again supporting electron transfer as the mechanism for initiating degradation.

3.1.5 Conclusions for TsGOH

The photolyses of TsGOH under various conditions; acidic, alkaline and 40% acetonitrile have shown the same products, although a slightly different distribution of products was seen at pH 9 than at pH 3 with the decarboxylation products becoming more significant. This is consistent with PIET being more favourable from the anion than the protonated carboxylate, although a considerable amount of the substrate is likely to be deprotonated even at pH 3. We have suggested that an initial ET in the excited state

produces a biradical intermediate which is able to react in a variety of ways to give most of the observed products. The major reaction of TsGOH has given TsH, formaldehyde, NH_3 and CO_2 as the photoproducts. However, we have also postulated some alternative mechanisms that can explain the products without invoking an initial ET but would require specific conformations of the molecule for the reactions to occur.

In the next section we examine the effects of having a more restricted conformational space upon these reactions by the introduction of aliphatic side-chains. If a particular alignment of orbitals is required then the yields may show a dependence upon the conformational space of the molecule. Subsequent sections examine the effects of potential electron donors or reactive groups in the amino acid side-chain upon the course of the photodegradation. The last two sections of this chapter investigate the effects of increasing the distance between the carboxylate and sulfonyl moieties, and having an ester instead of a carboxylate at the C terminus. Chapter 4 then extends this work to be applicable to peptide-like molecules by studying compounds with amide bonds including four tosyl dipeptides.

3.2 Aliphatic side-chains

3.2.1 Introduction

Now that we have comprehensive product data for TsGOH we shall look at the effects of side-chain structure on the product distribution. Reactive side-chains have the potential to participate in the photochemistry and may provide a complex mixture of products. Hence, amino acids with aliphatic side-chains were chosen initially in an attempt to look only at conformational effects. Three compounds were chosen to investigate different aspects of the effect of the side-chain structure upon the course of the photodegradation. The first was *N*-*p*-tosylvaline (TsVOH, **17**) which has a bulky *iso*-propyl side-chain that reduces the amount of conformational freedom the molecule has compared with TsGOH, and has side-chain methyl and methine hydrogens that may

participate in the photodegradation processes. The second was *N-p*-tosylproline (TsPOH, **18**) which has a three carbon side-chain attached to the nitrogen atom of the amino acid forming a five-membered ring. This has three consequences, the first being a restriction in the conformations the molecule can adopt, secondly the absence of a hydrogen atom on the nitrogen and thirdly there are now two hydrogen bearing carbon atoms α to the nitrogen. The last tosyl α-amino acid studied with an aliphatic side-chain was *N-p*-tosyl-2-amino-*iso*-butyric acid (TsAibOH, **19**), which contains the unnatural α-amino acid, 2-amino-*iso*-butyric acid that has two methyl groups at the α-C position. TsAibOH was studied primarily to look at the effect of the absence of a hydrogen atom at the α position.

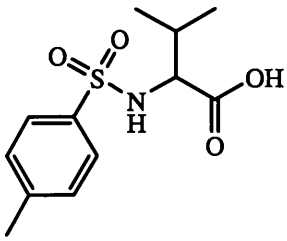

17

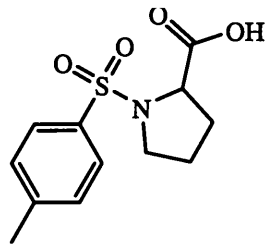

18

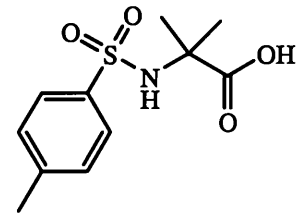

19

To our knowledge, these compounds have not been studied photochemically in the past, although the amino acids themselves are frequently components of molecules for PIET studies as shown in Chapter 1. A compound similar to TsVOH, tosylleucine, was studied by D'Souza and Day, who gave a yield of 22-48% for the amino acid upon photolysis.[25] Tosylleucine has an additional CH_2 in the side-chain compared with TsVOH and the photolyses were performed in aqueous solution so we may expect a similar result for TsVOH. It has been shown that the side-chain hydrogen atoms of amino acids are more labile to attack by hydroxyl radicals than the C_α-H,[87] hence we may see some side-chain involvement with these compounds.

After a brief overview of the methods used we will look at the results obtained for each of these three compounds and compare them with TsGOH. From this point

forward we shall assume that the substrates are in the deprotonated form, as the pK_a of the free amino acid carboxylate is ~2 and the substrate solutions had an apparent pH of ~3.

3.2.2 Method summary

The substrates were irradiated at a concentration of 10^{-2} mol dm^{-3} in 40% acetonitrile/60% H_2O solution that were pH unadjusted. Product analyses were carried out by the methods used for TsGOH with minor modifications i.e. HPLC of the raw photolysates and derivatised samples, and GC analysis for CO_2 all as described in Chapter 2. Products were identified and quantified by comparison with authentic standards where available or by comparison with an analogue that had similar UV absorption properties in HPLC. The data were plotted on graphs to identify a point early in the degradation where reliable values could be extracted for product distribution.

3.2.3 General observations for TsVOH, TsPOH and TsAibOH

The TsVOH solutions became cloudy initially and by the end of the irradiation, had become opaque with a slightly cream colouration. The TsPOH and TsAibOH solutions remained clear and colourless throughout the photolyses. The changes in the apparent pH and the percentage degradation after 60 mins irradiation are shown in Table 3.6. A comparison of the degradation rate with that of TsGOH in aqueous solution is shown in Figure 3.9.

Table 3.6 Change in apparent pH and conversion at 60 min irradiation.

Substrate	Initial apparent pH	Apparent pH at 60 min	Degradation at 60 min/%
TsVOH	3.3	3.6	36
TsPOH	n.m.	n.m.	65
TsAibOH	3.3	3.5	38

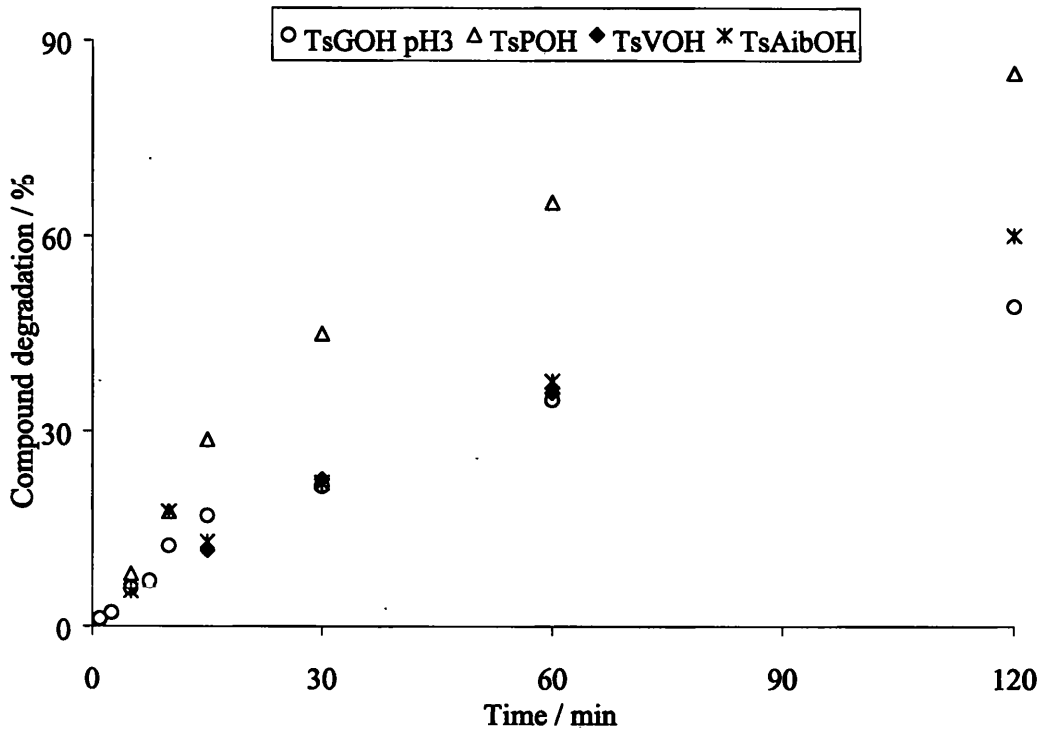

Figure 3.9 Comparison of the degradation rates of TsVOH, TsPOH and TsAibOH with TsGOH.

3.2.4 *N-p*-tosylvaline

HPLC analysis of the raw photolysate with detection at 228 nm showed that TsH was the major aromatic product of the irradiation. The only other aromatic product was TsOH. Analysis for DNP derivatised compounds with detection at 354 nm showed the major aldehyde product to be *iso*-butyraldehyde, which was identified by comparison of its DNP RT and UV spectrum with those of an authentic sample, and by coelution with an authentic sample. An additional DNP peak was also observed at 20.6 minutes but was not identified. It was tentatively quantified using a HCHO DNP standard. Valine, CO_2, NH_3 and *iso*-butylamine were quantified by AccQTag™ (see Chapter 2). Another peak was found in the AccQTag™ analysis at 16.9 min which could not be identified. The mole fractions of products identified by HPLC are given in Table 3.7, and CO_2 mole fractions are given in Table 3.8 and their relationship to TsVOH degradation is shown in Figure

3.10. The plot shows that in general the mole fractions of products decrease with an increase in degradation like those of TsGOH.

Table 3.7 Product mole fractions for TsVOH.

Time/ min	Degradation/%	Product mole fractions						
		TsH	TsOH	NH_3	valine	*iso*-butylamine	*iso*-butyraldehyde	20.6 min DNP[a]
15	12	0.60	0.09	0.63	0.02	0.05	0.69	0.12
30	23	0.57	0.09	0.69	0.02	0.05	0.60	0.10
60	36	0.56	0.09	0.74	0.02	0.05	0.55	0.09

[a]Quantified using a HCHO DNP standard

Table 3.8 CO_2 mole fractions for TsVOH.

Time/min	Degradation/%	CO_2 mole fraction
5	6	0.73
10	9	0.92
15	13	0.91
30	23	0.78
60	47	0.62
120	60	0.87

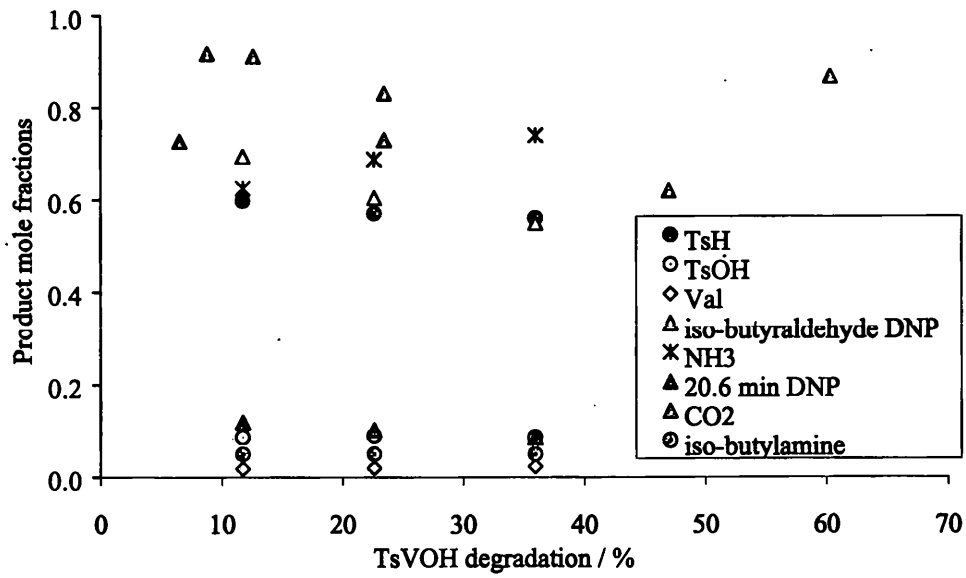

Figure 3.10 The product mole fractions from TsVOH photolysis.

The rate of degradation for TsVOH is similar to that of TsGOH at pH 3, as verified by a control experiment for TsGOH to ensure that the acetonitrile had no effect upon the rate or products. A slight colouration was observed upon photolysis but little or no precipitate was seen in 40% aq. acetonitrile. The change in apparent pH was minor.

The product data and the plots of product mole fractions for TsVOH show that the major products are TsH, NH_3 and *iso*-butyraldehyde in 60-70% yield and CO_2 in 60-90% yield. This suggests that the major route of degradation for TsVOH is analogous to TsGOH, with *iso*-butyraldehyde observed instead of formaldehyde. Consideration of the product mole fractions of a 12% degraded sample supports the proposal of a degradation scheme for TsVOH analogous to that of TsGOH. The analogue to glyoxylic acid would be 3-methyl-2-oxo-butanoic acid which may be the unidentified DNP derivative that was found in a similar yield to glyoxylic acid (~12%). TsOH and valine were both found although the former in higher yields than the latter, 9% and 2% respectively. This may be explained by decarboxylation of TsVOH to give tosyl-*iso*-butylamine and CO_2. Photolysis of the former yields TsOH and TsH which, as we shall see in Section 4.3.7, are the major products of the photodegradation of tosyl alkyl amines. This pathway accounts for some of the additional CO_2 that is not accounted for by this scheme and the higher mole fraction of TsOH compared with valine. In contrast to TsGOH, no $TsNH_2$ was found, possibly indicating a steric influence. A degradation scheme (Scheme 3.7) is suggested at ~12% degradation which shows that we can account for 95% of the degraded substrate.

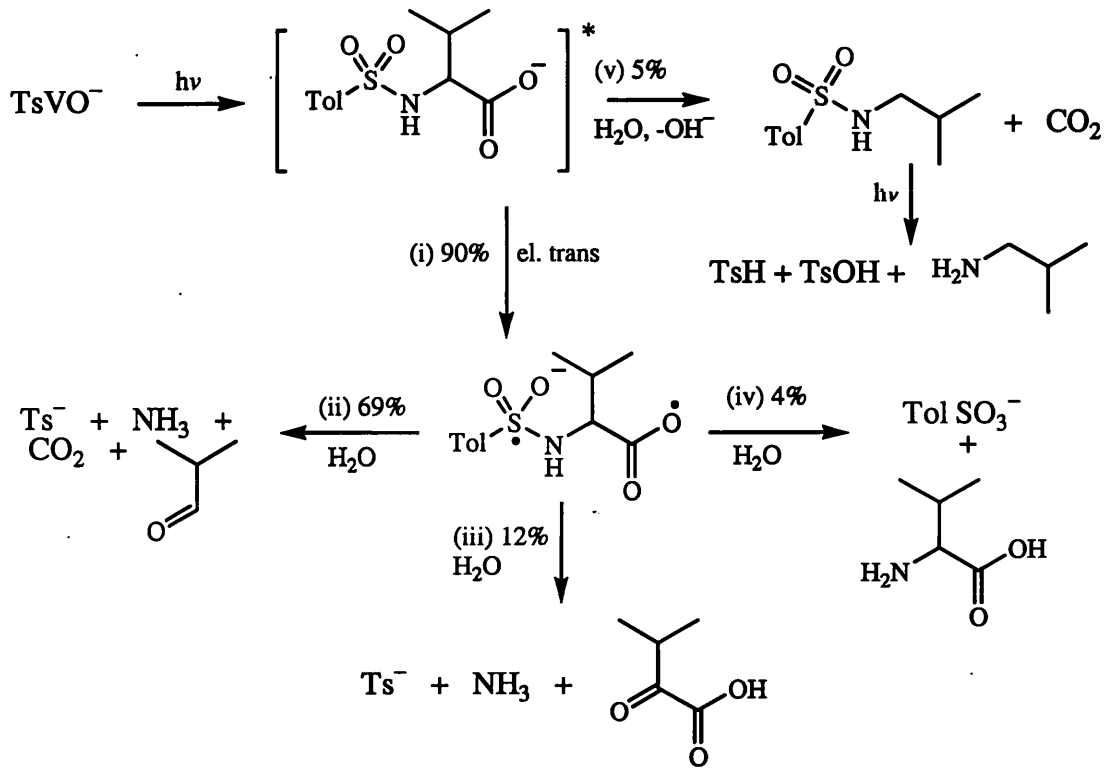

Scheme 3.7 Possible pathways of photodegradation of TsVOH at 12% degradation with accountancy for product distribution.

The degradation scheme accounts for most of the observed products by initial ET in the excited state to give a biradical intermediate that undergoes three separate pathways to the products in approximately the same yields as those observed for TsGOH. The formation of tosyl-*iso*-butylamine would be analogous to tosylmethylamine in TsGOH but it could not be found in the HPLC chromatograms and was assumed to be formed based upon the observation of *iso*-butylamine. It is possible that the known photodegradation of the tosylated amine (Section 4.3.7) occurs faster than that of the substrate.

Another possible route of degradation for TsVOH would involve the side-chain CH which has been shown in valine to be more susceptible to hydroxyl radical attack than the α-CH.[87] Nukuna *et al.* did a study of $^{1}H/^{2}H$ exchange, which showed that whilst the α-H in Ala and Gly was susceptible to hydroxyl radical abstraction, the side chain

hydrogens of other amino acids are more prone to abstraction than the α-H due to deactivation of the latter by the carboxylate group. On this basis we might expect the side-chain CH to be cleaved in a Norrish type II mechanism involving a six-membered transition state to give $TsNH_2$ as one of the products (Scheme 3.8). However, we did not find any $TsNH_2$ so it seems that the side-chain is not involved in the photodegradation of TsVOH unlike the parent valine. As will be seen later we have looked for the α,β-unsaturated photoproduct with a number of substrates and have not found any evidence for its formation.

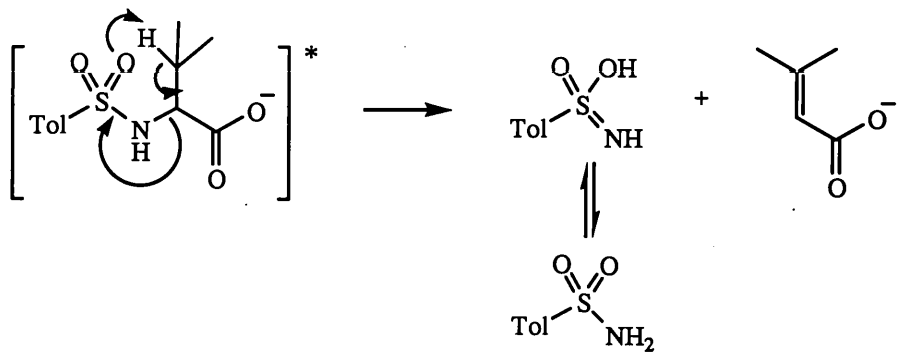

Scheme 3.8 A possible mechanism for production of $TsNH_2$ involving a six-membered transition state and the side-chain hydrogens.

It appears that the bulky side-chain of TsVOH does not significantly change the product distribution and the products can be accounted for by the same mechanisms suggested for TsGOH. So the limited conformational space of this molecule can still accommodate the same type of photochemistry.

3.2.5 *N-p*-tosylproline

HPLC analysis of the raw photolysate with detection at 228 nm showed that TsH and TsOH were again the major aromatic products of the irradiation. Two other peaks were found in the HPLC analysis at 13.7 and 16.7 min which had λ_{max} 223 and 228 nm respectively indicative of a tosylated compound, so they were tentatively quantified using a

TsPOH standard. Analysis for DNP derivatised compounds with detection at 354 nm showed a number of small peaks that were not identified but were tentatively quantified using a HCHO DNP standard. These had retention times of 7.3, 7.8, 7.9 and 15.8 min. The first three are shorter RT than any of the authentic compounds analysed previously and are therefore likely to be very polar molecules.

There were a number of other unidentified products in the photolysates including some AccQTag™ derivatives with RTs of 12.9, 14.6, 16.7 and 17.7 min. The product mole fractions are summarised in Table 3.9 although some of the minor unidentified ones have been omitted and CO_2 mole fractions are given separately in Table 3.10. The data are presented graphically in Figure 3.11, which shows a similar pattern to TsGOH.

Table 3.9 Product mole fractions for TsPOH.

Time/ min	Degradation/ %	Product mole fractions								
		TsH	TsOH	$TsNH_2$	13.7 min[a]	16.7 min[a]	NH_3	7.3 min DNP[b]	7.8 min DNP[b]	7.9 min DNP[b]
5	8	0.50	0.67	0.00	0.00	0.03	0.10	0.04	0.43	0.32
10	17	0.38	0.49	0.02	0.00	0.03	0.07	0.03	0.10	0.10
15	28	0.29	0.41	0.01	0.00	0.03	0.11	0.03	0.05	0.05
30	45	0.27	0.40	0.01	0.02	0.03	0.10	0.03	0.07	0.04
60	65	0.22	0.40	0.01	0.02	0.03	0.11	0.03	0.02	0.03
120	85	0.15	0.31	0.01	0.02	0.03	0.11	0.03	0.01	0.01

[a]Quantified from TsPOH, [b] quantified from HCHO DNP.

Table 3.10 CO_2 mole fractions for TsPOH

Time/min	Degradation/%	CO_2 mole fraction
5	10	0.55
10	23	0.40
15	21	0.65
30	34	0.62
60	57	0.74
120	81	0.76

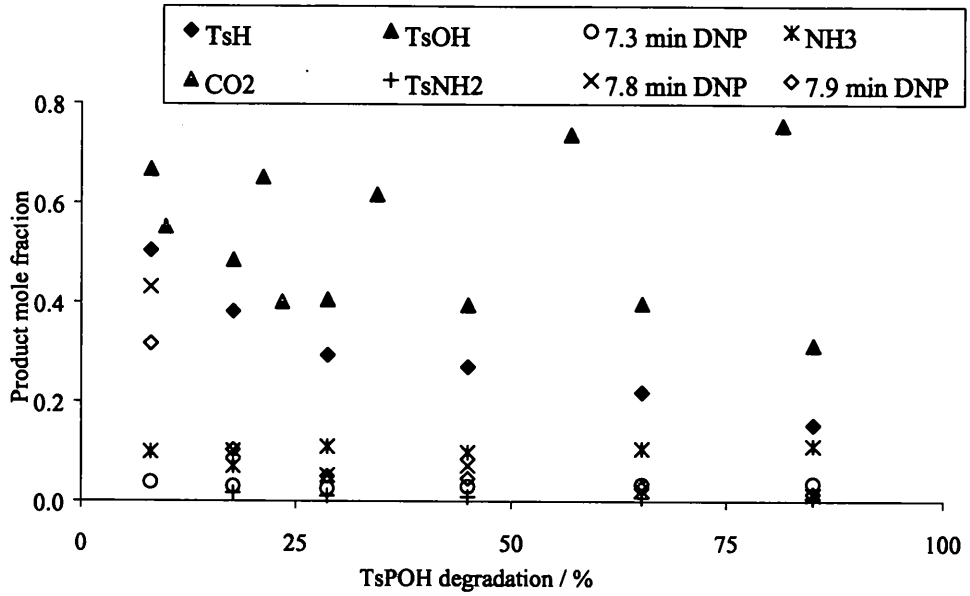

Figure 3.11 Product mole fractions for TsPOH.

The rate of degradation for TsPOH was higher than previous compounds indicating that the tertiary sulfonamide may be a better absorber. Subsequent compounds support this reason as will be seen later. A slight colouration occurred with photolysis but little or no precipitate was seen in 40% aq. acetonitrile.

At 18% degradation the major product of TsPOH photolysis is CO_2 (65%) suggesting that the main route for degradation involves decarboxylation of the molecule. Assuming that the same mechanism can be applied as for TsGOH, then the co-products should be TsH and 4-aminobutanal (Scheme 3.9). The imine precursor may be hydrolysed prior to derivatisation with the DNP reagent; however, NH_3 would not be formed unlike the previous examples as only one N-C would break and the nitrogen would remain attached to the carbon chain. TsH was found in only 38% yield and three DNP derivatives were observed in a combined yield of 23%, any of which could be 4-aminobutanal DNP that may even give two separable stereoisomers by HPLC. The two largest DNP peaks account for only 10% each of the degraded material, although it is possible that the suggested products are unstable in aqueous solution or in the DNP reagent solution. It is also possible that oligomerisation may occur due to the presence of the two reactive functional groups and hence the compound is detected by the method used.

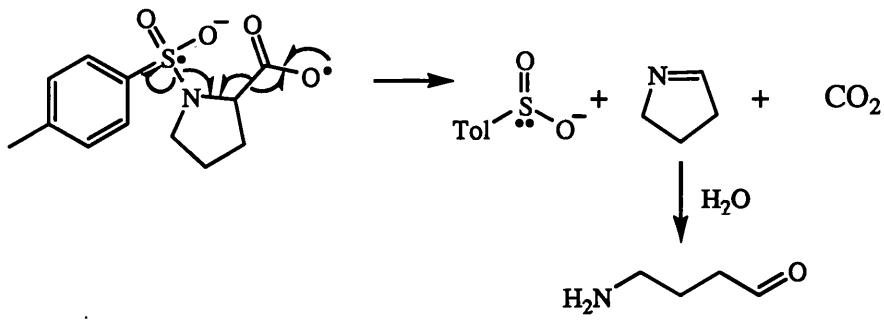

Scheme 3.9 Cleavage of bonds in the biradical intermediate for TsPOH to give the major products expected by comparison with previous compounds.

The unaccounted for DNP peak or peaks could be the analogue of glyoxylic acid DNP stereoisomers formed by α-H abstraction in the biradical intermediate (Scheme 3.10). Again no NH_3 would be formed. Assuming that the scheme for TsGOH can be applied to TsPOH we would expect a mole fraction of ~12%. One of the major DNP peaks plus the small one does indeed give 13% although the identity has not been confirmed.

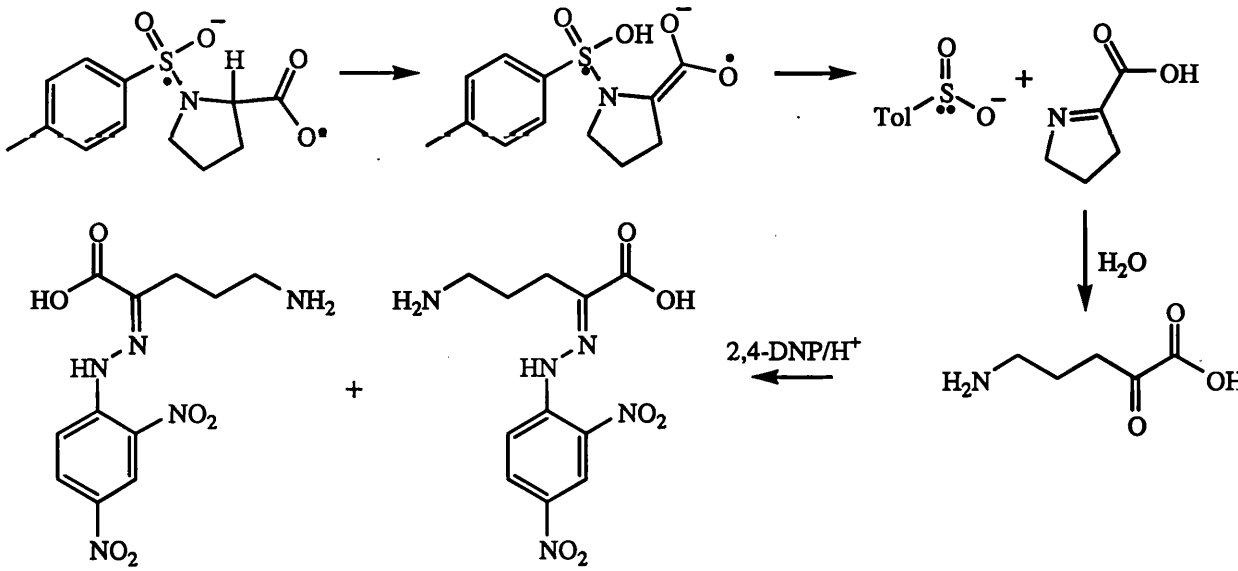

Scheme 3.10 A possible cleavage of bonds in the biradical intermediate of TsPOH to give a product analogous to glyoxylic acid that reacts with DNP reagent.

TsOH was found in 49% yield but no proline was found. A possible reason for the lack of proline may be that TsPOH is readily decarboxylated and the tosylpyrrolidine

that forms was photodegraded by a radical mechanism and disproportionates to give TsH plus TsOH and the amine plus an aldehyde (Scheme 3.11), as suggested for TsVOH. Alternatively tosylpyrrolidine may just be hydrolysed to give TsOH and the amine. The peak eluting at 16.7 min of the raw photolysate analysis could be tosylpyrrolidine based upon RT and λ_{max} (228 nm) but this has not been confirmed. The mole fraction of TsOH suggests that whatever the mechanism, this is a major route of degradation for TsPOH.

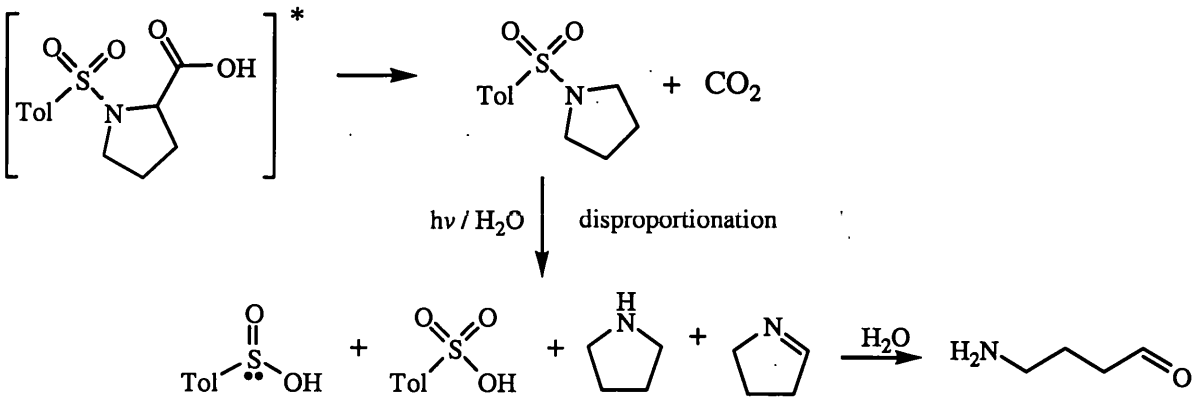

Scheme 3.11 A tentative mechanism involving decarboxylation of TsPOH.

A number of other AccQTag™ derivatives were found that have not been identified. However, any compounds with an amine group would be derivatised by the AccQTag™ reagent so both the amine and the aminoaldehydes suggested in the three previous schemes are likely candidates.

A very small amount of $TsNH_2$ was found although a plausible mechanism for its formation is elusive. The identity of the peak at 13.7 min has not been resolved either.

The results from TsPOH indicate that the main route of degradation involves decarboxylation, possibly by more than one route to give the identified products in ~65% yield. Tentative DNP derivatised products may account for the remaining substrate. However some of the expected products may be unstable, hence, their lack of detection. The absence of the amine hydrogen has made a significant difference to the observed products with TsOH being observed in greater yield than TsH whereas it was a minor product in previous examples. However, proline was not found suggesting that TsOH must

be formed by a different mechanism from that of previous substrates, with one possibility depicted in Scheme 3.11.

3.2.6 *N-p*-tosyl-2-amino*iso*butyric acid

HPLC analysis of the raw photolysate with detection at 228 nm showed that TsH was the major aromatic product of the irradiation. TsOH and $TsNH_2$ were found as minor products. Analysis for DNP derivatised compounds with detection at 354 nm showed a small peak corresponding to acetone DNP. NH_3, Aib and *iso*-propylamine were all analysed as their AccQTag™ derivatives and an additional peak was observed at 17.3 min that remained unidentified. The product mole fractions are summarised in Table 3.11 and CO_2 mole fractions are given separately in Table 3.12. The data are presented graphically in Figure 3.12, which shows a similar pattern to TsGOH.

Table 3.11 Product mole fractions for TsAibOH.

Time/ min	Degradation/%	Product mole fractions						
		TsH	TsOH	$TsNH_2$	acetone	NH_3	Aib	*iso*propylamine
5	5	0.47	0.06	0.00	0.08	0.56	0.04	0.03
10	18	0.25	0.03	0.01	0.05	0.53	0.02	0.02
15	13	0.63	0.07	0.00	0.10	1.17	0.05	0.05
30	22	0.57	0.08	0.01	0.10	1.19	0.05	0.04
60	38	0.59	0.07	0.01	0.10	1.25	0.05	0.04
120	60	0.53	0.08	0.01	0.10	1.23	0.05	0.03

Table 3.12 CO_2 mole fractions for TsAibOH.

Time/min	Degradation/%	CO_2 mole fraction
5	5	1.04
10	11	0.96
15	13	1.25
30	28	0.98
60	43	0.98
150	74	0.95

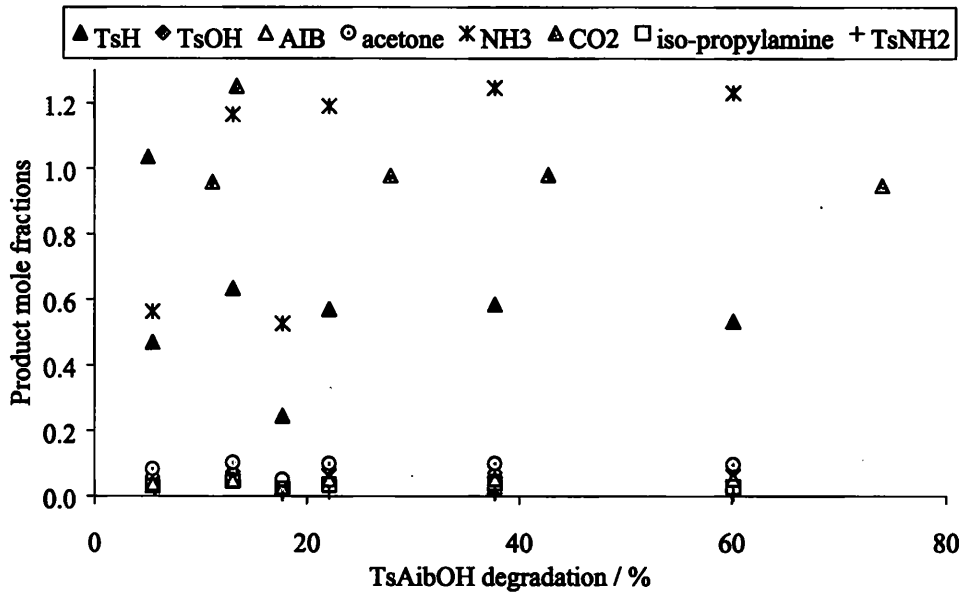

Figure 3.12 Product mole fractions for TsAibOH.

The rate of degradation for TsAibOH is similar to that of TsGOH at pH 3 and like the previous two substrates, TsAibOH exhibited a slight colouration upon photolysis but little or no precipitate was observed. The change in apparent pH was minor.

The photolyses of TsAibOH gave products analogous to those seen in the first two tosyl amino acids with the main products being TsH, NH_3, acetone and CO_2. Assuming that TsH comes only from this route, the value at ~12% degradation will be in the region of 60%. A problem was observed with the measurement of acetone DNP, which gave a value approximately four times lower than that expected. NH_3 and CO_2 were considerably higher with almost 100% yield. The latter may be explained in part by *iso*-propylamine, which was found in 5% yield and is analogous to *iso*-butylamine in TsVOH, and hence could come from tosyl-*iso*-propylamine, although the latter was not observed in the HPLC data. As with all previous compounds a very small amount of $TsNH_2$ was found that like most other products can be explained by analogy with TsGOH. TsOH and 2-amino-*iso*-butyric acid were both observed in about 6% yield thus giving a low value for S-N cleavage, again consistent with findings in previous compounds. A degradation scheme is suggested that accounts for 76% of the degraded material at 13% degradation

(Scheme 3.12). The two methyl groups at the α position appear to have little effect upon the product distribution in comparison with the previous tosyl amino acids, the main difference is that a product analogous to glyoxylic acid in TsGOH is not possible due to the absence of an α-H, and this may account for the enhanced value in TsAibOH of the main pathway compared with the analogous one of TsGOH.

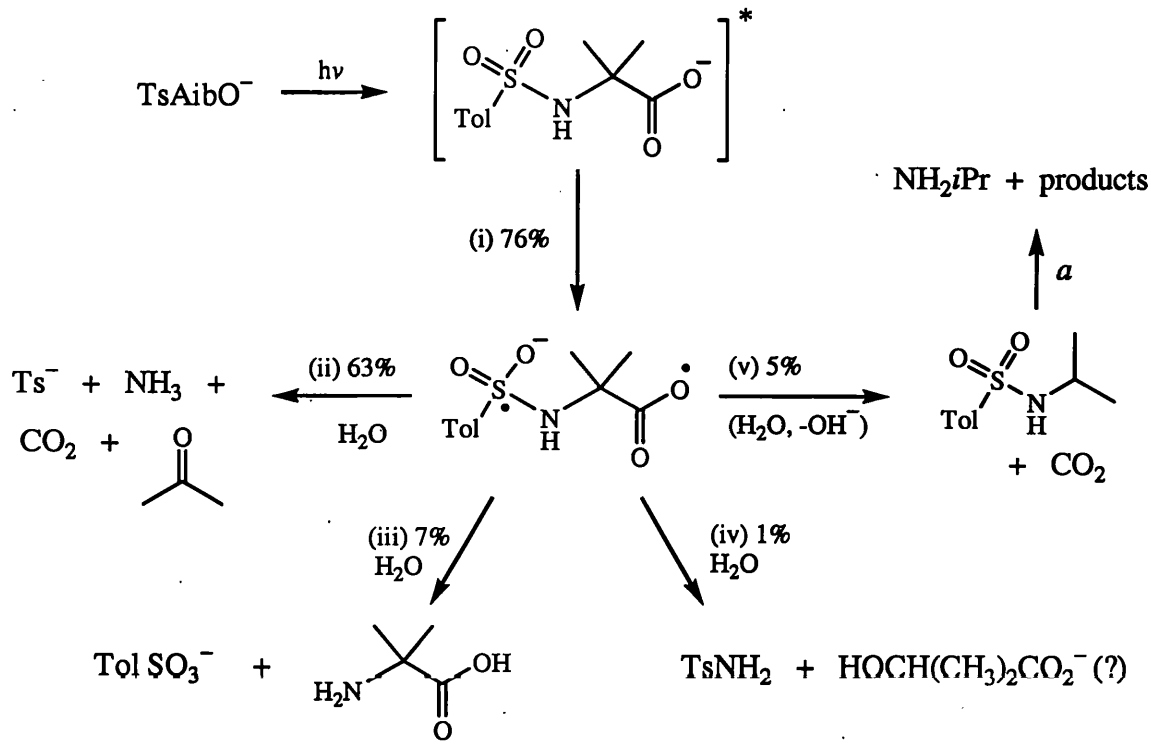

Scheme 3.12 Possible pathways of photodegradation of TsAibOH at 13% degradation that accounts for the observed products. [a] See Section 4.3.7.

3.2.7 Conclusions for compounds with an alkyl side-chain

The three compounds discussed in this section have revealed some photoproducts analogous to those of TsGOH with broadly similar distributions. The most obvious difference is the absence of a dehydrodimer being formed from all these compounds. This may be due to steric hindrance preventing dimerization although the decarboxylated product was not found with TsVOH or TsAibOH. However, an amine was found in both cases which could have resulted from detosylation of the decarboxylated

product. We had thought that the presence of bulky side-chains would alter the relative yields for each pathway but the effect was small in the case of TsVOH. TsPOH was investigated for both the effect of the five-membered ring and the absence of a hydrogen on the nitrogen atom. It would appear to have altered the product distribution in favour of TsOH over TsH although CO_2 was still predominant. The photolysates of this compound proved to be difficult to analyse and hence the product identity was not investigated further. The main reason for studying TsAibOH was to examine the effects of the absence of the α-H. The main effect appears to be an increase in the major pathway analogous to TsGOH and no new pathways were found.

In summary, the scheme and mechanisms suggested for TsGOH are further supported by the results obtained from TsVOH, TsPOH and TsAibOH at this stage. In the next section we will look at the effects of aromatic side-chains upon the product distributions which could, in principle offer an additional donor for PIET.

3.3 Aromatic side-chains

3.3.1 Introduction

TsVOH, TsPOH and TsAibOH have shown little difference in photoproducts compared with TsGOH indicating that an aliphatic side-chain does not participate in the degradation processes and that conformational restraints also have little effect on the course of the reactions. An aromatic side-chain however, may affect the course of the reaction as well as being a very bulky group. We shall look at two compounds in this section. The first is *N*-*p*-tosylphenylalanine (TsFOH, **20**), which has a benzyl side-chain. The second compound is *N*-*p*-tosyl-*O*-methyltyrosine (TsY(OMe)OH, **21**), which has a methoxy group at the *para* position of the side-chain aromatic ring. This group is a good electron donor and hence may offer degradation pathways different from those seen in previous compounds.

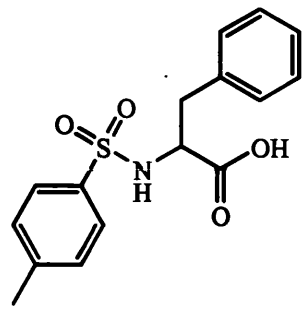

20

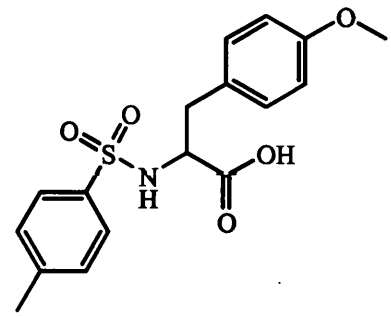

21

3.3.2 General observations for TsFOH and TsY(OMe)OH photolyses

The TsFOH solutions became cloudy upon irradiation for periods of greater than 30 mins. The apparent pH was found to increase from 3.1 to 3.3 after 60 mins irradiation and the degradation reached 35%.

The TsY(OMe)OH solutions remained clear throughout the irradiations. The apparent pH increased from 3.2 to 3.3 after 60 min irradiation, and the degradation had reached 39%. Figure 3.13 shows that TsFOH and TsY(OMe)OH had a similar rate of degradation to TsGOH.

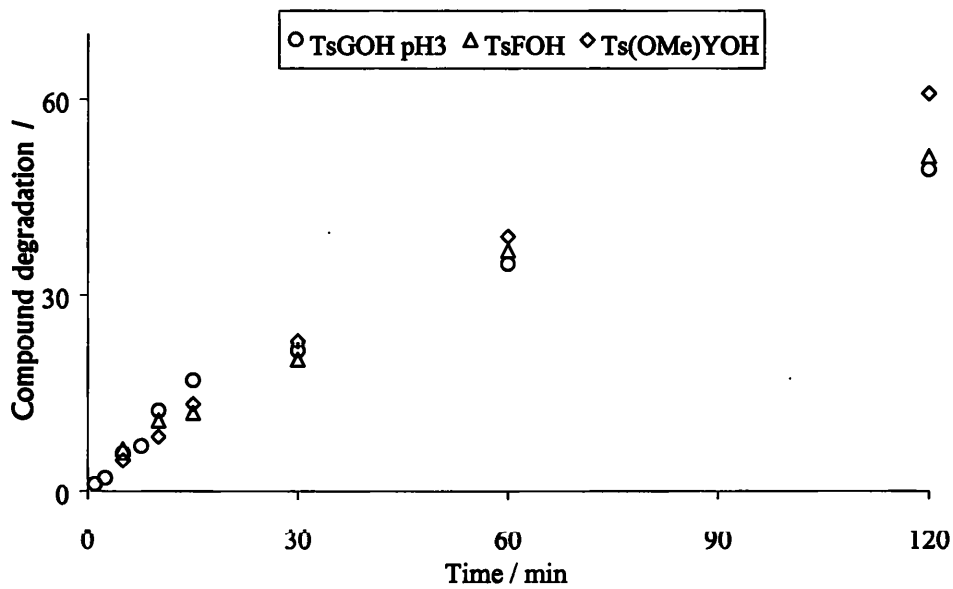

Figure 3.13 The rate of degradation of TsFOH and TsY(OMe)OH compared with TsGOH.

3.3.3 *N-p*-tosylphenylalanine

The HPLC chromatogram with detection at 228 nm showed that TsH was the major aromatic product. The minor aromatic products included TsOH and $TsNH_2$. An additional peak at 11.7 min had a UV spectrum with a λ_{max} at 239 nm. It is thought that this may be the imine precursor of phenylacetaldehyde that would be formed prior to hydrolysis, existing as its conjugated enamine tautomer in acidic solution (*cf* the UV spectrum of styrene, λ_{max} (cyclohexane) 248 nm). Biggs and co-workers had observed an intermediate thought to be the imine of phenylacetaldehyde during a methanolysis of an epoxide.[88] This had a λ_{max} 258 nm in acidified methanol. We do not need to quantify this peak, as phenylacetaldehyde was analysed as its DNP derivative.

The analysis for DNP derivatives revealed a number of peaks that have been identified as the DNP derivatives of phenylacetaldeyde, benzaldehyde and the *syn* and *anti* stereoisomers of phenylpyruvic acid DNP. The stereoisomers were found to interconvert in solution, particularly when exposed to daylight. Phenylpyruvic acid is known to be unstable degrading to benzaldehyde.[89]

AccQTag analysis also showed a number of peaks that were identified as NH_3, phenyalanine and phenethylamine. The formation of phenethylamine was investigated by irradiation of *p*-tosylphenethylamine and phenylalanine and was found in the photolysates of both compounds. The product mole fractions are shown in Table 3.13, Table 3.14 and Table 3.15 and illustrated graphically in Figure 3.14 and Figure 3.15.

Table 3.13 Product mole fractions for TsFOH.

Time/ min	Degradation/ %	Product mole fractions						
		TsH	TsOH	$TsNH_2$	Phe	phenyl-pyruvic acid	phenyl-acetaldehyde	benzaldehyde
5	2	0.88	0.14	0.05	0.03	0.37	1.35	0.09
10	5	0.83	0.13	0.04	0.02	0.28	0.94	0.07
15	9	0.69	0.07	0.03	0.03	0.20	0.60	0.04
30	20	0.56	0.04	0.02	0.03	0.13	0.36	0.02
60	35	0.53	0.04	0.02	0.03	0.10	0.28	0.02
120	56	0.50	0.03	0.02	0.03	0.07	0.20	0.02

Table 3.14 Product mole fractions for TsFOH.

Time/min	Degradation/%	Product mole fractions	
		phenethylamine	NH_3
5	6	0.03	0.35
10	11	0.05	0.56
15	12	0.05	0.54
30	20	0.05	0.52
60	37	0.06	0.51
120	51	0.05	0.48

Table 3.15 CO_2 mole fractions for TsFOH.

Time/min	Degradation/%	CO_2 mole fraction
5	12	0.28
10	16	0.33
15	22	0.43
30	30	0.47
60	47	0.56

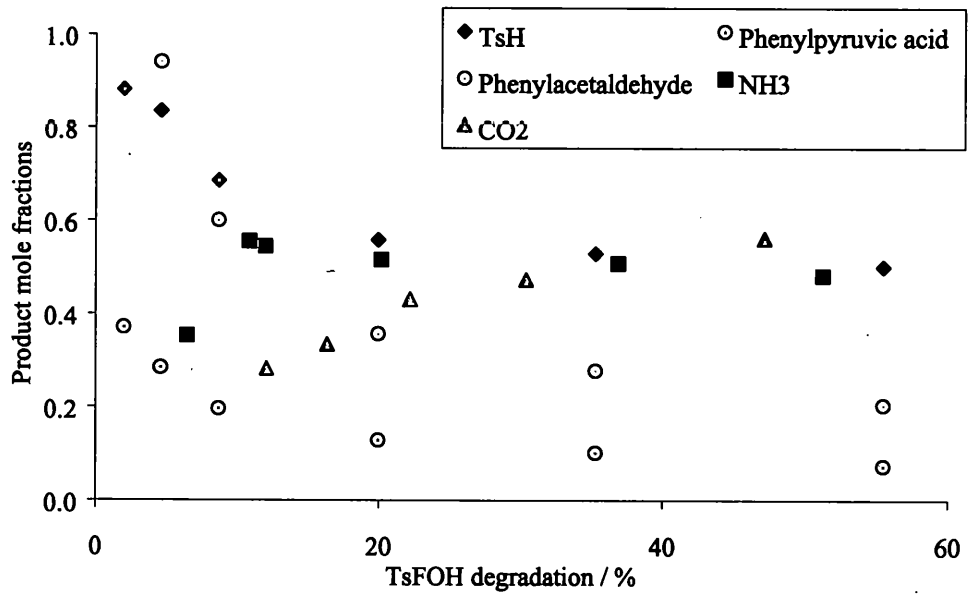

Figure 3.14 Major product mole fractions of TsFOH photolysis.

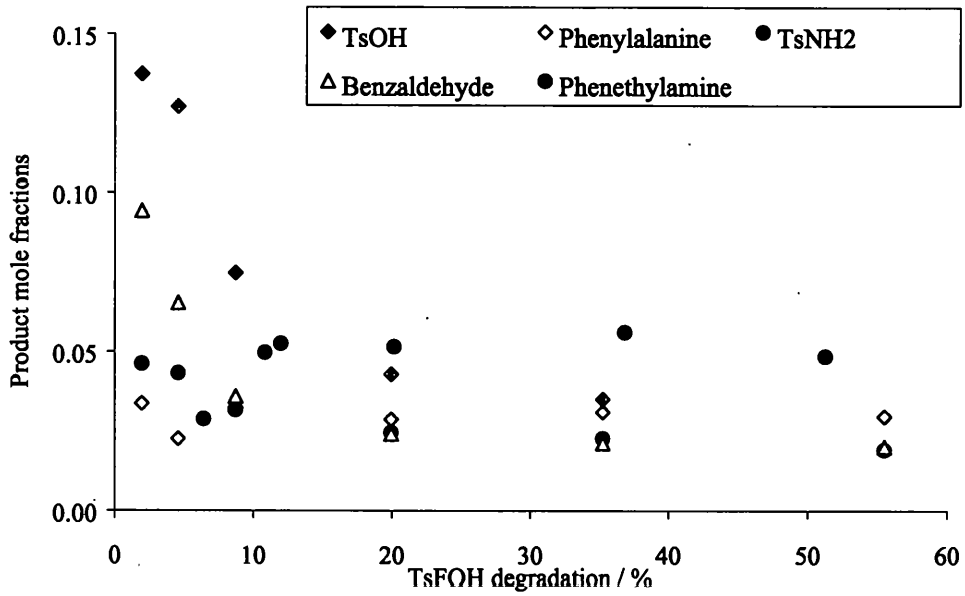

Figure 3.15 Minor product mole fractions of TsFOH photolysis.

The degradation rate of TsFOH is similar to that of TsGOH suggesting that the aromatic side-chain has not affected the rate of absorption. The change in apparent pH is also small consistent with that observed in the previous compounds.

The products identified for TsFOH show analogous degradation pathways to the previous compounds. A degradation scheme similar to the one suggested to TsGOH is proposed for TsFOH using the product mole fractions at 10% degradation (Scheme 3.13).

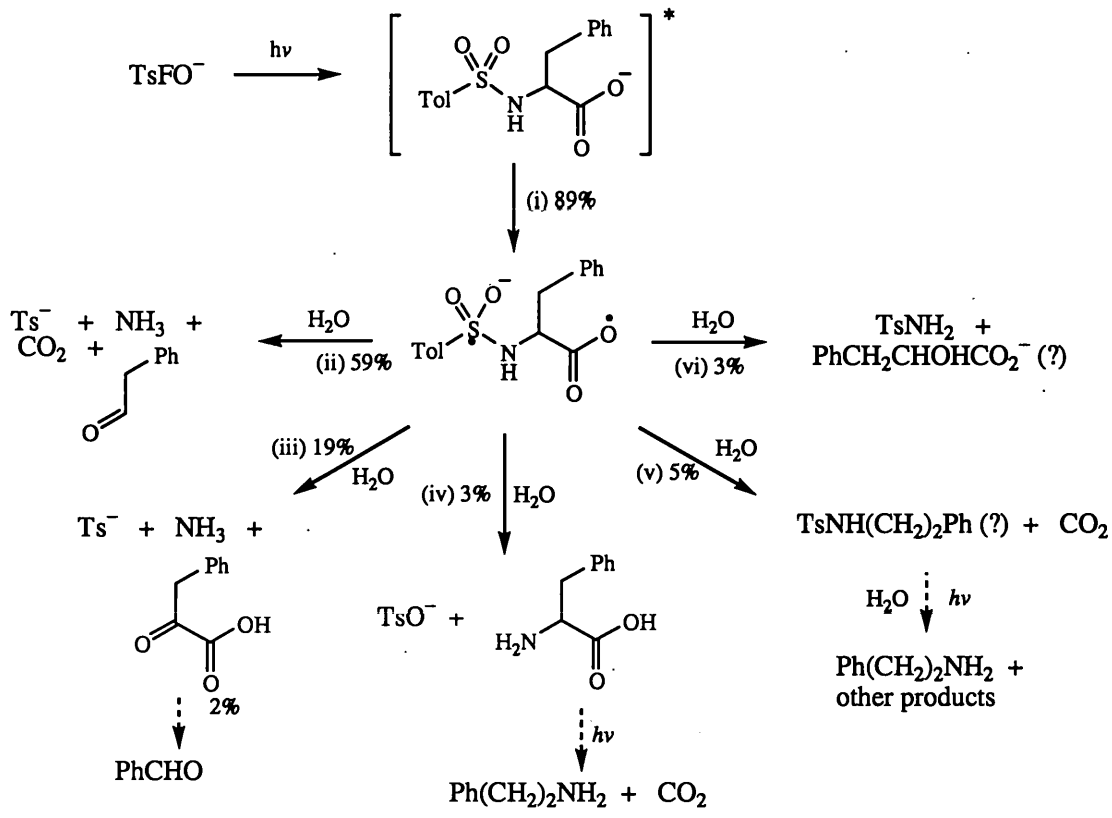

Scheme 3.13 A possible degradation scheme for TsFOH at 10% degradation.

As with TsGOH we can explain all of the observed products from a biradical generated from an initial ET in the excited state (i). The product distribution is also similar to TsGOH suggesting that the aromatic ring has not influenced the course of degradation. The predominant process (ii) from this intermediate gives TsH, phenylacetaldehyde, NH_3 and CO_2. The mole fraction of CO_2 was considerably lower than expected at only 28% whereas this scheme predicts a value of 67%. This figure was reached at the later stages of degradation so it is likely that there was greater inaccuracy for the low degradation samples where the levels of CO_2 are very low. Abstraction of the α-H gives further TsH, NH_3 and another carbonyl compound, phenylpyruvic acid (iii). Phenylpyruvic acid is known to be unstable in air and is the likely source of benzaldehyde.[89] TsH is only 9% lower than the predicted value consistent with its photodegradation at a slower rate than TsFOH. Route (iv) can be explained as shown in (Scheme 3.5) by formation of a cyclic intermediate to

give TsOH and phenylalanine by hydrolysis. The mole fraction of the former is too high (8%) when compared with that of phenylalanine (3%). The most probable reason is that TsOH may arise indirectly via route (v) which gives tosylphenethylamine by decarboxylation, and the tosyl amine may then be photodegraded to give phenethylamine and other products. We were not able to find evidence for tosylphenethylamine, but evidence from TsGOH suggests that decarboxylation is a feasible pathway and we have shown that tosylphenethylamine photodegrades to give phenethylamine. As we shall see in Section 4.3.7, tosyl alkyl amines photodegrade to give the amine and TsOH as some of the photoproducts.

A number of other products are speculative at present due to small amounts involved which would probably be below our levels of detection by HPLC. The co-products of $TsNH_2$ are a case in point. $TsNH_2$ may be produced by hydrolysis to give phenyllactic acid (vi) as suggested for TsGOH or via proton abstraction from a six-membered transition state to give cinnamic acid (Scheme 3.14) as suggested for TsVOH. The mole fraction of either compound is expected to be only 3% and this could be a combined value from both routes. Even when concentrated photolysate samples were injected no candidates for either compound were observed, although cinnamic acid is itself photolabile.[90]

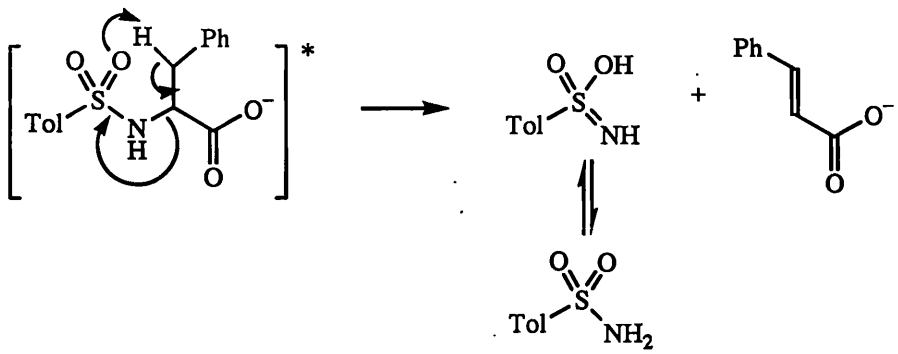

Scheme 3.14 A possible mechanism for production of $TsNH_2$ involving a six-membered transition state and the side-chain hydrogens of TsFOH.

3.3.4 *N-p*-tosyl-*O*-methyl tyrosine

Analysis of a raw photolysate gave a HPLC chromatogram with detection at 228 nm that showed the major aromatic product of the TsY(OMe)OH photolysis was TsH. A smaller peak corresponding to TsOH was also seen plus a number of other peaks. These all had a λ_{max} near 225 nm indicating that they were all tosylated products and hence they were quantified relative to TsY(OMe)OH. DNP analysis with detection at 354 nm revealed five peaks. Two were identified as the stereoisomers of glyoxylic acid DNP. The other three were postulated to be the two stereoisomers of *p*-methoxyphenylpyruvic acid DNP and *p*-methoxyphenylacetaldehyde DNP based upon their RT, λ_{max} and by analogy with the products of TsFOH photolysis. Standards were not available for these compounds so quantification was relative to HCHO DNP.

AccQTag™ analysis gave peaks corresponding to NH_3 and *O*-methyl tyrosine plus an additional three peaks that have not been identified. Table 3.16 gives the product mole fractions found in a 30% degraded sample, CO_2 mole fractions are given in Table 3.17.

Table 3.16 Product mole fractions for TsY(OMe)OH at 30% degradation.

Product	Mole fraction
TsH	0.45
TsOH	0.10
13.1 min	0.10[a]
13.6 min	0.04[a]
13.8 min	0.07[a]
24.7 min	0.05[a]
NH_3	0.45
O-methyl tyrosine	0.02
Glyoxylic acid DNP	0.19
p-methoxyphenylpyruvic acid DNP	0.10[b]
p-methoxyphenylacetaldehyde DNP	0.39[b]

[a]Quantified from a TsY(OMe)OH standard, [b]Quantified from a HCHO DNP standard

Table 3.17 CO_2 mole fractions for TsY(OMe)OH.

Time/min	Degradation/%	CO_2 mole fraction
5	5	0.40
10	8	0.53
15	13	0.58
30	23	0.61
60	39	0.55
120	61	0.61

The degradation rate of TsY(OMe)OH is similar to that of TsGOH suggesting that the aromatic side-chain has not affected the rate of absorption. The change in apparent pH is also small consistent with that observed in the previous compounds.

The product mole fractions show that the major products are TsH, NH_3, CO_2 and possibly *p*-methoxyphenylacetaldehyde which are analogous to the major route in all previous tosyl amino acids. This was observed in approximately 40% yield based upon the DNP derivative of *p*-methoxyphenylacetaldehyde and TsH. CO_2 values were higher than the latter compounds but mole fractions are gradually increasing throughout the degradation and may therefore be due to a secondary reaction. A DNP derivative thought to be *p*-methoxyphenylpyruvic acid DNP was observed in 10% yield which is about the same as glyoxylic acid from TsGOH. The main difference observed for this compound was the formation of a product, glyoxylic acid in 19% yield, which must come from side-chain cleavage. It was thought that the introduction of a good electron donor in the side-chain might provoke a side-chain cleavage and this has proved to be the case. A mechanism is proposed in Scheme 3.15 that involves an initial ET from the side-chain aromatic group to the sulfonyl in the excited state followed by cleavages that lead to the glyoxylic acid and a postulated product for the side-chain moiety. We will see in a subsequent section that we have evidence for an analogous product from another substrate.

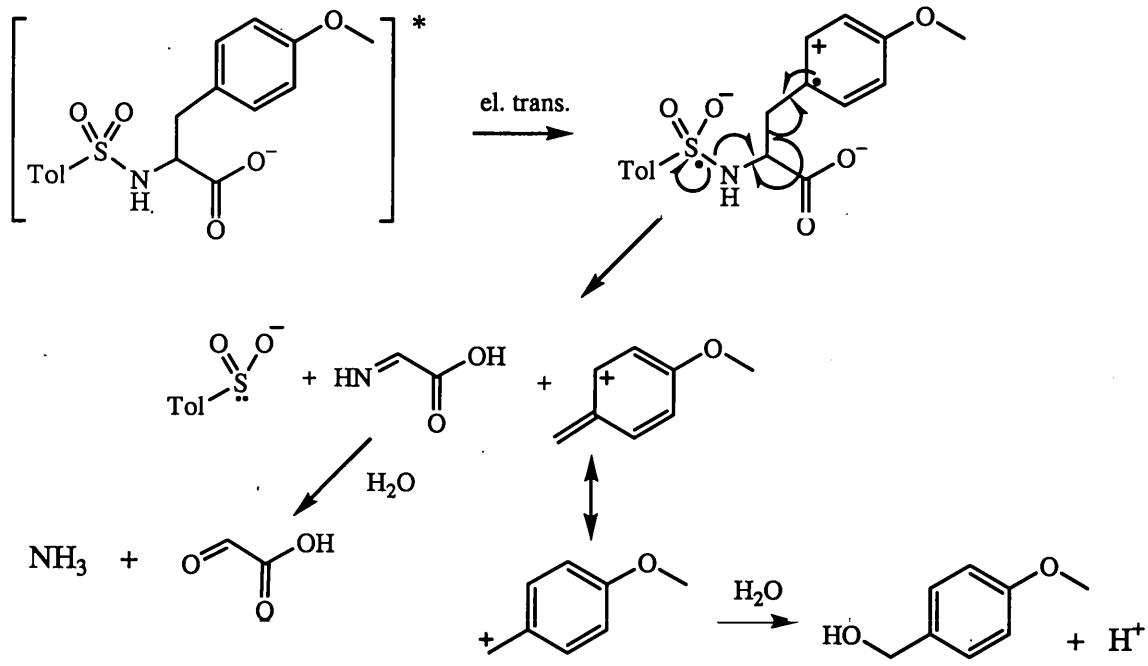

Scheme 3.15 A mechanism for side-chain cleavage in TsY(OMe)OH.

Griesbeck and co-workers have observed a side-chain cleavage in phthaloyl protected Phe and Tyr esters, which they suggested was a consequence of electron transfer from the aromatic group to the phthaloyl acceptor.[91] A higher yield was found for Tyr than Phe, just as we have found for the tosyl protected amino acids.

The ET from the side-chain to the sulfonyl could be due to a charge transfer transition in TsY(OMe)OH. We investigated the possibility of additional absorption bands in TsY(OMe)OH compared with TsGOH and tyrosine in the ground state by comparison of their UV spectra. Figure 3.16 shows an overlay plot for TsY(OMe)OH compared with the combined spectra of TsGOH and tyrosine. It is evident from this that there are no additional absorptions in the ground state of TsY(OMe)OH compared with the other compounds. However, this still does not rule out charge transfer in the excited state. We do have evidence at a later stage that this reaction can occur without the methoxy group present. Further evidence for the chromophore of TsY(OMe)OH not involving the side-chain aromatic ring is seen in the plot of degradation against time (Figure 3.13) which

shows that TsY(OMe)OH degrades at the same rate as other compounds such as TsFOH and TsGOH indicating that they all have the same chromophore.

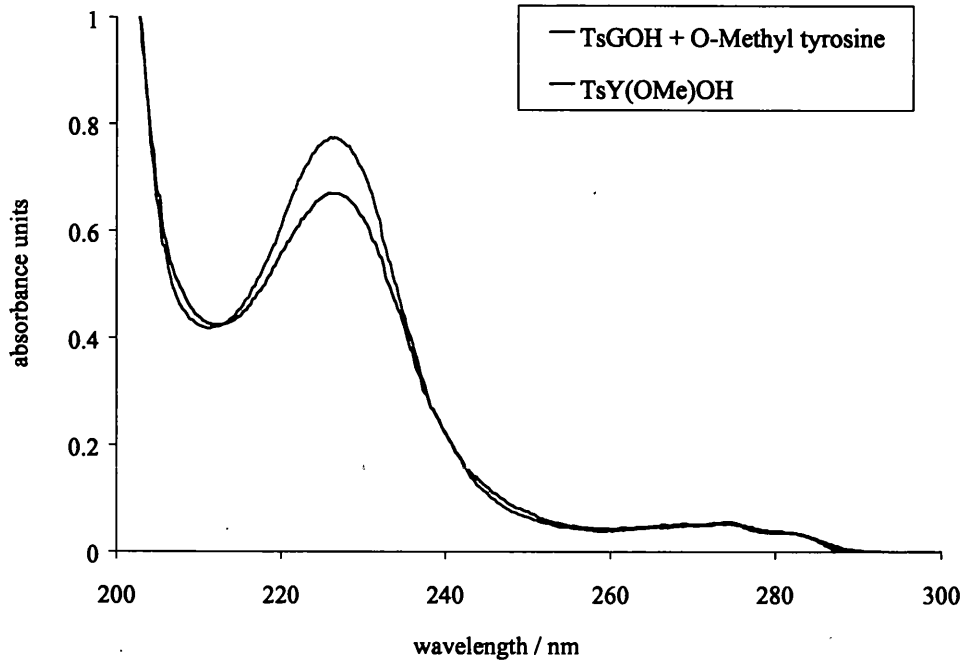

Figure 3.16 The UV spectrum of TsY(OMe)OH compared with the combined UV spectra of TsGOH and *O*-methyl tyrosine.

As with all other tosyl amino acids the yield for S-N hydrolysis was poor; TsOH was found in 10% yield and 2% of *O*-methyl tyrosine was recorded. The four unidentified peaks all have a UV spectrum with a λ_{max} of 224-228 nm indicating that the tosyl group has been retained in the product. The peak eluting at 24.7 min may be the decarboxylated product as the late RT suggests a molecule less polar than TsY(OMe)OH. Scheme 3.16 shows that 78% of the degraded material can be accounted for at 30% degradation. The unidentified peaks in the analyses may account for the remainder.

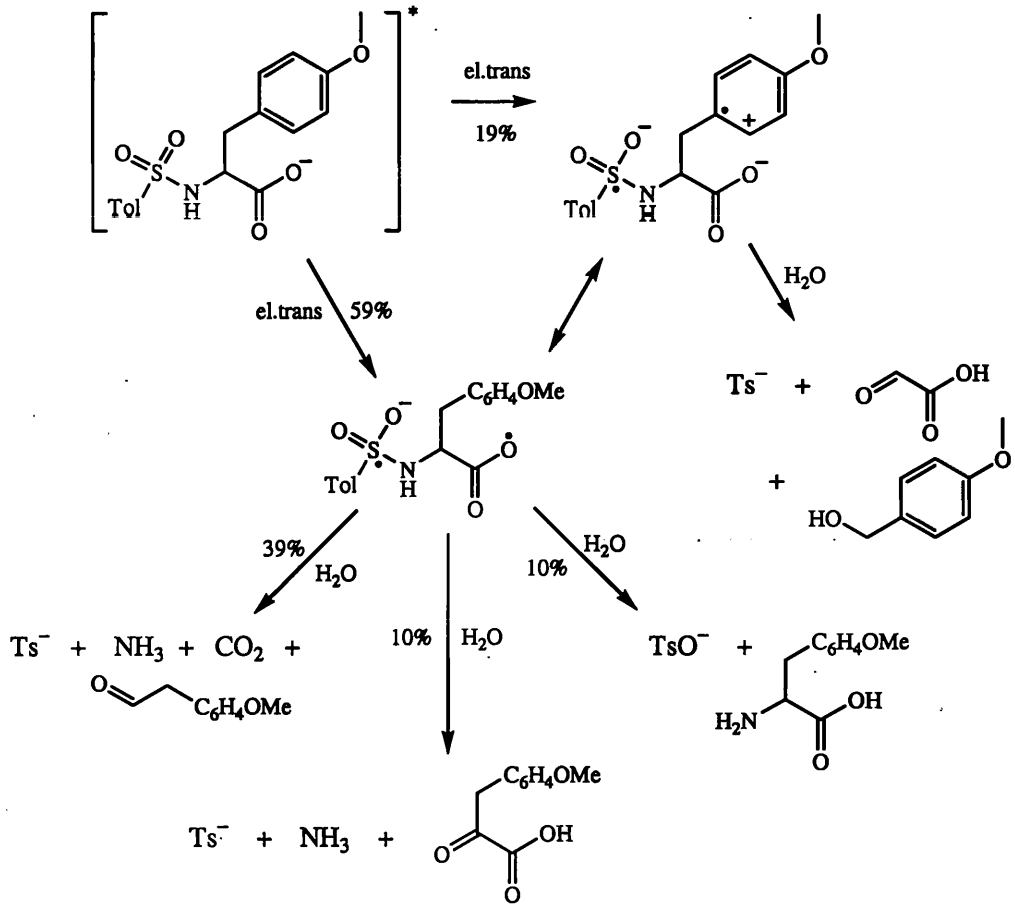

Scheme 3.16 A possible degradation scheme for TsY(OMe)OH at 30% degradation.

No evidence was found with TsFOH or TsY(OMe)OH for analogues of the dimers observed with TsGOH consistent with the products observed in the previous section and assumed to be due to steric reasons or exclusion by conformational factors.

3.3.5 Conclusions

The presence of the phenyl ring does not appear to play a part in the photodegradation of TsFOH. The major route is analogous to that observed for TsGOH i.e. electron transfer or proton transfer from the carboxylate group to the sulfonyl group with the subsequent breakdown of the molecule to give CO_2 and an imine, which is hydrolysed. The minor pathways that are observed are all analogous to those seen with TsGOH.

However, for TsY(OMe)OH the presence of a methoxy group on the side-chain aromatic ring has introduced a previously unseen cleavage of the side-chain. The consequences for this are a reduction in competition from other routes, in particular the major route of previous compounds accounted for 60% of the degradation but in TsY(OMe)OH it was only 40%. This suggests that other potentially reactive groups in the side-chains may also invoke new routes of photodegradation. In the next section we shall look at another amino acid with a potentially reactive side-chain.

3.4 Another potentially reactive side-chain

3.4.1 Introduction

We have seen in the previous section that an electron donor in the side-chain of the amino acid results in side-chain cleavage. This is thought to occur from a biradical that is generated by ET from the aromatic ring. We shall now look at *N-p*-tosylmethionine (TsMOH, **22**) where a side-chain sulfur atom is readily oxidised i.e. a good electron donor, and in the case of phthaloyl methionine has been found to participate in cyclisation reactions.[92]

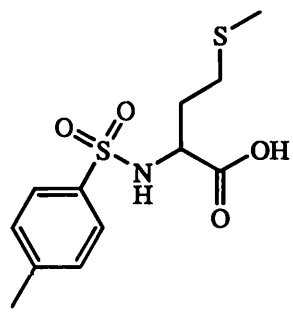

22

3.4.2 *N-p*-tosyl methionine

The photolysates were slightly cloudy after 60 min irradiation. The apparent pH was initially 3.2 and had not changed after 60 min irradiation, at which time the

degradation had reached 24%. A plot of the degradation versus time revealed a similar trend to that of previous compounds.

HPLC analysis of the raw photolysate with detection at 228 nm showed that the major aromatic product was TsH. TsOH and $TsNH_2$ were minor products produced in roughly equal quantities. Another peak at 11.1 min had a λ_{max} 228 nm suggesting that it was a tosylated compound. This was not identified but was quantified using a TsMOH standard.

Analysis of DNP derivatives gave five peaks. All had UV spectra indicative of a DNP derivative and were quantified from a HCHO DNP standard. The major peak is thought to be the analogue of HCHO DNP from TsGOH and this may be analysed as two separable stereoisomers on HPLC due to the sulfur atom but prediction of the likelihood of this is not possible as no similar compounds have been analysed. Two of the smaller ones are likely to be the analogues of glyoxylic acid DNP stereoisomers from TsGOH, although prediction of RT is not possible. Unfortunately no standards were available for confirmation of peak identity.

AccQTag™ analysis gave peaks for NH_3 and methionine plus three other compounds that were not identified. One of these had an earlier RT than methionine indicating a more polar compound. CO_2 was measured in a separate experiment. The product mole fractions are given in Table 3.18 and Table 3.19 and a plot of the product mole fractions versus degradation for 5-30% substrate conversion is shown in Figure 3.17. The unidentified 11.1 min product and the three minor DNPs have been omitted from this graph for clarity. The plot shows a similar distribution to previous compounds.

Table 3.18 Product mole fractions for TsMOH.

Time/ min	Degradation/ %	Product mole fractions										
		TsH	TsOH	$TsNH_2$	11.1 min[a]	NH_3	Met	7.2 min DNP[b]	13.7 min DNP[b]	18.3 min DNP[b]	19.0 min DNP[b]	20.2 min DNP[b]
15	8	0.77	0.08	0.09	0.05	0.52	0.02	0.03	0.06	0.03	0.15	0.65
30	14	0.79	0.06	0.07	0.03	0.58	0.03	0.03	0.06	0.03	0.15	0.67
60	24	0.79	0.06	0.06	0.02	0.61	0.04	0.02	0.05	0.04	0.14	0.71

[a]Quantified from TsMOH standard, [b]quantified from a HCHO DNP standard

Table 3.19 CO_2 mole fractions for TsMOH.

Time/min	Degradation/%	CO_2 mole fraction
10	8	0.43
15	10	0.52
30	19	0.52
60	32	0.47
150	53	0.52

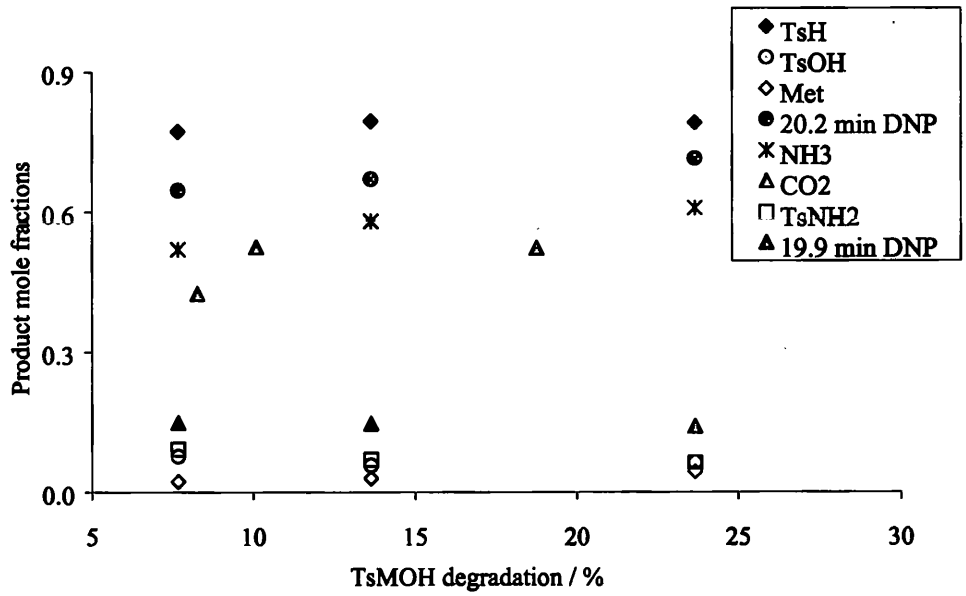

Figure 3.17 Mole fractions from TsMOH photolysis.

TsMOH was studied as an example of an amino acid with a potentially reactive side-chain group. The results indicate that its photodegradation follows a similar pattern to those observed with previous tosyl amino acids with the major degradation route giving

TsH, NH_3, CO_2 and a DNP derivative at 20.2 min which could be 3-(methylthio)-propanal. The latter was observed in an apparent 65% yield, which is higher than the CO_2 values but may reflect a difference in molar absorption coefficient from that of the formaldehyde DNP used as the standard for quantification. Other DNP derivatives were found which could be the analogues of glyoxylic acid. As with other 2-oxo acids, stereoisomers would be expected, thus accounting for two of the DNP derivatives. A low yield was observed for S-N cleavage to give TsOH (8%) and methionine (2%). The lower yield of methionine may reflect its further degradation or an initial decarboxylation of TsMOH as suggested for previous compounds. By analogy with previous suggestions and evidence provided later, the decarboxylated compound could be photolysed to TsH and TsOH plus an amine. There were a number of AccQTag™ derivatives that could be the decarboxylated methionine. An unidentified peak in the HPLC analysis of the photolysate at 11.1 min had a λ_{max} at 228 nm which is indicative of a tosylated compound. No other tosylated amino acids have produced photoproducts with such a short RT so this compound could well arise from a reaction involving the methionine side-chain generating additional polar groups. It was not investigated further as it only accounted for 5% of the degradation products. A degradation scheme is suggested that accounts for at least 93% of the observed products at 8% degradation (Scheme 3.17). $TsNH_2$ could also arise from a β-H abstraction as described for TsFOH (Scheme 3.14).

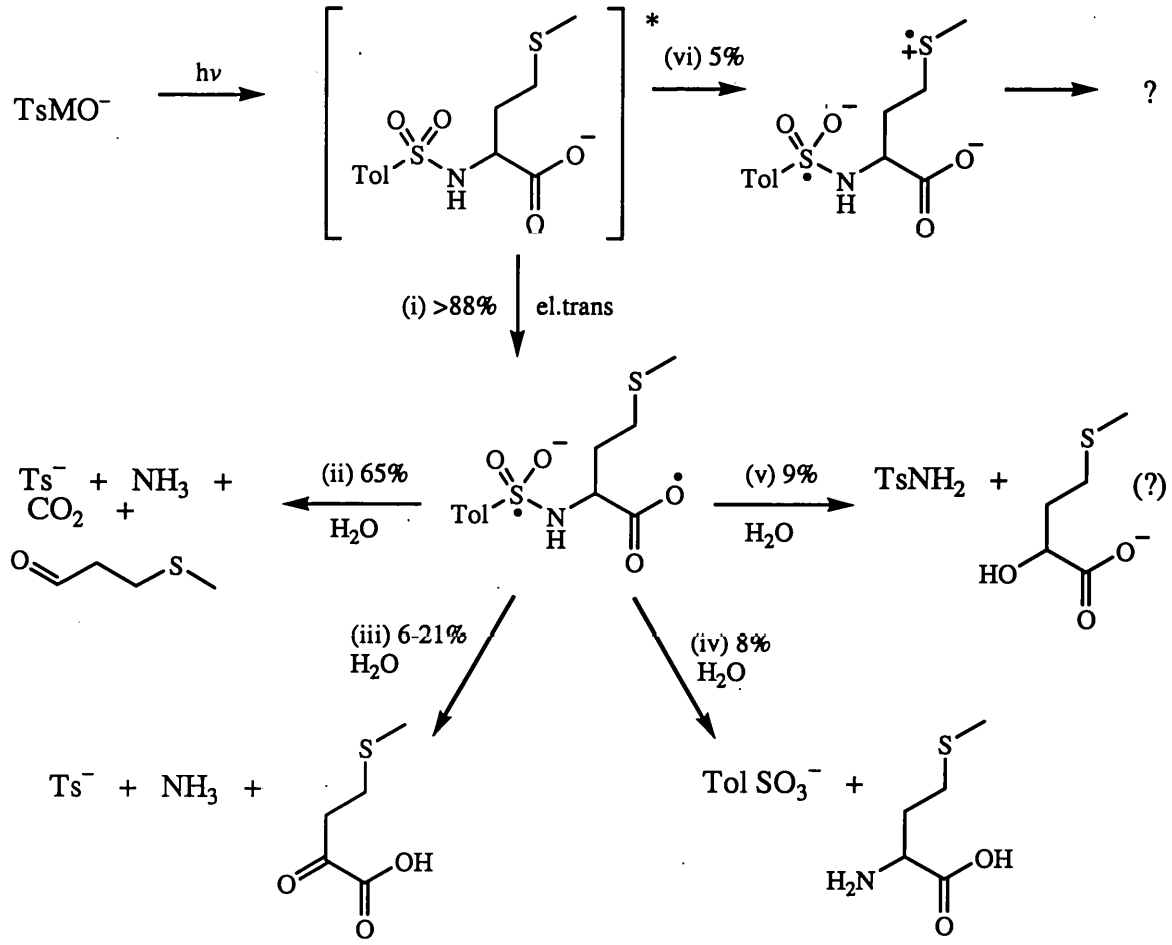

Scheme 3.17 Possible pathways of photodegradation of TsMOH with accountancy for the product distribution at 8% degradation.

The sulfur atom of the methionine side-chain does not appear to have made a large impact upon the course of the degradation in comparison with other tosyl amino acids. The major route still appears to be same as for TsGOH i.e. ET in the excited state to give a biradical that cleaves to give TsH, CO_2 and an imine that is hydrolysed to the aldehyde and NH_3.

3.4.3 Conclusions

TsMOH has given similar results to TsGOH, which is the case for all except two of the other tosyl α-amino acids studied. The exceptions were TsAibOH that could not undergo C_α-H abstraction and TsY(OMe)OH where side-chain cleavage was observed. It

appears that the major degradation pathway for all tosyl α-amino acids is similar regardless of the side-chain structure i.e. ET from the carboxylate group to the sulfonyl group and the resultant cleavages that lead to TsH, NH_3, an aldehyde and CO_2.

We now turn to two further aspects of the influence of structure on the photochemical properties of these compounds: increasing the distance between the carboxylate and the sulfonyl groups, and modifying the carboxylate function. In the next section we shall look at the results of a compound with two carbon atoms between the carboxylate and the sulfonyl, and the following section looks at the results for two esters.

3.5 Further separation of sulfonamide and carboxyl function

3.5.1 Introduction

The influence of functional group proximity on the photochemistry of tosyl amino acids was investigated by studying a compound with an increased carbon chain length, *N-p*-tosyl-β-alanine (TsβAOH, **23**). This compound has one more carbon atom between the carboxylate and the sulfonyl than in TsGOH and the absence of a side-chain allows ready comparison between the two compounds. The DNMBS derivative of βAla has been studied by other workers as discussed in Chapter 1, who found a four fold improvement in the yield of the amino acid compared with the glycine derivative.[37] Their studies were also carried out in aqueous solution so are comparable to ours.

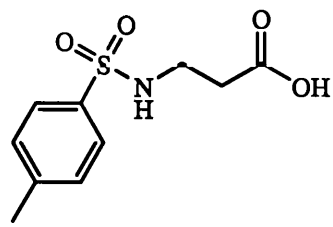

23

3.5.2 *N-p*-tosyl-β-alanine

The solutions acquired a milky colour upon irradiation. The apparent pH was initially 3.6 and had not changed after 60 min, at which point the degradation had reached 36%. A plot of degradation versus time is similar to that of previous compounds including TsGOH.

HPLC analysis of the raw photolysate with detection at 228 nm showed three products. The major aromatic products were TsH and TsOH. A smaller peak at 16.8 min peak has not been identified. Its UV-vis spectrum had a λ_{max} 228 nm indicating a tosylated compound so was quantified using a TsβAOH standard.

Analysis for DNP derivatives with detection at 354 nm gave one major peak identified as that of 3-oxo-propionic acid. Two smaller ones were not identified but accounted for only 2% of the degradation.

AccQTag™ analysis showed only two peaks that correspond to NH_3 and β-alanine. The product mole fractions are summarised in Table 3.20, and, except for the high values of NH_3, are illustrated graphically in Figure 3.18.

Table 3.20 Product mole fractions for TsβAOH.

Time/ min	Degradation/%	Product mole fractions					
		TsH	TsOH	16.8 min[a]	NH_3	β-alanine	3-oxo-propionic acid
15	10	0.55	0.20	0.15	1.36	0.21	0.69
30	19	0.49	0.17	0.09	1.18	0.20	0.53
60	36	0.40	0.16	0.06	1.05	0.16	0.43
120	50	0.41	0.15	0.06	1.02	0.18	0.41

[a]Quantified relative to a TsβAOH standard

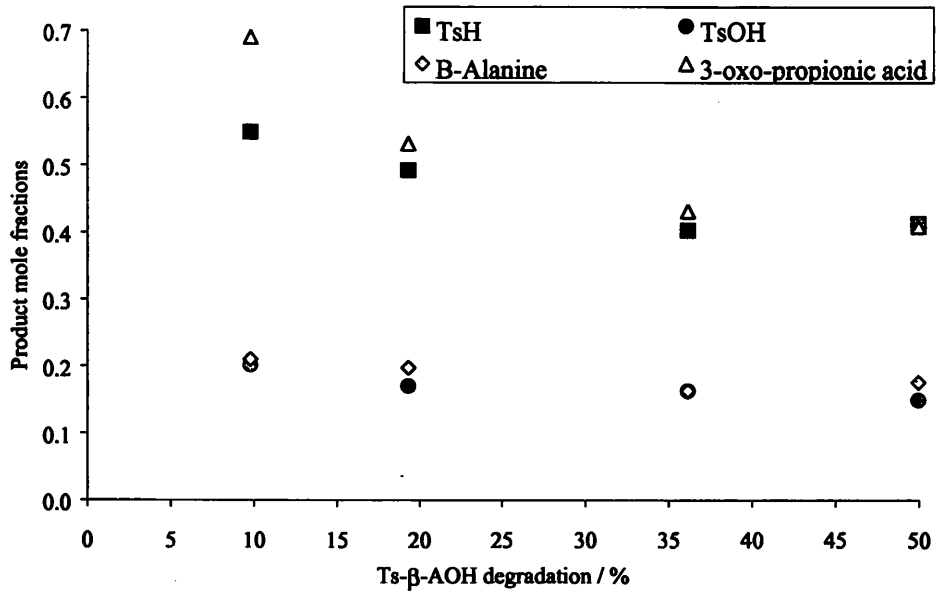

Figure 3.18 TsβAOH mole fractions.

Figure 3.18 clearly shows that the products appear to be divided into two pathways. The major products of TsβAOH degradation are TsH and 3-oxo-propionic acid in 53% yield for a 19% degraded sample (Table 3.20) and a good correlation was found for 3-oxo-propionic acid *vs* TsH; slope = 0.91, R^2 = 1.00. Table 3.20 shows that the mole fractions for NH_3 were higher than these two products. The three products are best explained by H-abstraction from the β-C in the excited state (Scheme 3.18). This is similar to the alternative mechanism suggested for the production of glyoxylic acid from TsGOH, which is analogous to the mechanism suggested by other workers for the thermolysis of sulfones where the H atom was thought to lie in the same plane as the sulfone oxygen making it easily accessible to the oxygen.[84]

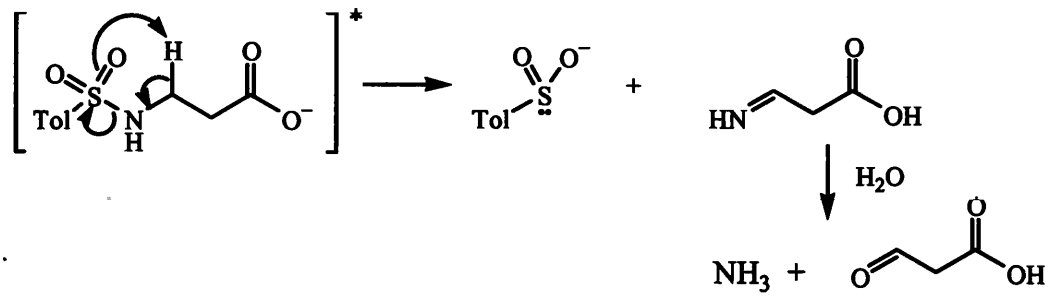

Scheme 3.18 Formation of 3-oxo-propionic acid and co-products from the excited state by C_β-H abstraction.

The reactions of TsGOH and TsβAOH both involve H-abstraction by a sulfonyl oxygen at the carbon atom next to the nitrogen. However, in TsGOH we had proposed an ET mechanism which is difficult to apply in the case of TsβAOH. The yield for this reaction in TsβAOH is much higher than for C_α-H-abstraction of the previous compounds which were around 12%. So increasing the carbon chain length has prevented the cleavages that produced CO_2 and HCHO in TsGOH, and resulted in an analogue of glyoxylic acid being formed.

The minor products, TsOH and β-alanine could, however, be the result of an ET from the carboxylate group. We can invoke a similar mechanism to that proposed for TsGOH i.e. formation of a biradical intermediate which cyclizes in this case to give a six-membered ring that is then hydrolysed to yield β-alanine and TsOH in ~20% yield (Scheme 3.19). This is a higher yield than observed in previous compounds. A good correlation was found for β-alanine *vs* TsOH; slope = 1.15, $R^2 = 0.97$.

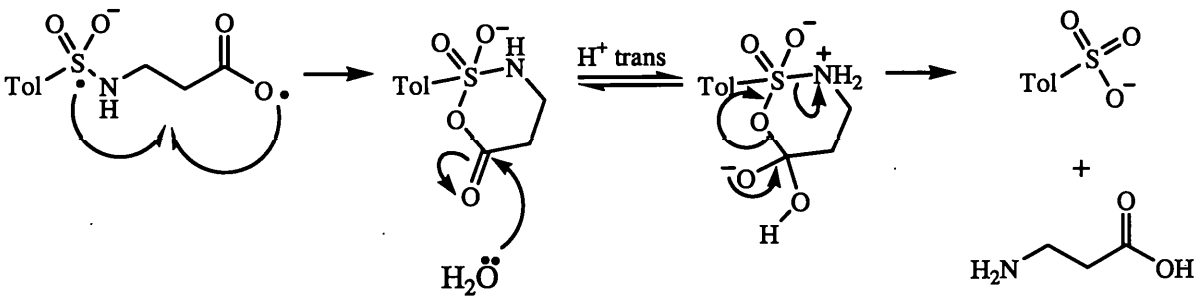

Scheme 3.19 Mechanism for S-N cleavage following an initial ET in the photodegradation of TsβAOH (anion shown) to give β-alanine and TsOH.

Thus, we are able to account for 73% of the substrate at 19% degradation with these two pathways, which both showed good correlations for their products.

3.5.3 Conclusions

The results from TsβAOH have shown that increasing the carbon chain length gives improved yields for the free amino acid consistent with the DNMBS derivative of

βAla studied by Corrie and Papageorgiou.[37] Presumably this is because the molecule is unable to cleave in the same manner as the tosyl α-amino acids, or, perhaps, because the cyclisation to a six-membered ring is more favourable than that to a five-membered ring. We have proposed a mechanism that involves ET for the formation of β-alanine. However, the formation of the aldehyde cannot be explained readily using ET and instead we have suggested H-abstraction from a five-membered ring transition state analogous to that observed in the thermolysis of sulfones.[84] Increasing the distance between the carboxylate and the sulfonyl moieties has altered the proportions for some pathways and prevented others, most notably the decarboxylative ones.

In the next section we will look at the effects of converting the carboxylate of tosylated α-amino acids to a different functional group, namely an ester.

3.6 Ester derivatives of tosyl α-amino acids

3.6.1 Introduction

We saw in Section 3.1 that the pH of the solution had little effect upon the products observed for TsGOH but it is likely that even at pH ~3 the majority of the substrate will be deprotonated. The deprotonation state of all of the other compounds studied is difficult to determine as they were all irradiated in solutions containing 40% acetonitrile. We now turn to esters where this ambiguity is eliminated.

In the case of tosyl α-amino acids we have found that most of the reactions could be explained by ET in the excited state to give a biradical intermediate. The major products were found to be TsH, NH_3, CO_2 and an aldehyde. The side-chain groups generally had little effect unless they contained an electron donor. Lengthening the carbon chain appears to have precluded the decarboxylative pathways in favour of H-abstraction at the carbon adjacent to the nitrogen atom and also given an improved yield for the free amino acid.

In this section we consider the effect on the photochemistry when the carboxylate group of tosylated α-amino acids is replaced by that of an ester. We have studied the ester derivatives of two compounds discussed in the previous sections. The first is *N*-*p*-tosylglycine methyl ester (TsGOMe, **24**) which is of course the simplest example that we could choose. The second is *N*-*p*-tosylphenylalanine methyl ester (TsFOMe, **25**) which has a benzyl side-chain. The major route of degradation for the compound with the free carboxylate involved cleavage of bonds to produce CO_2 and other products. The DNMBS derivative of glycine methyl ester was studied by Corrie and co-workers who reported a yield of 44% for glycine methyl ester upon photolysis in aqueous solution.[37] We shall start by looking at the results obtained for TsGOMe, and compare them with those of TsGOH to see if S-N cleavage has an improved yield, and then look at TsFOMe.

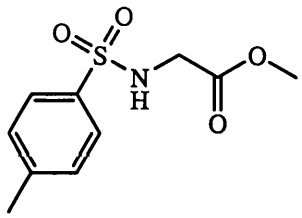

24

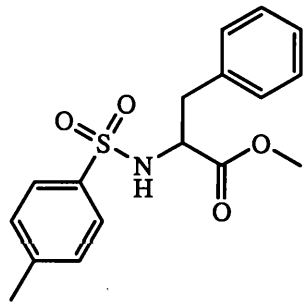

25

3.6.2 General observations for TsGOMe and TsFOMe

The TsGOMe and TsFOMe solutions acquired a milky colour upon irradiation. The apparent pH of a TsGOMe solution decreased from 5.0 to 4.1 after 60 min irradiation and degradation had reached 32%. The apparent pH of a TsFOMe solution decreased from 6.8 to 3.4 after 60 min irradiation and degradation had reached 32%.

3.6.3 *N-p*-tosylglycine methyl ester

HPLC analysis of the raw photolysate with detection at 228 nm showed that TsH was the major tosyl product. The only other peak was TsOH.

Analysis for DNP derivatives showed four peaks. These were identified as the two stereoisomers of glyoxylic acid DNP and the two stereoisomers of methyl glyoxylate DNP by comparison of RT, UV spectra and coelution with a standard. Methyl glyoxylate was the major product and this was found to degrade under the analytical conditions of DNP derivatisation to glyoxylic acid DNP stereoisomers.

AccQTag analysis showed six peaks, two of which correspond to NH_3 and glycine. Glycine methyl ester was not detected by AccQTag™ but that could be for one or two reasons; first the GOMe derivative has a low response factor, and second, GOMe is hydrolysed to glycine under the conditions used. The amount of glycine observed is therefore taken to be a minimum value for glycine methyl ester mole fractions. The other peaks have not been identified but all had a later RT than glycine, indicating less polar compounds. The mole fractions for the identified products are summarised in Table 3.21 and shown on a plot versus substrate degradation in Figure 3.19.

Table 3.21 Product mole fractions for TsGOMe.

Time/ min	Degradation/%	Product mole fractions						
		TsH	TsOH	$TsNH_2$	Gly	NH_3	glyoxylic acid	methyl glyoxylate
10	4	0.60	0.23	0.00	0.03	0.68	0.23	0.80
15	7	0.66	0.15	0.02	0.02	0.74	0.18	0.64
30	18	0.52	0.10	0.01	0.01	0.87	0.14	0.48
60	32	0.45	0.10	0.01	0.01	0.64	0.12	0.41
120	49	0.39	0.11	0.01	0.01	0.51	0.12	0.37

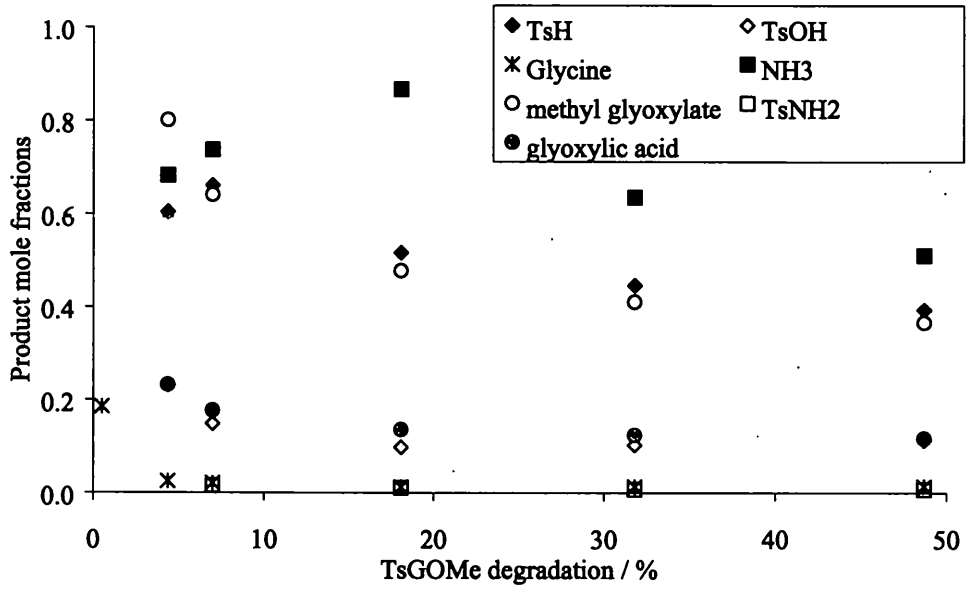

Figure 3.19 TsGOMe product mole fractions.

The apparent pH of TsGOMe was found to decrease after 60 min irradiation. This is most likely due to the appearance of acidic products such as TsH and TsOH. The degradation proceeded at a rate similar to those of most of the previous compounds.

The major products of the TsGOMe photolyses were TsH, NH_3 and methyl glyoxylate. TsH was found in 66% yield at 7% degradation, at which point methyl glyoxylate accounted for 64% of the substrate and NH_3 for 74%. We found that methyl glyoxylate DNP degraded to glyoxylic acid DNP under the analytical conditions employed. Therefore, methyl glyoxylate may be as high as 82% if we include the value for glyoxylic acid. Glyoxylic acid could not come from photocleavage of the ester to give TsGOH as our earlier photolyses of TsGOH have shown that formaldehyde is the major aldehyde formed from TsGOH and it was not observed in the TsGOMe photolysates. We can explain the formation of methyl glyoxylate by an initial ET from the ester bond to the sulfonyl to give a biradical intermediate. C_α-H abstraction and subsequent bond cleavage gives methyl glyoxylate and co-products *cf.* glyoxylic acid from TsGOH (Scheme 3.20).

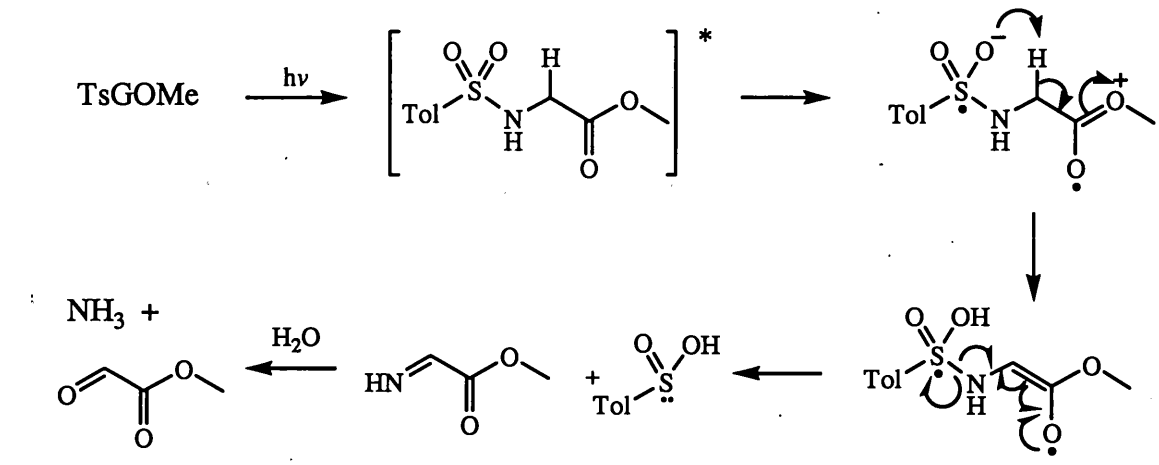

Scheme 3.20 Formation of methyl glyoxylate and co-products from a biradical intermediate.

TsOH was observed at 15% yield in a 7% degraded sample. Unfortunately we could not acquire values for glycine methyl ester due to analytical problems, so we have assumed that it corresponds to the measured value of TsOH based upon evidence from earlier compounds such as TsGOH. The production of TsOH and glycine methyl ester can also be explained in a similar manner to the analogous reaction with TsGOH i.e. ET to give a biradical intermediate which can cyclise and is then hydrolysed to give the products (Scheme 3.21).

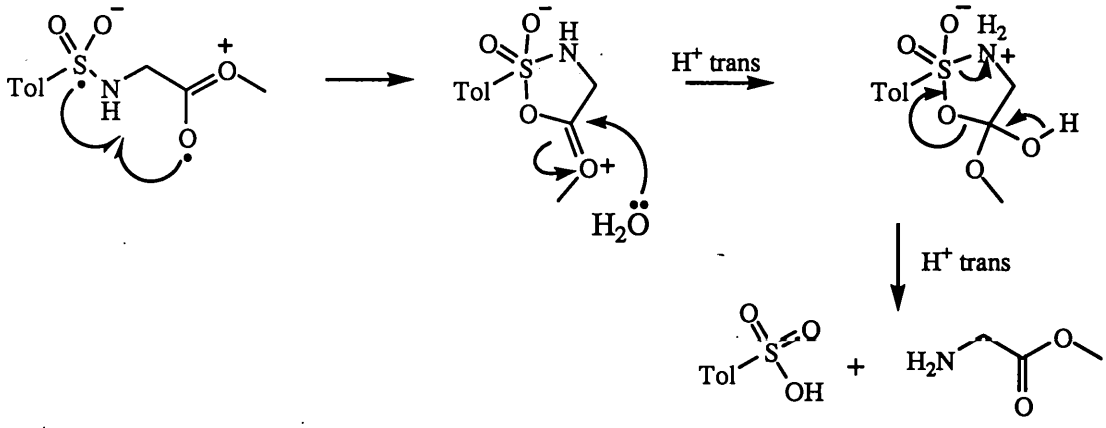

Scheme 3.21 Mechanism for S-N cleavage to give glycine methyl ester and TsOH.

A small amount of $TsNH_2$ (2%) was found, which can also be explained from the biradical intermediate in a similar manner to TsGOH. At 7% degradation we can

propose a scheme that accounts for 99% of the degraded TsGOMe (Scheme 3.22) by an initial ET transfer.

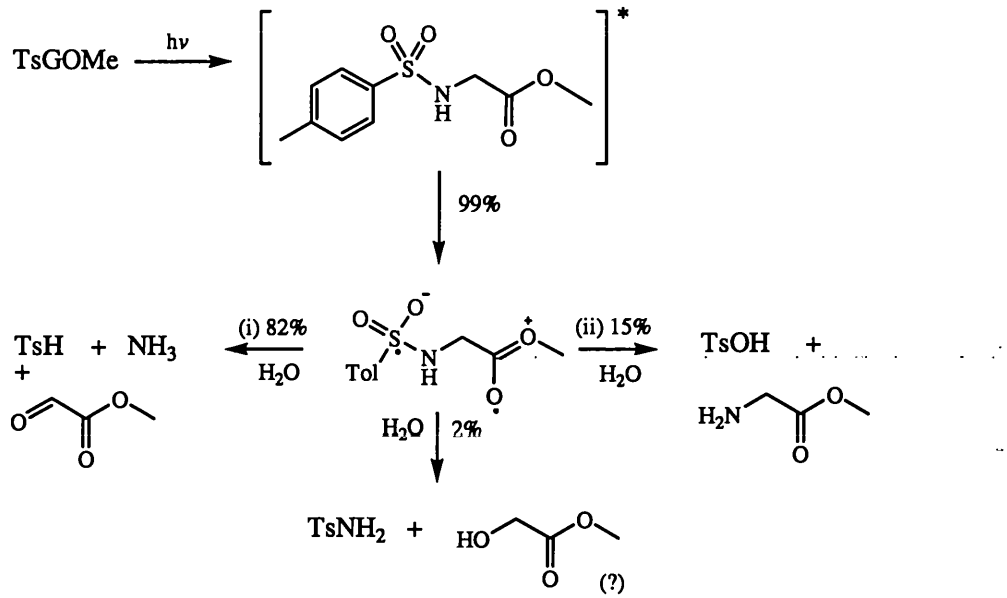

Scheme 3.22 A possible scheme for TsGOMe degradation with 99% product accountancy at 7% degradation.

3.6.4 *N-p*-tosylphenylalanine methyl ester

HPLC analysis of the raw photolysates with detection at 228 nm showed five peaks. The major tosyl product was TsH and a smaller peak was identified as TsOH. $TsNH_2$ was also found as a very small peak in some of the more degraded photolysates. A peak at 11.8 min had a λ_{max} at 240 nm, which could be an imine precursor of an aldehyde as proposed for TsFOH. A peak at 16.5 min had a λ_{max} at 200 nm consistent with an aromatic compound and was identified as benzaldehyde. The 19.2 min peak had a λ_{max} at 291 nm and is thought to be methyl phenylpyruvate based upon peaks observed during a HPLC analysis in the synthesis of methyl phenylpyruvate DNP. Both benzaldehyde and methyl phenylpyruvate were quantified as their DNP derivatives.

Analysis for DNP derivatives revealed a number of peaks which were identified as benzaldehyde DNP, and the stereoisomers of the following compounds:

methyl glyoxylate DNP, phenylpyruvic acid DNP and methyl phenylpyruvate DNP. The latter was the major product.

AccQTag analysis showed two peaks that correspond to NH_3 and phenylalanine. The problems noted in the analysis of glycine methyl ester were found for phenylalanine methyl ester so we could not quantify this product. The mole fractions for the products obtained are summarised in Table 3.22, and a plot of these versus mole fractions is shown in Figure 3.20.

Table 3.22 Product mole fractions for TsFOMe.

Time/ min	Degradation/ %	Product mole fractions							
		TsH	TsOH	$TsNH_2$	NH_3	phenyl-pyruvic acid	methyl phenyl-pyruvate	benz-aldehyde	methyl glyoxylate
15	8	0.61	0.28	0.00	0.80	0.12	0.92	0.00	0.07
30	17	0.45	0.21	0.00	0.56	0.10	0.64	0.02	0.04
65	39	0.37	0.14	0.02	0.61	0.08	0.42	0.02	0.03
120	54	0.39	0.11	0.02	0.59	0.07	0.36	0.02	0.03

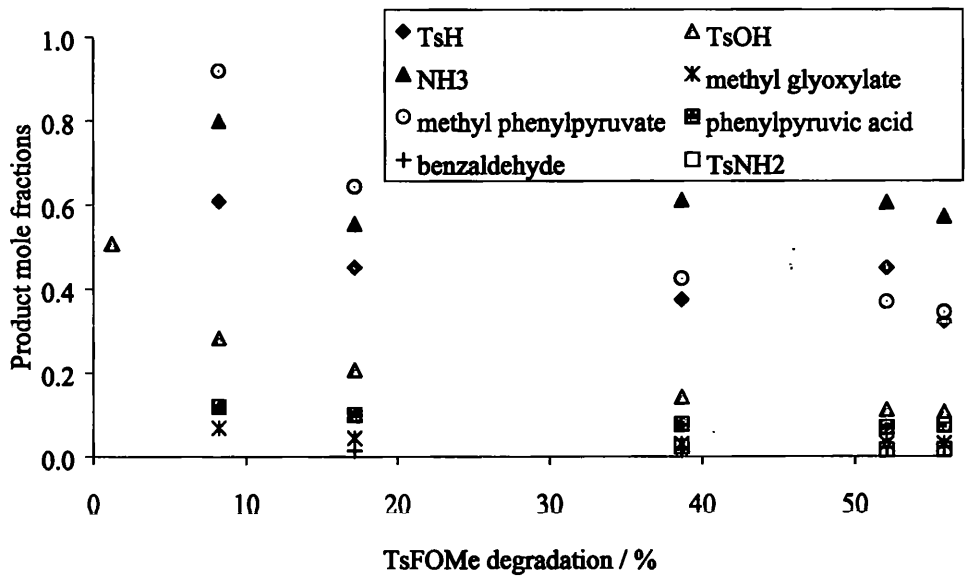

Figure 3.20 TsFOMe product mole fractions.

The apparent pH of TsFOMe was found to decrease after 60 min irradiation. This is most likely due to the appearance of acidic products such as TsH and TsOH. The degradation proceeded at a rate similar to those of most of the previous compounds.

The major products from TsFOMe were analogous to those of TsGOMe i.e. TsH, NH_3 and methyl phenylpyruvate. The latter was found in 64% yield in a 17% degraded sample, although the yield may be higher as the problems noted for the analysis of esters in TsGOMe were apparent in TsFOMe. Also, benzaldehyde is a degradation product of phenylpyruvic acid,[89] so the yield for methyl phenylpyruvate may be as high as 76%. An alternative hypothesis is cleavage of the ester bond during photolysis but this is unlikely as no TsFOH or its major degradation products were found. TsOH was higher than in TsFOH, but as for TsGOMe we were unable to quantify its possible coproduct, phenylalanine methyl ester. Esters of amino acids are known to cyclise with another molecule to give a diketopiperazine. The HPLC data were scrutinized for the diketopiperazine of phenylalanine but it was not found.

A surprising result was the production of methyl glyoxylate (2% yield). This can be explained by electron transfer from the phenyl group to the sulfonyl (*cf* TsY(OMe)OH, Section 3.3.4) with the subsequent breaking of bonds that leads to the observed products (Scheme 3.23). The product from the side-chain is thought to be benzyl alcohol which, as will be seen later, we detected in the photolysis of another tosylated derivative of phenylalanine. Another conceivable product for the side-chain aromatic group was *o*-cresol, resulting from addition of water to the aromatic ring, which was also sought but not found.

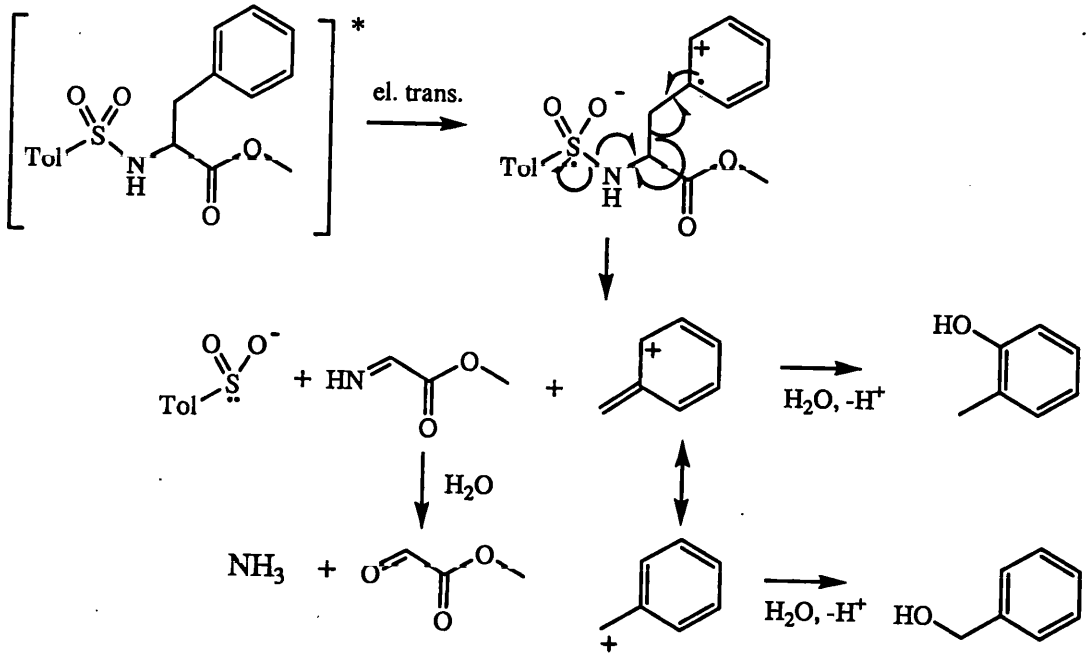

Scheme 3.23 A possible mechanism for the production of methyl glyoxylate from TsFOMe.

We are now able to suggest a degradation scheme for TsFOMe (Scheme 3.24) that explains the observed product distribution, where the value for a particular route is derived from the uniquely associated product. We are able to account for 99% of the degradation at 17% conversion.

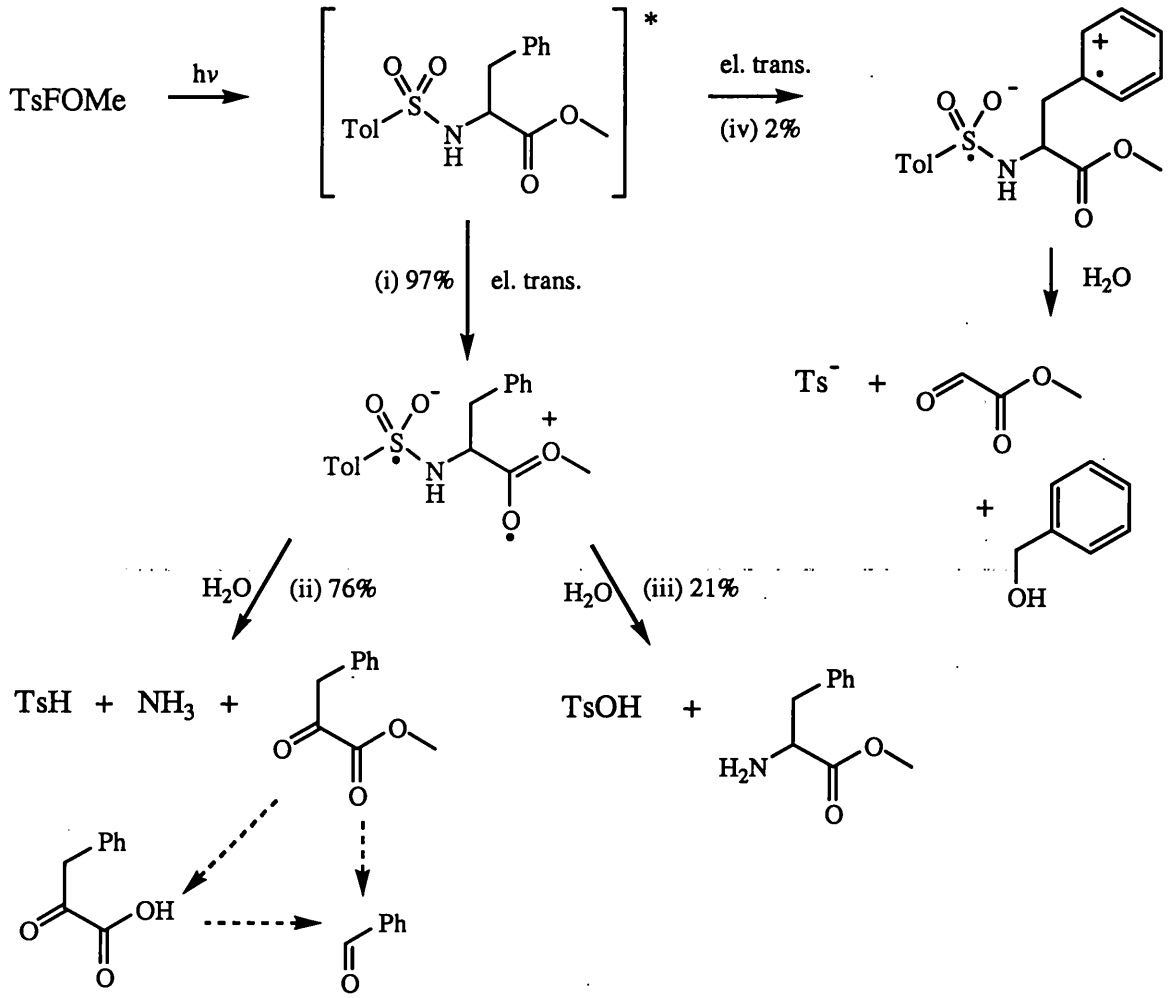

Scheme 3.24 A scheme for TsFOMe degradation at 17% conversion.

3.6.5 Conclusions

TsGOMe and TsFOMe have shown some similar reactions to those of TsGOH and TsFOH, the main difference being that the decarboxylative reactions cannot occur, so the other pathways have become more important. The major reaction involved the C_α-H to give an aldehyde as the final product. A reaction to give the free amino ester looked to be more important than in the tosylated α-amino acids although quantification was difficult. This result is in agreement with that of other workers who found that TsGOMe gave a yield for glycine methyl ester of 44%.[37] This change in product distribution is similar to that for TsβAOH. It appears that increasing the carbon chain length or conversion of the carboxylate to a different functional group such as an ester has a similar effect.

The unexpected result in TsFOMe was the side-chain cleavage that was not observed in TsFOH. This shows that when a good electron donor such as a carboxylate is not present, other groups may donate electrons instead. The photochemistry of all the compounds discussed so far can be predominantly explained by ET to give a biradical which then cleaves by a variety of pathways depending upon the functional groups that are present.

In the next chapter we look at compounds that have an amide instead of a carboxylate group. These do not suffer hydrolysis under the conditions used and have an added significance with the peptide bond as a potential donor in PIET.

Chapter 4: The Photochemistry of Tosyl Amino Amides

4.1 Introduction

In the previous chapter we saw that, in general, tosyl α-amino acids photodegrade in the same manner irrespective of the side-chain groups. The major products were TsH, NH_3, CO_2 and an aldehyde for all of the compounds studied. However, an electron donor in the side-chain was found to reduce the yield for this pathway due to an additional pathway leading to side-chain cleavage. A minor pathway for tosyl α-amino acids involved H-abstraction at the carbon adjacent to the nitrogen. When the carbon chain was extended, as in TsβAOH, or the carboxylate was changed to an ester, this minor pathway became the major one. In this chapter we shall look at the effects of changing the carboxylate group to an amide, which may be a model for a peptide bond and hence this terminology is used for all of the compounds discussed in this chapter. Peptide bonds are known to participate in ET reactions as discussed in Chapter 1, so we anticipated some different photochemistry with these compounds, and this proved to be the case.

We have studied the methyl amide derivatives of all the tosyl amino acids discussed in Chapter 3, hence this chapter follows a similar order. The first section looks at the tosylated methyl amide derivatives of glycine and compounds with unreactive side-chains. One of these prompted a study of some tosyl alkyl amines and these are included at the end of the first section. Next we look at the effects of having aromatic or sulfur containing side-chains and then a brief look at the effect of extending the carbon chain in this series.

In the final section we consider the tosyl derivatives of four glycyl dipeptides. These were studied to seek evidence for longer range PIET and its possible conformational dependence upon bulky groups distal to the tosyl moiety. It is hoped that all of the compounds studied will give insight into the areas discussed in Chapter 1, i.e PIET,

removal of protecting groups, arylsulfonamide drug photostability and the mechanisms of photodegradation in peptide-like compounds.

First, though, a brief summary of the methods that were used to study the compounds discussed in this chapter.

4.2 Method summary

Full experimental details are given in Chapter 2. All of the compounds in this chapter except for *N*-*p*-tosylglycylglycine (TsGGOH) were studied in 40% aq. acetonitrile. The analytical methods were as described previously i.e. HPLC analysis of the products including the analysis of DNP and AccQTag™ derivatives. TsGGOH was studied in aqueous solution that had the pH unadjusted (~3) and the pH adjusted to 9 with 1M NaOH as described for TsGOH. Analysis was by the same HPLC methods as the other compounds in this chapter but additionally NH_3 and CO_2 were measured by gas electrodes.

The assignment of HPLC peaks was confirmed by comparison of UV-vis spectra and RT with those of authentic samples, and by co-elution with an authentic samples. Further confirmation of product identity was sought by LC-MS for four of the compounds.

4.3 Glycine and amino acids with aliphatic side-chains

4.3.1 Introduction

The first compound to be discussed is *N*-*p*-tosylglycine-*N'*-methyl amide (TsGNMA, **26**) where the amino acid does not have a side-chain, making it the simplest one of this section. Next we shall look at *N*-*p*-tosylvaline-*N'*-methyl amide (TsVNMA, **27**) which has a bulky *iso*-propyl side-chain. The third example is *N*-*p*-tosylproline-*N'*-methyl amide (TsPNMA, **28**) with the five-membered ring as part of the amino acid and hence no hydrogen on the sulfonamide nitrogen. The final compound in this section, *N*-*p*-tosyl-*N'*-

methyl-2-amino-*iso*-butyramide (TsAibNMA, **29**) which contains an unnatural amino acid with two methyl groups at α-C.

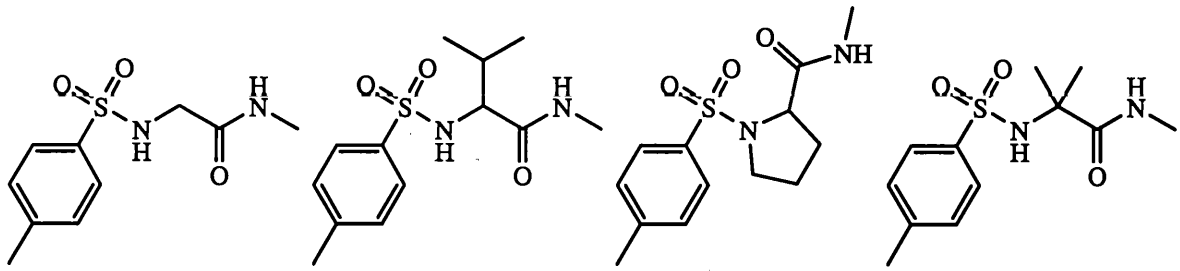

26 **27** **28** **29**

The results obtained with TsAibNMA prompted the study of some tosyl alkyl amines: tosylmethylamine (TsNHMe, **30**), tosylethylamine (TsNHEt, **31**), tosyl-*iso*-propylamine (TsNH*i*Pr, **32**), tosyl-2-butylamine (TsNH-2-Bu, **33**) and tosyl-*tert*-butylamine (TsNH*t*Bu, **34**). These are examined to look for C-C bond cleavage in compounds where ET is not possible.

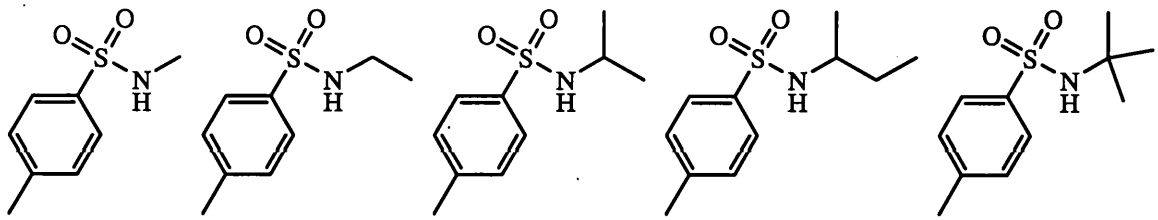

30 **31** **32** **33** **34**

4.3.2 General observations

Two of the compounds studied, TsGNMA and TsVNMA became bright yellow upon photolysis. TsPNMA solutions remained colourless whilst the TsAibNMA solutions became a very pale yellow. The tosyl alkyl amine solutions all remained colouless upon photolysis.

Table 4.1 shows the changes in apparent pH and the degradation after 60 min irradiation. Degradation rates were similar to those of the tosyl amino acids, although TsGNMA was slightly slower and TsPNMA was slightly faster than the rest.

Table 4.1 Change in apparent pH and conversion at 60 min irradiation.

Substrate	Initial apparent pH	Apparent pH at 60 min	Degradation at 60 min/%
TsGNMA	5.9	5.3	26
TsVNMA	5.9	5.1	33
TsPNMA	7.7	3.9	44
TsAibNMA	5.3.	6.9	38
TsNHMe	-	-	36
TsNHEt	6.7	3.6	35
TsNH*i*Pr	-	-	37
TsNH-2-Bu	-	-	37
TsNH*t*Bu	-	-	32

4.3.3 *N-p*-tosylglycine-*N'*-methyl amide

HPLC analysis of the raw photolysates with detection at 228 nm showed three peaks, the largest of which was TsH. The other two were identifed as TsOH and TsGOH. The yellow component of the photolysate eluted at 4.7 min and had a λ_{max} 455 nm.

The analysis for DNP derivatives with detection at 354 nm gave two peaks that were identified as the stereoisomers of *N*-methyl glyoxamide DNP. AccQTag™ analysis showed peaks that correspond to NH_3, glycine, methylamine and glycine *N*-methyl amide. The product mole fractions are shown in Table 4.2 and illustrated graphically in Figure 4.1.

Table 4.2 Product mole fractions for TsGNMA 40% aq. acetonitrile photolysate.

Time/ min	Degradation/ %	Product mole fractions							
		TsH	TsOH	TsGOH	Glycine *N*-methyl amide	Methyl-amine	Glycine	NH_3	methyl glyoxamide
10	7	0.36	0.12	0.18	0.08	0.21	0.002	0.49	0.72
15	8	0.60	0.08	0.20	0.12	0.33	0.002	0.85	0.89
30	16	0.49	0.11	0.17	0.09	0.24	0.002	0.73	0.77
60	26	0.60	0.07	0.12	0.13	0.19	0.003	0.81	0.80
120	41	0.59	0.05	0.07	0.14	0.16	0.003	0.76	0.73

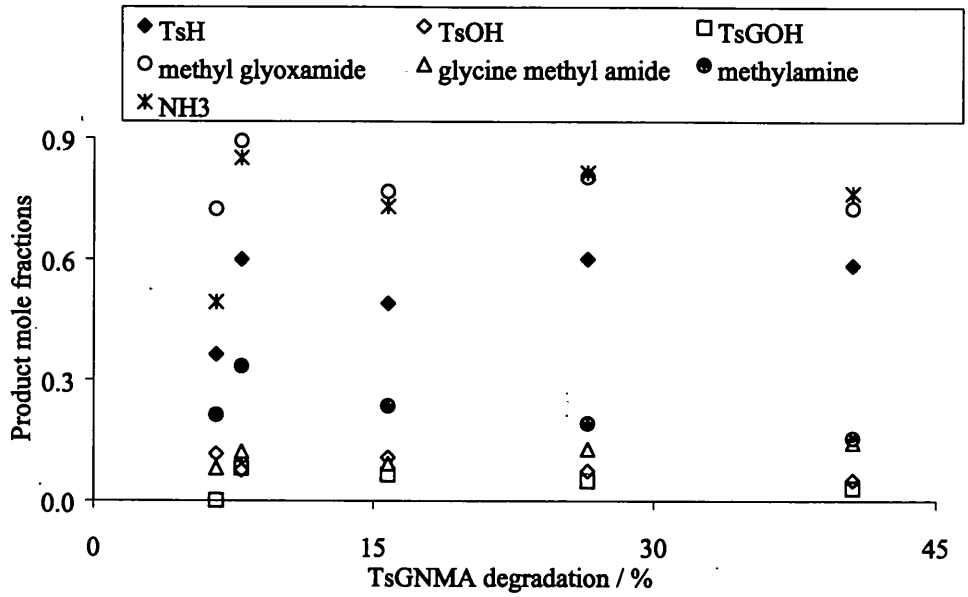

Figure 4.1 TsGNMA product mole fractions.

The formation of bright yellow photolysate solutions was unexpected and we shall consider this phenomenon in Section 4.10. As we shall see, this provides support for the ET mechanisms proposed in the photodegradation of the tosylated amino compounds. The slight decrease in the apparent pH is consistent with the production of acidic compounds such as TsH and TsOH.

The major photoproducts from TsGNMA are TsH, NH_3 and *N*-methyl glyoxamide. As with TsGOH, we have found good correlations between these products (Table 4.3) with gradients close to one indicating that they are produced in equal amounts throughout the photolysis.

Table 4.3 Correlations for TsGNMA.

Products	R^2	Gradient	Intercept
NH_3 vs TsH	0.99	1.15	0.0003
methyl glyoxamide vs TsH	0.99	1.05	0.0004
NH_3 vs methyl glyoxamide	1.00	0.90	0.0002

These products can be explained by a mechanism analogous to the one suggested for the major aldehydes in TsGOMe and TsFOMe photolyses, and the minor aldehydes of

the tosyl amino acids such as TsGOH. However, in the case of TsGNMA, ET would occur from an amide bond rather than an ester bond or carboxylate group, followed by a C_α-H abstraction (Scheme 4.1). We did not find any glyoxylic acid suggesting that *N*-methyl glyoxamide is more stable to hydrolysis than methyl glyoxylate, as would be expected.

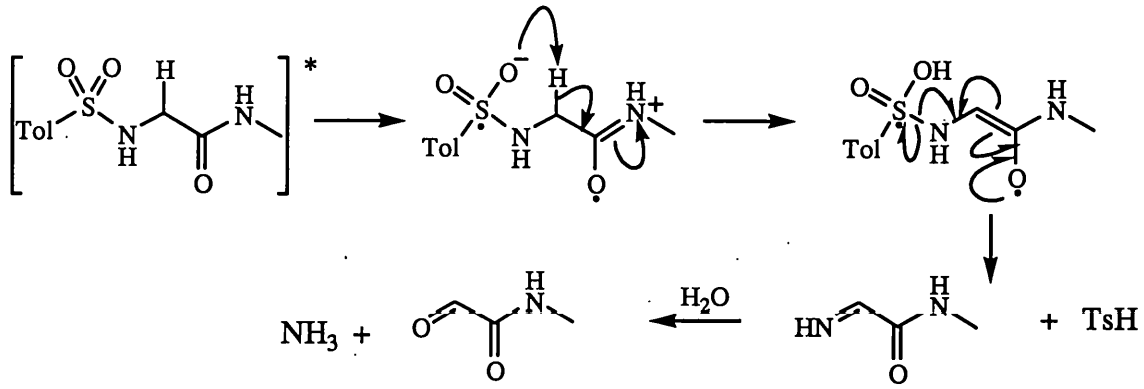

Scheme 4.1 A mechanism for C_α-H abstraction to give the major products of TsGNMA photolysis.

TsOH and glycine *N*-methyl amide were found in similar yields and again can be explained with a mechanism similar to that advanced previously for S-N cleavage to yield the free amino acid moiety. The biradical now involves the amide bond as shown above, which may cyclise as suggested for TsGOH to give an intermediate with a five-membered ring. Attack of water, however, can lead to not only S-N but peptide bond cleavage too and another significant pair of products, methylamine and TsGOH (Scheme 4.2), found with yields of 33% and 20% respectively, at 8% conversion. The latter degrades further so does not match the amine quantitatively.

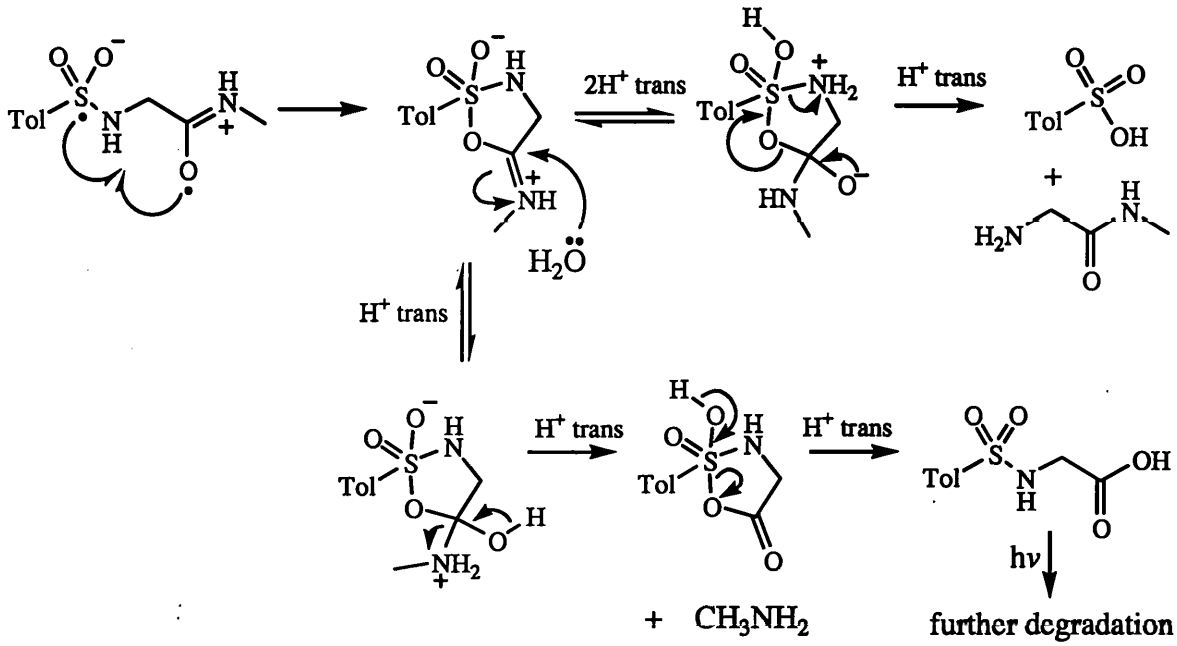

Scheme 4.2 Mechanisms for S-N and peptide bond cleavages.

The mechanism proposed for the TsGNMA peptide bond cleavage has intermediates that are analogous to those suggested by other workers who observed an unusual peptide bond acidolysis in Aib containing dipeptides (Scheme 4.3).[93]

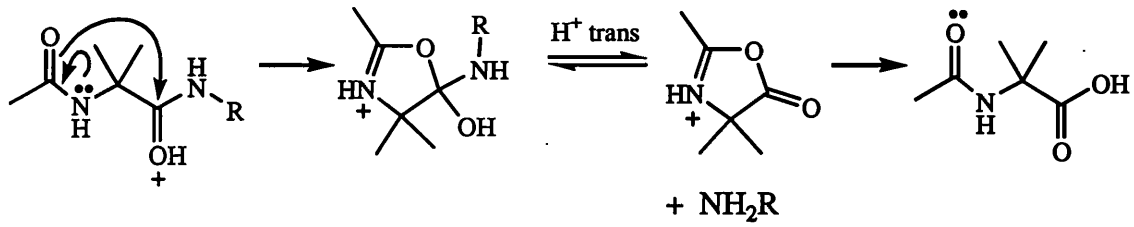

Scheme 4.3 Mechanism for peptide bond acidolysis.

An alternative mechanism for the peptide bond cleavage could involve homolytic cleavages analogous to that proposed for the major products of TsGOH (Scheme 4.4). However, this can be discounted for a number of reasons; firstly, we have observed TsGOH which supports Scheme 4.2, and secondly, we did not find any formaldehyde.

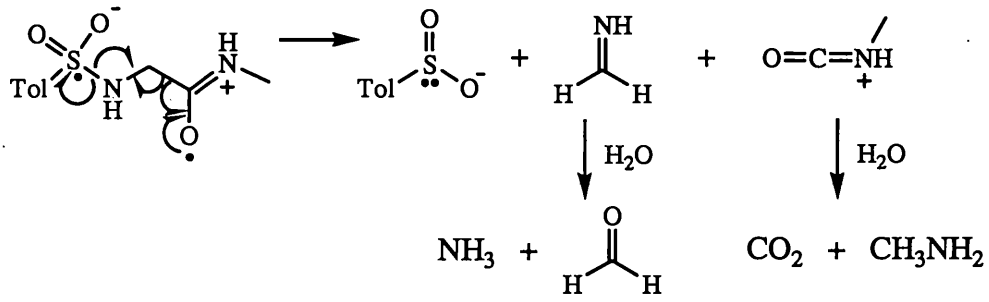

Scheme 4.4 An alternative mechanism for peptide bond cleavage in TsGNMA.

Scheme 4.5 shows the proposed degradation scheme for TsGNMA based upon the results obtained at 16% degradation. An initial ET from the amide bond to the sulfonyl gives a biradical intermediate that could react by the three pathways discussed above to give all of the observed products. Scheme 4.5 accounts for 97% of the degraded substrate with the value for each route calculated as an average of all the observed products as they were all unique to a single pathway.

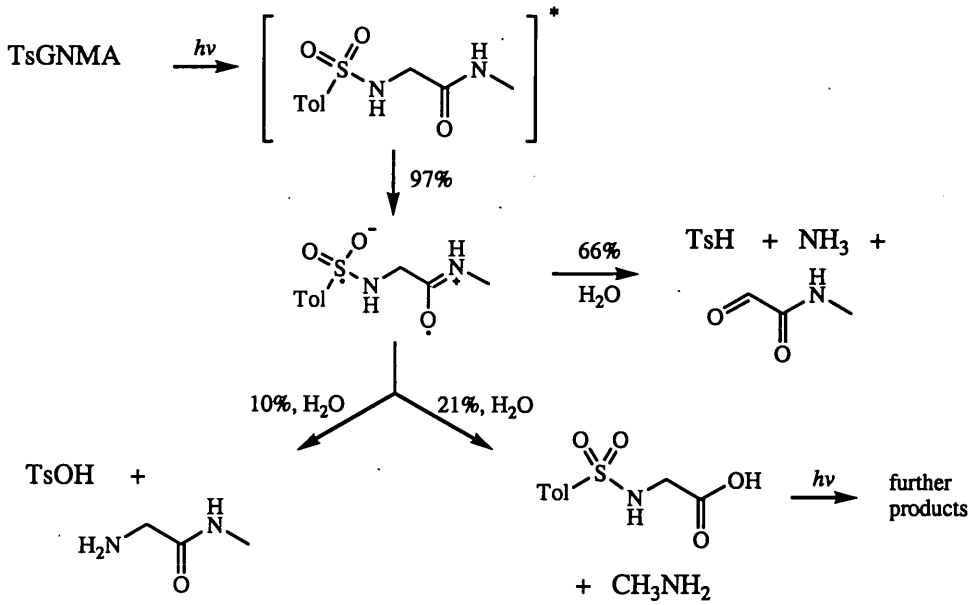

Scheme 4.5 A possible degradation scheme for TsGNMA at 16% degradation.

4.3.4 *N-p*-tosylvaline-*N'*-methyl amide

HPLC analysis of the raw photolysates showed four peaks, the major one being TsH. Two of the others were identified as TsOH and $TsNH_2$. A small one at 10.8 min was

not identifed. It had a λ_{max} 236 nm indicating that it was an aromatic compound. The yellow component of the photolysate eluted at 8.5 min.

Analysis for DNP derivatives gave five peaks. The one with the latest RT was identified as *iso*-butyraldehyde DNP. By comparison with previous cases, two more are likely to be the stereoisomers of *N*-methyl-3,3-dimethylpyruvamide DNP which would be expected to have an earlier RT than *iso*-butyraldehyde DNP as they would be more polar molecules.

AccQTag™ analysis gave peaks that were identified as NH_3 and methylamine, and two unidentified peaks, one of which is could be valine methyl amide. The product mole fractions are given in Table 4.4 and illustrated graphically in Figure 4.2.

Table 4.4 Product mole fractions for TsVNMA 40% aq. acetonitrile photolysate.

Time/ min	Degradation /%	Product mole fractions										
		TsH	TsOH	10.8 min[a]	$TsNH_2$	NH_3	methyl -amine	13.7 min DNP[b]	15.2 min DNP[b]	15.4 min DNP[b]	18.1 min DNP[b]	*iso*-butyraldehyde[b]
15	12	0.43	0.09	0.00	0.04	0.39	0.10	0.06	0.03	0.05	0.17	0.03
30	20	0.56	0.05	0.02	0.05	0.44	0.11	0.08	0.05	0.04	0.13	0.05
60	33	0.56	0.05	0.01	0.04	0.46	0.11	0.08	0.06	0.02	0.08	0.05

[a]Quantified by comparison with a TsVNMA standard, [b]quantified from a HCHO DNP standard.

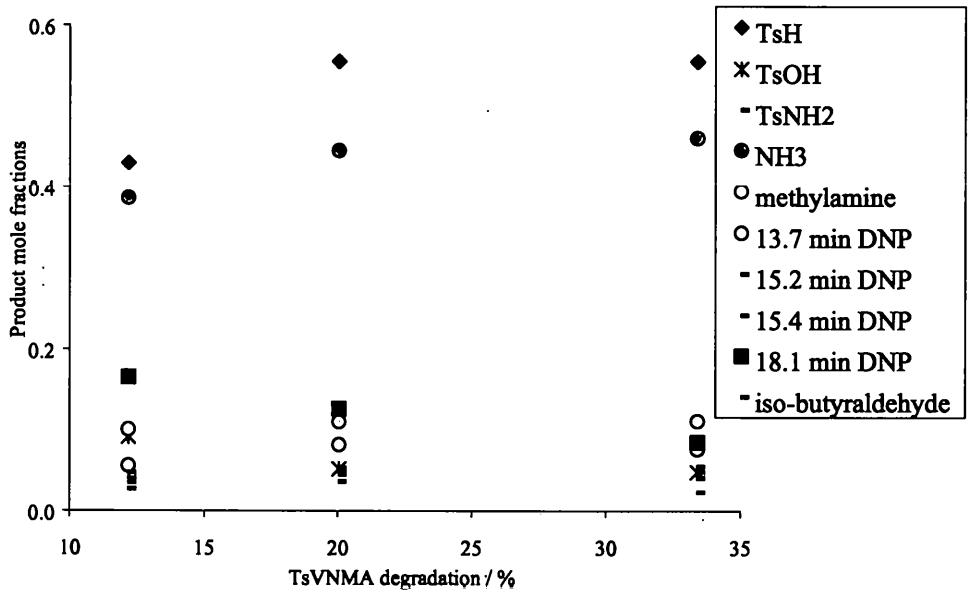

Figure 4.2 TsVNMA product mole fractions versus degradation.

TsVNMA, like TsGNMA became bright yellow upon photolysis and gave similar results to TsGNMA, although some of the products were not observed in such high yields. A slight decrease in the apparent pH is again consistent with the observed products. The major products were TsH and NH_3 in ~50% yield, which is about 10% lower than for TsGNMA. *N*-methyl-3-methyl-2-oxo-butanamide is expected as a co-product resulting from C_α-H abstraction (Scheme 4.6) and would be analysed as its DNP derivative. Stereoisomers would be expected for the DNP derivative as observed for all previous α-keto carbonyl compounds. A number of DNP derivatives were found but the two highest yields account for only 23% of the degraded substrate. This could be due to a stability problem or an analytical one as an authentic standard was not available so values were estimated using a HCHO DNP standard.

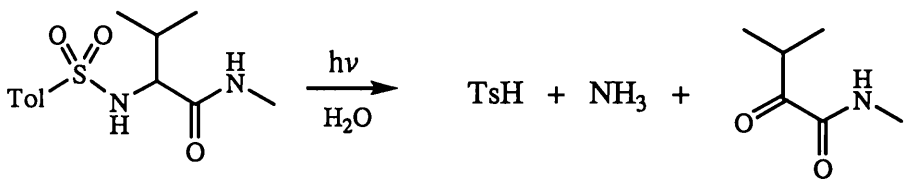

Scheme 4.6 The products expected from C_α-H abstraction in TsVNMA (*cf* Scheme 4.1).

TsOH was only found in 5% yield and its expected coproduct, valine *N*-methyl amide could not be measured as an authentic standard was not available. A peak in the AccQTag™ analysis eluted after valine as would be expected for the valine *N*-methyl amide so it was believed to be present. Assuming that the yield of TsOH is the yield for S-N cleavage, this is lower than the value observed in TsGNMA. Methylamine was found in 11% yield and may come from a net hydrolysis of the peptide bond as suggested for TsGNMA in Scheme 4.2 and give TsVOH as its co-product. However, TsVOH was not found although it may have been photodegraded as it was formed, as its major degradation product, *N*-methyl-3-methyl-2-oxo-butanamide was found. Again this route has a lower value than the analogous one in TsGNMA.

Scheme 4.7 accounts for all the identified or suspected products at 20% degradation of TsVNMA. Routes (ii) and (iii) have a lower value than for TsGNMA possibly reflecting steric hindrance of the *iso*-propyl group in allowing formation of the cyclic intermediate postulated for both routes. Route (i) on the other hand, does not require a cyclic intermediate and although closer to the corresponding result with TsGNMA, its smaller contribution indicates hindrance to C_α-H abstraction. It appears, however, that TsVNMA has one additional route (iv) compared with TsGNMA to give $TsNH_2$ in 5% yield.

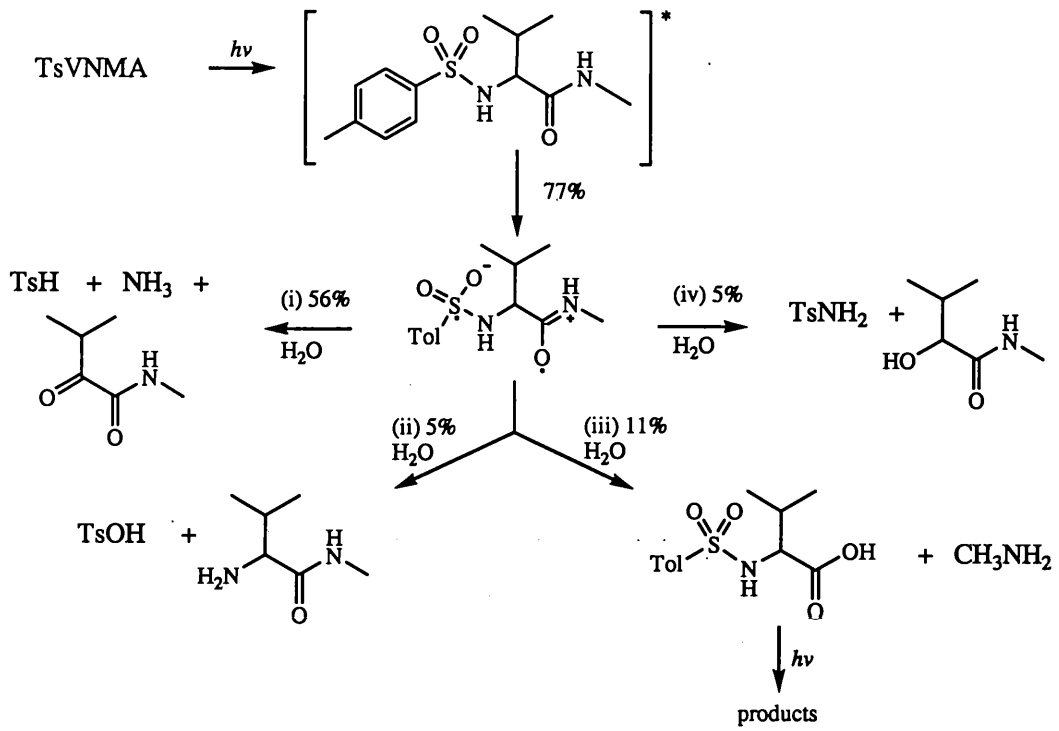

Scheme 4.7 A possible degradation scheme for TsVNMA at 20% degradation.

The production of $TsNH_2$ in TsVNMA but not in TsGNMA may be a result of the other pathways having more steric hindrance in the former than the latter. An alternative mechanism, however, that is not possible with TsGNMA, involves a Norrish Type II mechanism (Scheme 4.8) as suggested for TsVOH (Section 3.2.4) that leads to a photolabile product. We have no direct evidence for either mechanism.

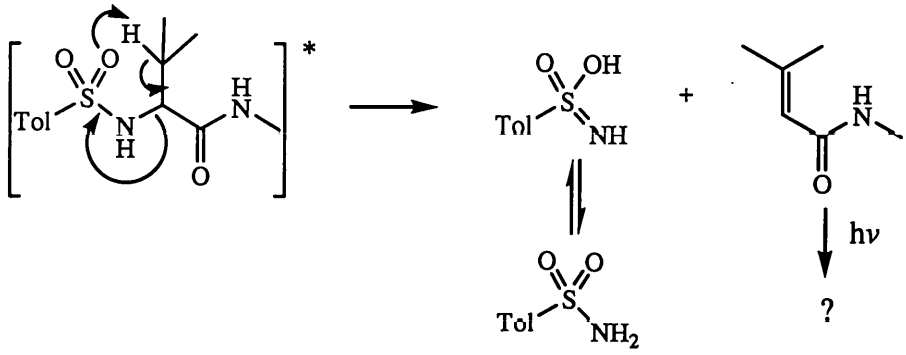

Scheme 4.8 A possible mechanism for production of $TsNH_2$ involving a six-membered transition state and the side-chain hydrogens (*cf* Scheme 3.8).

4.3.5 *N-p*-tosylproline-*N'*-methyl amide

HPLC analysis of the raw photolysate with detection at 228 nm showed that TsH was the major aromatic product and that TsOH was the only minor one.

Analysis for DNP derivatives with detection at 354 nm showed four peaks that have not been identified but had λ_{max} typical of the DNP derivatives of aliphatic aldehydes; 361, 374, 359 and 353 nm. These were quantified using a HCHO DNP standard.

Analysis for AccQTag™ derivatives revealed a very small amount of NH_3 plus four other peaks that were not identifed. One of these is likely to be proline methyl amide as it had a slightly later RT than proline, which was not found.

The product mole fractions are shown in Table 4.5 and illustrated graphically in Figure 4.3 plotted against TsPNMA degradation.

Table 4.5 Product mole fractions for TsPNMA

Time/ min	Degradation/%	Product mole fractions						
		TsH	TsOH	NH_3	7.1 min DNP	7.3 min DNP	7.8 min DNP	13.5 min DNP
15	14	0.65	0.26	0.02	0.26	0.13	0.02	0.10
30	24	0.65	0.27	0.02	0.19	0.10	0.03	0.13
60	44	0.63	0.26	0.02	0.11	0.06	0.04	0.15

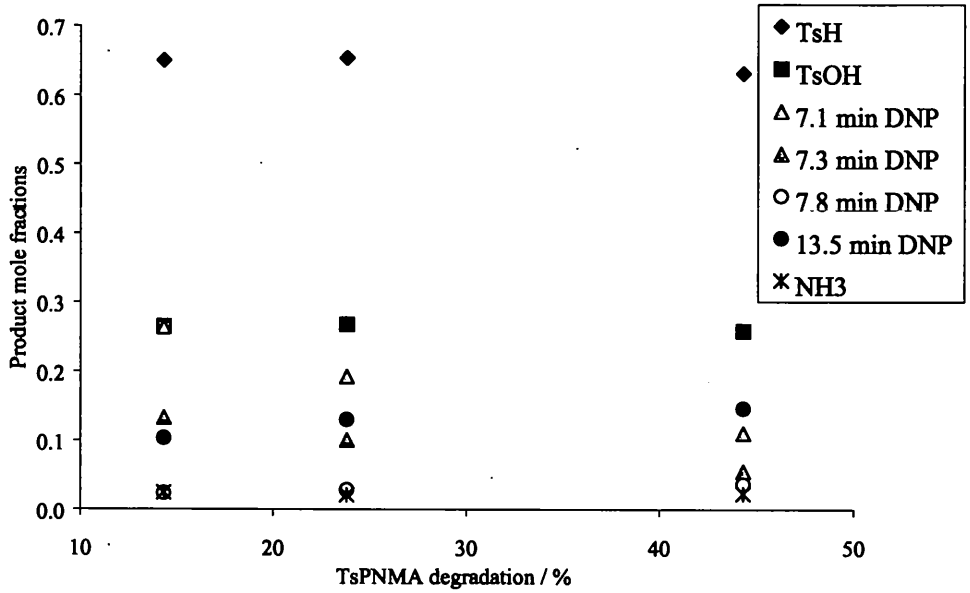

Figure 4.3 TsPNMA product mole fractions versus degradation.

TsPNMA, unlike the two previous compounds, did not become yellow upon photolysis suggesting that a hydrogen atom on the sulfonamide nitrogen is important for the formation of the yellow species. The apparent pH of the TsPNMA photolysates showed a much greater decrease than with TsGNMA and TsVNMA.

The absence of methylamine or TsPOH suggests that little or no peptide bond cleavage occurred. If, as we had proposed, a cyclic intermediate is required for this outcome, the intermediate with TsPNMA would require two five-membered rings fused together (Scheme 4.9). Amide bond cleavage and S-N cleavage both require attack of water at the amide carbonyl, however, the latter results in relief of the ring strain and may be more favourable than the former which retains the ring strain. At 20% conversion, 26% TsOH was produced which is the highest yield of any of the tosyl amino acid derivatives so far. Proline *N*-methyl amide could not be measured as a standard was not available but the AccQTag™ HPLC was consistent with it being a significant product. Thus, the cyclic mechanism appears to be supported by the high yield for S-N cleavage and the lack of amide bond cleavage in TsPNMA which would require a strained intermediate.

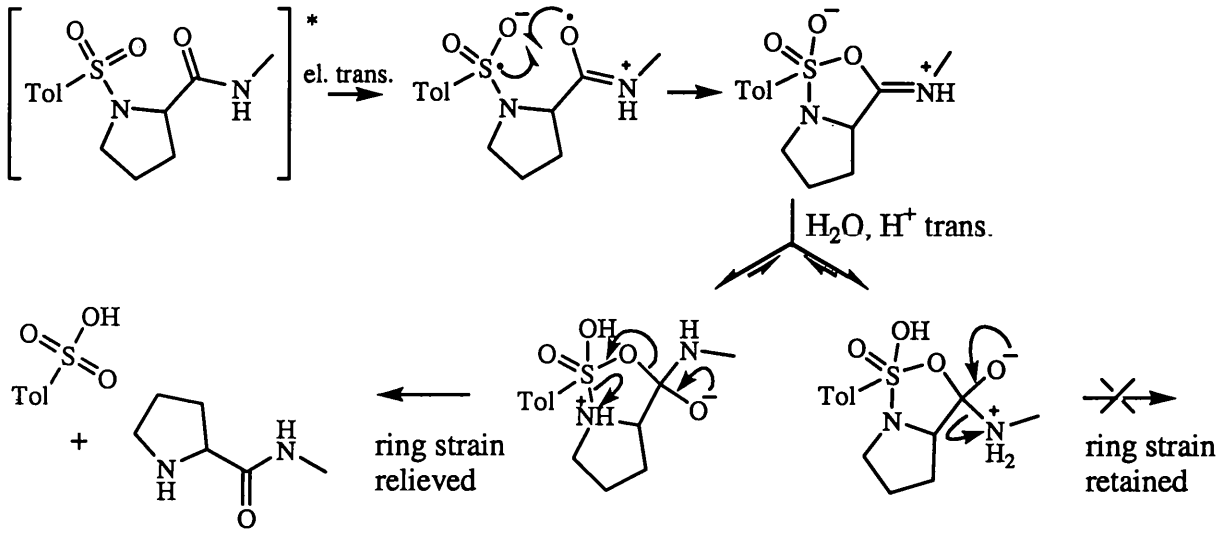

Scheme 4.9 Mechanism for S-N and peptide bond cleavages inTsPNMA.

The major product was TsH observed in 65% yield which is very similar to the yield of TsH from TsGNMA. Its expected co-product would be an α-keto carbonyl compound from C_α-H abstraction that would have been analysed as the two stereoisomers of its DNP derivative (Scheme 4.10). Four DNP peaks were observed with the two largest ones giving a maximum yield of 39%. The low yield of DNP products compared with TsH could be due to the quantitation using a HCHO DNP standard or a stability problem with carbonyl product as suggested for the analogous products of TsPOH. As with TsPOH, no NH_3 is expected as the nitrogen is retained in the final product.

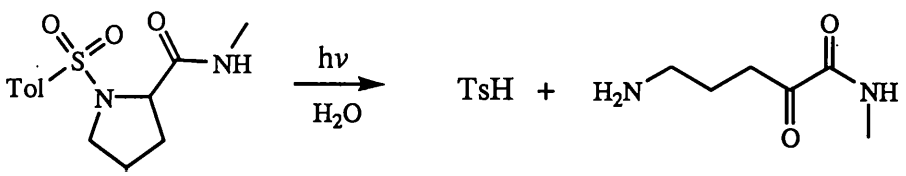

Scheme 4.10 The products expected from C_α-H abstraction in TsPNMA (*cf* Scheme 4.1).

The other two DNP derivatives accounted for 12% of the degraded substrate. These could come from C_β-H abstraction (Scheme 4.11) in a mechanism similar to that proposed

for sulfone compounds[84] and the alternative mechanism proposed for C_α-H abstraction in TsGOH that does not involve ET. The aldehyde would be likely to form two stereoisomers with the DNP reagent.

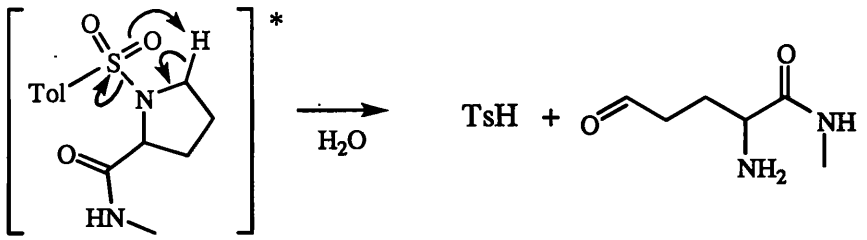

Scheme 4.11 A possible mechanism for C_δ-H abstraction in TsPNMA.

A tentative degradation scheme that accounts for the yields of the observed tosyl products is shown in Scheme 4.12 where TsH has been assigned to two pathways, (i) and (iii), with the carbonyl and the aldehyde DNP derivatives respectively.

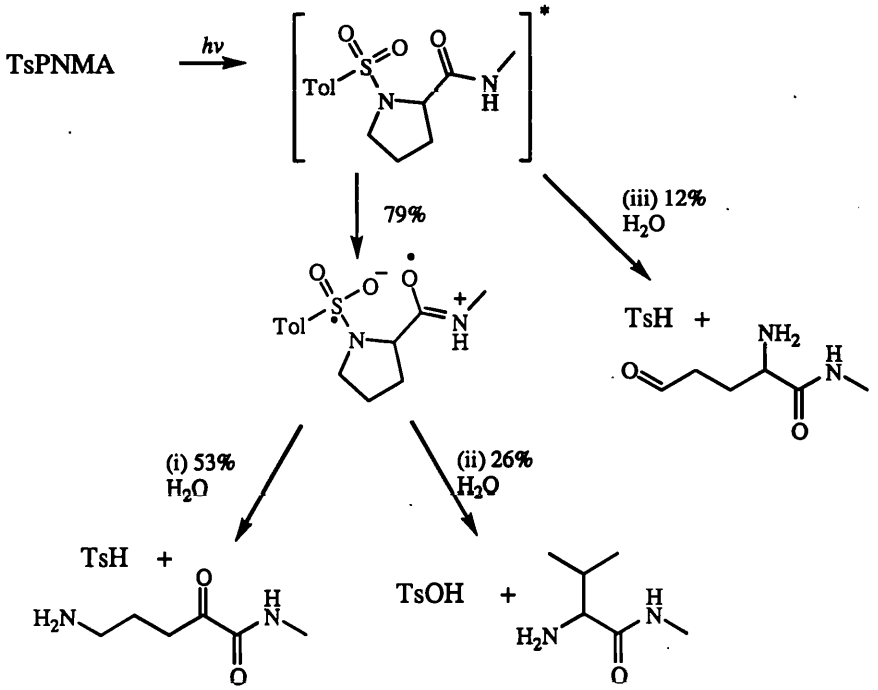

Scheme 4.12 A possible degradation scheme for TsPNMA at 14% conversion.

TsPNMA has revealed a number of differences to the previous amide derivatives, TsGNMA and TsVNMA. It did not become yellow upon photolysis, nor did it exhibit any amide bond cleavage. The latter appears to have been compensated for by an enhanced amount of S-N cleavage to give TsOH and proline *N'*-methyl amide in the highest yield yet.

4.3.6 *N-p*-tosyl-*N'*-methyl-2-amino-*iso*-butyramide

HPLC analysis of the raw photolysates with detection at 228 nm showed the major aromatic product to be TsH. TsOH and $TsNH_2$ were minor products. Analysis for DNP derivatives with detection at 354 nm showed two peaks that were identified as acetone DNP and methyl pyruvamide DNP. AccQTag™ analysis gave peaks for NH_3, *N'*-methyl-2-amino-*iso*-butyramide (AibNMA) and methylamine. The product mole fractions are given in Table 4.6 and shown graphically in Figure 4.4. An experiment for CO_2 analysis gave mole fractions of 0.05 and 0.06 at 28% and 40% degradation respectively.

Table 4.6 Product mole fractions for TsAibNMA.

Time/ min	Degradation/%	Product mole fractions							
		TsH	TsOH	$TsNH_2$	NH_3	Aib-NMA	methyl-amine	methyl pyruvamide	acetone[a]
10	6	0.67	0.12	0.02	0.49	0.44	0.27	0.16	0.07
15	11	0.54	0.10	0.03	0.66	0.34	0.26	0.14	0.06
30	22	0.50	0.08	0.03	0.64	0.34	0.22	0.13	0.05
60	38	0.49	0.08	0.03	0.63	0.29	0.21	0.13	0.05

[a]Reported values for acetone are low due to quantification problems of the DNP derivative as noted in Chapter 2

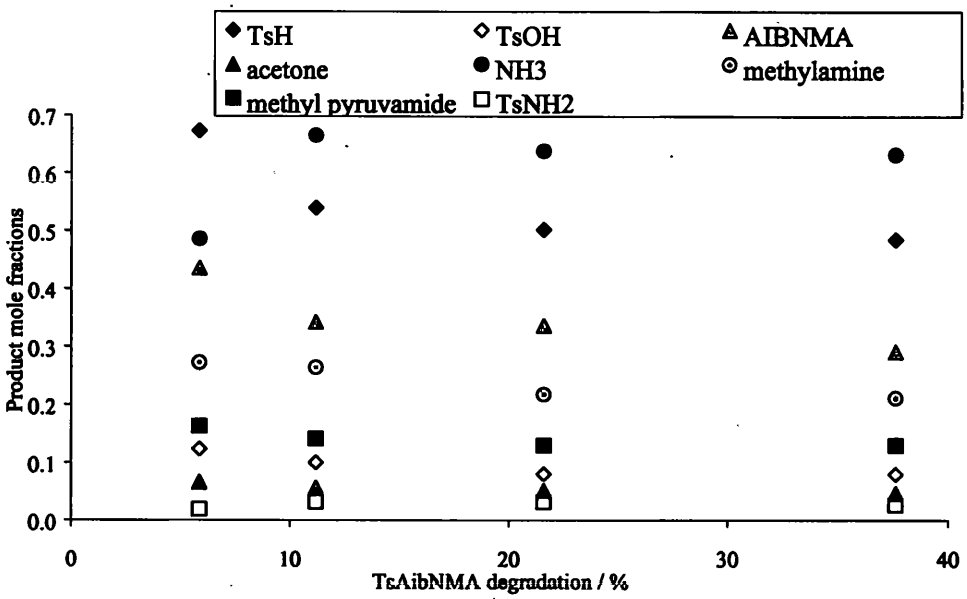

Figure 4.4 Product mole fractions of TsAibNMA photolysis.

TsAibNMA became only very pale yellow upon photolysis further suggesting that the C_α-H is important for the formation of a yellow species. The product mole fractions for TsAibNMA show that its photolysis has yielded products analogous to those observed in the three previous compounds. However, peptide bond cleavage was observed in the highest yield in TsAibNMA (26%), reflecting the influence of the α-H being replaced by a methyl group. S-N cleavage to give the free AibNMA was also seen in slightly higher yields than for TsGNMA and TsVNMA and for most of the compounds in the previous chapter, although TsOH and AibNMA values did not correlate well in this case. The higher yields apparent for both peptide bond and S-N cleavage could be seen as support for a common intermediate such as the cyclic system that has been proposed (*cf.* Scheme 4.2).

Methyl pyruvamide (15%) was a surprising product as it implicates a C_α-C cleavage (Scheme 4.13) analogous to the mechanism proposed for C_α-H abstraction proposed as one consequence of PIET in other compounds (e.g. Scheme 4.1). The sulfonic ester would be readily hydrolysed and detected as TsH in HPLC analysis.

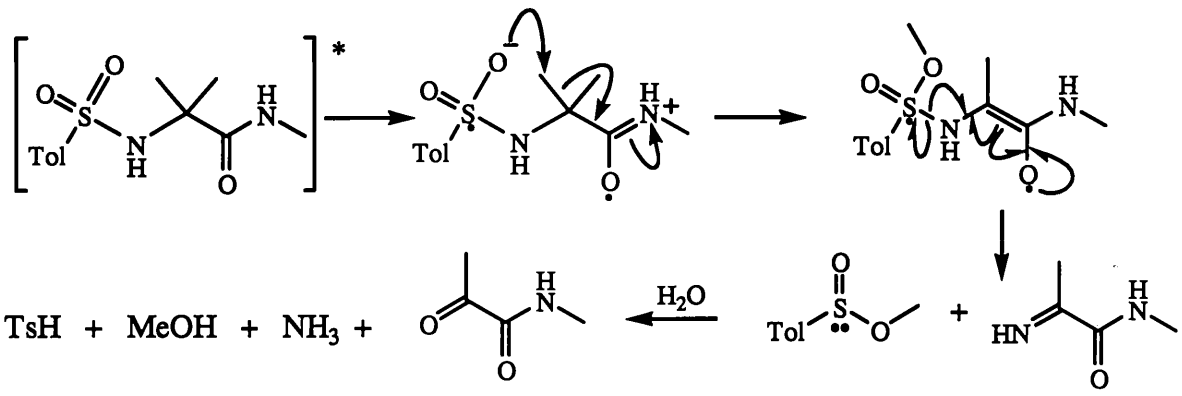

Scheme 4.13 A mechanism for C_α-C bond cleavage in TsAibNMA.

A degradation scheme analogous to those proposed earlier is shown in Scheme 4.14, but it fails to account for the total yield of some products. The most notable example is TsH, which had a measured yield of 54%, yet the scheme only accounts for 14%. However we also measured a 6% yield for acetone, but as reported earlier (TsAibOH Section 3.2.6), we encountered problems quantifying acetone, the values being seriously underestimated. If our control experiment with acetone was valid (Section 2.5.7), the value is more likely to be around 24%, close to the measured value of methylamine. This suggests that a further 24% TsH can be accounted for by TsAibOH degradation, but that still leaves 16% unaccounted for. TsAibOH was not found, although it could be photodegraded as soon as it is produced. Another explanation could be that the peptide bond cleaves by the alternative mechanism suggested for TsGNMA (Scheme 4.4), but this would require a higher yield for CO_2 to match the methylamine mole fractions and still gives the same value for TsH as Scheme 4.14.

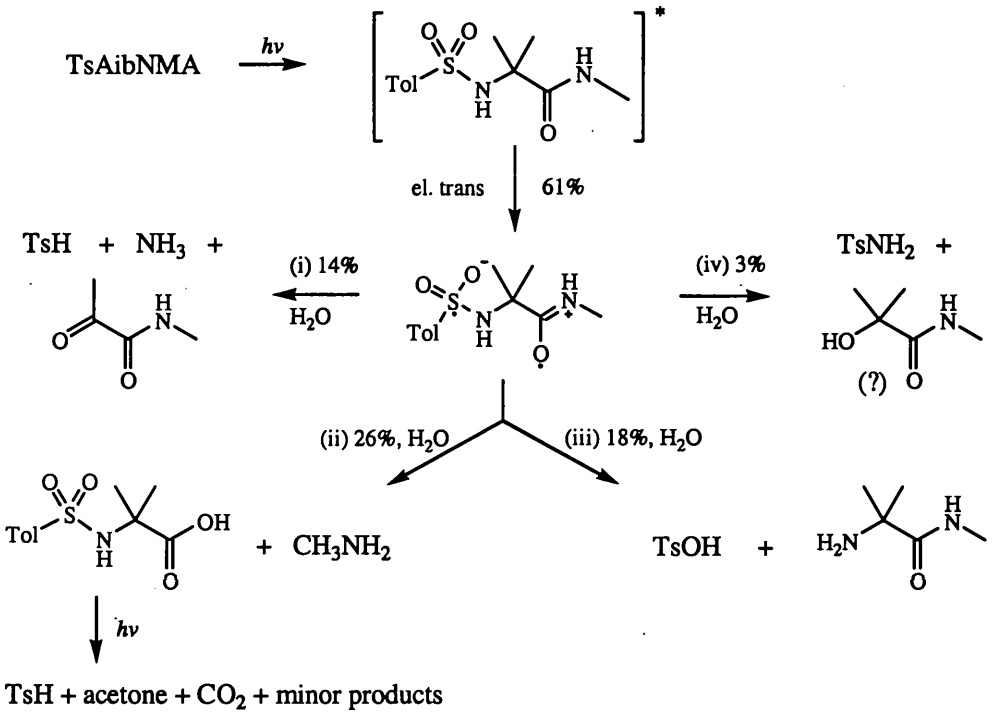

Scheme 4.14 A possible degradation scheme for TsAibNMA at 11% degradation.

The mechanism for $TsNH_2$ has been proposed as a radical cleavage (TsGOH, Scheme 3.6) or a Norrish Type II mechanism involving side-chain hydrogens (TsVOH, Scheme 3.8). The latter would give *N*-methyl methylacrylamide as the coproduct, which was sought in the photolysates but not found, although this could be photolabile. Scheme 4.14 shows the product of the radical cleavage but the co-product was not sought either and the mechanism therefore remains equivocal.

TsAibNMA has shown increased values for amide cleavage and S-N cleavage compared with TsGNMA. However, perhaps the most significant outcome of replacing the hydrogen atom by a methyl group in TsAibNMA was the apparent C_α-C bond cleavage. This, and the apparent mass balance problems with the PIET pathway prompted us to examine a series of tosyl alkyl amines where there there is little or no scope for intramolecular ET.

4.3.7 Tosyl alkyl amines

Five tosyl alkyl amines were studied to investigate the C-C cleavage observed in TsAibNMA and also to gain further insight into other pathways that we have found. As we saw in Table 4.1, the rate of degradation is similar to that of other compounds confirming that the chromophore has not changed. Table 4.7 gives the product mole fractions found for each of the tosyl alkyl amines at approximately 20% conversion.

Table 4.7 Product mole fractions for the tosyl alkyl amines at ~20% degradation.

	Product mole fractions						
Substrate	TsH	TsOH	$TsNH_2$	NH_3	parent amine	DNP derivative of C_α-H abstraction	DNP derivative of C_α-C cleavage
TsNHMe	0.38	0.35	0.05	0.40	0.60	0.40	-
TsNHEt	0.44	0.17	0.03	0.30	0.48	0.47	-
TsNH*i*Pr	0.61	0.17	0.01	0.62	0.30	0.28[a]	0
TsNH-2-Bu	0.61	0.18	0	0.70	0.30	0.10	0.01
TsNH*t*Bu	0.32	0.35	0	0.02	0.73	-	0.04

[a]Quantification problems of acetone as its DNP derivative noted in Chapter 2

It is immediately apparent from the above table that C-C cleavage is not a favourable process in the tosyl alkyl amines. In particular, the last compound, TsNH*t*Bu has no α-CH bonds and might be expected to exhibit a higher yield for C-C cleavage than was actually found. Instead, the yield of the amine has reached 73%, the highest observed yet. Most of the tosyl amino acid compounds discussed previously have shown good correlations between TsOH and the amino moiety, but all the compounds in the above table have a yield for the amine that is approximately double the value of TsOH. However, in Chapter 1 we saw that Pete and co-workers had proposed a radical cleavage for tosyl alkyl amines followed by disproportionation.[29] If valid, it is likely that the tosyl alkyl amines we have studied undergo a radical cleavage followed by disproportionation to give the observed products.

A degradation scheme is suggested for TsNH*i*Pr in Scheme 4.15, where the values for individual routes are based partly upon the measured values; route (i) is a

disproportionation of the aromatic radical to give TsOH in 17% yield (Table 4.7) and TsH. The remaining TsH (44%) is accounted for by disproportionation with the amine radical to give an imine coproduct, route (ii), that ultimately gives acetone and NH_3 in 44% yield. This leaves ~17% NH_3 that could be a product of the disproportionation of the amine radical, route (iii), which also yields the amine and further acetone. This leaves 22% of the substrate unaccounted for that may react to give more of the amine and an unidentified product, route (iv). Some of the products in Scheme 4.15 have been accounted for using their measured values from Table 4.7, whereas others such as *iso*-propylamine and acetone are based upon their coproducts. The calculated value for *iso*-propylamine is 39% from the sum of routes (iii) and (iv), which is only 9% higher than the measured value. The scheme predicts a value of 61% for acetone, considerably higher than measured, however, we have noted previously the problems with its quantification.

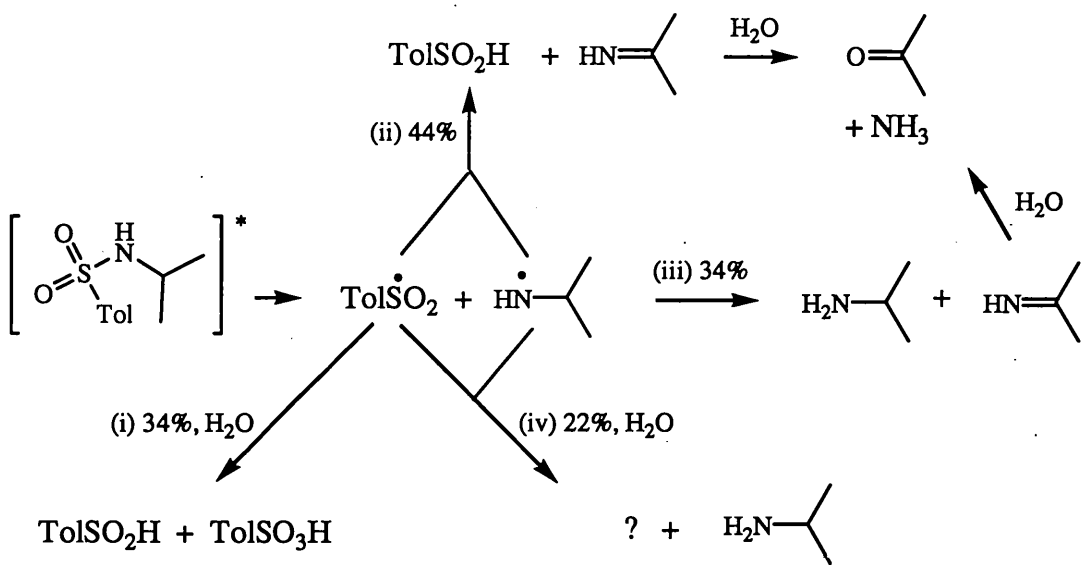

Scheme 4.15 A possible degradation scheme for photodegradation of tosyl alkyl amines.

The lack of C-C cleavage in these compounds coupled with the higher yields observed for the amines suggests that the photochemistry of tosyl amino acids and their

derivatives is better explained by an alternative mechanism such as the one based on PIET that we have favoured hitherto. Homolysis may play some part, however, in those cases such as the tertiary sulfonamide, TsPOH whose product distribution is not well explained by PIET.

4.3.8 Conclusions

The methyl amide compounds discussed in this section have shown a number of differences from the esters and carboxylates in Chapter 3, the first being the formation of a yellow species upon photolysis. The requirements for this at present are a hydrogen on the sulfonamide nitrogen and at the α C position. We shall see further adjustments to these requirements later. This series of compounds has also shown differences to one another in the values obtained for C_α-H abstraction and the net S-N hydrolysis, the latter giving higher yields when the former becomes less favourable.

Two unexpected cleavages were found in the amide bonds and the C-C side-chain of TsAibNMA. The latter is not a favourable reaction in compounds such as the tosyl alkyl amine which also lack a suitable donor for PIET. It seems that the majority of the products observed in all of the other compounds studied are best explained by ET in the excited state.

In the next section we look at the effects of an aromatic ring in the side-chain upon the photodegradation of methyl amide derivatives.

4.4 Aromatic side-chains

4.4.1 Introduction

This section describes the influence of two structural features 1) introducing an aromatic side-chain, 2) changing a carboxylate or ester to a methyl amide in TsFOH, TsFOMe and TsY(OMe)OH. First we will look at *N*-*p*-tosylphenylalanine-*N'*-methyl amide (TsFNMA, **35**), which has a benzyl side-chain and then *N*-*p*-tosyl-*O*-

methyltyrosine-*N'*-methyl amide (TsY(OMe)NMA, **36**) which has a methoxy group at the *para* position of the side-chain aromatic ring. We had seen evidence for side-chain cleavage in TsFOMe and TsY(OMe)OH, so we will be looking for the effects of the methyl amide upon this reaction in particular

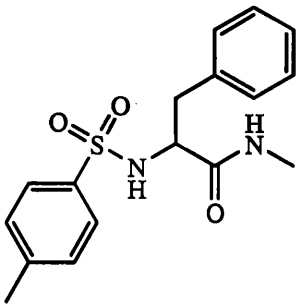

35

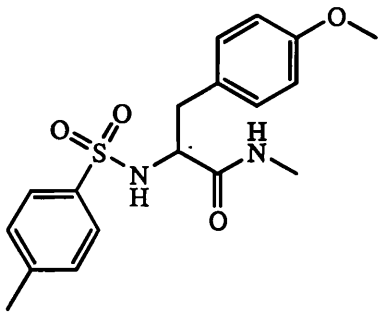

36

4.4.2 General observations for TsFNMA and TsY(OMe)NMA

The TsFNMA solutions became bright yellow upon irradiation. The apparent pH was found to decrease from 6.2 to 5.8 after 60 mins irradiation and the degradation reached 32%. A plot of degradation vs time was similar to that of TsGOH.

In contrast with most other amide derivatives, the TsY(OMe)NMA solutions remained colourless throughout the photolyses. The apparent pH increased from 4.7 to 6.4 after 60 min irradiation and the degradation had reached 20% which is slower by ~10% than that observed for TsGOH and other compounds.

4.4.3 *N-p*-tosylphenylalanine *N'*-methyl amide

HPLC analysis of the raw photolysate with detection at 228 nm showed four peaks, two of which were identified as TsOH and TsH. The two unidentified peaks at 13.0 and 13.5 min had λ_{max} 348 nm and 239 nm. The latter was thought to be an imine precursor of a carbonyl compound, *cf.* phenylacetaldehyde in the TsFOH photolyses. Further evidence was sought in the photodiode array data of the DNP derivatised sample by

examining a chromatogram at 228 nm. All of the peaks of the original photolysate were present with the exception of the 239 nm peak suggesting that the 239 nm compound does react with the DNP reagent. The yellow component which eluted at 12 min will be considered in Section 4.10. Benzyl alcohol was identified as a minor product from a 30% degraded sample. Quantitation was not possible from the original data due to the low response factor of benzyl alcohol and the small injection volumes that had been used.

Analysis for DNP derivatives with detection at 354 nm showed two main products and three minor ones. The former were identified as *N*-methyl glyoxamide and *N*-methyl phenylpyruvamide, and further confirmation was obtained by LC-MS which gave MH^+ 268 and 358 respectively. The minor products were identifed as phenylpyruvic acid, benzaldehyde and phenylacetaldehyde.

AccQTag analysis showed a number of peaks that correspond to NH_3, methylamine, phenylalanine, phenethylamine and two unidentified peaks. The complete results are summarised in Table 4.8 and Table 4.9.

Table 4.8 Product mole fractions for TsFNMA.

Time/ min	Degradation/ %	Product mole fractions						
		TsH	TsOH	N-methyl glyoxamide	methyl phenyl-pyruvamide	phenyl-pyruvic acid	benz-aldehyde	phenyl-acetaldehyde
15	12	0.21	0.09	0.21	0.28	0.03	0.05	0.00
30	21	0.24	0.06	0.20	0.25	0.03	0.03	0.01
60	32	0.27	0.05	0.20	0.23	0.02	0.03	0.01
120	48	0.25	0.04	0.17	0.19	0.02	0.03	0.01

Table 4.9 Product mole fractions for TsFNMA continued.

Time/ min	Degradation/ %	Product mole fractions				
		NH3	methylamine	phenylalanine	phenylalanine *N*-methyl amide	phenethylamine
15	12	0.62	0.20	0.002	0.08	0.01
30	21	0.77	0.16	0.001	0.09	0.01
60	32	0.78	0.13	0.001	0.11	0.01
120	48	0.53	0.08	0.001	0.09	0.01

The product mole fractions enable us to propose a degradation scheme for TsFNMA (Scheme 4.16) based upon evidence from previous compounds. At 10% conversion, 60% of the degraded substrate can be accounted for by two main pathways that both involve ET, (i) and (v). The scheme also illustrates that there may be electronic interactions within the charge-separated biradical that reflects the donor potential from both amide and side-chain functions.

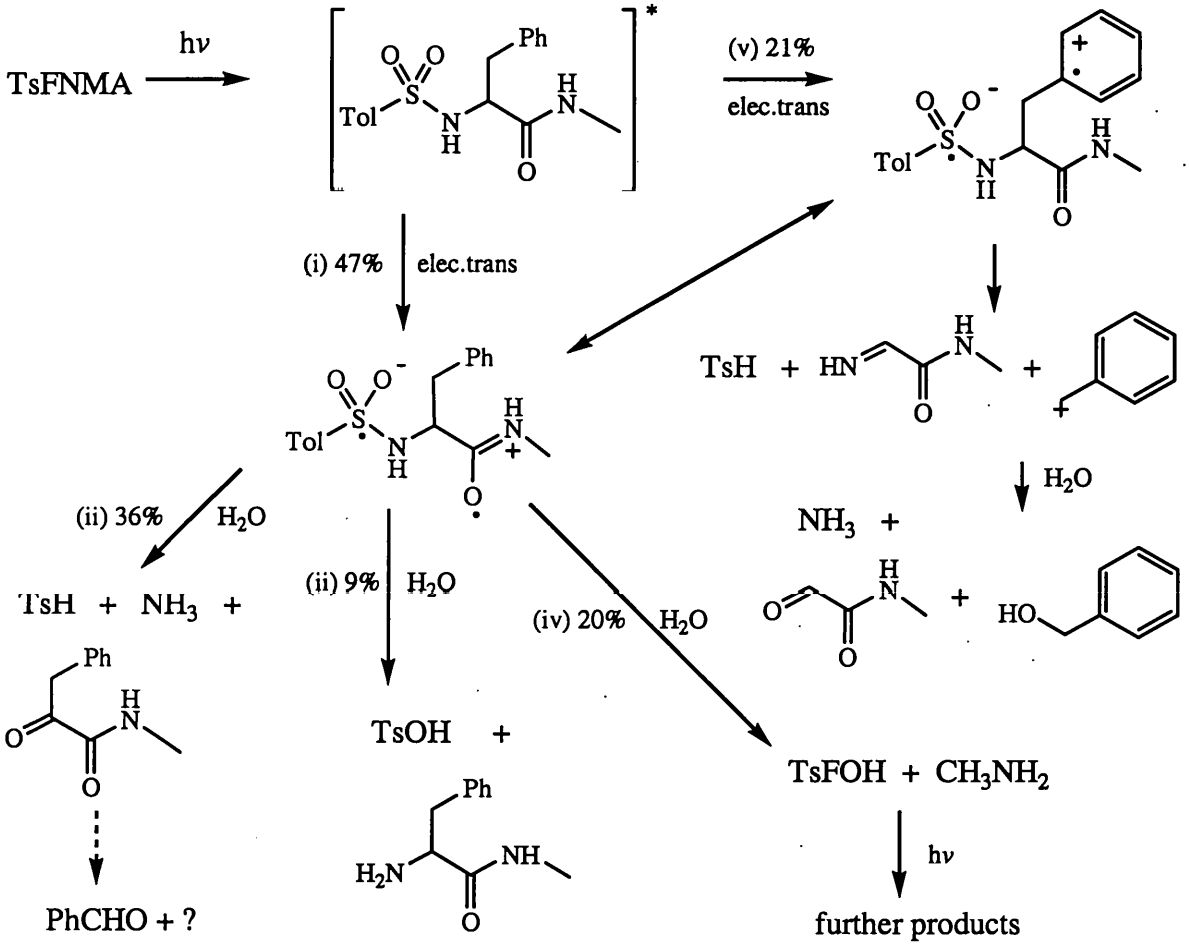

Scheme 4.16 A degradation scheme for TsFNMA at 10% conversion.

The product mole fractions for TsFNMA showed a similar yield for amide bond cleavage to that observed in previous compounds, about 20%. The alternative mechanism suggested with homolytic bond cleavages (Scheme 4.4), can, as with

TsGNMA, be discounted due to the lack of phenylacetaldehyde that would be expected in an equal yield to methylamine if the alternative mechanism was valid. The yield for TsOH and phenylalanine *N*-methylamide are also similar to previous compounds. So, the aromatic group does not appear to have influenced either of these reactions.

However, the yield of C_α-H abstraction is much lower than for TsGNMA and TsVNMA; only 28% compared with ~60%. This would be due to competition with a side-chain cleavage to give *N*-methyl glyoxamide in 21% yield (Scheme 4.17), a process that occurs in a much higher yield than seen with TsFOMe (~2%) and not seen at all with TsFOH. This indicates that ET from the aromatic group is more competitive in TsFNMA than in either of the other two compounds. Next we look at a compound with a methoxy group on the aromatic ring to see if this enhances the side-chain cleavage even further.

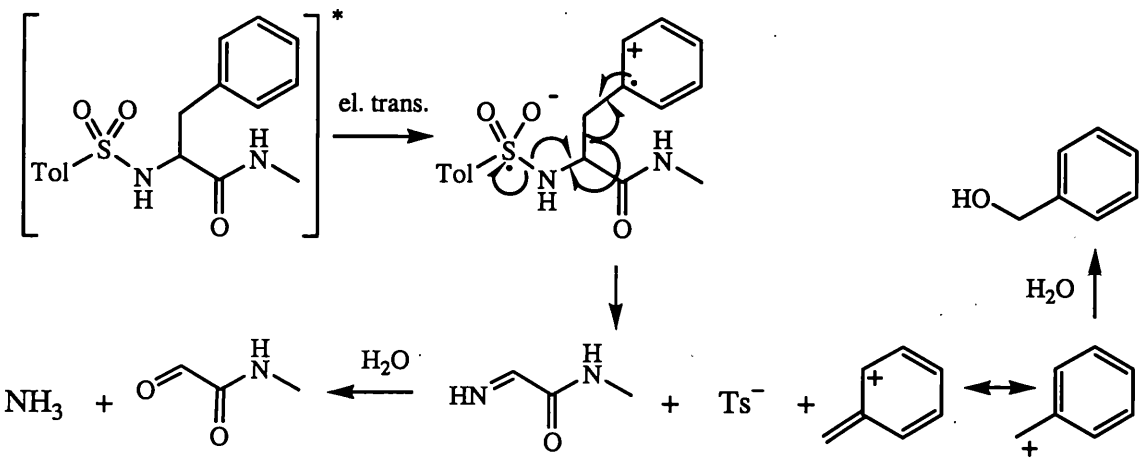

Scheme 4.17 A mechanism for side-chain cleavage involving ET from the aromatic side-chain.

4.4.4 *N-p*-tosyl-*O*-methyltyrosine-*N'*-methyl amide

HPLC analysis with detection at 228 nm showed that TsH was the major aromatic product and TsOH was a minor one. An unidentified peak eluting at 13.0 min had λ_{max} 224 nm and 273 nm, whilst another unidentified peak at 24.6 min had λ_{max} 229 nm. The latter is indicative of a tosylated compound so was quantified using a TsY(OMe)NMA standard.

Analysis of the DNP derivatives with detection at 354 nm gave four peaks. Two were identifed as the stereoisomers of *N*-methyl glyoxamide DNP. The other two were thought to be the stereoisomers of *N*-methyl-*p*-methoxyphenylpyruvamide DNP based upon the RT compared with those of the stereoisomers of *N*-methylphenylpyruvamide DNP.

Analysis of the AccQTag™ derivatives showed five peaks. Two were identified as NH_3 and methylamine and one was likely to be *O*-methyltyrosine *N*-methylamide based upon its RT. The other two have not been identified. The product mole fractions are shown in Table 4.10.

Table 4.10 Product mole fractions for TsY(OMe)NMA.

Time/ min	Degradation/ %	Product mole fractions						
		TsH	TsOH	24.6 min[a]	NH_3	methyl-amine	*N*-methyl glyoxamide[b]	*N*-methyl *p*-methoxy phenylpyruvamide[b]
15	6	0.21	0.31	0.20	0.70	0.02	1.32	0.15
30	12	0.35	0.20	0.13	0.76	0.03	1.08	0.11
60	20	0.32	0.18	0.11	0.84	0.03	1.02	0.11

[a]Quantified using a TsY(OMe)NMA standard, [b]quantified using a HCHO DNP standard

TsY(OMe)NMA did not become yellow upon photolysis indicating that ET from the peptide bond is important for the formation of the yellow species. The product mole fractions at 20% conversion show clearly that the major degradation route was the side-chain cleavage in >90% yield. The sum of the DNP derivatives appears to exceed 100% so suggesting a small error in the quantification relative to formaldehyde DNP. It remains clear, however, that *N*-methyl glyoxamide is the major product in the degradation in conjunction with NH_3 (84%) and TsH (32%). TsH is rather low but TsOH is rather high, if it arises as before, from the net hydrolysis of the S-N bond, although none of the AccQTag™ peaks were identifed as *O*-methyl tyrosine *N'*-methyl amide due to the lack of a standard. The DNP derivatives at 17.4 and 25.5 min could be stereoisomers of the C_α-H abstraction product; *N*-methyl-*p*-methoxy phenylpyruvamide DNP with a yield of ~11%. Very little amide bond cleavage occurred which, again, contrasts with the behaviour of

other amide derivatives where ~20% cleavage was observed. A degradation scheme is suggested that accounts for all of the identified products assuming that the sum of the DNP derivatives is equal to the NH_3 yield (Scheme 4.18).

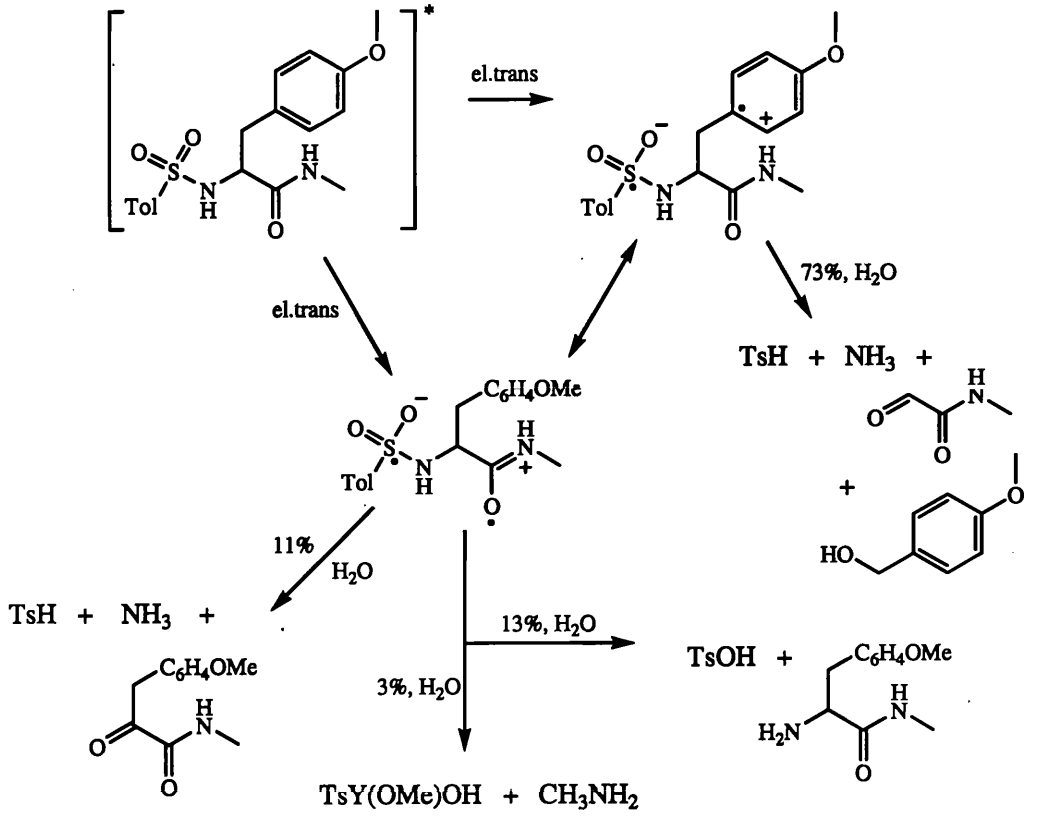

Scheme 4.18 A possible degradation scheme for TsY(OMe)NMA at 20% degradation.

TsY(OMe)NMA has given good support to the hypothesis that side-chain cleavage of aromatic amino acids is due to electron donation from the side-chain aromatic group. It is also a good example of the effects of introducing a different functional group into the molecule that is a better electron donor than the others already present. In TsY(OMe)NMA side-chain cleavage was observed in preference to peptide bond cleavage although the latter has been shown to occur in ~20% yield in some of the previous amide derivatives without the side-chain donor.

4.4.5 Conclusions

The results obtained for TsFNMA and TsY(OMe)NMA have shown some important differences to those of previous compounds, most notably in the increasing values for side-chain cleavage through the series. In TsY(OMe)NMA the side-chain cleavage occurred at the expense of the C_α-H abstraction and the amide bond cleavage indicating that ET from the aromatic ring was in competition with ET from the aromatic side-chain which contains a better ET donor than in TsFNMA due to the methoxy group.

In the next section we look at another compound with a good electron donor in the side-chain.

4.5 Further donor competition from a side-chain: a methionyl derivative

4.5.1 Introduction

We have seen in the previous section that an electron donor in the side-chain of the amino acid results in side-chain cleavage. This is thought to occur from a biradical that is generated by ET from the aromatic ring. We shall now look at *N*-*p*-tosylmethionine *N'*-methyl amide (TsMNMA, **37**) which has a sulfur atom in the side-chain of methionine that is known to be a good electron donor.[92] We saw with TsMOH that the side-chain had little influence upon the photodegradation, will it be more effective in the methyl amide?

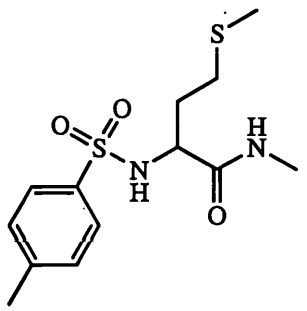

37

4.5.2 *N-p*-tosylmethionine-*N'*-methyl amide

The photolysates were bright yellow upon irradiation for 15 min. At 60 min the apparent pH had decreased from 6.0 to 5.1. Degradation reached 33% at 60 min which is similar to TsGOH and the majority of other compounds.

HPLC analysis of the raw photolysate with detection at 228 nm showed that TsH was the major aromatic product accompanied by a small amount of TsOH and $TsNH_2$. An unidentified peak at 10.5 min had λ_{max} 228 nm, indicative of a tosylated compound and was quantified using a TsMNMA standard.

Analysis for DNP derivatives with detection at 354 nm gave four peaks thought to be two sets of stereoisomers of *N*-methyl 4-methylsulfanyl-2-oxo-butyramide and 3-(methylthio)-propanal DNP. These had λ_{max} 344 - 369 nm and were quantified using a HCHO DNP standard. AccQTag™ analysis gave peaks that were identified as NH_3 and methylamine plus two other unidentifed peaks, one of which may be methionine *N*-methyl amide according to its RT compared with methionine. The product mole fractions are shown in Table 4.11.

Table 4.11 Product mole fractions for TsMNMA

Time/ min	Degradation/ %	Product mole fractions									
		TsH	TsOH	$TsNH_2$	10.5 min[a]	NH_3	methyl -amine	7.1 min DNP[b]	12.2 min DNP[b]	15.0 min DNP[b]	17.3 min DNP[b]
15	12	0.39	0.07	0.03	0.05	0.10	0.07	0.00	0.00	0.04	0.00
30	21	0.43	0.07	0.02	0.04	0.08	0.06	0.02	0.01	0.05	0.01
60	33	0.47	0.09	0.02	0.04	0.08	0.05	0.02	0.01	0.05	0.01

[a]Quantified using a TsMNMA standard, [b]quantified using a HCHO DNP standard

A major product was expected to be the imine or ketone resulting from C_α-H abstraction, which would be analysed as its DNP derivative. However, the value for the largest DNP was only 4%. Quantification may be difficult due to the possible instability of the compound or because formaldehyde DNP is an unsuitable standard, although the latter should cause only small errors. NH_3 was also obtained in a low yield (10%), consistent

with the amount of DNP derivative found. TsH, however, was observed in 39% yield and would be the expected co-product for the ketone and NH_3. It is possible that TsH arises from a photoreaction involving ET from the methionine side-chain (Scheme 4.19). Analogous reactions have been found with phthaloyl derivatives of methionine.[92]

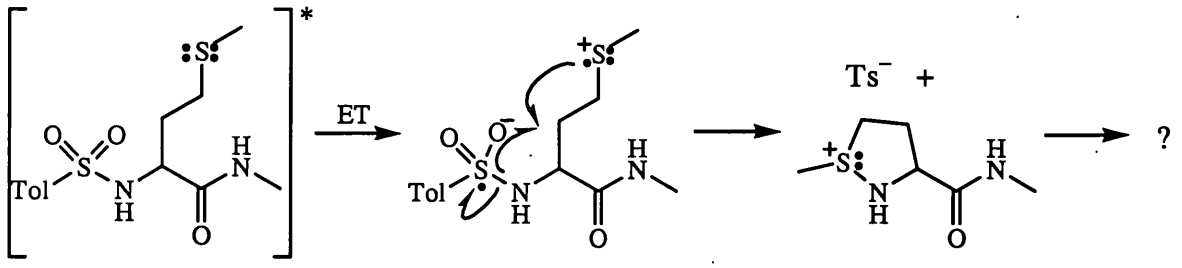

Scheme 4.19 A possible mechanism involving ET from the methionine side-chain.

The S-N cleavage was approximately 7% based upon quantification of TsOH which is similar to the value for TsMOH but slightly lower than the same cleavage in TsGNMA and higher than TsVNMA. Peptide bond cleavage was also 7% based upon the measurement of methylamine, which is also lower than that seen in TsGNMA and TsVNMA. The sulfur containing side-chain appears therefore to have had a small influence upon the yields of these two reactions, although the amide bond has not made a difference relative to the carboxylate. A lower yield for $TsNH_2$ was seen in TsMNMA than in TsMOH so the amide bond has made a difference to this reaction which was suggested to involve an α-lactam or a six-membered ring transition state.

Scheme 4.20 is based upon our previous mechanisms and shows the products that we can account for at 12% degradation and assumes that TsH comes from two routes, (ii) and (iii), the former having unidentified co-products.

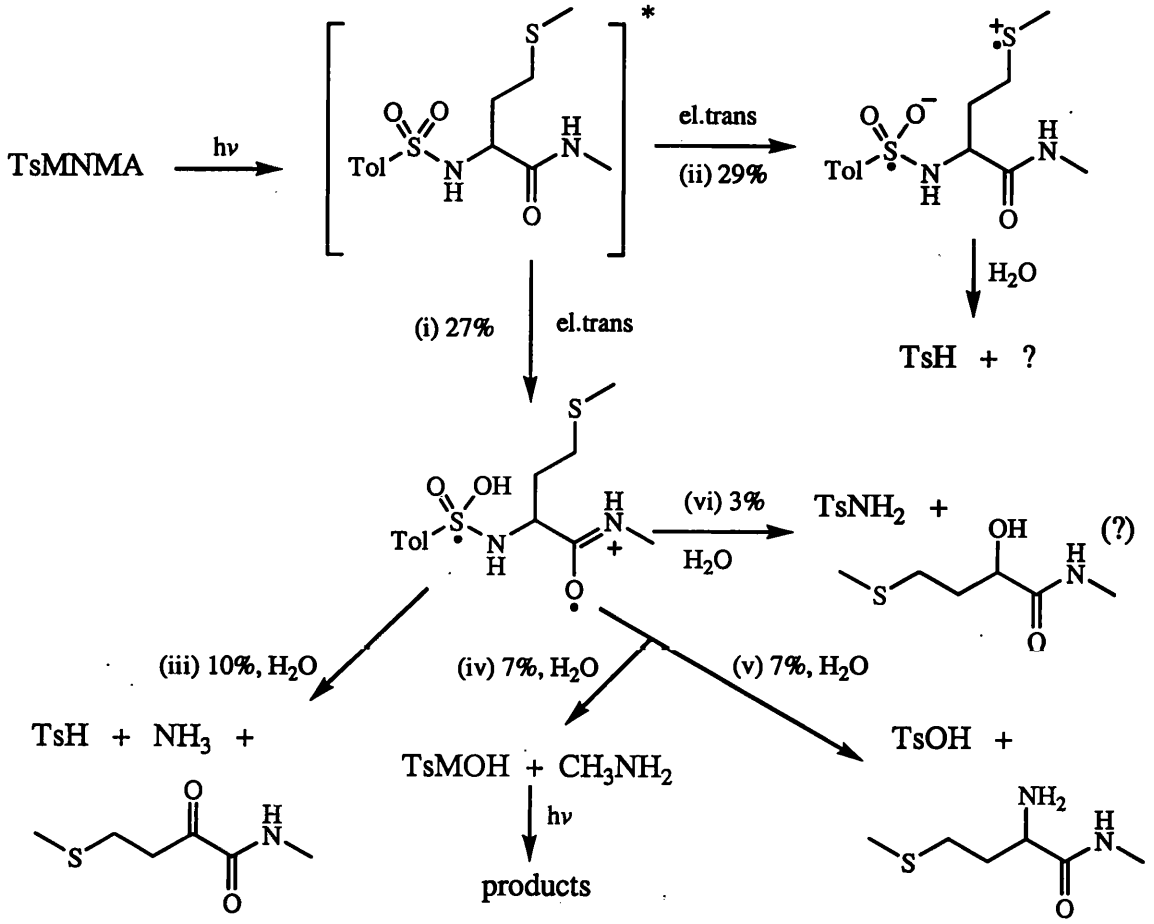

Scheme 4.20 Possible pathways of photodegradation of TsMNMA with accountancy for the product distribution at 12% degradation.

Overall, the accountancy for the degraded material was low, only 56%. The low yields for DNP derivatives compared with other methyl amide derivatives suggests that the sulfur in the side-chain may be participating in the degradation process to give TsH (29%) and unidentified or undetected products. This did not appear to be the case with TsMOH where the major process involved decarboxylation, and shows the importance of the carboxylate group in the degradation of tosyl amino acids. It demonstrates how degradation routes may be influenced by the choice of the carboxyl function in appropriate cases.

In the next two sections we look at the effect of increasing the distance between the amide bond and the sulfonyl group, and the photochemistry of tosyl dipeptides

of the type GX where ET from a distant carboxylate may be possible via the peptide bond to the sulfonyl group.

4.6 Increasing the distance between the amide bond and the sulfonyl group

4.6.1 Introduction

We now consider the effect upon the photodegradation of changing the carboxylate function of TsβAOH to an amide function by examining the photoproducts of *N*-*p*-tosyl-β-alanine-*N'*-methyl amide (TsβANMA, **38**). This has one more carbon atom between the amide bond and the sulfonyl than TsGNMA, and the absence of a side-chain means that TsβANMA can be readily compared to TsGNMA as well as to TsβAOH. TsβANMA was of particular interest in probing the structural requirements for the formation of a yellow species.

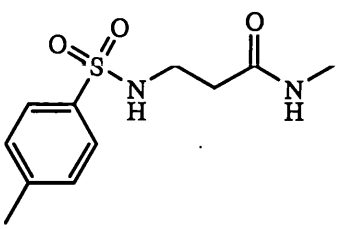

38

4.6.2 *N*-*p*-tosyl β-alanine *N'*-methyl amide

The photolysates remained colourless up to 60 min irradiation. The apparent pH of the 60 min photolysate decreased from 7.3 to 4.0 and degradation reached 34% similar to TsGOH and most other compounds.

HPLC analysis with detection at 228 nm showed the only aromatic products to be TsH and TsOH. Analysis for DNP derivatives with detection at 354 nm gave a large peak thought to be *N*-methyl-3-oxo-propionamide DNP and a small one that was identified

as 3-oxo-propionic acid DNP. AccQTag™ analysis gave peaks identified as NH_3 and methylamine and a large peak that may be β-alanine *N*-methyl amide. The product mole fractions are shown in Table 4.12.

Table 4.12 Product mole fractions for Ts-β-ANMA.

Time/ min	Degradation/%	Product mole fractions					
		TsH	TsOH	NH_3	methyl-amine	3-oxo-propionic acid	9.8 min DNP[a]
15	11	0.38	0.23	0.66	0.04	0.02	0.41
30	18	0.47	0.28	0.80	0.05	0.01	0.49
60	34	0.35	0.29	0.59	0.04	0.01	0.43

[a]Quantified using a 3-oxo-propionic acid DNP standard

The products of the photolysis appear to be similar to those in Ts-β-AOH with the main products being TsH, NH_3 and *N*-methyl 3-oxo-propionamide in approximately 40% yield, which could come from C_β-H abstraction as suggested for TsβAOH.

Cleavage of the S-N bond via a net hydrolysis was observed in 23% yield based upon TsOH quantification, similar to that of TsβAOH but higher than most of the other methyl amides studied. The increased length of the carbon chain has resulted in a low yield for peptide bond cleavage, with only 4% methylamine observed. This is consistent with the association we have made thus far between peptide bond cleavage and PIET, and with the absence of decarboxylation in the photochemistry of the parent acid, TsβAOH reported in Chapter 3. The TsβANMA results suggest that PIET appears to be less favourable with increasing distance between the donor and acceptor but still possible if we invoke ET to explain the peptide bond and S-N cleavages (Scheme 4.21).

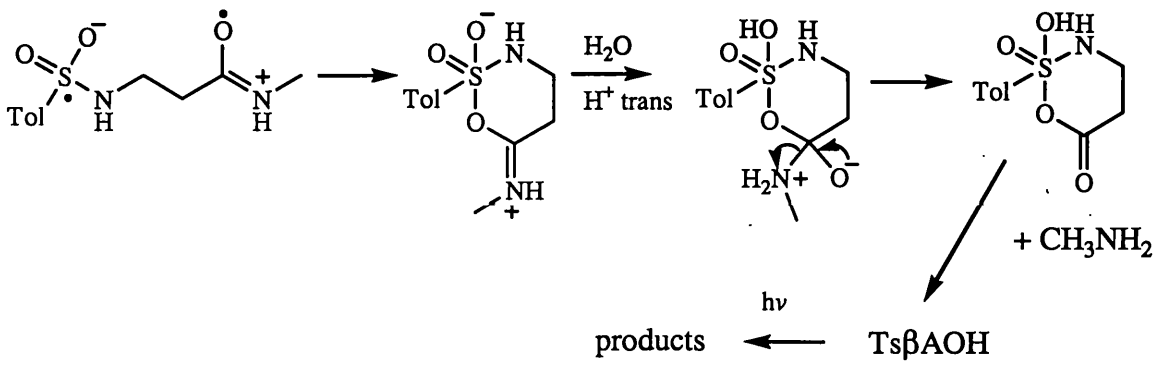

Scheme 4.21 A mechanism involving PIET in TsβAOH.

4.7 Conclusions for the methyl amide series

The methyl amides, with some notable exceptions, have shown consistently a distinctive and potentially informative photoyellowing property which will be more fully discussed in Section 4.10.

The side-chain cleavage was found to be greater in the aromatic compounds than the ones in the previous chapter that had carboxylate groups or esters. With a good electron donor in the side-chain this actually became the dominant reaction. We have also found two unexpected cleavages in this series: 1) amide bond cleavage, 2) side-chain cleavage. The former was found to be affected by the side-chain structure and was reduced when other reactions such as production of the free amino moiety or side-chain cleavage became more favourable.

We have suggested that the peptide bond cleavage is a consequence of PIET in which the group acts as an electron donor. This has interesting consequences for protein photochemistry and in the next section we report results obtained with four tosyl dipeptides of the type GX. We shall note the effects of side-chain groups and a carboxylate group distal to the sulfonyl moiety upon the course of the photoreaction.

4.8 Tosyl dipeptides

4.8.1 Introduction

We have seen that a C_α-H abstraction is important in the methyl amide series but other reactions such as amide bond cleavage and S-N cleavage are affected by the structure of the side-chain to a small extent where the side-chains are aliphatic. Aromatic or sulfur side-chains can have a greater effect. We have seen that β-amino acids also alter the course of reaction.

In this section we shall look at compounds where the carboxylate is distal to the sulfonyl moiety by studying a series of tosyl dipeptides. The first one is the simplest that we could choose, *N-p*-tosylglycylglycine (TsGGOH, **39**) which was studied extensively under the same conditions as TsGOH and afforded considerable product data. Then we shall compare the results with those of three compounds with aliphatic side-chains in the C-terminal amino acid in order to probe possible conformational effects on long range electron transfer. They are: *N-p*-tosylglycylalanine (TsGAOH, **40**), *N-p*-tosylglycylvaline (TsGVOH, **41**) and *N-p*-tosylglycylproline (TsGPOH, **42**).

39

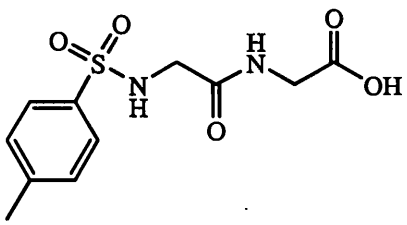

40

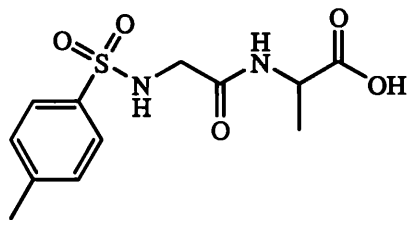

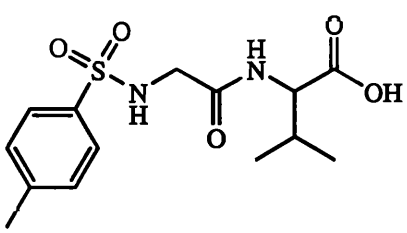

41

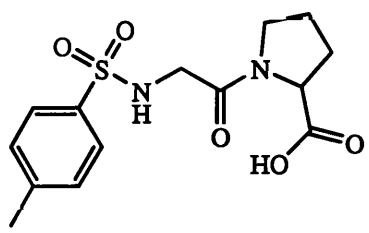

42

4.8.2 General observations for the tosyl dipeptides

TsGGOH solutions became bright yellow under all photolysis conditions. The TsGAOH solutions became a paler yellow and the TsGVOH solutions became a very pale yellow. TsGPOH solutions however, became bright orange upon photolysis. All compounds had a similar degradation rate to TsGOH in aqueous solution.

Table 4.13 Change in pH and conversion at 60 min irradiation.

Substrate	Initial pH[a]	pH at 60 min[a]	Degradation at 60 min/%
TsGGOH unadjusted (H_2O)	3.0		39
TsGGOH alkaline (H_2O)	9.0		37
TsGGOH (40% aq. acetonitrile)			40
TsGAOH (40% aq. acetonitrile)	3.3	3.6	30
TsGVOH (40% aq. acetonitrile)	3.3	3.5	30
TsGPOH (40% aq. acetonitrile)	3.1	3.5	30

[a]This is an apparent pH for all compounds dissolved in 40% acetonitrile/60% H_2O

4.8.3 *N-p*-tosylglycylglycine

HPLC analysis with detection at 228 nm showed that TsH was the major aromatic compound under all three conditions. The next largest peak was identified as TsGOH. Minor peaks were identified as TsOH, $TsNH_2$ and TsGNMA. The latter was not found in the low degradation samples of TsGGOH pH 3 photolysis, but gave larger peaks in all of the alkaline samples. A peak appeared in the alkaline irradiation at 4 min that was not significant in the unadjusted solution. This has not been identified. The yellow component eluted at 5.6 min and had a UV-vis spectrum with λ_{max} 486 nm.

Analysis of DNP derivatives with detection at 354 nm revealed two peaks that were identified as the stereoisomers of *N*-oxo-acetylglycine DNP. These had λ_{max} 360 and 364 nm. The synthesized sample of *N*-oxoacetylglycine DNP gave two peaks in a HPLC chromatogram, which were separated and identified as stereoisomers. Solutions of the two isolated compounds were found to interconvert both thermally and photochemically. The

retention times and peak spectra gave a good match with the two DNP derivative peaks obtained from TsGGOH photolysates (Figure 4.5).

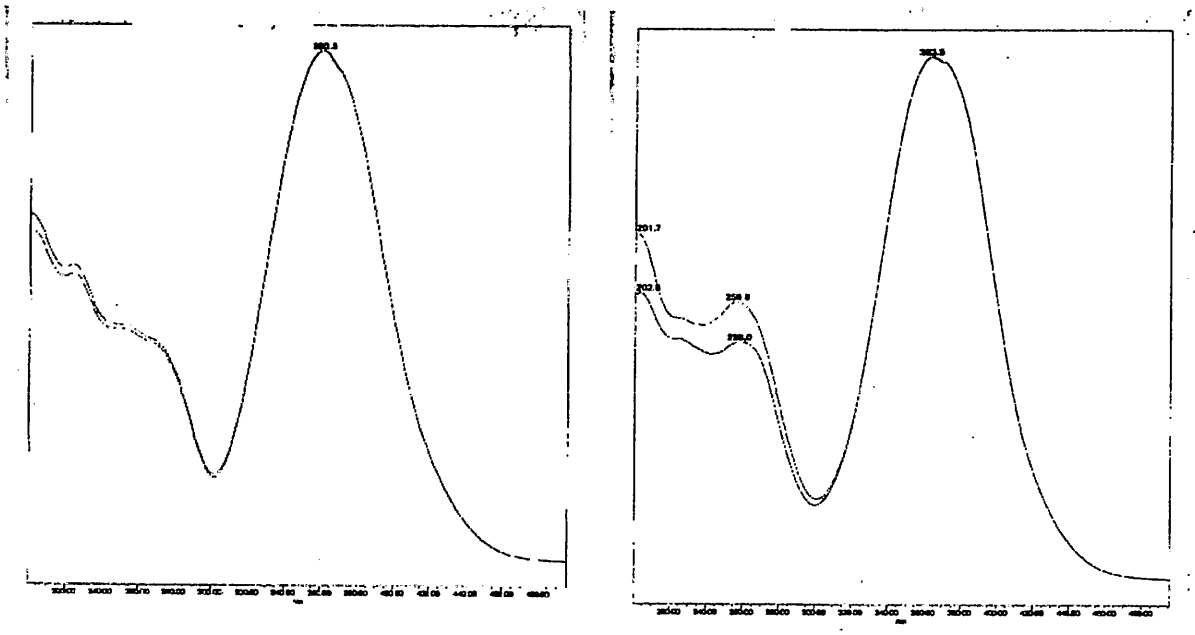

Figure 4.5 Left: Spectra obtained from *N*-oxoacetylglycine DNP 16.5 min peak (red line) and the 16.5 min DNP derivative from a TsGGOH photolysate (pink line). **Right:** Spectra obtained from *N*-oxoacetylglycine DNP 19.2 min peak (green line) and the 19.2 min DNP derivatives from a TsGGOH photolysate (blue line).

Glycylglycine and glycine were quantified by AccQTag™ analysis. NH_3 and CO_2 were measured by gas electrode. An experiment in 40% aqueous acetonitrile gave similar results for CO_2 as the pH unadjusted experiment. The product mole fractions are shown in Table 4.14 for the unadjusted solution and Table 4.15 for the alkaline solution.

The unadjusted solution had some precipitate forming after 30 mins irradiation. No solid was seen in the alkaline solution at any point of the irradiation. The insoluble product from irradiation of the unadjusted solution has been shown to be predominantly TsGOH by both TLC and HPLC analysis. FT-IR spectroscopy was inconclusive.

Table 4.14 Product mole fractions for TsGGOH pH unadjusted photolysates.

Time/ min	Degradation/%	Product mole fractions								
		TsH	TsOH	$TsNH_2$	TsGOH	CO_2	NH_3	glycine	glycyl-glycine	*N*-oxo-acetyl-glycine
2.5	4	0.18	0.17	0.00	0.28	0.00	0.34	0.20	0.06	0.53
5	7	0.20	0.13	0.00	0.20	0.00	0.37	0.22	0.07	0.55
10	13	0.21	0.09	0.01	0.16	0.01	0.38	0.23	0.07	0.60
15	17	0.26	0.08	0.03	0.15	0.02	0.42	0.24	0.08	0.63
30	26	0.29	0.05	0.02	0.12	0.03	0.43	0.25	0.08	0.64
60	39	0.29	0.04	0.02	0.09	0.06	0.44	0.25	0.09	0.65
120	57	0.27	0.04	0.02	0.06	0.08	0.51	0.22	0.09	0.65

Table 4.15 Product mole fractions for TsGGOH pH 9 photolysates.

Time/ min	Degradation/ %	Product mole fractions									
		TsH	TsOH	$TsNH_2$	TsGOH	TsGNMA	CO_2	NH_3	Gly	GlyGly	*N*-oxo-acetyl-glycine
10	9	0.23	0.11	0.00	0.19	0.05	0.08	0.18	0.28	0.10	0.72
15	13	0.26	0.08	0.04	0.18	0.10	0.14	0.19	0.24	0.09	0.65
30	22	0.26	0.05	0.03	0.20	0.10	0.16	0.22	0.30	0.11	0.63
60	37	0.26	0.03	0.04	0.19	0.08	0.19	0.26	0.25	0.09	0.59
120	57	0.26	0.02	0.03	0.14	0.06	0.25	0.31	0.23	0.09	0.54

A change in initial pH had no effect upon the rate of degradation, confirming that the rate of the photochemical reaction is dependent upon the absorption of radiation, as observed in TsGOH. The presence of the solid in only the unadjusted solution is consistent with the main component being the acid, TsGOH.

Both solutions showed the same products with the exception of the unidentified peak at 4 mins in the alkaline irradiation. The overall pattern is broadly similar for the two irradiations suggesting that the degradation pathways are the same. Some of the products such as TsH, TsOH, glycine, NH_3 and CO_2 could be produced in part from the further degradation of TsGOH as well as the degradation of TsGGOH i.e. they are both primary and secondary products. Both solutions showed one main pathway, C_α-H abstraction in ~60% yield based upon the *N*-oxo-acetylglycine which is similar to the value observed in

the photolysis of TsGNMA, indicating that the second amino acid has not influenced the yield for this type of reaction. However, TsH and NH_3 were found in much lower yields (~30%) as sometimes seen previously. Peptide bond cleavage occurred in a similar yield to that seen in many of the methyl amide compounds (~20%), as did S-N cleavage to give TsOH and glycylglycine (8%). Loss of CO_2 was dependent upon the pH of the solution with higher yields found in alkaline solution consistent with ET being favourable from the deprotonated molecule. A tentative degradation scheme is proposed that accounts for all of the products observed at 13% conversion (Scheme 4.22).

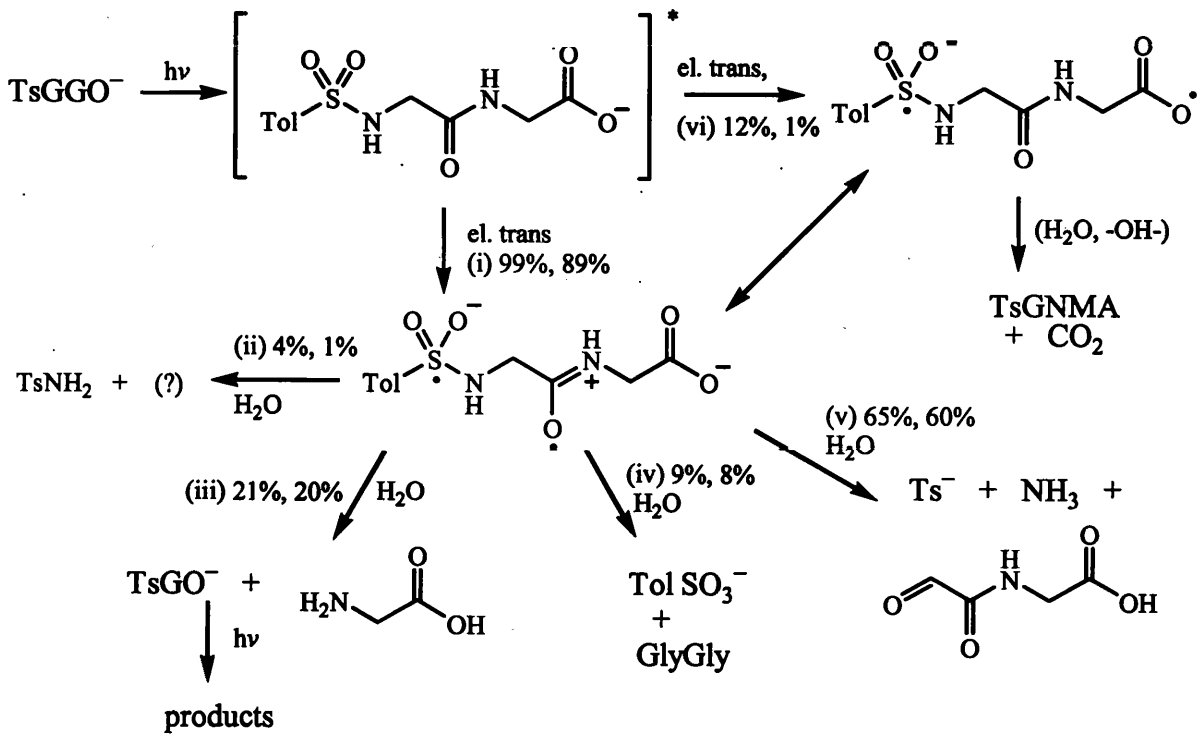

Scheme 4.22 Possible pathways of photodegradation of TsGGOH at 13% degradation and accountancy for product distributions in pH 3 (red) and pH 9 (blue) aqueous photolysates (for simplicity, only the anion is shown).

This scheme accounts for 90% and more than 100% of the substrate in the unadjusted and alkaline irradiations respectively. It is likely that the values of the DNP

derivative have a small error due to quantification using a formaldehyde DNP standard and possibly explains the high accountancy calculated for the alkaline solution.

The identification of TsGNMA in the TsGGOH photolyses provides further evidence for the higher decarboxylation that was found in the alkaline solutions of TsGOH. This supports the hypothesis for electron transfer in the excited state of the deprotonated molecule, which can occur more readily than proton transfer from the carboxylate group (Scheme 4.23).

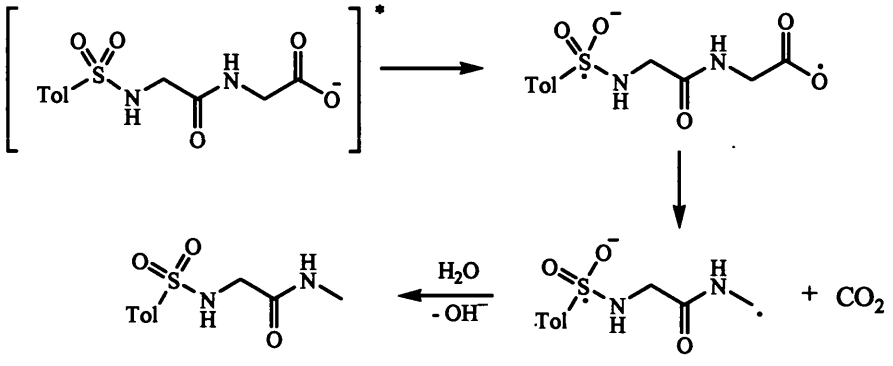

Scheme 4.23 A mechanism for TsGGOH decarboxylation in alkaline solution.

The photodegradation of TsGGOH proceeds primarily via a pathway involving ET that leads predominantly to C_α-H abstraction as seen in the ester and methyl amide derivatives of tosyl amino acids. We have also observed all of the other reactions seen in the methyl amide series. The most significant of these for TsGGOH is the route involving hydrolysis of the peptide bond to give TsGOH and glycine. Comparison of the unadjusted irradiation with the alkaline irradiation has shown the main difference to be a higher rate of decarboxylation at high pH as observed for TsGOH. The next three compounds have increasingly bulkier groups in the amino acid residue distal from the sulfonyl group. So we shall now look at the effect that this has upon the course of the photodegradation with particular interest focused on a possible conformational influence on the long-range decarboxylation process.

4.8.4 *N-p*-tosylglycylalanine

Analysis of the raw photolysate with detection at 228 nm showed three peaks identified as TsOH, TsH and TsGOH. The coloured component eluted at 6.4 min and had λ_{max} 457 nm. Analysis for DNP derivatives with detection at 354 nm showed two main peaks at 12.6 min and 14.2 min., and one small peak at 17.5 min. These had λ_{max} 362 and 363 nm, consistent with a typical DNP derivative such as HCHO DNP from which they were quantified. It was thought that the two main peaks could be stereoisomers of *N*-oxoacetylalanine DNP (*cf.* *N*-oxoacetylglycine DNP from TsGGOH). This is supported by the LC-MS analysis of the first peak which gave the appropriate MH^+ value of 325. The results for the other two peaks were inconclusive. AccQTag analysis shows a number of peaks that correspond to NH_3, glycine, alanine and glycylalanine. CO_2 results were obtained separately for samples that were 7-70% degraded. The product mole fractions obtained for 20-30% degraded solutions are summarised in Table 4.16.

Table 4.16 Product Mole fractions for TsGAOH at 20-30% degradation.

Product	mole fraction
TsH	0.36
TsOH	0.05
TsGOH	0.04
N-oxoacetylalanine DNP	0.86
17.6 min DNP	0.12
NH_3	0.78
glycine	0.003
glycylalanine	0.10
alanine	0.01
CO_2	0.10

Table 4.16 shows that the main products are the DNP derivatives thought to be *N*-oxo-acetylalanine and almost as much NH_3. TsH is lower than both of these, as observed for TsGGOH. Assuming that the yield for the C_α-H abstraction is 78-86%, this is higher than the same route in TsGGOH. The yields for the amide bond cleavage is lower than in

TsGGOH, although S-N cleavage is about the same. This implies that cyclisation of the proposed biradical may be more difficult in TsGAOH than TsGGOH due to the methyl side-chain. CO_2 values, however, are similar so the loss of some conformational space would appear not to have affected decarboxylation. We shall now see if TsGVOH has a more pronounced effect due to a more bulky side-chain.

4.8.5 *N-p*-tosylglycylvaline

HPLC analysis with detection at 228 nm showed three peaks identified as TsOH, TsH and TsGOH as a minor peak. An unidentified peak eluted at 8.9 min. It was not possible to obtain a UV-vis spectrum of the coloured component due to a very low absorbance.

Analysis for DNP derivatives with detection at 354 nm showed two main peaks at 20.4 min and 23.4 min., and two smaller peaks at 26.6 min. and 29.4 min. It was thought that the two main peaks could be stereoisomers of *N*-oxoacetylvaline DNP (*cf* *N*-oxoacetylglycine DNP from TsGGOH). This is supported by the LC-MS analysis of the two main peaks which both had the appropriate MH^+ value of 354.

AccQTag analysis shows a number of peaks that correspond to NH_3, glycine, valine and glycylvaline. CO_2 results were obtained in a separate experiment from 7-70% degradation. The product mole fractions at 20-30% degradation are summarised in Table 4.17.

Table 4.17 Product mole fractions at 20-30% degradation of TsGVOH.

Product	mole fraction
TsH	0.32
TsOH	0.05
8.9 min	0.03
N-oxoacetylvaline DNP	0.74
26.6 min DNP	0.07
29.4 min DNP	0.04
NH_3	0.75
glycine	0.002
glycylvaline	0.06
valine	0.01
CO_2	0.06

TsGVOH product mole fractions appear to be very similar to those of TsGAOH. A small decrease is seen in the yield for S-N cleavage which is only 6% based on the values of TsOH and glycylvaline. The yield of NH_3 is similar yield to that from TsGAOH although the DNP thought to be *N*-oxo-acetylvaline is lower (which may be due to the error of quantification from HCHO DNP). The most noticeable difference to TsGGOH and TsGAOH is the reduced yield for CO_2, which as we will see for TsGPOH, correlates well with the colour of the compound photolysates. Here it suggests a conformational influence on the longe range ET implicated in decarboxylation.

4.8.6 *N-p*-tosylglycylproline

HPLC analysis with detection at 228 nm showed three peaks which were identified as TsOH, TsH and TsGOH. The coloured component eluted at 7.6 min and had λ_{max} 495 nm. Analysis for DNP derivatives with detection at 354 nm showed two peaks at 12.5 min and 14.5 min. These are consistent with the stereoisomers of *N*-oxoacetylproline DNP (*cf N*-oxoacetylglycine DNP from TsGGOH), an assignment that is supported by the LC-MS analysis of both peaks which gave the expected value for MH^+, 352. AccQTag analysis showed a number of peaks that correspond to NH_3, glycine, proline and glycylproline. CO_2 results were obtained from 2-60% degradation. The product mole

fractions at 20-30% degradation are summarised in Table 4.18. A plot of the CO_2 mole fractions are shown in Figure 4.6 for all of the tosyl dipeptides studied.

Table 4.18 Product mole fractions at 20-30% degradation of TsGPOH.

Product	mole fraction
TsH	0.30
TsOH	0.03
TsGOH	0.02
15.0 min	0.04
N-oxoacetylproline DNP	0.68
NH_3	0.59
glycine	0.006
glycylproline	0.05
proline	0.02
CO_2	0.30

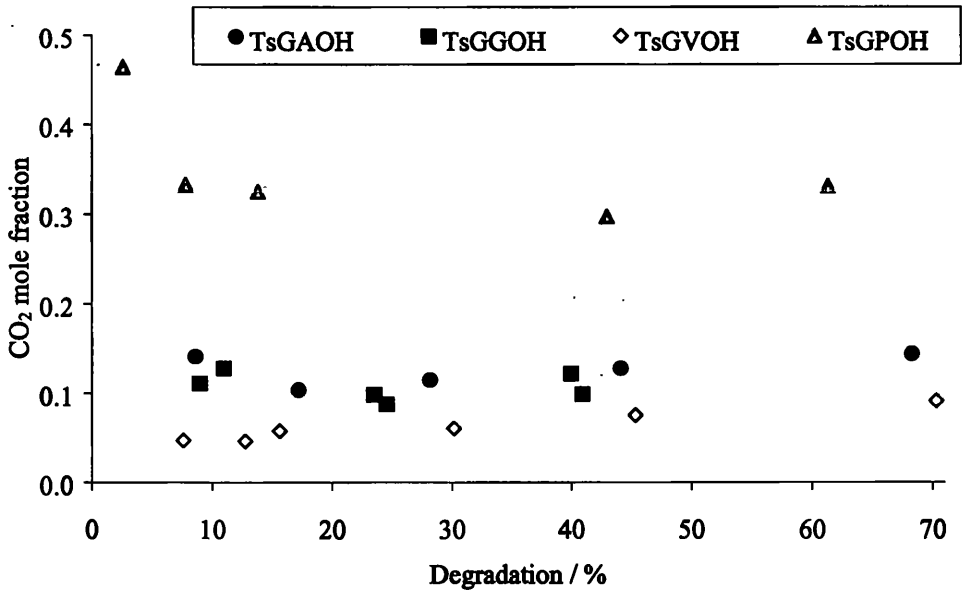

Figure 4.6 The CO_2 mole fractions for all of the tosyl dipeptides.

TsGPOH had a much higher yield for CO_2 than any of the other tosyl dipetides studied (Figure 4.6) and it was also the compound with the deepest colouration. Indeed, the CO_2 mole fractions and the colour appear to correlate well for all of the tosyl dipeptides, a

high CO_2 value corresponds to a more intense colour of the photolysate. However, no peaks were found in the chromatograms that could account for the decarboxylated product, so it may degrade too rapidly for detection by HPLC. The high yield for this route appears to have reduced the yield of the C_α-H abstraction products to about 60%, which is similar to that seen in TsGGOH. However, TsGPOH exhibited very little peptide bond cleavage (2%) or S-N cleavage (4%) both of which were proposed to occur from a cyclic intermediate presumably due to the CO_2 releasing route being more competitive.

4.9 Conclusions for the tosyl dipeptides

All four tosyl dipeptides show a similar product distribution, C_α-H abstraction after an initial ET being the major route as observed with the methyl amide series. The peptide bond and S-N cleavages have been shown to be affected by the C-terminal amino acid, as has the production of CO_2. The peptide bond cleavage showed a significant decrease in all of the tosyl dipeptides compared with TsGGOH, whereas the S-N cleavage exhibited a smaller decrease. The production of CO_2 showed a decrease with increasing steric hindrance with the exception of TsGPOH. However, we have noted differences in TsPOH and TsPNMA that have been difficult to explain in relation to similar compounds and TsGPOH may therefore involve a different mechanism to the other tosyl dipeptides. The production of CO_2 does appear to be associated with the variation in the colour of the compounds, especially in the case of TsGPOH so this matter will be examined in detail in the next section.

4.10 The photoyellowing of tosyl amino acid amides

One striking feature of the photochemistry of tosyl amino acid derivatives has been the frequent observation of an intense yellowing of the photolysate of many members of the series of compounds investigated. If the cause of this phenomenon could be determined, further insight might be gained into the mechanisms of photodegradation.

The yellow colour has been found to be stable for a number of weeks if the photolysate solution is kept in a sealed tube in the cold and dark i.e. in a fridge at < 4 °C. The colour appears to slowly disappear overnight when the solutions are exposed to air and light or when diluted with H_2O. However, this was not rigorously tested.

This thesis has described a number of compounds that have become yellow and many that have not, so we are in a position to propose a basic structural requirement for the photoyellowing phenomenom.

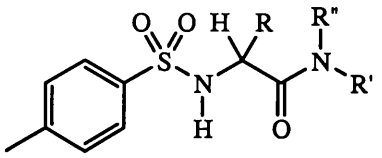

43

A minimal structure, **43,** is based upon evidence from all of the compounds studied. Firstly, only tosyl carboxamides exhibit photoyellowing. It is not seen in the tosyl amino acids and their ester derivatives suggesting that N is required on the carboxylate function. However, TsPNMA, which has a tertiary sulfonamide, did not become yellow suggesting that a hydrogen on the sulfonamide nitrogen is also important. Furthermore, only a very slight colouration was seen with TsAibNMA indicating that the C_α-H is important. When side-chain chemistry was dominant, as in TsY(OMe)NMA, no colouration occurred indicating that the main chain is involved in the photoyellowing. TsGNMA, which has no side-chain, also becomes yellow. Neither of R′ and R″ need to be a hydrogen as TsGPOH actually gave a more intense colouration than any of the other

compounds, perhaps showing that the more polarizable tertiary nitrogen is beneficial. Finally, TsβANMA did not become yellow suggesting that only α-amino acids derivatives can exhibit this phenomenom.

The UV-vis spectrum for the yellow components of the compounds that became yellow were closely similar with TsGPOH having the longest wavelength maximum. Figure 4.7 shows an overlay of the spectra for all of the compounds that became yellow.

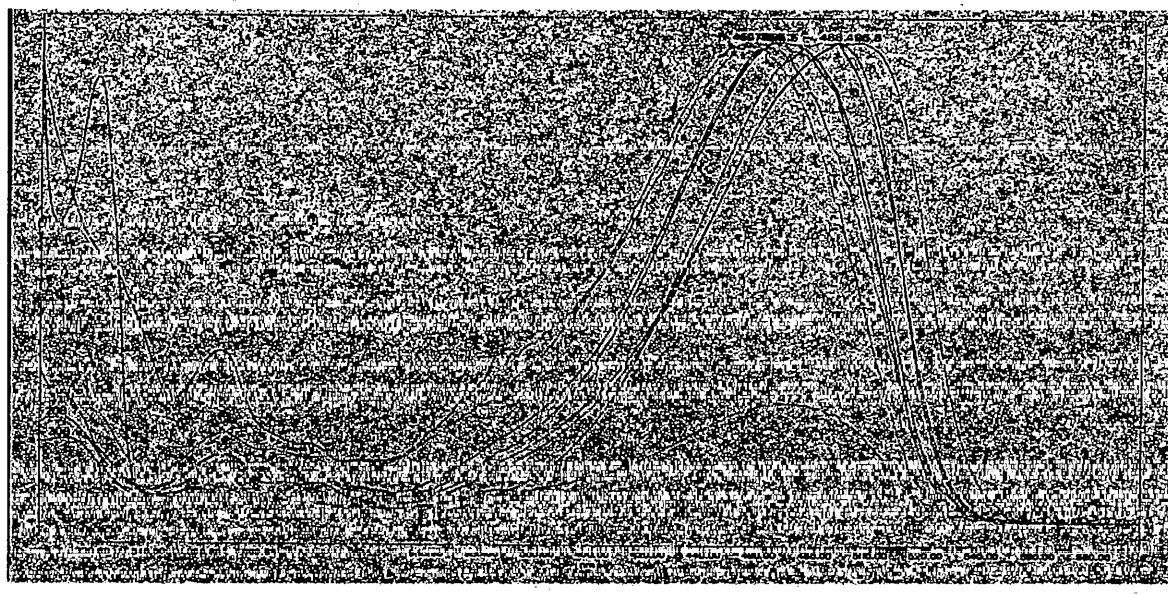

Figure 4.7 UV-vis spectra of the yellow components of TsGNMA, TsGGOH, TsGAOH, TsGVOH, TsVNMA, TsMNMA, TsFNMA and TsPNMA photolysates.

Although attempts to isolate the yellow material were unsuccessful, analysis of TsFNMA by LC-MS with detection at 400 nm gave two peaks that both had MH^+ 333.1. This is the same value as that expected for the protonated molecular ion of TsFNMA, which suggests that the yellow colour may be due to a rearrangement of the starting material or possibly a long-lived radical.

The observations made have led us to suggest that a cyanine type structure may be responsible for the photoyellowing. Cyanine systems are known to exhibit intense absorption at longer wavelength than the corresponding conjugated alkene.[6] This is

exemplified by the difference between cyanine dyes and the corresponding anhydro-base dyes shown in Figure 4.8 with their absorption maxima.

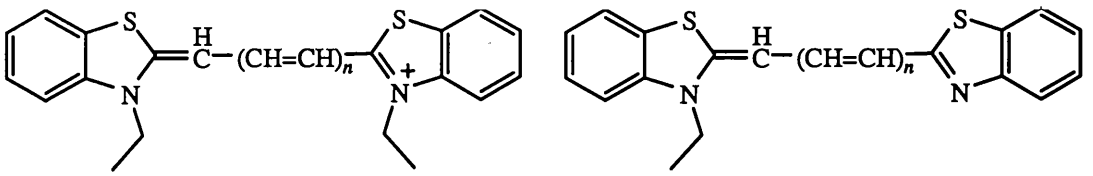

$n = 0, \lambda_{max} = 423$
$n = 1, \lambda_{max} = 569$
$n = 2, \lambda_{max} = 649$
$n = 3, \lambda_{max} = 760$

$n = 0, \lambda_{max} = 393$
$n = 1, \lambda_{max} = 461$
$n = 2, \lambda_{max} = 494$
$n = 3, \lambda_{max} = 522$

Figure 4.8 The difference in absorption maxima for some cyanine dyes (left) and the corresponding anhydro-base dyes (right).[6]

A mechanism is suggested in Scheme 4.24 that leads to a cyanine-type structure from compounds with the basic structural requirements identified earlier.

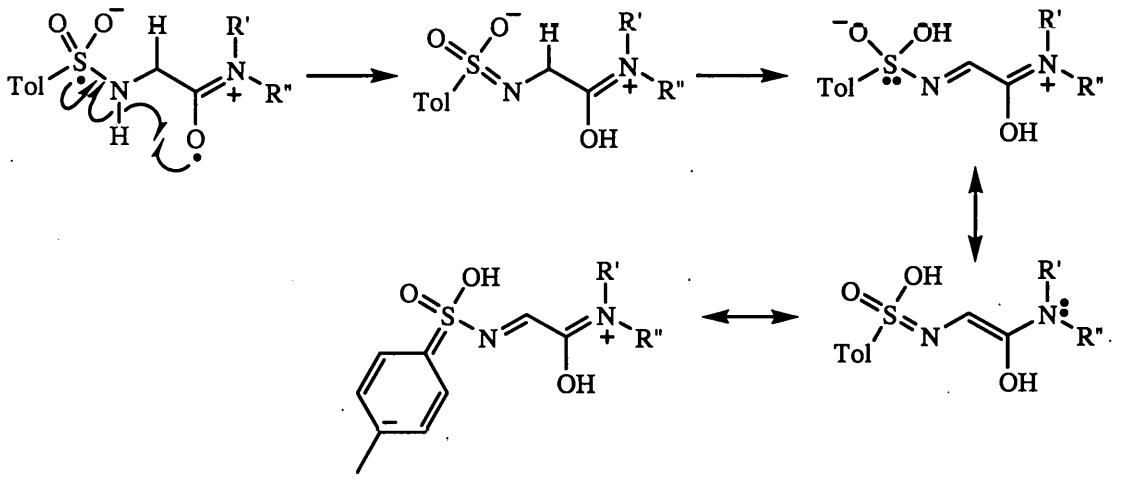

Scheme 4.24 A possible mechanism for the formation of a yellow cyanine-type species.

The cyanine–type structure hypothesis is supported by the evidence cited for the basic structural requirements at the beginning of this section. The requirement of N rather than O on the carboxyl function is consistent with N being more polarizable and

therefore able to participate more readily in electron delocalised structures. Also the proposed cyanine-type compound requires H on the sulfonamide nitrogen and at the α-C. The single major absorption band observed in the UV-vis spectra of all the yellow photolysates implies that a single chromophore is involved, which is supported by the cyanine-type structure that does not involve the side-chain. The conjugated system is possible with α-amino acids but not with β-amino acids. The involvement of the peptide bond nitrogen is consistent with TsGPOH having an absorption maxima at a longer wavelength than the other tosyl dipeptides studied, due to tertiary amide being more polarizable than secondary amides.

The proposed cyanine system also provides a system that may readily decarboxylate in the case of the tosyl dipeptides (Scheme 4.25). TsGPOH had the highest mole fractions for CO_2 and the most intense colour showing that the more favourable the formation of a yellow species then the greater likelihood of decarboxylation. TsGVOH has a much more restricted conformational space that may inhibit the alignment required for this reaction, which is supported by TsGVOH being the least coloured and having the lowest values for CO_2 of all the tosyl dipeptides.

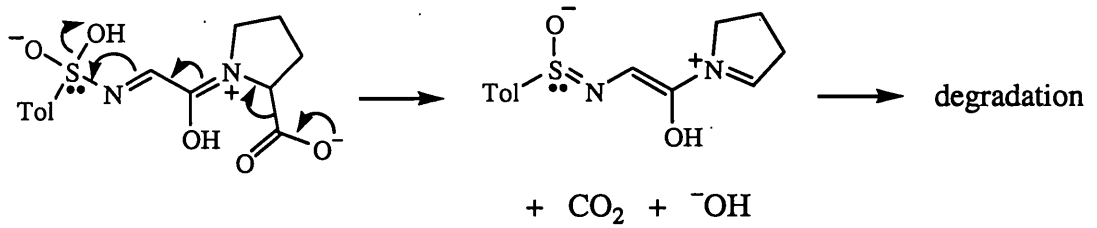

Scheme 4.25 A mechanism for the decarboxylation of tosyl dipeptides.

If these conjectures are valid, they endorse PIET as the key process in the photochemistry of tosyl amino amides. The cyanine-type species can be incorporated into the photodegradation scheme for TsGNMA as shown in Scheme 4.26, which illustrates how the yellow species may be kinetically accessible through the excited state but not from the ground state.

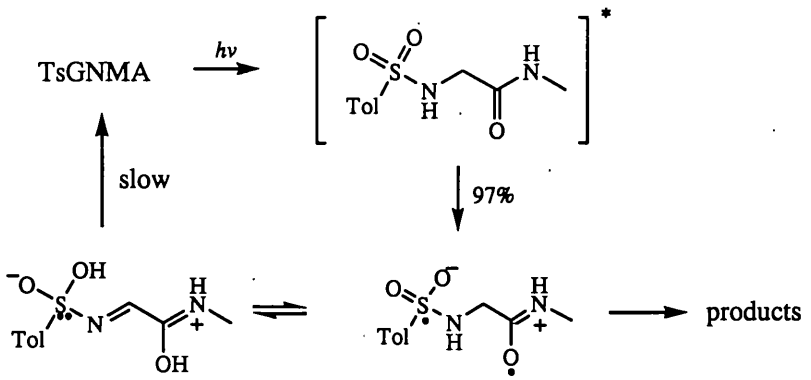

Scheme 4.26 A degradation scheme for TsGNMA, based upon Scheme 4.5, extended to incorporate the yellow species.

The formation of a coloured species upon absorption of light that can return to the colourless ground state species thermally is known as photochromism, a well known and technically important process.[90] A familiar example is the use of photochromic lenses in spectacles.

Chapter 5: Overview

5.1 Summary

The photochemistry of arylsulfonamides is important for three main reasons: firstly as models for PIET in biological systems, secondly the potential of arylsulfonyls for photoremovable protecting groups in organic synthesis and finally because arylsulfonamide pharmaceuticals are known to be photolabile. In Chapter 1, we saw that there continues to be a vast amount of research in the first area, with many workers keen to gain insight into the mechanisms of photosynthesis in order to contribute towards the design of artificial systems that could have application in a wide range of areas. The second area also continues to receive interest but not to the same extent, generally because of the poor yields that have been reported. Many attempts have been made to design electron donors capable of absorbing at > 300 nm to avoid the destruction of the compounds involved. However, little progress has been made in identifying the unwanted products or mechanisms. This also tends to be the case with pharmaceutical stability testing. If a compound is unstable it may be rejected in the late stages of development, but without determining the reason for the observed photoinstability, such problems cannot be readily anticipated.

Our aim was to study a range of model compounds to gain insight into all of the aforementioned areas and possibly to enable prediction of the outcome of photochemical reactions involving arylsulfonyl compounds. We have performed extensive studies of twenty-seven tosylated compounds, twenty-two of which were amino acid derivatives, and by a comprehensive product analysis using predominantly HPLC we have been able to identify all of the major degradation products and also many minor ones. From the product data we have been able to propose degradation schemes that involve an initial PIET step to produce the majority of the photoproducts.

We found that the tosyl amino acids generally photodegrade by a process that involves loss of CO_2, which, indeed has been noticed by other workers, although the co-products have not been identified. All of the tosyl amino acids produced a carbonyl compound that could react with DNP reagent and hence was readily observable by HPLC, unlike the underivatised compound. The introduction of bulky side-chains, including an aromatic or a potentially reactive sulfur-containing side-chain produced little change in the product distribution. However, a good electron donor attached to the aromatic side-chain resulted in side-chain cleavage, as well as all of the previously observed photoreactions but in lower yield than reported for other compounds. In all of the tosyl α-amino acids the yield for recovery of the amino acid was poor, typically < 10%, regardless of the side-chain structure.

On increasing the distance between the carboxylate and sulfonyl moieties, as in a β-amino acid, the yield for the free amino acid was increased to ~ 20%. However the main reaction still involved production of a carbonyl compound but with retention of the carboxylate group.

A different carboxylate function such as an ester, also gave a low yield for S-N cleavage and the major photoproducts were identified as carbonyl componds that could be explained by a C_α-H abstraction that had been seen as a minor outcome from the tosyl α-amino acids, and analogous to the products from the β-amino acid. However, problems were found with the stability of the ester function under the analytical conditions used leading to difficulties in product quantification.

Amide derivatives were then studied, which provided more stable photoproducts for analysis and produced some interesting photoreactions that had not been anticipated. Firstly we found peptide bond cleavage in most of the tosyl amino amides studied in yields of around 20%. The only compound that did not undergo this reaction was a proline derivative that would have produced a strained intermediate in our proposed mechanism and may preferentially undergo S-N cleavage to relieve ring-strain. A lower yield was also seen when a good electron donor was present in the side-chain. In all cases

the main photoreaction afforded products arising from a C_α-H abstraction as with the ester derivatives. This work was then extended to four tosyl dipeptides to look at the influence of bulky groups and a carboxylate in the C-terminal amino acid. A conformational effect was found for the loss of CO_2 and peptide bond cleavage, although C_α-H abstraction remained as the dominant pathway.

A striking observation for a number of the tosyl amino amides was the production of bright yellow photolysates. By considering the data acquired and the structural requirements for the formation of a coloured species, we have suggested that photochromism involving a cyanine-type structure as behaviour consistent with the proposed mechanisms of photodegradation involving an initial PIET step that we have suggested for all of the tosyl amino derivatives studied.

5.2 Conclusions

We had anticipated that this project may contribute to PIET processes in peptide models and we have seen photoreactions that are indicative of ET from a number of possible sites. The Tyr and Phe derivatives have shown the importance of a good electron donor in the side-chains of amino acids. We have also found many examples of peptide bond cleavage which may be seen as evidence for this important group acting as an electron donor and facilitator of electron movement through peptide chains. The carboxylate has also been shown to participate in longer-range PIET, possibly via an intermediate peptide bond.

The literature had shown poor yields for deprotection of tosylated amines and we have provided comprehensive product analysis that enables prediction of competing reactions. Most notably, the hydrogen at the α-C is particularly labile and the formation of imine compounds is a likely outcome of photolyses unless reducing agents are used. This may provide a useful approach to the formation of imines and carbonyl compounds rather than the amines as previously attempted.

The photoinstability of drugs is difficult to predict. However, guidelines exist for the photostability testing and the outcome of a reaction may be predicted based upon comparison with analogous compounds. In the case of arylsulfonamides we have shown the most likely site of reaction to be the α-C which may react by a hydrogen abstraction to give an imine and the arylsulfonyl group, or possibly by side-chain cleavage. The presence of electron donors in the group attached to the α-C makes the latter more likely, whilst electron donors such as carboxylates and peptide bonds make cleavages at other sites of the molecule likely. Discolouration of sulfonamide drugs may even be due to photochromism as suggested for our compounds and hence may not result in photodegradation. Photoreactions of drug compounds are obviously undesirable and the appropriate precautions must be taken.

In conclusion, we have studied the photochemistry of a large range of tosylated amino acids and their derivatives. Comprehensive product data have been acquired from which we have been able to propose some possible mechanisms for the degradations that have implied PIET as an important process and enabled us to identify the likely mechanisms of photodegradation in simple compounds. We anticipate that the conclusions from this work may be widely applicable to the photochemistry of more complex arylsulfonamides.

5.3 Further work

There have been a number of instances where authentic standards have not been available and the photoproduct identity has been assumed by analogy with other compounds. LC-MS has been a useful tool in confirming the identity of some of these photoproducts but could have been used much more extensively if time and facilities allowed. In particular a number of DNP derivatives, the co-products of $TsNH_2$ and the side-chain cleavages remain speculative and their identity could give important insight into

some of the minor pathways. Further development of LC-MS methods is required for comfirmation, or otherwise, of the speculative products.

One avenue considered during this work was the trapping of radicals, which may have been useful in establishing some features of the degradation pathways and perhaps eliminating a radical origin of photoyellowing. ESR spectroscopy could also aid in the identification of a biradical species and although it is difficult to perform upon aqueous solutions, warrants further investigation.

A very interesting concept conceived at a late stage of the project was that of a possible photochromic process being involved in the formation of a yellow species. Indeed, LC-MS again proved particularly useful in proposing this hypothesis and it warrants further study with different compounds.

References

1 T. Hamada, A. Nishida, and O. Yonemitsu, *Journal of the American Chemical Society*, 1986, **108**, 140.

2 T. Hamada, A. Nishida, and O. Yonemitsu, *Tetrahedron Letters*, 1989, **30**, 4241.

3 M. Bruncko and D. Crich, *Journal of Organic Chemistry*, 1994, **59**, 4239.

4 A. Albini and E. Fasini, 'Drugs: Photochemistry and Photostability', The Royal Society of Chemistry, London, 1998.

5 H. H. Tonnesen, 'Photostability of Drugs and Drug Formulations', Taylor and Francis, London, 1996.

6 'S341: Photochemistry: Light, Chemical Change and Life', The Open University Press, 1987.

7 'S327: Living Processes: Bioenergetics', The Open University Press, 1995.

8 R. R. Hill, J. D. Coyle, D. Birch, E. Dawe, G. E. Jeffs, D. Randall, I. Stec, and T. M. Stevenson, *Journal of the American Chemical Society*, 1991, **113**, 1805.

9 R. R. Hill, G. E. Jeffs, F. Banaghan, T. McNally, and A. R. Werninck, *Journal of the Chemical Society-Perkin Transactions 2*, 1996, 1595.

10 L. Serrano-Andres and M. P. Fulscher, *Journal of the American Chemical Society*, 1998, **120**, 10912.

11 J. Deisenhofer, O. Epp, K. Miki, R. Huber, and H. Michel, *Journal of Molecular Biology*, 1984, **180**, 385.

12 J. Deisenhofer and M. Michel, *Abstracts of Papers of the American Chemical Society*, 1988, **196**, 277.

13 D. A. Williamson and B. E. Bowler, *Journal of the American Chemical Society*, 1998, **120**, 10902.

14 E. Galoppini and M. A. Fox, *Journal of the American Chemical Society*, 1996, **118**, 2299.

15 M. A. Fox and E. Galoppini, *Journal of the American Chemical Society*, 1997, **119**, 5277.

16 A. Polese, S. Mondini, A. Bianco, C. Toniolo, G. Scorrano, D. M. Guldi, and M. Maggini, *Journal of the American Chemical Society*, 1999, **121**, 3446.

17 S. H. Pullen, M. D. Edington, S. L. Studer-Martinez, J. D. Simon, and H. A. Staab, *Journal of Physical Chemistry A*, 1999, **103**, 2740.

18 C. A. Slate, D. R. Striplin, J. A. Moss, P. Y. Chen, B. W. Erickson, and T. J. Meyer, *Journal of the American Chemical Society*, 1998, **120**, 4885.

19 G. Jones, V. Vullev, E. H. Braswell, and D. Zhu, *Journal of the American Chemical Society*, 2000, **122**, 388.

20 H. A. Wagenknecht, E. D. A. Stemp, and J. K. Barton, *Journal of the American Chemical Society*, 2000, **122**, 1.

21 M. Aoudia and M. A. J. Rodgers, *Journal of the American Chemical Society*, 1997, **119**, 12859.

22 B. Nyasse, L. Grehn, U. Ragnarsson, H. L. S. Maia, L. S. Monteiro, I. Leito, I. Koppel, and J. Koppel, *Journal of the Chemical Society-Perkin Transactions 1*, 1995, 2025.

23 A. Lebouc, P. Martigny, R. Carlier, and J. Simonet, *Tetrahedron*, 1985, **41**, 1251.

24 I. Schon, *Chemical Reviews*, 1984, **84**, 287.

25 L. D'Souza and R. A. Day, *Science*, 1968, **160**, 882.

26 L. D'Souza and R. A. Day, *Archives of Biochemistry and Biophysics*, 1970, **141**, 690.

27 J. P. Pete, C. Portella, A. Abad, and D. Mellier, *Tetrahedron Letters*, 1971, 4555.

28 J. P. Pete and C. Portella, *Journal of Chemical Research (S)*, 1979, 20.

29 J. P. Pete, D. Mellier, and C. Portella, *Tetrahedron Letters*, 1971, 4559.

30 M. Z. A. Badr, M. M. Aly, and A. M. Fahmy, *Journal of Organic Chemistry*, 1981, **46**, 4784.

31 B. Weiss, H. Durr, and H. F. Haas, *Angewandte Chemie-International Edition in English*, 1980, **19**, 648.

32 J. A. Pincock and A. Jurgens, *Tetrahedron Letters*, 1979, 1029.

33 B. Umezawa, O. Hoshino, and S. Sawaki, *Chemical and Pharmaceutical Bulletin*, 1969, **17**, 1115.

34 B. Umezawa, O. Hoshino, and S. Sawaki, *Chemical and Pharmaceutical Bulletin*, 1970, **18**, 182.

35 T. Hamada, A. Nishida, and O. Yonemitsu, *Heterocycles*, 1979, **12**, 647.

36 R. Kossai, B. Emir, J. Simonet, and G. Mousset, *Journal of Electroanalytical Chemistry*, 1989, **270**, 253.

37 J. E. T. Corrie and G. Papageorgiou, *Journal of the Chemical Society-Perkin Transactions 1*, 1996, 1583.

38 G. Papageorgiou and J. E. T. Corrie, *Tetrahedron*, 1999, **55**, 237.

39 J. Monig, R. Chapman, and K. D. Asmus, *Journal of Physical Chemistry*, 1985, **89**, 3139.

40 G. Jones, L. N. Lu, V. Vullev, D. J. Gosztola, S. R. Greenfield, and M. R. Wasielewski, *Bioorganic & Medicinal Chemistry Letters*, 1995, **5**, 2385.

41 G. Jones, L. N. Lu, H. N. Fu, C. W. Farahat, C. Oh, S. R. Greenfield, D. J. Gosztola, and M. R. Wasielewski, *Journal of Physical Chemistry B*, 1999, **103**, 572.

42 H. H. Tonnesen, *International Journal of Pharmaceutics*, 2001, **225**, 1.

43 E. Selvaag and P. Thune, *Acta Dermato-Venereologica*, 1996, **76**, 405.

44 T. Oppenlander, *Chimia*, 1988, **42**, 331.

45 K. Kuokkanen, *Acta Allergol*, 1972, **27**, 407.

46 T. J. Dougherty, *Photochemistry and Photobiology*, 1987, **45**, 879.

47 International Conference on Harmonisation. Tripartite Guidelines: Photostability Testing of New Drug Substances and Products, 1996.

48 P. L. Russ and E. A. Caress, *Journal of Organic Chemistry*, 1976, **41**, 150.

49 A. Beecham, *Journal of the American Chemical Society*, 1957, **79**, 3257.

50 R. W. Holley and A. D. Holley, *Journal of the American Chemical Society*, 1949, **71**, 2129.

51 W. J. Pope and C. S. Gibson, *Journal of the Chemical Society*, 1912, **101**, 1703.

52 R. G. Kostyanovsky, G. V. Shustov, and N. L. Zaichenko, *Tetrahedron*, 1982, **38**, 949.

53 J. R. Piper and T. P. Johnston, *Journal of Organic Chemistry*, 1968, **33**, 636.

54 C. Remsen and D. Palmer, *American Chemistry Journal*, 1886, **8**, 241.

55 A. I. Vogel, '*Practical Organic Chemistry*', Longman, 1956.

56 R. Schoenheimer, *Hoppe-Seylers Zeitschrift fur Physiologische Chemie*, 1926, **154**, 222.

57 A. F. Beecham, *Journal of the American Chemical Society*, 1957, **79**, 3262.

58 M. Y. Malov, G. K. Semenova, Krasil'nikov, II, and O. V. Arapov, *Russian Journal of Applied Chemistry*, 1997, **70**, 1280.

59 E. W. McChesney and W. Swann, *Journal of the American Chemical Society*, 1937, **59**, 1116.

60 M. Bovarnick and H. T. Clarke, *Journal of the American Chemical Society*, 1938, **60**, 2426.

61 T. B. Johnson and H. G. Guest, *American Chemistry Journal*, 1909, **42**, 340.

62 S. G. Pyne, M. J. Hensel, and P. L. Fuchs, *Journal of the American Chemical Society*, 1981, **104**, 5719.

63 M. Raban and F. B. Jones, *Journal of the American Chemical Society*, 1971, **93**, 2692.

64 J. W. Hinman, E. L. Caron, and H. N. Christensen, *Journal of the American Chemical Society*, 1950, **72**, 1620.

65 E. Kaiser and E. P. Gunther, *Journal of the American Chemical Society*, 1956, **78**, 3841.

66 J. A. Bajgrowicz, A. E. Hallaoui, R. Jacquier, C. Pigiere, and P. Viallefont, *Tetrahedron*, 1985, **41**, 1833.

67 K. Walther, U. Kranz, and H. G. Henning, *Journal Fur Praktische Chemie*, 1987, **329**, 859.

68 G. A. Molander and P. J. Stengel, *Tetrahedron*, 1997, **53**, 8887.

69 J. R. Bartels-Keith, *Journal of the Chemical Society*, 1960, 1662.

70 G. L. Clark and H. Kao, *Journal of the American Chemical Society*, 1948, **70**, 2151.

71 E. A. Braude and E. R. H. Jones, *Journal of the Chemical Society*, 1945, 498.

72 S. A. Barker, J. C. Bevington, J. S. Brimacombe, and E. D. M. Eades, *Journal of the Chemical Society*, 1962, 4508.

73 H. Heaney, G. Papageorgiou, and R. F. Wilkins, *Tetrahedron*, 1997, **53**, 14381.

74 A. Ross and R. N. Ring, *Journal of Organic Chemistry*, 1961, **26**, 579.

75 H. Li Chum and P. Krumholz, *Inorganic Chemistry*, 1974, **13**, 514.

76 A. E. Opara and G. Read, *Journal of the Chemical Society. Perkin Transactions II*, 1973, 1221.

77 H. Reinheckel, A. Jovtscheff, and S. Spassov, *Monatshefte fur Chemie*, 1965, **96**, 1185.

78 P. M. Pojer and I. D. Rae, *Australian Journal of Chemistry*, 1970, **23**, 413.

79 M. M. Shemyakin, G. A. Ravdel, and E. S. Chaman, *Doklady Chemistry (English Translation)*, 1956, **195**, 106.

80 M. Alvaro, H. Garcia, S. Iborra, M. A. Miranda, and J. Primo, *Tetrahedron*, 1987, **43**, 143.

81 W. S. Fones, *Journal of Organic Chemistry*, 1952, **17**, 1534.

82 J. H. Jones, B. Liberek, and G. T. Young, *Journal of the Chemistry Society (C)*, 1967, 2371.

83 I. Ojima, H. J. C. Chen, and X. G. Qiu, *Tetrahedron*, 1988, **44**, 5307.

84 J. W. Cubbage, B. W. Vos, and W. S. Jenks, *Journal of the American Chemical Society*, 2000, **122**, 4968.

85 G. J. Karabatsos, B. L. Shapiro, F. M. Vane, J. S. Fleming, and J. S. Ratka, *Journal of the American Chemical Society*, 1963, **85**, 2784.

86 E. Grosjean, P. G. Green, and D. Grosjean, *Analytical Chemistry*, 1999, **71**, 1851.

87 B. N. Nukuna, M. B. Goshe, and V. E. Anderson, *Journal of the American Chemical Society*, 2001, **123**, 1208.

88 J. Biggs, N. B. Chapman, A. F. Finch and V. Wray, *Journal of the Chemistry Society (B)*, 1971, 55.

89 O. Sciacovelli, A. Dell'Atti, A. De Giglio, and L. Z. Cassidei, *Naturforsch*, 1976, 5.

90 'S341: Light, Chemical Change and Life: a source book in photochemistry', ed. J. D. Coyle, R. R. Hill, and D. R. Roberts, 1988.

91 A. G. Griesbeck, A. Henz, J. Hirt, V. Ptatschek, T. Engel, D. Loffler, and F. W. Schneider, *Tetrahedron*, 1994, **50**, 701.

92 A. G. Griesbeck, H. Mauder, I. Muller, E. M. Peters, K. Peters, and H. G. Vonschnering, *Tetrahedron Letters*, 1993, **34**, 453.

93 C. J. Creighton, T. T. Romoff, J. H. Bu, and M. Goodman, *Journal of the American Chemical Society*, 1999, **121**, 6786.